

An Experimental Investigation of a Joined Wing Aircraft Configuration Using Flexible, Reduced Scale Flight Test Vehicles

by

Jenner Richards
B.Eng., University of Victoria, 2009

A Dissertation Submitted in Partial Fulfillment
of the Requirements for the Degree of

DOCTOR OF PHILOSOPHY

in the Department of Mechanical Engineering

© Jenner Richards. 2014
University of Victoria

All rights reserved. This Dissertation may not be reproduced in whole or in part, by photocopy or other means, without the permission of the author.

An Experimental Investigation of a Joined Wing Aircraft Configuration Using Flexible, Reduced Scale Flight Test Vehicles

by

Jenner Richards
B.Eng., University of Victoria, 2009

Supervisory Committee

Dr. Afzal Suleman, Supervisor
(Department of Mechanical Engineering)

Dr Curran Crawford, Departmental Member
(Department of Mechanical Engineering)

Dr. Pan Agathoklis, Outside Member
(Department of Electrical Engineering)

Supervisory Committee

Dr. Afzal Suleman, Supervisor
(Department of Mechanical Engineering)

Dr Curran Crawford, Departmental Member
(Department of Mechanical Engineering)

Dr. Pan Agathoklis, Outside Member
(Department of Electrical Engineering)

Abstract

The United States Air Force has specified a need for the next generation, High Altitude, Long Endurance aircraft capable of carrying advanced sensor arrays over very large distances and at extreme altitudes. These extensive set of requirements has required a radical shift away from the conventional wing & tube configurations with a new focus placed on extremely light weight and unconventional structural and aerodynamic configurations. One such example is the Boeing Joined wing SensorCraft Concept.

The Joined wing concept has potential structural and sensor carrying benefits, but along with these potential benefits come several challenges. One of the primary concerns is the aeroelastic response of the aft wing, with potential adverse behaviours such as flutter and highly nonlinear structural behaviour of the aft wing under gust conditions. While nonlinear computation models have been developed to predict these responses, there exists a lack of experimental ground and flight test data for this unique joined wing configuration with which to benchmark the analytical predictions. The goal of this work is to develop a 5m, scaled version of the Boeing Joined Wing configuration and collect data, through a series of ground and flight based tests, which will allow designers to better understand the unique structural response of the configuration.

A computational framework was developed that is capable of linearly scaling the aeroelastic response of the full scale aircraft and optimize a reduced scale aircraft to exhibit equivalent scaled behaviour. A series of reduced complexity models was developed to further investigate the flying characteristics of the configuration, test avionics and instrumentation systems and the develop flight control laws to adequately control the marginally

stable aircraft. Lessons learned were then applied the 5m flight test article that was designed and constructed by the author.

In the final stage of the project, the decision was made to relax the aeroelastically scaled constraint in order to allow additional softening of the structure to further investigate the nonlinear behaviour of the aircraft. Due to the added risk and complexity of flying this highly flexible aircraft the decision was made to produce the final aeroelastically scaled article at the 1.85m scale. This model was designed, developed and ground tested in the lead up to a follow on project which will see additional flight testing performed in conjunction with Boeing Inc.

Table of Contents

Supervisory Committee	ii
Abstract.....	iii
Table of Contents.....	v
List of Tables	viii
List of Figures.....	ix
Acknowledgments	xiv
Dedication.....	xvi
Chapter 1 - Introduction to the USAF SensorCraft Project	1
1.1 Introduction.....	2
1.2 Background and Motivation.....	3
1.3 Literature Review.....	4
1.3.1 Previous Studies into the Joined Wing Configuration	5
1.3.2 Previous Studies into Aeroelastic Scaling.....	8
1.3.3 Nonlinear Aeroelastic Analysis Methods.....	10
1.4 Summary of Proposed Work.....	11
1.5 Contributions.....	12
1.6 Collaborations	13
1.7 Layout of this Document.....	14
Chapter 2 - Feasibility Study and Scaling Framework	16
2.1 The Need for Feasibility Investigations	17
2.2 Scaling of Boeing Joined Wing SensorCraft.....	17
2.2.1 Choosing the Governing Physics	17
2.2.2 Non-dimensionalizing the Governing Equations	18
2.2.3 Scaling Factors.....	20
2.2.4 Scaling Methodology	23
2.3 Initial Test Point Feasibility Study.....	25
2.3.1 Structural Layout of Baseline Structure.....	25
2.3.2 Scaled Frequency and Mode Shape Matching	26
2.3.3 Results of Feasibility Study	28
2.4 Advanced Scaling Framework	29
2.4.1 Analysis Tools	29
2.5 Conclusions.....	37
Chapter 3 - Preliminary Configuration Design and Testing	39
3.1 Estimate of Scaled performance.....	40
3.1.1 Aerodynamic Prediction Using Vortex Lattice Methods	40
3.1.2 Aerodynamic Corrections Using Higher Order CFD.....	42
3.1.3 Stability Analysis	49
3.1.4 Proposed Modifications	50
3.2 Avionics and Control	55
3.2.1 Crow Mixing of Surfaces for Drag Rudder Effect.....	55
3.2.2 Split Surfaces for Drag Rudder Effect	56
3.2.3 Vertical Rudder in Boom.....	57
3.2.4 Aileron Differential and Trim Tabs	58
3.3 Reduced Scale Testing and Simulation.....	61
3.3.1 Simulation.....	61
3.3.1.1 6 Degree of Freedom Flight Simulation	61
3.3.2 Reduced Scale Flight Testing	64
3.5 Conclusions.....	72
Chapter 4 - 5m Configuration Evaluation and Testing	74
4.1 Design of 5m RPV	75
4.1.1 Structural Sizing.....	75

4.1.2	Design of Propulsion System.....	83
4.1.3	Landing Gear Design	86
4.1.4	Power Management.....	90
4.1.5	Avionics and Control	91
4.1.6	Camera Systems.....	93
4.1.7	Ground Control Station.....	95
4.2	Fabrication	101
4.2.1	Internals Fabrication	101
4.2.2	Tooling Fabrication.....	102
4.2.3	Composite Layups	104
4.2.4	Final Assembly	105
4.2.5	Part fabrication and Integration.....	108
4.3	Flight Test Planning	110
4.4	Ground Testing	111
4.4.1	Static Thrust Test	111
4.4.2	Bifilar Pendulum Test (BFPT).....	111
4.4.3	Static Load Testing	113
4.4.4	Landing Gear Drop Test	114
4.4.5	Range and Electro Magnetic Interference (EMI) Tests	115
4.4.6	Additional Testing	115
4.5	Reduced Complexity Flight Tests	116
4.6	Flight Testing	117
4.6.1	Flight Test Location	117
4.6.2	Flight Test	118
4.7	Post Flight Analysis	119
4.7.1	Mission Summary	119
4.7.2	Takeoff.....	120
4.7.3	Cruise Segment	122
4.7.4	Range and EMI	125
4.7.5	Landing Segment	125
4.7.6	Fuel Usage	126
4.7.7	Mission Duration	127
4.7.8	Roll Oscillations/Dutch Roll.....	128
4.8	Conclusions.....	131
Chapter 5 - Aeroelastically Scaled to Aeroelastically Tuned Demonstrator		133
5.1	Linearly Scaled 5m Aircraft Modifications.....	134
5.2	Investigation of Nonlinearities and Design Space Exploration.....	135
5.2.1	Low Fidelity Analysis.....	136
5.3	Aeroelastically Tuned SensorCraft RPV for Investigating Aft Wing Buckling	143
5.4	Aeroelastically Tuned “Mini” SensorCraft Configuration.....	145
5.5	Conclusions.....	146
Chapter 6 - Nonlinear Test Article Design, Testing and Tuning		148
6.1	Aeroelastically Tuned Mini SensorCraft Design	149
6.1.1	Redesign of Generation 1 Mini SensorCraft Configuration.....	149
6.1.2	Detailed Design of Aeroelastically Tailored Model	155
6.2	Fabrication	161
6.2.1	Structural components.....	161
6.2.2	Test Rigs and Instrumentation	161
6.2.3	As Built Data.....	161
6.3	Ground Test Planning	164
6.3.1	Static and Dynamic Load Testing	164
6.3.2	Load case 1a: Forward Wing Loading	165
6.3.3	Load Case 1b: Boom Loading	166

6.3.4	Load Case 1c: Dynamic Structural Response of Forward Wings	166
6.3.5	Load Case 2a: Forward Wing and Boom Loading of Assembled Configuration	167
6.3.6	Load Case 2b: Equivalent 3g Pull-up Flight Maneuver Clearance	167
6.3.7	Load Case 2c: Dynamic Structural Response of Aircraft	168
6.4	Ground Testing	168
6.4.1	Static Load Testing	168
6.4.2	Flightworthiness Checks	189
6.4.3	Modifications to Instrumentation System for Flight Based Measurements	193
6.4.4	Flight Clearance Load Testing	197
6.5	Flight Test Planning	198
6.5.1	Rigid Flights.....	198
6.5.2	Flexible Flights	199
6.6	Flight Testing	200
6.6.1	Generation 2 Rigid Flights.....	200
6.7	Aeroelastically Tuned Mini Flights.....	203
6.8	Conclusions	205
Chapter 7	- Conclusions and Future Work.....	206
7.1	Conclusions	207
7.2	Recommendations and Future Work.....	213
Literature Cited	214

List of Tables

Table 1 - Summary of Key Scaling Parameters	21
Table 2 - Key Geometric And Operational Values	21
Table 3 - Reference Quantities Used in Subsequent Analyses	41
Table 4 - Test Matrix for CFD Analysis	46
Table 5 - Dynamic Stability for Baseline Configuration	49
Table 6 - Dynamic Stability for Configuration with Addition of Vertical Surface	51
Table 7- Stability for Configuration with Addition of Conventional Tail Surfaces	52
Table 8 – Reduced Complexity Models Used in This Work	65
Table 9 – Summary of Bifilar Pendulum Test Results for the GSRPV	113
Table 10 – Summary of Mission Limits	120
Table 11 – Measured Roll Oscillations vs Calculated Dutch Roll Frequency	128
Table 12 - Control Surface Scheduling.....	152
Table 13 - Load Application Interface Details.....	173
Table 14 - Measured Straing GUI Details	176

List of Figures

Figure 1. Joined wing SensorCraft Concept ^[1]	2
Figure 2. SensorCraft Concepts (From Left to Right : Lockheed Martin, Northrup Grumman, Boeing).....	3
Figure 3 - Relative Scale of Boeing Baseline Aircraft, 5m Remotely Piloted Vehicle and 1.85m Mini SensorCraft	22
Figure 4 - Beam Elements and Point Masses Used to Model Internal Structure	25
Figure 5 - Element Geometry	27
Figure 6 - Output of Code that Compares the Displacements of Non-Conformal Meshes.....	32
Figure 7 - Optimization Loop Used to Match Scaled Modal Response.....	33
Figure 8 - Optimization Loop Used to Match Scaled Modal Response by Matching Stiffness and then Mass Distribution	34
Figure 9 - Graphical Process Flow of Benchmark Case	35
Figure 10 – Comparison of Baseline (Left) and Optimized Reduced Scale (Right) Modal Responses.....	36
Figure 11. Beam Model Used for Initial Scaling Study.....	37
Figure 12. Comparison of Baseline Modal Results (Points) and Results of Optimized Beam Model (Lines) ...	37
Figure 13 - Control Surface Locations and Naming	41
Figure 14 - Vortex Lattice Models of Baseline.....	42
Figure 15 – Boom Geometry Before (Left) and After (Right) Geometry Cleanup	44
Figure 16 - Computational Domain	44
Figure 17 - Surface Mesh of Baseline Configuration and Detail showing Inflated Boundary Layer	45
Figure 18 - Comparison of Aerodynamic Predictions (VLM & CFD) With Wind Tunnel Results	48
Figure 19 - Boeing SensorCraft in the Transonic Dynamics Tunnel at NASA Langley ^[28]	48
Figure 20 - Eigenvalues of Baseline Geometry	49
Figure 21 - Configuration with Vertical Tail Surface.....	50
Figure 22 – Configuration with Addition of Conventional Tail Surfaces.....	52
Figure 23 - Effect of Resolved Lift Increment on Aircraft Yaw.....	55
Figure 24 - Locations of Split Drag Rudders at Outboard Elevator (Top) and Outboard Flap (bottom) Stations	57
Figure 25 - Side View Showing Rudder Location	58
Figure 26 - Right Rolling Maneuver using Aileron Differential	59
Figure 27 - Flexible Drag Tab Used to Counteract Adverse Yaw	59
Figure 28 - Six Degree of Freedom Flight Simulator	62
Figure 29 - Screenshot from RealFlight G5 Simulator Used for Pilot Familiarization	63
Figure 30 - Flat Plate Foamie in flight during a flight test.....	66
Figure 31 - Twist Corrected Foamie	67

Figure 32 - Mini SensorCraft Construction	68
Figure 33 - Various Generation 1 Mini SensorCraft RPVs	69
Figure 34 - QT1.1 UAV.....	70
Figure 35 - Autonomous Catapult Takeoff Test	71
Figure 36 - Wing Cross Section Showing Structure Makeup of Wings	75
Figure 37 - Internal Aircraft Structure.....	76
Figure 38 – Internal and External View of High Fidelity FE Mesh.....	77
Figure 39 - Sample Test Coupons (Left) Undergoing Tensile Testing (Right)	78
Figure 40 - Location of Trimming Weight Bays (1 in fuselage, 2 in wings, 3 in tail and 4 in nose).....	79
Figure 41 - Fuselage Layup	80
Figure 42 - Foreword Wing Layup	81
Figure 43 - Aft Wing Layup	82
Figure 44 - Boom Layup.....	82
Figure 45 - Cutaway of Propulsion System Viewed from Side	84
Figure 46 - Exhaust Outlet Showing Custom Double Walled Thrust Tube (Left) and Stainless Steel Flashing on Structure to Prevent Heat Damage to Structure (Right).....	84
Figure 47 - Fuel Cell Used in 5m Rigid Aircraft	86
Figure 48 - Tricycle Landing Gear Layout and Custom OLEO Strut.....	87
Figure 49 -Gear Sizing of the Geometrically Scaled RPV for Aft and Foremost CG Location	88
Figure 50 - Mini SensorCraft Used to Evaluate Proposed Landing Gear Geometry	88
Figure 51 - Finite Element Analysis of Landing Gear.....	89
Figure 52 - Avionics Bay showing Battery Compartment, Switch Banks, Pneumatic Fill Valves and Pressure Readouts	91
Figure 53 - Piccolo II/ RxMUX System Concept	93
Figure 54 - In Flight View from FPV Camera On Vertical Boom	94
Figure 55 - Video Diversity Switch Used at Ground Station.....	95
Figure 56 - Initial Mobile Command Center: Computer Station (top and lower right), Interior of Custom Trailer (Lower Left) and Deployed Setup (Lower Right).....	96
Figure 57 – Interior Side View (Left) and Exterior Top View (Right) of Mobile Command Unit	97
Figure 58 - Aft Compartment from Inside Main Compartment.....	98
Figure 59 - Aft Compartment from Rear Doors	98
Figure 60 – Main Compartment Showing Three Primary Workstations	99
Figure 61 – Exterior View with Antenna Mast Deployed (Left) and at Night (Right).....	100
Figure 62 - Exploded View Showing Interlocking Bulkheads	101
Figure 63 - Internal Structure of Rigid RPV Fuselage.....	102
Figure 64 - Mold Fabrication Process.....	103

Figure 65 - Male Plugs Used for Producing Air Intake Skins (left) and Outlet Skins (Right)	103
Figure 66 - Laying Up Bottom Fuselage Skin	104
Figure 67 - Conformal Fuselage Access Door.....	105
Figure 68 - Procedure used to Bond Internal Structure and Skins	106
Figure 69 - Assembly of Wing Structure	107
Figure 70 - Assembly of the Aircraft Using Custom Jig	108
Figure 71 - Some of The Custom Components Fabricated (Forward Wing Shown).....	109
Figure 72 - Paint Scheme Chosen for Aircraft Rigid RPV (Left) and Actual Aircraft After Paint (Right).....	109
Figure 73 - Installed Static Thrust Test Rig.....	111
Figure 74 - Author in Front of BFPT about Pitch Axis	112
Figure 75 - Static Loading of Aircraft	113
Figure 76 - Improved Static Loading Rig Showing Loading of Front Wings	114
Figure 77 - Landing Gear at Impact (Left); Landing Gear after Test (Right).....	115
Figure 78 - Mini SensorCraft fleet (left); Mini SensorCraft in flight	116
Figure 79 - Aerial Photo of Foremost Airstrip (left), Approved Airspace (right).....	117
Figure 80 - GSRPV Flight from Ground Perspective (Left); Tail Boom Camera Perspective (Right)	118
Figure 81 - GSRPV on Final Approach.....	119
Figure 82 - Aircraft GPS Position (Left); Altitude Profile for Flight (Right).....	120
Figure 83 - Airspeed and Throttle During Takeoff Run	121
Figure 84 - Aircraft Roll Immediately After Takeoff	121
Figure 85 - Points Chosen to Investigate CL and CD.....	122
Figure 86 - Comparison of Calculated Polars vs Flight Test Data.....	123
Figure 87 - Aileron Travel Throughout Flight.....	124
Figure 88 - z-Acceleration throughout Flight	124
Figure 89 - Acknowledgement Ratio Along Flight Path	125
Figure 90 - Fuel Burn Over Mission.....	127
Figure 91 - Sample of Mini SensorCraft Flight Data Showing Roll Oscillations.....	129
Figure 92 - PSD Analysis of Mini SensorCraft Roll Angle Showing Roll Oscillation Freq.	129
Figure 93 - Simulated Open Loop Response of GSJWSC to Chirped Bank Command (0.384 Hz).....	130
Figure 94 - Simulation of Roll Response to Chirped Bank Command (Gains From Flight Tests)	130
Figure 95 – Internal and External View of High Fidelity FE Mesh.....	134
Figure 96 - Beam Locations shown in Blue (Left) and visualization of their Cross Sections (Right).....	136
Figure 97 - DOFs used as Design Variables in Parametric Studies.....	137
Figure 98 - Generic Beam Cross Section Showing Three Variables used to tune Stiffness	137
Figure 99 - Framework Used to Match Experimental Results and Investigate Nonlinearities of Joined Wing	139
Figure 100 - Load Cases used in Tuning Baseline Beam Model.....	140

Figure 101 – Nonlinearity Sensitivities Due To Joint Stiffness’s (parameters with little to no effect are not shown)	140
Figure 102 - Sensitivity to Structural Member Stiffness (parameters with little to no effect are not shown)...	141
Figure 103 - Effect of Joints on Nonlinear Response (parameters with little to no effect are not shown)	142
Figure 104 - Effect of Running Stiffness on Nonlinear Response (parameters with little to no effect are not shown).....	142
Figure 105 - Part of Design Space Showing Different Nonlinear Responses.....	143
Figure 106 - Structural Layout of Structural Model Used in Aeroelastic Framework.....	145
Figure 107 – Updated Internal Layout of Generation 2 Minis.....	150
Figure 108 - Updated Elevator Servo Locations and Control Rods.....	150
Figure 109 - Custom Bracket used to Mount GoPro and Adjust CG.....	151
Figure 110 - RF Transparent Portions of Mini Structure (Shown Transparent)	152
Figure 111 – Control Surface Layout	153
Figure 112 - Close-up of Right Elevator Showing Constrained Degrees of Freedom.....	154
Figure 113 - Main Components of Compliant Structure	155
Figure 114 - Forward and Aft Wing Internals (Left and Right Respectively).....	156
Figure 115 - Aerodynamic Shells Employing Single Line of Attachment Ensuring No Load Transfer to Skins	157
Figure 116 - Hinge Sealing Tape Showing Adhesive Along One Edge Only	158
Figure 117 - Gap Sealing Techniques (Left shows Flexible Tape and Right Showing Lap Joint Using Hinge Tape).....	158
Figure 118 - Strain Gauge (Red) and Accelerometer (Green) Spanwise Locations (Mirrored on Left Side of AC)	159
Figure 119 - Camera Field of View for Capturing Aft Wing Structural Response in Flight.....	160
Figure 120 - As Built Mass Properties of Aeroelastically Tuned Aircraft.....	163
Figure 121 - Hard Point Locations Used for Load Application (Mirrored on LHS)	165
Figure 122 - Line of Contact Between Aircraft and Test Fixture	165
Figure 123 - Load Case 1a Loading.....	166
Figure 124 - Load Case 1b Load Applied to Boom.....	166
Figure 125 - Load Case 2a Loading.....	167
Figure 126 - Load Case 2b Loading	168
Figure 127 - Static Loading Test Setup	169
Figure 128 - Aircraft/Jig Contact.....	170
Figure 129 – Phidget® Load Cell And 1046 Data Acquisition Board	171
Figure 130 - Load Application Interface.....	172
Figure 131 - Half Bridge CCT Used to Measure Bending Strain.....	174

Figure 132 - Custom Bridge Completion Circuit Used for Strain Based Ground Testing Measurements	174
Figure 133 - Custom Interface for Calculating, Filtering and Displaying Measured Strain	176
Figure 134 - Top View Showing Optical Targets	177
Figure 135 - Photomodeler Interface Showing Deformed and Unreformed Geometry	178
Figure 136 - 3-Axis Accelerometer on Aft Wing	179
Figure 137 - Load Case Summary	180
Figure 138 - Cantilever Wing and Boom Test Results vs Baseline FE Model	180
Figure 139 - Comparison of Measured Strains with Those Predicted by Baseline FE Model	181
Figure 140 – Spectral Response of Cantilever Wing (Blue) vs Predicted (Red)	182
Figure 141 – FE model of SensorCraft Configuration Showing Updated Taped Beam Inboard Wing Sections	183
Figure 142 - Modifications To Baseline Nastran Model to Capture as Tested Configuration (Baseline on Left, Updated Right)	184
Figure 143 - Discreet Bending Moment Distribution Due to Ladder Shaped Aft Spar	184
Figure 144 - Modified Material Properties Used in Subsequent Optimization (Baseline on Left, Updated Right)	185
Figure 145 - ModelCenter Process Used to Tune Baseline Model	185
Figure 146 – Locations Used to Measure Structural Displacements	186
Figure 147 - Strain and Displacement Results of Baseline FEM Configuration	187
Figure 148 - Pareto Front Showing Optimal Designs in Terms of Minimized Displacement and Strain RMS Errors	188
Figure 149 - Strain and Displacement Results of Optimized FEM Configuration	188
Figure 150 - Testing Process Flow	190
Figure 151 - Bifilar Pendulum Test in Pitch Axis	191
Figure 152 - Calculation of Launch Speeds and Trajectories in Preparation For Flight Testing	193
Figure 153 - Hardware Architecture for Capturing Strain Data In-Flight	194
Figure 154 - Custom Designed Printed Circuit Board for Remote Strain Readings	195
Figure 155 - Data Logger Output, 18-Hour Test	196
Figure 156 - Pilot Station Heads Up Display	197
Figure 157 - Flight Testing of Generation 2 Mini	201
Figure 158 - Z-acceleration Due To Pilot Induced Doublet Maneuver	202
Figure 159- Z-acceleration Due To Auto-Pilot Induced Doublet Maneuver	203

Acknowledgments

I would like to acknowledge all of the individuals who assisted and supported me during the execution of my Dissertation. Developing and operating an aircraft of this complexity is a very large undertaking and would not have been possible without their support. In particular, I would like to acknowledge my thesis supervisor, Professor Afzal Suleman. From the outset of this project, Dr. Suleman has provided guidance, technical and logistic support for the successful completion of this thesis and has shown me a great deal of respect and trust, giving me the freedom that very few students are ever afforded.

I would like to acknowledge our collaborators Dr. Robert Canfield, Tyler Aarons and Anthony Ricciardi from Virginia Tech for the very useful discussions, insights and contributions to resolving the complex design issues related to the SensorCraft configuration. A special thanks goes to Jeffery Garnand Royo who was instrumental throughout the project and who has since become a great friend. The project was supported by the Air Force Research Laboratories at Wright Patterson Air Force Base in the U.S.A. and the technical feedback provided by Max Bair, Ned Lindsley and Ray Kolonay are kindly acknowledged. I would also like to acknowledge the assistance of Jon Harwood who provided me technical guidance in the areas of composites design and fabrication and was always willing to help the project succeed. The partnership with Camosun College prototyping centre was an important aspect during the development and manufacturing of the 5m flight model. The pilot Kelly Williams was also instrumental to the flight operations, offering hundreds of volunteer hours and providing expert knowledge and piloting the aircraft on many flight test campaigns. Throughout the process a number of Co-op and visiting students were always keen to lend a hand and help with the nitty gritty details. They included Willem Brussow, Ryan Flagg, Shayan Rahimi, Peter Lu, Kurt Fairfield and Andre Coelho.

Finally, I would like to thank my Fiancé, Newsha, who has always supported me and encouraged me to keep pursuing my passions. She has been a constant in a period of my life that has had so many unknowns. Thank you everyone for your help!

Dedication

I would like to dedicate this work to my parents, Linda and Donald Richards, who have always been my greatest supporters. They have given me the confidence to take on any project while teaching me the discipline to see it through to completion.

Chapter 1 - Introduction to the USAF SensorCraft Project



1.1 Introduction

High Altitude, Long Endurance (HALE) unmanned aerial vehicles (UAVs) are capable of providing revolutionary intelligence, surveillance and reconnaissance (ISR) capabilities over vast geographic areas when equipped with advanced sensor packages. The benefit of these platforms is becoming more apparent with their recent use in military roles, as well as their increasing adoption for civilian applications. As their use becomes more widespread, the demand for additional range, endurance and capability has increased and designers are now looking towards non-conventional configurations to meet the increasing demands.

One such configuration is the joined-wing concept. A joined-wing aircraft is one that typically connects a front and aft wings in a diamond like planform. One such example is the Boeing Joined Wing concept, pictured in Figure 1 below. Boeing's concept is a proposed solution to the United States Air Force Research Laboratory's (AFRL) SensorCraft Request for Proposals.

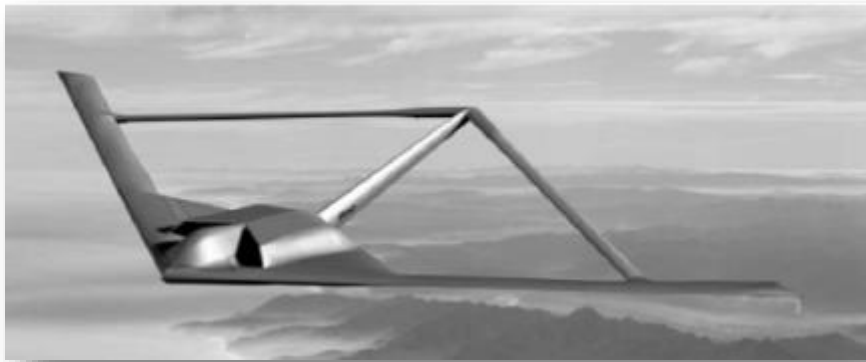


FIGURE 1. JOINED WING SENSORCRAFT CONCEPT^[1]

While the Joined Wing Sensor Craft (JWSC) configuration offers potential benefits with regard to aerodynamic efficiency, airframe weight, and sensing capability, structural design is governed by the unique issue of elastic (buckling) stability resulting from the aft wing supporting, in compression, part of the forward wing structural loading. It has been shown already that this is a highly nonlinear phenomenon, involving geometric nonlinearities and follower forces that tend to flatten the entire configuration, leading to structural overload

due to the loss of the aft wings' ability to react forward wing load. Severe gust encounter is likely to be the critical design condition, with flight control system interaction in the form of Gust Load Alleviation (GLA) playing a key role in minimizing the structural loads [2].

Previous work has been focused on investigating the non-linear response computationally and some scale models have been developed and investigated in wind tunnels. However, no flight test data exists for a HALE joined wing configuration which exhibit these non-linearities and the AFRL has identified a requirement for "independent analysis of a configuration that demonstrates significant structural and aerodynamic nonlinearities that AFRL can utilize for validation and benefit demonstration of the AFRL MDICE-based suite of analysis tools". The subject of this PhD work is the analysis, design, manufacture, instrumentation, testing and parameter identification of a 1/9th scale flight test vehicle based on the Boeing Joined Wing SensorCraft concept (*Boeing 410-E8 Configuration*).

1.2 Background and Motivation

The United States Air Force Research Laboratory is presently investigating the requirements of the next generation HALE ISR platform. One such set of requirements has been conceived and is the basis of the SensorCraft program. Several companies have developed SensorCraft Concepts including Boeing, Lockheed Martin and Northrop Grumman. Figure 2 shows three of the candidate designs.



FIGURE 2. SENSORCRAFT CONCEPTS (FROM LEFT TO RIGHT: LOCKHEED MARTIN, NORTHRUP GRUMMAN, BOEING)

Traditional aircraft design typically begins with the development of the airframe first and then a selection of sensors are chosen to integrate into that platform. With the SensorCraft project however, this process is reversed and an aircraft platform is specifically designed around an optimized collection of sensors. This, along

with the increased requirements in terms of endurance and range, has resulted in a departure from conventional configurations as is apparent with the Boeing Joined Wing Concept.

The joined-wing configuration offers many potential benefits over conventional aircraft designs. Foremost is the ability to incorporate conformal radar antennae in the fore and aft wings to provide persistent 360 degree, foliage penetrating surveillance ^[3]. Among other potential benefits are reduced induced drag, a stiffer and potentially lighter wing structure, and direct lift/side force control. These benefits do come at a cost however. Previous computational studies of joined-wing aircraft configurations have shown the importance of geometric nonlinearity due to large deflections and follower forces that may lead to buckling of the aft wing ^[2] This potential buckling represents a unique and challenging aeroelastic design problem. The non-linear behavior, which is a result of the joined wing configuration and advanced, lightweight structural design, could be removed by strengthening the wing to a point where these non-linear behaviors vanish; however, this would result in large penalties in aspect ratio and structural weight, greatly reducing the performance of the aircraft. To avoid these penalties, nonlinear aeroelastic design, analysis and testing are required to ensure that the Joined Wing SensorCraft is able to sustain the nonlinear responses required to complete the proposed ISR mission.

A scaled RPV provides a low cost and effective way to investigate these non-linear aeroelastic responses and to validate/tune existing computational models. The RPV developed in this work has also serves as a useful test bed for investigating additional technologies such as redundant control surface scheduling and stability/control methods for highly flexible structures. The platform may also be implemented in later work for aspects such as stick to stress investigation and gust load alleviation schemes.

1.3 Literature Review

There have been many studies on the joined-wing concept, aeroelastic model scaling, optimizing for nonlinear response and using wing twist for aircraft control. Some of these studies were completed externally and some

local to the AFRL and Air Force Institute of Technology (AFIT). This section provides a review of past studies and frames their role in relation to the present course of investigation.

1.3.1 Previous Studies into the Joined Wing Configuration

The joined-wing concept has been proposed in a series of patents by Wolkovitch in the 1970s, and a subsequent overview was published 1986^[4]. His arguments for this new configuration were several potential advantages over conventional aircraft:

1. Lighter weight and higher stiffness
2. Less induced drag
3. Reduced parasite, transonic and supersonic drag
4. Built-in direct lift and side force capability
5. Good stability and control in normal flight and at the stall

Wolkovitch also showed that the wing bending axis is tilted, with respect to the horizontal, because of the out-of-plane arrangement of the joined wing surfaces. This effect allows the unique benefit of concentrating material near upper leading edge and lower trailing edge to increase structural rigidity. (Referred to here as the Wolkovitch effect^[4]).

More detailed aerodynamic and structural studies by Kroo, Gallman and Smith^[5] have confirmed the Wolkovitch effect and defined some additional characteristics of joined-wing structures that are advantageous to the design. Further analysis by Kroo et al, of nonlinear finite element models, demonstrated aft-wing buckling with very large deflections. The findings pointed out a need to incorporate a nonlinear analysis methodologies early into the design phase of aircraft employing the joined wing configuration. These findings have also been demonstrated in work performed at the US Air Force Institute of Technology by Y.I. Kim et al^[6] as well as the need for multidisciplinary optimization.

The joined-wing configuration exhibits very flexible wings due to the high aspect ratio and optimal lift-to-drag (L/D) of the HALE aircraft design requirements. Since highly flexible wings experience large deflections, linear assumptions may no longer be valid. Thus, nonlinear analysis is essential both locally and globally. Traditional preliminary aircraft design investigates local nonlinearities like skin panel buckling. Due to the design requirements mentioned above, global nonlinearities, such as front or aft wing buckling are shown to be of concern^[7].

Previously, joined-wing designers have only considered nonlinear buckling response with respect to the design of the aft wing. Front wing buckling had been overlooked until the high-fidelity model and analysis of Blair, et al. "Because the wing bends up and forward, both the aft and front wings have the potential to buckle whenever compression is present". "The joined-wing configuration exhibited large geometric nonlinearity below the critical buckling eigenvalue. Thus, nonlinear analysis was required to model correctly this joined-wing configuration"^[8]. This study will attempt to confirm this experimentally to further the understanding of nonlinear response for unconventional designs

Smith and Kroo continued their research, along with Cliff, and built a demonstrator joined wing aircraft^[9]. The objectives were to demonstrate good handling qualities and validate the design methods used for the joined wing configuration. It was evaluated with wind tunnel tests in a 12-foot wind tunnel at 1/6 of the full-scale. The assessment of performance, stability and control confirmed that the tools used for design were suitable for a complicated configuration like a joined wing.

A survey of joined-wing configurations conducted by Livne explores the fact that the joined-wing concept is of significant interest to a number of disciplines^[10]. The joined-wing concept requires a multidisciplinary approach to effectively realize the analysis and design problem. The configuration requires an optimized design which takes advantage of the interactions between nonlinear structural behavior and aeroelastic response. Livne recognizes that there are significant aeroelastic scaling challenges for the joined-wing.

Typically, the aft wing of the joined-wing configuration braces the high-aspect-ratio forward wing. To take advantage of this structural redundancy, the joint must be designed to transfer the moment while resisting instabilities. These instabilities include divergence and flutter caused by excessive moment, shear and axial reaction loads at the joint ^[11]. Lin, et al investigated joint fixity influence on the stiffness and strength characteristics of a joined-wing. They found that the rigid joint was the best compromise for combined strength and stiffness benefits.

Once a promising configuration is designed, analytical aeroelastic analysis, and then experimental analysis of an aeroelastically scaled model must be accomplished to reduce the risk for full-scale production of this unique configuration. Two recent examples illustrate the detailed steps of these processes with aeroelastic characteristics in mind. The first entails the use a joined wing flight demonstrator designed in house at AFRL that had limited success (only one short flight before crashing), while the second focuses on scaling a joined-wing model for valid experimental analyses in a wind tunnel.

The AFRL study led by Blair et al ^[12] investigated the joined wing configuration using a flight test article, loosely based on Joined Wing SensorCraft geometry. A test article was built and flown unsuccessfully. The aircraft crashed on the second flight attempt however and no meaningful structural data resulted from these flights.

Additional studies internal to the AFRL were performed that investigated the linear and nonlinear effects of the joined wing configuration. Blair and Canfield stressed that two critical phenomena contribute to structural failure: Large deformation aerodynamics and geometrically nonlinear structures ^[13]. Blair, Canfield and Roberts then concluded that non-linear deformations were critical in the weight-optimized aluminum joined-wing structure ^[8]. Rasmussen, et al ^[14], continued this vein of research by automating the analyses and investigated various configurations, concluding that lightweight joined wing designs were possible but with the result being highly nonlinear.

Recent studies performed by Demasi et al ^{[15] [16] [17] [18]} pointed out the importance of nonlinear analysis in the design of the joined wing configuration as well as the snap buckling instability of a joined wing configuration.

They further concluded that factors such as the relative flexibility of the fore/aft wings, wing joint connectivity and anisotropy of the composites structures can all have a large effect on the nonlinear response.

1.3.2 Previous Studies into Aeroelastic Scaling

The early foundations of scaling methodology has its roots in dimensional analysis. Initial efforts in this field were summarized in Macagno's Historico-Critical Review of Dimensional Analysis^[19]. In this work, the history of dimensional analysis was examined from the first notions about dimensions in early civilizations, to the more complete methods of more modern times.

Later the well-known Pi Theorem was introduced. This was first proven by French mathematician J. Bertrand. The first application of the theorem in the general case became widely known due to the works of Raleigh. The formal generalization was presented by A. Vaschy in 1892,^[20] who demonstrated the concept on the classical pendulum theory using four primary quantities. Later, in 1914, Buckingham provided an updated proof and provided various additional examples. Finally, Bridgeman^[21] clarified and consolidated the developments and his work remains a classic reference in the areas of dimensional analysis and similitude.

Bisplinghoff et al^[22] presented the concept of applying scaling theory to aeroelastic applications in *Aeroelasticity* using classical analytical aerodynamic and structural formulations. There he introduced the derivation of scaling parameters to scale several fundamental phenomena such as static aeroelasticity, restrained and unrestrained flutter as well as dynamic stability. Aerodynamics were modelled using potential flow including compressibility and unsteady flow. The work also shows the fundamental importance of matching the scaled mass and stiffness distributions as well as aerodynamics. It also points out an important note that the reduced scale structure often does not and can not match that of the full scale article. Finally, the work also provided a series of chapters focused on the design, construction and testing of reduced scaled models.

Another source of scaling guidelines is presented in the AGARD Manual on Aeroelasticity ^[23] where some additional phenomena such as heat transfer and compressibility are addressed as well as additional notes on model construction and testing.

Further studies of aeroelastic systems were presented by Jennifer Heeg et al ^[24] in *Wind Tunnel to Atmospheric Mapping for Static Aeroelastic Scaling*. Here it was shown that a practical wind tunnel model can be designed and built such that multiple flight vehicle test conditions map to the wind tunnel envelope. This however requires a relaxation of scaling requirements present in the dynamic problem that are not critical to the static aeroelastic problem.

French used optimization, combined with finite element modeling, to design an aeroelastically (static) scaled model. The optimization process sought to match the scaled displacements through the constraining of the flexibility matrix, while minimizing the structural weight. These results were then validated using physical load test results. French and Eastep ^[25] modified the methodology presented in Ref. ^[26] to include scaling for dynamic aeroelasticity. The stiffness of a low aspect ratio wind tunnel model was designed to match the stiffness of a target model. The optimization minimized the structural weight while satisfying displacement matching constraints (by constraining a common flexibility matrix). Physical static load tests validated the analysis and optimization. . A two-step optimization procedure was used. First, the wing structure was designed to minimize the differences in scaled static deflections between the design and target model. Then, assuming the stiffness design was complete and accurate, nonstructural masses were designed by constraining the reduced modal frequencies to match while minimizing the differences in mode shapes. Total non-dimensional masses were also constrained to match. The technique was used to design a low aspect ratio wind tunnel model.

Starting in the late 1990's, Friedmann, Presente, and others ^{[27] [28] [29] [30] [31]} published a series of papers on active flutter suppression of a two-dimensional wing section and associated scaling laws for incompressible and compressible flow. Friedman and Peretz ^[32] continued the scaling work while applying modern

computational methods and showed that the methods applied previously to fixed wing aircraft can also be applied to rotary wing configurations.

Pereira, et al ^[33] ^[34] investigated two potential methods of scaling in the design of a wind tunnel model of a fore/aft wing assembly. The first proposed method was to scale using the natural frequencies (assuming that the reduced frequencies would match since the aerodynamic effects were neglected). The second was to match the scaled natural frequencies and reduced flutter. The culmination of this effort was the fabrication of the aeroelastically scaled wing set that was tested in an open section wind tunnel at the Portuguese Air Force Academy.

Bond et al later showed that matching scaled natural frequencies alone is not sufficient for producing an accurately scaled model. She proved this by optimizing two cantilever wing structures with matching natural frequencies but very different mode shapes and aeroelastic responses. She then proceeded to achieve better results through matching the first three natural frequencies, first three mode shapes and the first buckling eigenvalue (in an attempt to capture the nonlinear behavior). The resulting scaled structure exhibited good aeroelastic matching throughout the velocity profile. The nonlinear results were less accurate with the buckling mode of the scaled aircraft matching to within 60% of the predicted full scale buckling load.

Wan and Cesnik's scaling investigations sought to derive scaling laws for transient aeroelasticity that also included nonlinear stiffness ^[35] ^[36]. During this work the validity of neglecting the Froude number in the scaling process was investigated using two scaled, highly flexible flying wing aircraft. One aircraft considered Froude number matching while the other did not. Extensive verification was carried out and the conclusion was that the Froude number played an important role in the scaling and should not be neglected.

1.3.3 Nonlinear Aeroelastic Analysis Methods

Throughout this work there is a requirement to analytically predict the static aeroelastic response of the flight test articles. Several commercial codes such as ZAERO ^[37] and MSC NASTRAN ^[38] have been shown to reliably

couple high fidelity linear FE structural analysis with linear aerodynamics to analyze linear aeroelastic trim but these codes do not account for the large structural nonlinearities seen in the SensorCraft Configuration.

However, several research codes have been developed that directly couple nonlinear beam element structural models with linear aerodynamics models. The NATASHA code was developed by Patil and Hodges^[39] based on Peter et al's previous work on air loads and inflow formulations^{[40] [41]} as well as Hodges geometrically exact intrinsic beam formulations^{[42] [43]}.

Ricci et al^{[44] [45]} developed the Next Generation, Conceptual Aero Structural Sizing, or NeoCASS, framework which couples a nonlinear beam formulation with aerodynamics models of varying fidelity. Drela developed the ASWING software code^{[46] [47] [48]} for the aerodynamic, structural, and control-response analysis of aircraft with flexible wings and fuselages of high to moderate aspect ratio. It employs unsteady lifting line aerodynamics and a structural formulation based on geometrically nonlinear isotropic beam analysis.

Cesnik and Brown^{[36] [49] [50]} use strain based structural analysis along with the inflow aerodynamics in the development of the University of Michigan Nonlinear Aeroelastic Simulation Toolbox (UM/NAST) package which they used as their basis in the development of a highly flexible aircraft flown to validate the code^[51].

Ricciardi^[52] developed a computation framework as part of the current SensorCraft investigation. His framework employs vortex lattice aerodynamics as well as a beam formulation that is capable of calculating sensitivities, aerodynamic response and nonlinear aeroelastic trim. Perhaps of greatest importance, the code overcomes a lot of the deficiencies the research codes described here (lower order structural formulations) through the inclusion of higher fidelity FE models through the integration with NASTRAN solvers.

1.4 Summary of Proposed Work

The purpose of the proposed work is to develop a set of flight and ground test data characterizing the nonlinear structural response of a 1/9th scale SC concept. The complexity of the JW configuration and related systems requires a systematic approach to understand the various design issues. To this end, a family of flight

test demonstrators of increasing complexity were designed, fabricated and tested. The project is unique in its overall scope as it includes many aspects of aircraft design, analysis, fabrication, instrumentation, testing and analysis.

Efforts will be focused on developing a computational framework to investigate and develop methods for aeroelastically scaling full scale behaviors to that of the reduced scale article and test point. An investigation into the primary non-linear behaviors of the configuration, and their response to primary design variables, will serve as design support for future efforts. While aeroelastic scaling is applied more regularly to wind tunnel models, the scaling of flight test articles is done very rarely due to the challenges of balancing the conflicting constraints of the scaling process and those required for flight worthiness.

Developing these flight test articles in-house requires a huge amount of initial setup and overhead. An additional benefit of this work are the facilities, best practices and knowledgebase that are required to design, fabricate and test unmanned aircraft. At the outset of this work the University of Victoria had no capabilities for fabrication and operation of unmanned systems. However, as a result of this work (and the vision and dedication of Professor Afzal Suleman), the University of Victoria Center for Aerospace Research was opened in summer of 2012 and is now a hub for UAV design in Western Canada.

1.5 Contributions

The contributions resulting from the thesis are in the area of airworthiness investigation, aeroelastic modeling, performance evaluation and structural characterization of a novel Joined-Wing (JW) aircraft configuration. The JW design has been studied at length but no data exists that quantifies the highly non-linear response of a weight optimized vehicle in flight. The purpose is to provide data and independent analysis of a configuration that demonstrates significant structural and aerodynamic nonlinearities that AFRL, and the aerospace community as a whole, can utilize for validation of existing analysis and design tools and methodologies.

The main contributions of the present thesis are as follows:

- An in-depth literature review of the JW configuration including geometric non-linearity. Also, a review on current aeroelastic scaling methodologies is presented.
- Develop and implement two aeroelastic scaling methodologies and investigate the suitability of several optimization methods using simple test cases.
- Investigate and characterize the stability and control of the JSWC concept in flight. Develop and evaluate a control scheme capable of controlling a marginally stable, highly flexible aircraft configuration, while also providing the potential for gust load alleviation and/or redundant flight control. It is noted that the JW configuration does not have a vertical stabilizer. This requires a more complex flight control system based on gain-scheduling of the longitudinal control surfaces.
- Investigate the JWSC structural response, including sensitivities to geometric variables common to the joined wing configuration, and compare to experimental results of both an extensive ground based static loading regime as well as to responses measured in flight.
- Provide project transitional guidance for follow up programs at the AFRL as well as serve as a resource to other programs developing flight test programs.

1.6 Collaborations

The scope of this project requires the collaboration between several entities, with the project being divided between three main groups. Project guidance and support is provided by the US AFRL with Ned Lindsley acting as the point of contact, along with the assistance of Peter Flick and Maxwell Blair. Instrumentation and detailed flight test planning is led by Virginia Polytechnic Institute and State University (Virginia Tech or VT). In addition, technical guidance was supplied by Dr R Canfield at Virginia Tech and several VT students were instrumental in assisting in flight test operations. The student involved in the initial phases was Tyler Aarons, who was aided by then research assistant, Jeffery Garnand-Royo. Upon completion of the initial flight tests Tyler Aarons graduated leaving Jeffery in charge of instrumentation and flight test planning for the subsequent Aeroelastically Tailored phase of the project. Jeffery also offered a great deal of assistance in flight test

operations. Later in the project, when the decision was made to develop the flexible Joined Wing aircraft to specifically investigate Non-linear structural response, Virginia Tech student Anthony Ricciardi played an instrumental role in the development of a framework for investigating non-linear aeroelastic behavior.

The University of Victoria was responsible for the design, fabrication and flight testing of the test articles. The PhD candidate is the principle investigator and was responsible for all efforts performed at UVic. Throughout this work several undergraduate students have assisted with work ranging from fabrication to piloting the flight test aircraft. More specifically, the following undergraduate students have performed the following tasks: Ryan Flagg (assisted in procurement and acquisition of parts), Willem Brussow (assisted with composite manufacturing), Peter Lu & Kurt Fairfield (flight test support) and Shayan Rahimi (assisted with instrumentation) who all worked at some point on this project. These students were instrumental in the success of this project.

Camosun College also assisted in some areas of the manufacturing. This included the rapid prototyping of several aircraft components as well as the machining of the larger molds using their 5-axis CNC center. Harwood Custom Composites also assisted by providing design guidance and composites manufacturing advice when called upon. HCC also fabricated 3 of the 9 Mini SensorCraft used in the project.

1.7 Layout of this Document

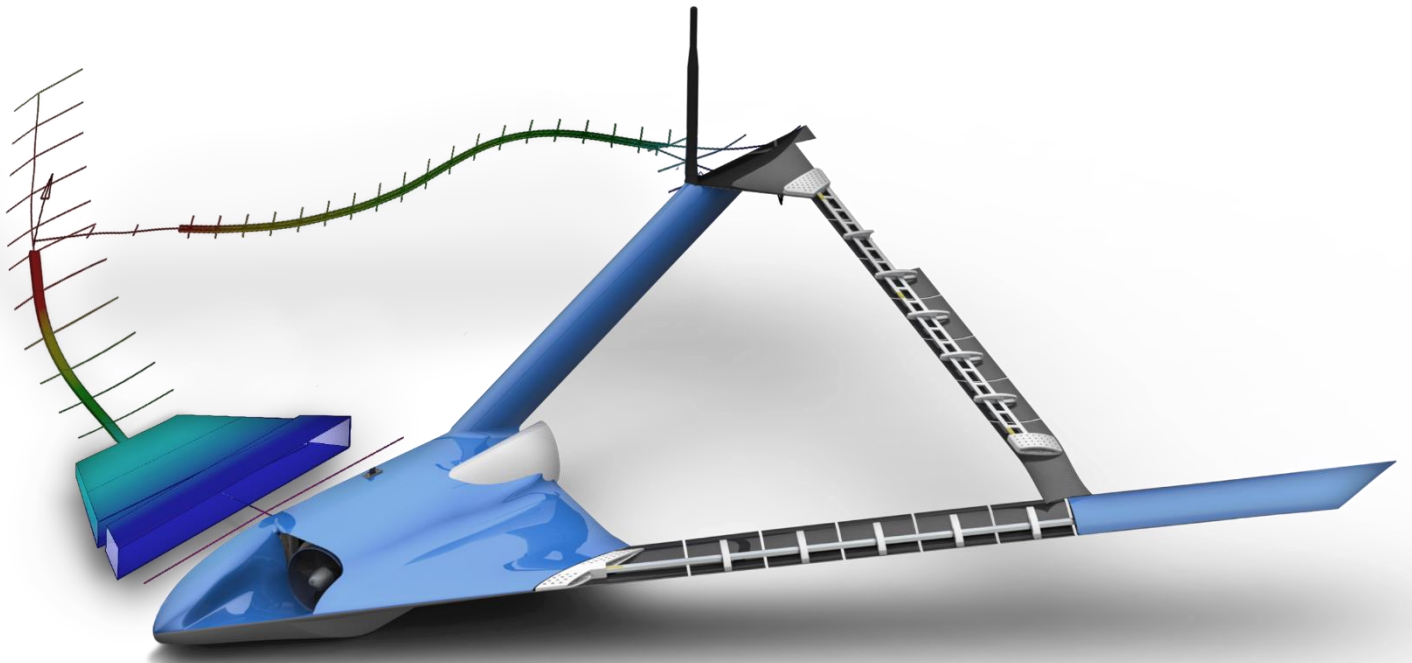
The layout of this dissertation is primarily chronological, as it happened throughout the project's lifespan. Some small reorganization was required to preserve the flow, especially in cases where work was performed in parallel. The first section describes the initial phase of the project which sought to determine if the chosen scale and test point location used to evaluate this configuration was feasible. It also outlines some of the preliminary scaling efforts, as well as an initial computation framework developed for performing geometry based, aeroelastic scaling.

The next chapter details the preliminary analysis of the SensorCraft configuration. This includes preliminary work to determine the stability and control characteristics of the aircraft as well as stability augmentation methods. The chapter also outlines some of the reduced scale testing (which was actually carried out for the entire duration of this work) using a series of reduced complexity models.

Next, the 5m span, Geometrically Scaled RPV is introduced. The detailed design and construction is discussed as well as a series of ground tests and flight test planning that was performed in preparation for initial flight testing. The chapter finishes by describing the initial flight test campaign and some of the conclusions drawn after analysis of the flight test data.

At a certain point a decision was made to focus exclusively on the nonlinear response of the aircraft, rather than the linear aeroelastic behavior, as initially intended. Chapter 5 presents some of the work performed to investigate the non-linear behavior of the configuration and sensitivities to the primary structural components of the aircraft. The chapter concludes by presenting the Flexible Mini SensorCraft configuration, the aircraft chosen for evaluating nonlinear behavior in flight. Finally, the design, development and testing of the Flexible Mini is presented, including fabrication, instrumentation, ground testing and flight test planning.

Chapter 2 - Feasibility Study and Scaling Framework



2.1 The Need for Feasibility Investigations

The Boeing Joined Wing SensorCraft Concept has a wing span roughly equivalent to a Boeing 737 jet liner. In order to better understand the physics of this concept, without building an expensive full scale demonstrator, a reduced scale model must be designed. However, scaling the physics of such a complex system goes far beyond merely scaling down the size. Limits are imposed by parameters the designer has little or no freedom to change, such as air properties and gravitational accelerations. This constrains the ability to scale the physics of the aircraft and some compromises must be made. In some cases these compromises are too great and as a result the physics are not adequately captured at the reduced scale. In other cases, the resulting design is rendered infeasible (for instance, the aircraft may be impossible to manufacture using existing methods or may require material properties that cannot be achieved). For these reasons, a feasibility study was performed to evaluate the proposed test point and chosen scale of the 5m Remotely Piloted Vehicle (RPV). This section outlines the methodology used and the conclusions drawn from these initial investigations.

2.2 Scaling of Boeing Joined Wing SensorCraft

This section outlines the methodology chosen to scale the aircraft physics. The chosen set of governing equations is introduced, non dimensionalized and reduced to yield a set of scaling parameters.

2.2.1 Choosing the Governing Physics

Aeroelastically scaled models are constrained by a set of scaling parameters, used to map the full scale test point, stiffness, mass and geometry to the reduced scale test point. These scaling parameters are derived from a chosen set of governing equations. Due to the limited time and resources, some assumptions are applied to simplify the scaling process. In the present case, a simplified physics model is chosen: the small disturbance, linear potential partial differential equations (PDE).

The choice of scaling, based on the linear PDE equations above, allows the elimination of several constraints that would otherwise be present if a more complex procedure was chosen (i.e. one based on the Navier-Stokes

equations). For instance, the equations are based on thin airfoil theory which allows an arbitrary airfoil thickness to be assigned, assuming the mean camber line is maintained. Also, if inviscid incompressible flow is assumed, the equations of motion (EOM) will not constrain the Mach number or Reynolds number.

$$[M]\{\ddot{x}\} + [k]\{x\} = [A_k]\{x\} + [A_c]\{\dot{x}\} + [A_m]\{\ddot{x}\} + [M]\{a_g\} \quad (1)$$

Where:

$\{x\}$ *Vector of elastic degrees of freedom*

$[M]$ *Mass matrix of system*

$[K]$ *Stiffness Matrix*

$[A_i]$ *Aerodynamic Terms*

$\{a_g\}$ *Vector of Gravitational terms for the corresponding dof*

While limited, these physics are adequate for a low-cost exploration of flight mechanics. When the EOM describing this system are non-dimensionalized, they yield a set of parameters that are used for scaling the baseline aircraft.

2.2.2 Non-dimensionalizing the Governing Equations

When the above equations are written in non-dimensional form, three non-dimensional parameters appear:

reduced frequency $\kappa_1 = \frac{\omega_1 b}{V}$, an inertia ratio $\mu_1 = \frac{\rho S b^3}{m}$ and the Froude number $Fr = \frac{V}{\sqrt{bg}}$ as seen in the

following equation ^[52].

$$\langle \bar{\mathbf{m}} \rangle \{\ddot{\eta}\} + \langle \bar{\mathbf{m}} \bar{\omega}^2 \rangle \{\eta\} = \frac{1}{2} \frac{\mu_1}{\kappa_1^2} \left([\bar{\mathbf{a}}_k] \{\eta\} + \kappa_1 [\bar{\mathbf{a}}_c] \{\dot{\eta}\} + \kappa_1^2 [\bar{\mathbf{a}}_m] \{\ddot{\eta}\} \right) + \frac{1}{Fr^2 \kappa_1^2} \langle \bar{\mathbf{m}} \rangle [\Phi]^T \{\bar{\mathbf{a}}_g\} \quad (2)$$

where:

η = vector of modal coordinates

$\ddot{\eta}$ = second derivative of η wrt non dimensional time

$\dot{\eta}$ = first derivative of η wrt time

$\langle \bar{\mathbf{m}} \rangle$ = Diagonalized nondimensional mass

$\langle \bar{\mathbf{m}} \bar{\omega}^2 \rangle$ = Diagonalized nondimensional stiffness

μ_1 = inertia ratio between atmospheric and structural mass

κ_1 = first reduced frequency

$[\bar{\mathbf{a}}_i]$ = nondimensional aerodynamic influence coefficients

$\{\bar{\mathbf{a}}_g\}$ = nondimensional gravity vector

From this equation we can see that, in order for the reduced scale model to have an equivalent linear aeroelastic and flight dynamic response to the full scale, the following conditions must be met.

1. External Aerodynamics, A_i
2. Reduced Frequency, κ_1
3. Froude Number, F_R
4. Atmospheric to structural Inertia ratio, μ_{ij}
5. Nondimensional Modal Mass, $\langle \bar{\mathbf{m}} \rangle$
6. Nondimensional Mode Shapes and Frequencies, $[\Phi]$ & $\langle \bar{\omega} \rangle$
7. Optionally Reynolds and Mach Number depending on fidelity of Physics chosen, R_e & Mach

Here the external aerodynamics are assumed to be equivalent since the outer mold line (OML) of the configuration is preserved. The modal mass and stiffness are matched through optimization of the reduced scale structure to match the modal response of the full scale aircraft (after relevant scaling factors are applied as discussed below). Since the Eigen response is a function of the modal mass and stiffness, matching the modal response will also ensure that the mass and stiffness distributions are also equivalent.

Depending on the fidelity of the aerodynamics that are modelled, the non-dimensional quantities of Mach and Reynolds number may appear (though not shown explicitly in equation 2 above). However, matching these values is often difficult, requiring unrealistic operating conditions, or sometimes impossible using standard atmosphere and gravity (matching these conditions often requires the use of exotic gases as is often seen in trans-sonic wind tunnels). As a result, these quantities will not be considered in subsequent scaling efforts.

2.2.3 Scaling Factors

Since the equations of motion consist of the three fundamental properties of length (L), time (t) and mass (M), the Pi theorem tells us that we can choose 3 independent scaling parameters consisting of these quantities. Here we choose to scale the span (based on the desired reduced scale span of 5m), gravitational acceleration (since the reduced scale will operate at the same gravitational constant at full scale) and density (since we are choosing the test altitude based on the flight test range). Note that the subscripts of m and fs represent model scale and full scale respectively and scaling factors are represented by a double arrow accent.

$$\begin{aligned}\vec{L} &= \frac{b_m}{b_{fs}} = \frac{5m}{45m} = 0.1096 \\ \vec{g} &= \frac{g_m}{g_{fs}} = 1 \\ \vec{\rho} &= \frac{\rho_m}{\rho_{fs}} = \frac{\rho_{990m}}{\rho_{SL}} = 0.908\end{aligned}\tag{3}$$

\vec{L} is a fundamental quantity (length) while the gravity and scaling factors are surrogate parameters made up of the other primary quantities of mass and time. The above scaling factors can be used to solve for the two remaining fundamental scaling quantities, \vec{M} and \vec{t} , as follows. First, we observe that gravity is comprised of the fundamental quantities of length and time.

$$\vec{g} \equiv \frac{\vec{L}}{\vec{t}^2}\tag{4}$$

Therefore,

$$\vec{t} = \sqrt{\frac{\vec{L}}{\vec{g}}} = \sqrt{\frac{0.1096}{1}} = 0.331 \quad (5)$$

Similarly, the mass scaling factor can be calculated from the chosen density scaling factor ($\vec{\rho}$) to yield the mass scaling factor.

$$\vec{\rho} = \frac{\vec{M}}{\vec{L}^3} \quad (6)$$

hence,

$$\vec{M} = \vec{\rho}\vec{L}^3 = 0.908 \cdot 0.1096^3 = 1.2e - 3 \quad (7)$$

We can then calculate all surrogate parameters (such as Inertia, velocity etc) in a similar manner using the fundamental scaling terms. Some of these are summarized in Table 1 below. (It should also be noted that a column has been added for the scaling factors governing a smaller configuration, the *Mini SensorCraft*, which has been developed and will be discussed in an upcoming section).

TABLE 1 - SUMMARY OF KEY SCALING PARAMETERS

Parameter	Scale Factor for 5m Aircraft	Scale Factor for Mini SensorCraft	Symbol
Length Scale	0.1096	0.0405	\vec{L}
Air Density at Testpoint	0.908	1.00	$\vec{\rho}$
Gravity at test point	1	1	\vec{g}
Velocity	0.33	0.201	\vec{v}
Time	0.331	0.0201	\vec{t}
Mass	1.20e-3	6.67e-5	\vec{M}
Inertia	1.44e-5	1.10e-7	\vec{I}_J
Frequency	3.02	4.97	$\vec{\omega}$
Kinematic Visc. at Testpoint	0.0363	0.0082	$\vec{\nu}$

Using the calculated scaling factors and the constraints contained in the equations of motion, the actual geometric and operating properties of the reduced scale aircraft can be calculated. Table 2 below summarizes these values while Figure 3 demonstrates the geometric scaling graphically.

TABLE 2 - KEY GEOMETRIC AND OPERATIONAL VALUES

	Full Scale*	5m RPV	Mini SensorCraft	Units
Span	45.63	5	1.85	m
Density	1.21	1.113	1.225	Kg/m ³
MTOW	7.05E+04	84.21	4.70	kg
TP Velocity	86.43	28.61	17.40	m/s
Reynolds Number	2.18e7	7.91E+05	1.78E+05	-
Mach Number	0.254	0.085	0.025	-

**Full scale test point supplied by Boeing to correspond most adverse gust condition (fully fueled ascent condition shortly after takeoff).*

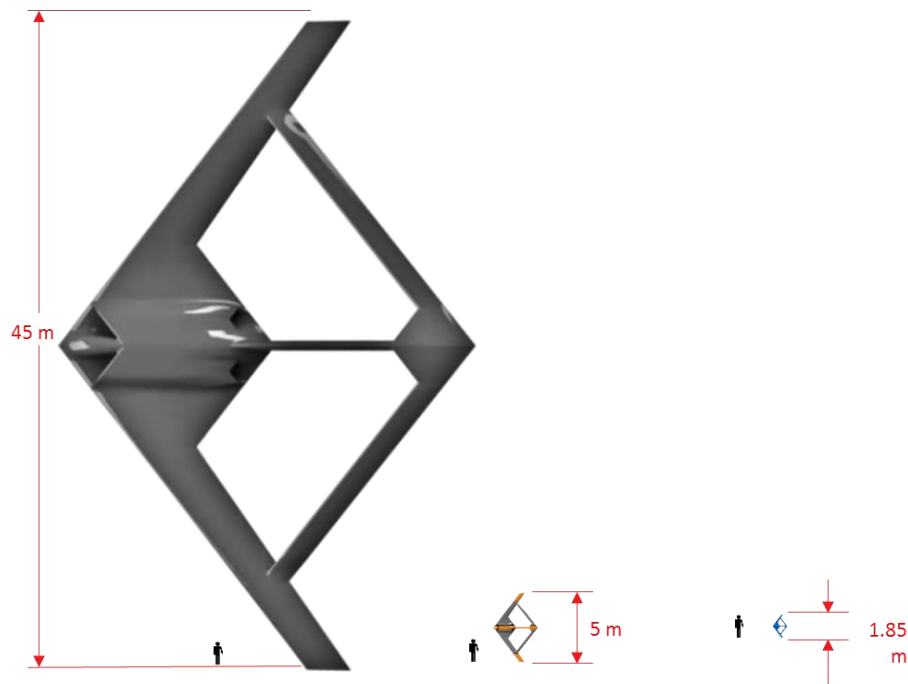


FIGURE 3 - RELATIVE SCALE OF BOEING BASELINE AIRCRAFT, 5M REMOTELY PILOTED VEHICLE AND 1.85M MINI SENSORCRAFT

The items highlighted blue in Table 2 above signify quantities that do not match the desired scaled results. Since Mach and Reynolds numbers are non-dimensional quantities that appear in higher order equations of motion, their values should be consistent for each reduced scale test point. However, for the reasons mentioned previously, their effects will be ignored and no attempt made at matching them.

While this discrepancy between full scale and reduced scale Re and Mach is not ideal, it is assumed that this omission will not overly affect the validity of the results. Mach number is important when considering

compressibility effects which are often ignored at low Mach numbers as seen here ($M_{\max} \approx 0.254$). Also, while the Reynolds number is quite a bit smaller for the 5m aircraft, it is still well above critical values at which we might expect scale effects such as laminar separation. Unfortunately, the Reynolds number experienced at the Mini configuration's scale is low enough that these effects may be of concern. However, methods to address these issues (such as tripping laminar flow with boundary layer devices) have been employed and will be discussed in following sections.

2.2.4 *Scaling Methodology*

As mentioned previously, the goal here is to reproduce the structural properties of the full scale aircraft by matching dimensionless mass and stiffness properties. One design approach for developing accurate mass and stiffness distributions is to scale down the exact geometry of the full scale aircraft. Unfortunately, this is not practical in the case of the SensorCrafts for several reasons. For one, the internal structure is not given. In addition, manufacture of scaled components may be very expensive and in some cases impossible due to their small resulting sizes.

While some advanced manufacturing techniques and exotic material could potentially be employed to match the mass and stiffness distributions, while still ensuring manufacturability, there exists another challenge in this project. The details of the full scale mass and stiffness distributions are not known directly as the internal structure is classified and therefore not made available. However, mass normalized modal shapes and natural frequencies of the aircraft were supplied for the *SensorCraft Boeing 410 E4-21R2* configuration at the outset of this project.

From the governing equations it can be shown that any model with the same scaled mass and stiffness distribution, over the same scaled geometry, will result in the same modal shapes and frequencies as those of the full sized aircraft (after appropriate scaling). By designing a model with similar modal response (mode shapes and frequencies) to the full scale aircraft, similarity of the mass/stiffness distributions will be achieved independent of internal structure. This then allows a simplified internal structure to be employed. The

requirements of the structure are to allow a proper stiffness distribution while still fitting into the available space, as well as not using up too much of the available mass allowance. Once this is achieved, concentrated masses can be added to attain the desired mass distribution and overall mass values. An alternate option to adding concentrated masses is to alter the geometry of the structure such that it affects the mass without altering the stiffness. (An example of changing mass distribution without affecting the spanwise stiffness distribution would be to change the thickness of the ribs in a standard spar/rib configuration).

The methodology chosen here is to first define a simplified internal configuration for the reduced scale aircraft that can be subsequently optimized. The geometry is defined using various physical parameters such as spar height, thickness or density. The parameters of this model can then be used as design variables in an optimization routine. The problem may be subject to constraints such as maximum stress or strain limits. The model is then optimized by adjusting the design variables to minimize an objective function with the goal of matching the desired modal response.

2.3 Initial Test Point Feasibility Study

Before proceeding with the detailed design and scaling of the RPV, an initial feasibility study was performed to determine the suitability of the chosen test point while utilizing common building methods and materials. It is possible that a particular combination of parameters would yield a test point that would require material properties beyond that commonly available (ie, extremely light/exceedingly stiff) in which case another test point would need to be considered. It was also desired to determine if the mass of the resulting structure would still allow for sufficient weight reservations for supporting systems and flight critical components.

2.3.1 Structural Layout of Baseline Structure

As a first approach, a simplified beam truss structure is chosen to simulate the wing structure. One dimensional, aluminum beam elements of rectangular cross section with variable heights are used to match the scaled stiffness distribution. The structural weight of these components contributes, along with the point masses, to make up the desired mass distribution. These point masses are positioned on nodes connecting beam elements as shown in the figure below.

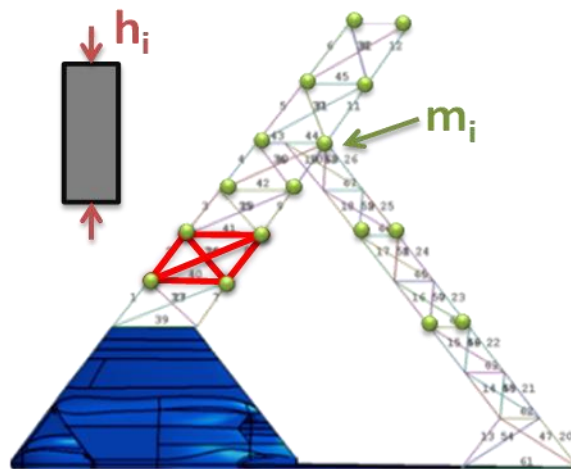


FIGURE 4 - BEAM ELEMENTS AND POINT MASSES USED TO MODEL INTERNAL STRUCTURE

Here the nodal locations are chosen so that they correspond to the reduced set of modal results supplied by Boeing. By ensuring the nodes are coincident with the full scale model no interpolation was required to compare displacements between the two models once scaling laws were applied.

For this initial feasibility study, a simplifying assumption was made that the relative stiffness of the fuselage was very high compared to the wing and therefore assumed rigid. This allowed fixed boundary condition to be applied on the root nodes of the forward wing. The initial modal results supplied by Boeing did not include the rigid body modes as the analysis was run with a fixed condition at the configurations center of gravity and therefore the fixed condition chosen here was determined to be sufficient for the initial study.

2.3.2 Scaled Frequency and Mode Shape Matching

This structure was simulated using ANSYS FEA software and integrated in an optimization routine using Phoenix Integration's ModelCenter Software. The objective of the optimization was to minimize both the error in the calculated mode shapes as well as the overall mass of the structure (not including point masses) as reflected by the objective following function.

$$\text{Objective} = k_1 M_{\text{structure}} + k_2 \text{RMS}_{\text{error}} \quad (8)$$

Where k_1 and k_2 represent weighting factors controlling the relative importance of the mass and RMS error. A genetic algorithm was used to solve the optimization problem subject to the following constraints.

- 1. Match scaled frequency of first three modes – the constraint is relaxed to allow frequency to be matched with to $\pm 5\%$*
- 2. Overall mass of the configuration within 5% of scaled takeoff weight minus 30 kg which is reserved for the fuselage, engines fuel and other items not modeled here.*
- 3. Equivalent stress due to 5g pull-up load not to exceed material yield limits*

The objective function serves to minimize both the mass of the aluminum load bearing structure (not including point masses) and the RMS of the difference in amplitude of the first three given and calculated mode shapes at all nodes. Within each loop of the optimization process, the following steps were performed.

4. *Assign values to the heights of each structural beam*
5. *Adjust values of point masses*
6. *Perform modal analysis and natural frequency calculation within ANSYS*
7. *Perform linear static analysis for 5g load case*
8. *Check RMS error in mode shapes using Excel*
9. *Calculate objective based on updated mass and mode shape RMS errors*
10. *Check frequency, mass and stress limit constraints*
11. *Check for convergence and iterate if necessary*

A solution was obtained which obeyed the target constraints while yielding an overall structural mass of 29.85 kg (for one set of half fore/aft wings) while adequately approximating the given mode shapes. A graphical representation of the resulting element dimensions is included in the following figure.

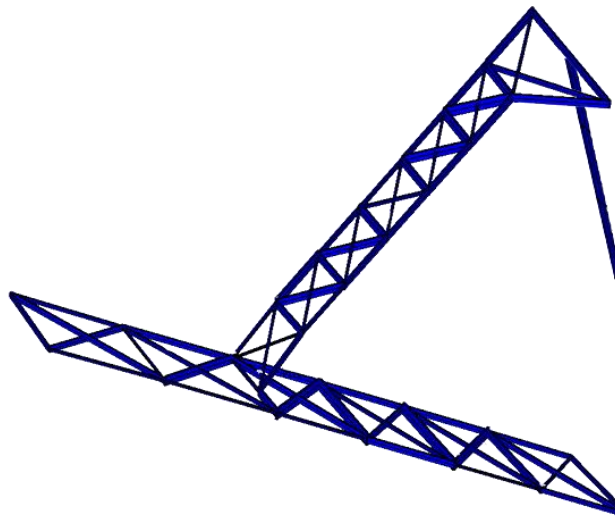


FIGURE 5 - ELEMENT GEOMETRY

One resulting area of concern was the robustness of the optimization routine used. Initially, a gradient based method was employed but with very poor results. It is believed that this is due to the coupling of mass and stiffness resulting from varying the height of the structural elements. As one area is made to be stiffer by the optimization, it also becomes heavier and therefore is required to be stiffer to support itself. Convergence so a global optimum was difficult to achieve which is why the genetic algorithm is used at the price of longer solve times.

2.3.3 Results of Feasibility Study

The Air Force's main concern at the outset of the feasibility study was that a structure that was sufficiently stiff, and strong enough to resist flight loads, may not be light enough to allow the incorporation of supporting systems and trimming weights.

Results of the feasibility study showed, that considering only the structural elements, a total mass for both wings would be 49.7 Kg. This then required approximately 4.5kg of distributed point masses in order to achieve the desired mass distribution and mass constraint. This 4.5kg of trimming mass was determined to be large enough to allow the incorporation of supporting systems such as actuators, wiring, instrumentation etc while still being able to achieve the desired mass distribution. The initial layout chosen here was also not very structurally efficient and it was predicted the overall structural mass would be less once a better structural layout was chosen.

This point was determined feasible by the US Air Force and the 5m test point chosen as the basis for current work.

2.4 Advanced Scaling Framework

The next step was to improve the framework used in the optimization. The goal was to develop a more robust tool capable of matching several mode shapes/frequencies of the Joined Wing structure simultaneously, while incorporating finite element models of varying fidelity (1, 2 and 3D elements). In addition, several other improvements were required, including a process for comparing non conformal meshes using a thin plate spline method for interpolating the supplied full scale displacements to the non-conformal mesh of the reduced scale model.

This section details this improved framework including the underlying analysis tools used and two methodologies investigated to improve the convergence of the problem. It also presents two benchmark studies performed including a simplified cantilever wing and a beam model of the Joined wing configuration.

2.4.1 Analysis Tools

Several commercial software packages were used in the scaling framework. In order to be integrated into the framework these codes had to be capable of being run from a command line using batch files or scripting routines in order to allow integration into ModelCenter. The following is a brief description of some of the tools used.

2.4.1.1.1 Phoenix Integration's ModelCenter

ModelCenter®, by Phoenix Integration, is a graphical environment for automation, integration, and design optimization. Within the programming environment you can create an engineering process and then explore the design space to find the best design. Some interfaces for integrating common software packages come standard and most others can be incorporated through the individual program's STKs and APIs. In addition there is the option of adding custom scripts within ModelCenter that can be programmed in a variety of languages including Java, C and Visual Basic.

ModelCenter can also be used to perform optimizations and features over 30 algorithms from leading research organizations including: Boeing's Design Explorer, Sandia Labs' DAKOTA, VR&D's DOT and BIGDOT, and SwarmOps.

2.4.1.1.2 Catia Computer Aided Design Software

Catia is a full featured CAD package that can be integrated directly into ModelCenter (MC). Within this framework, various geometries were generated in Catia and key parameters exposed as design variables. For example, in higher fidelity analyses of the Joined wing configuration variables such as spar width, skin thicknesses and number of ribs were exposed to ModelCenter. MC could then change these parameters and update the geometry for subsequent operations such as meshing.



2.4.1.1.3 ICEM Meshing Suite

ICEM meshing software is a robust program that can mesh a wide variety of geometry. ICEM is not integrated directly into ModelCenter but can be run from a command line using scripts programmed in the tcl scripting language. A custom wrapper was written in MC that can update the tcl script and call ICEM in batch mode. The script then automates the meshing and outputs the meshed geometry to disk for use in subsequent FE analysis.



2.4.1.1.4 ANSYS Finite Element Package

ANSYS is the primary FE solver used in this framework. It can be integrated into ModelCenter in a similar manner to ICEM. Modal and static/nonlinear analyses are run using batch commands and the results written to disk. Model center can update the input batch files and parse the subsequent results in order to drive the automation of the structural analysis.



2.4.1.1.5 Matlab Programming environment

Matlab was used extensively for many programmed functions such as calculating errors, constraints and comparing results to the baseline model. Matlab can be called directly from ModelCenter. Matlab was also used to generate plots to visualize results at each iteration. These plots were saved to disk and associated to the particular iteration so that the evolution of the design could be viewed during and after the optimization process.



Matlab was also used to interpolate the scale model displacement measurements to non-conformal points on the full scale model. Since the topology of the full scale and model scale aircraft differ, the supplied baseline results are at locations that may not correspond to results acquired for the ANSYS model. As a result, full scale results are interpolated using an infinite plate spline technique as can be seen in Figure 6.

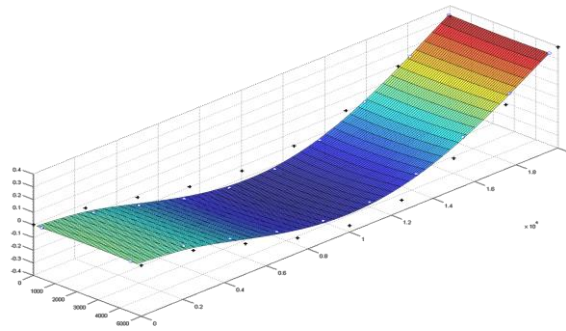


FIGURE 6 - OUTPUT OF CODE THAT COMPARES THE DISPLACEMENTS OF NON-CONFORMAL MESHES

2.4.1.1.6 Scripting Commands



A variety of tasks are performed using script commands. In this case the Visual Basic scripting language is used to perform tasks such as calculating the objective functions.

2.4.1.2 ZAERO Aeroelastic Analysis Code



The ZAERO software system is a powerful engineering tool that integrates all essential disciplines required for advanced aeroelastic design and analysis. ZAERO was not used in the optimization routine due to the heavier computational expense vs matching of the modal response (which does not require calculation of aerodynamics, only the structural response). However, ZAERO was included in the ModelCenter environment and was used to compare final results with supplied aeroelastic modes and also to rapidly calculate flutter conditions for subsequent sizing studies.

2.4.1.3 Strategy and Rationale

It was discovered in the feasibility study that the coupling between mass and stiffness, due to varying physical parameters such as beam heights, caused convergence issues due to the many local minima in the design space. As a result two different techniques were investigated in matching the desired modal response. The first method matches the response directly, by updating the mass and stiffness distributions simultaneously in one optimization routine (as with the feasibility study). The second method involves uncoupling the mass and stiffness optimization into two separate routines.

2.4.1.3.1 Method 1: Matching Modal Response Directly

This technique has the advantage in that it matches the modal response directly, whereas the other method matches the mass and stiffness distributions in separate routines. The process can be seen in Figure 7 below.

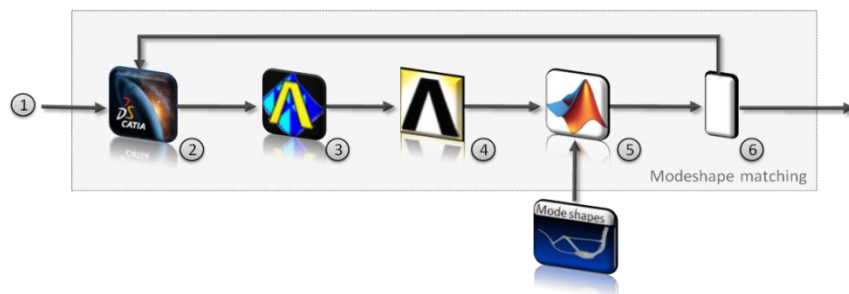


FIGURE 7 - OPTIMIZATION LOOP USED TO MATCH SCALED MODAL RESPONSE

Since the mass and stiffness are coupled in the thickness of the elements, gradient based methods were not very stable. In many cases the optimizer would try and drive up the mass by increasing the element thickness rather than adding point masses (which add no stiffness themselves). This resulted in some areas becoming too heavy, in which case the stiffness would need to be increased by thickening elements, thereby increasing the mass again. Although the gradient based algorithm was problematic, a genetic algorithm did converge to an acceptable result at the price of long computation times.

One strategy that was also adopted with good success was to uncouple mass and stiffness of the structural elements by assigning a very low density to the structural elements and letting the optimizer add additional

weight through point masses only. This then requires calculating the actual predicted weight of the structural components, if reasonable density values were assigned, and subtracting the resulting weight distribution from the distributed point masses. Unfortunately, this was a very laborious post processing procedure and, since the point mass distribution is discrete, the final redistribution of weight properties will not result in a totally equivalent distribution to the optimization output.

2.4.1.3.2 Method 2: Matching Modal Response through Mass and Stiffness Matching

This method assumes that a similarity of modal responses will be achieved if both the mass and stiffness distributions are matched. This routine is divided into two separate optimization loops as seen in Figure 8 below.

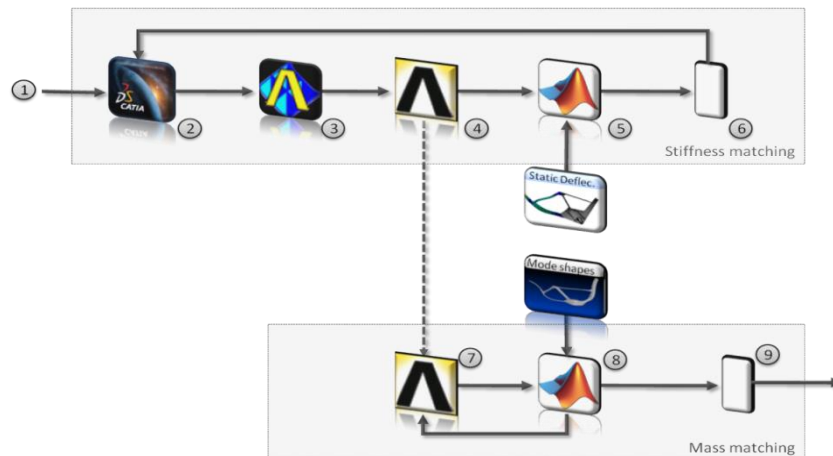


FIGURE 8 - OPTIMIZATION LOOP USED TO MATCH SCALED MODAL RESPONSE BY MATCHING STIFFNESS AND THEN MASS DISTRIBUTION

First, the stiffness is matched by reproducing a given set of displacements under a known load using an optimization routine which updates the element sizes/geometry. Next, a second optimization routine is run which matches the modal response by updating the mass distribution.

This method uncouples the mass and stiffness and was much more robust than the previous method. It also resulted in much faster convergence, especially when surrogate based methods were used to select starting points for the gradient based optimizer.

2.4.1.3.3 Comparison of Methods

As stated, method one was not very robust and required the use of a genetic algorithm to converge to an acceptable result. The second method was far superior but does have one major disadvantage: **It requires additional sets of displacements under given loads.** This information is crucial for this method and if not made available, method one is the only option.

2.4.1.4 Benchmarking the Scaling Framework

A simplified model was first chosen to benchmark the framework and investigate the methodologies described earlier as well as a variety of optimization methods. This simple model was chosen to represent a typical cantilever wing as a simple ladder structure where the poles and rungs of the ladder represent typical spars and ribs seen in a wing box.

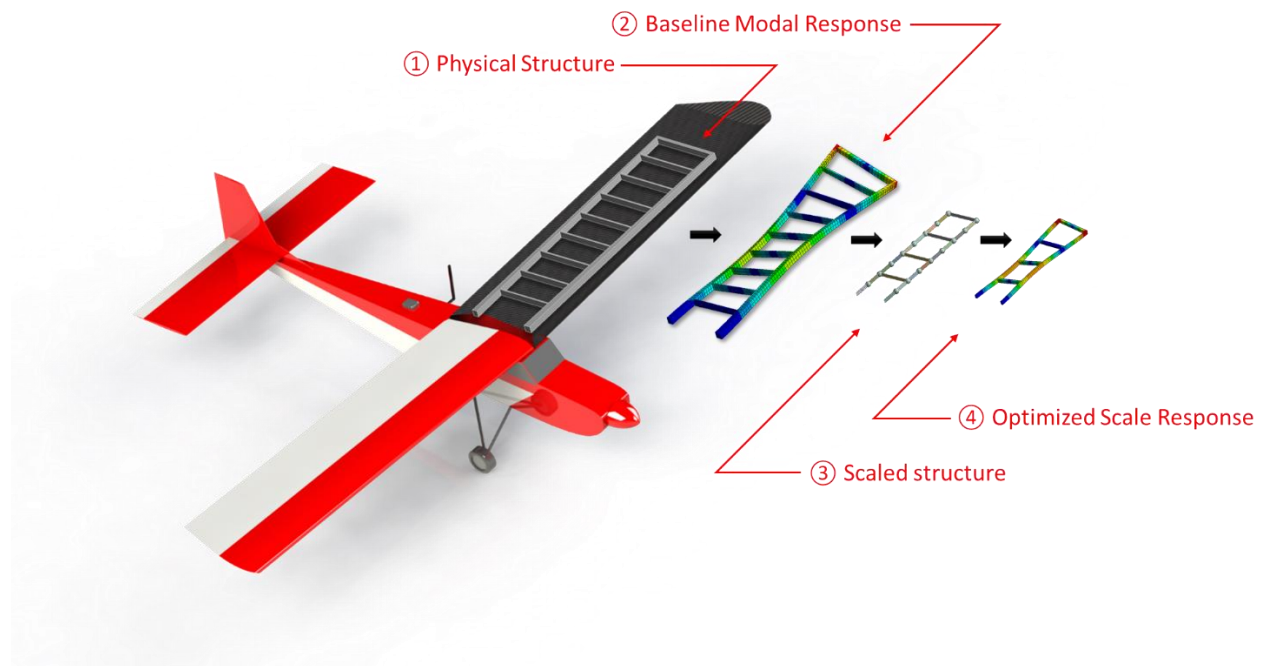


FIGURE 9 - GRAPHICAL PROCESS FLOW OF BENCHMARK CASE

Figure 9 above shows the process flow of the benchmark analysis. In step 1 a physical structure was designed for a typical UAV configuration. Next, in step 2, this structure was analyzed using Finite Element Analysis in order to generate baseline data in the form of mode shapes, frequencies and static deflections due to several

static load cases (information similar to that supplied for the baseline SensorCraft configuration). In step three it is assumed the physical structure of the baseline is not known and therefore a simplified structure is chosen (here it is again a ladder like structure but the topology is different, ie the number of ribs and aspect ratio). At step three a scale factor of 0.5 is chosen and the baseline results are also scaled. In step 4 the scaled structure from 3 is optimized in order to match the scaled baseline response. Here the individual shell thicknesses, material properties and point mass values were varied.

This baseline model was used to explore both proposed methodologies and various optimization algorithms. Good results were achieved with both methodologies but faster convergence was typically achieved with method 2. Figure 10 below shows a typical result that was achieved, resulting in very good modal matching between the baseline and reduced scale models. (Here the reduced scale model is shown at the same size as the baseline to aid in comparison).

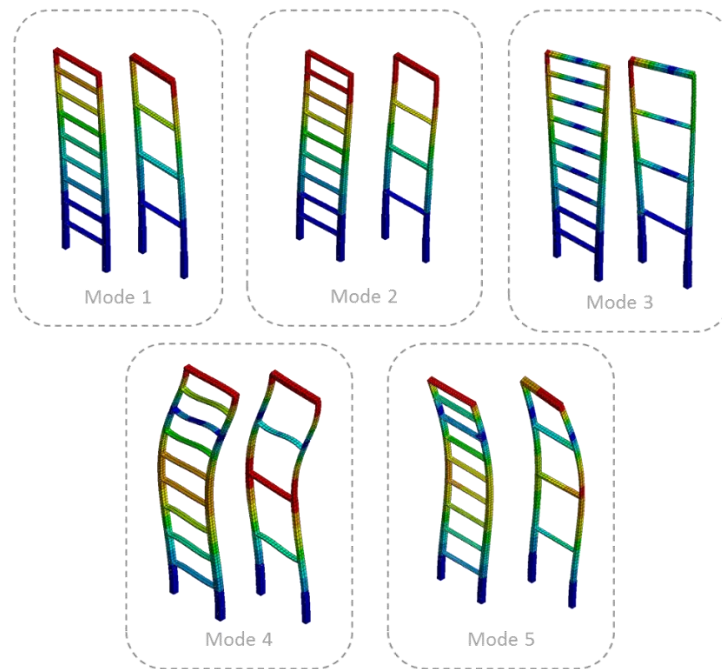


FIGURE 10 – COMPARISON OF BASELINE (LEFT) AND OPTIMIZED REDUCED SCALE (RIGHT) MODAL RESPONSES

Next, a test case was chosen to explore the Joined Wing Configuration. Here a simplified, 1d beam formulation was chosen as seen in Figure 11. Additional constraints were incorporated for this analysis, including the

requirement to match scaled moments of inertias and cg locations. This required the modelling of flight supporting systems such as actuators, engines, fuel etc. The locations of these components became variables in the optimization process in order to adjust the inertial properties as the optimizer redistributed mass throughout the structure to match the modal response.

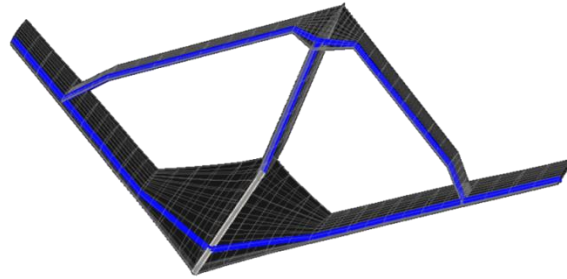


FIGURE 11. BEAM MODEL USED FOR INITIAL SCALING STUDY

Figure 12 below shows the results of some of the initial studies. Here the inertias and cg locations were matched within 5% and good agreement could be seen in the first 6 mode shapes. Here mode 5 showed some discrepancy along the aft wing which was determined to be due to the tradeoff between allowing additional mass to be distributed along the aft wing while still maintaining the cg constraints.

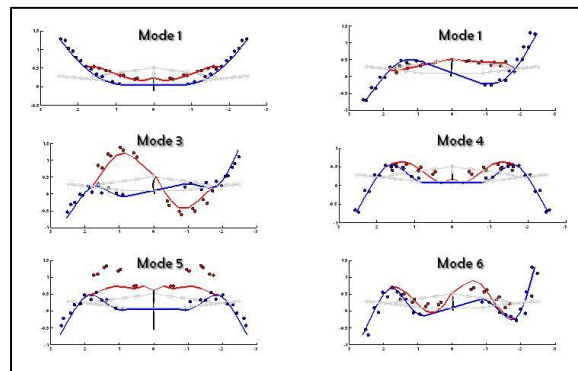


FIGURE 12. COMPARISON OF BASELINE MODAL RESULTS (POINTS) AND RESULTS OF OPTIMIZED BEAM MODEL (LINES)

2.5 Conclusions

The intent in the Feasibility stage was to determine whether the full sized aircraft could be scaled down to a 5m span (~1/9th scale) and flown at or near sea level. Some simplifying assumptions were made regarding the

governing physics and a set of scaling laws developed which were used to map characteristics from full to model scale. Several constraints were imposed based on physical quantities that cannot be easily manipulated (such as air viscosity and the gravitational constant) but these were shown to likely be of little consequence to the overall usefulness of results.

Since the internal structure of the full scale aircraft is classified, the internal details were not made available. However, the modal response of the full scale aircraft was supplied and it was shown that if the aerodynamics can be preserved (by scaling the outer mould line), a linear aeroelastically equivalent model can be achieved if the mode shapes and scaled frequencies are reproduced.

A quick initial study was summarized with the aim of proving that the chosen reduced scale design point was feasible. Using geometric parameter optimization to tailor the mass and stiffness distribution, it was shown that a feasible model could likely be produced that would have sufficient stiffness using common building materials, yet remain light enough to allow incorporation of all supporting systems required for a flight worthy aircraft.

An advanced Scaling Framework was introduced that is capable of optimizing more complex and representative aircraft geometry in a repeatable and automated way. A test case was run using a simplified cantilever wing design and showed very good results. This framework was then applied to a simplified beam model of the joined wing configuration in an attempt to match the first six mode shapes and frequencies.

While results using the simplified joined wing configuration were very promising, it was apparent that the optimization problem is very sensitive to the mass distribution and therefore the locations and weights of all the supporting systems. As a result it was determined that the first step must be to more accurately determine the space and component weight reservations throughout the aircraft. This would be achieved in the design of the Rigid 5m RPV (as detailed in the following chapter) and only after all components were defined would the final scaling be performed on a higher fidelity FE model.

Chapter 3 - Preliminary Configuration Design and Testing



The following chapter is a summary of the work done to evaluate the unique characteristics of the Joined Wing SensorCraft. A multi-fidelity approach is adopted to investigate the aerodynamics and to subsequently determine the flying characteristics. Several deficiencies were found in the design and therefore some potential solutions are presented as well as results of evaluations using simulation and reduced complexity flight testing.

3.1 Estimate of Scaled performance

A combination of Vortex Lattice and higher order computational fluid dynamics was used to predict the SensorCraft's performance. Non-dimensional stability derivatives and trim calculations were determined primarily using HASC and AVL code while FLUENT while used to compare/validate results and scope individual flight cases of particular concern. In addition, a quantitative estimation of the flight characteristics and trim states of the aircraft was performed using a series of reduced scale (1.58m span) Mini SensorCraft models. Flight test results were used to further refine aerodynamic parameters such as base drag and control surface derivatives.

3.1.1 Aerodynamic Prediction Using Vortex Lattice Methods

A detailed analysis of the joined wing flight dynamic stability was carried using Vortex Lattice Methods (VLM). These initial investigations were performed using HASC (High Angle of Attack Stability and Control) software ^[53] to determine dynamic stability and control characteristics for developing a 6dof simulator. Additional analyses were also performed using Athena Vortex Lattice code developed by Mark Drela et al at MIT ^[54].

There are two main motivations for detailed investigation of the flight characteristics for this aircraft. The first is that the initial analysis showed the aircraft had marginal yaw stability and it may be necessary to modify the outer mold line of the aircraft to reduce or eliminate this. The second motivation is that the present configuration does not have a rudder surface and some form of yaw authority is required, whether through scheduling of other surfaces or the addition of a new surface on which to include a rudder.

The following sections introduce the baseline results as well as three alternate configurations and methods to improve yaw stability while introducing a form of control authority. It should also be noted that unless otherwise stated, all results specified are for the flight condition specified in Table 3 below.

TABLE 3 - REFERENCE QUANTITIES USED IN SUBSEQUENT ANALYSES

Reference Quantity	Symbol	Value	Units
Planform Area	S	1.39	m ²
Mean Aerodynamic Chord	\bar{c}	0.404	m
Span	b	5	m
Air Density/Altitude	$\rho/Alt.$	1.180/400	Kg/m ³ , m

The mass properties assigned to the aircraft correspond to the supplied full scale test point after having been scaled by the derived scaling factors to map them to the reduced scale test point.

The baseline configuration is defined by the supplied CAD geometry of the aircraft. Since no control surfaces are specified from the given geometry, the following control surface layout is used for the present work. Figure 13 shows the chosen locations and the numbering of the control surfaces.

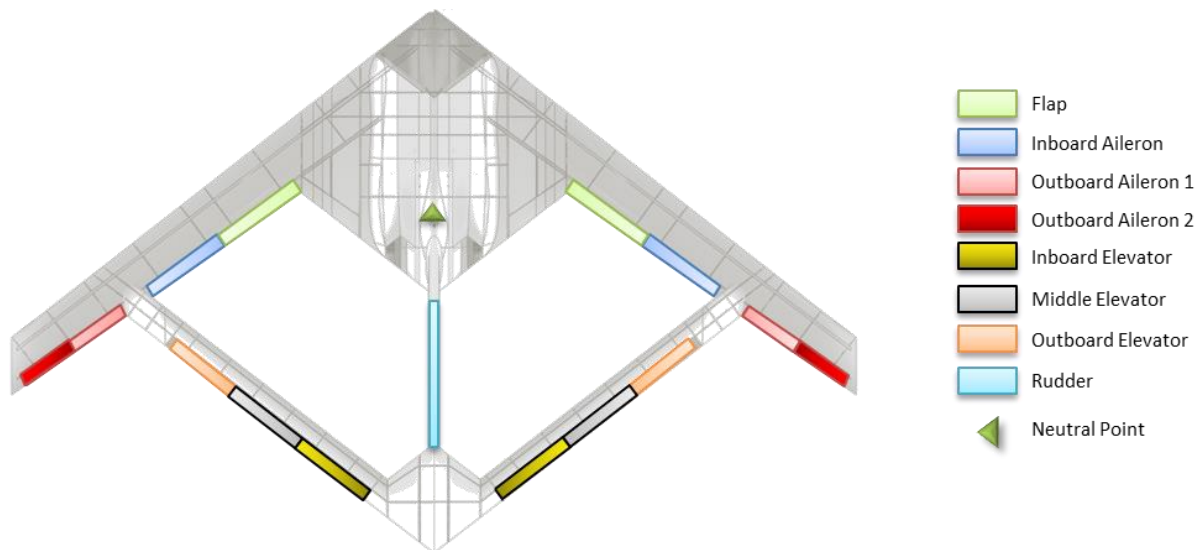


FIGURE 13 - CONTROL SURFACE LOCATIONS AND NAMING

Figure 14 below shows the discretized baseline geometry. The large figure on the left is a representation of the geometry with the airfoil thicknesses rendered along with the control surfaces. The top right model is the HASC geometry and the lower right shows the model used with AVL.

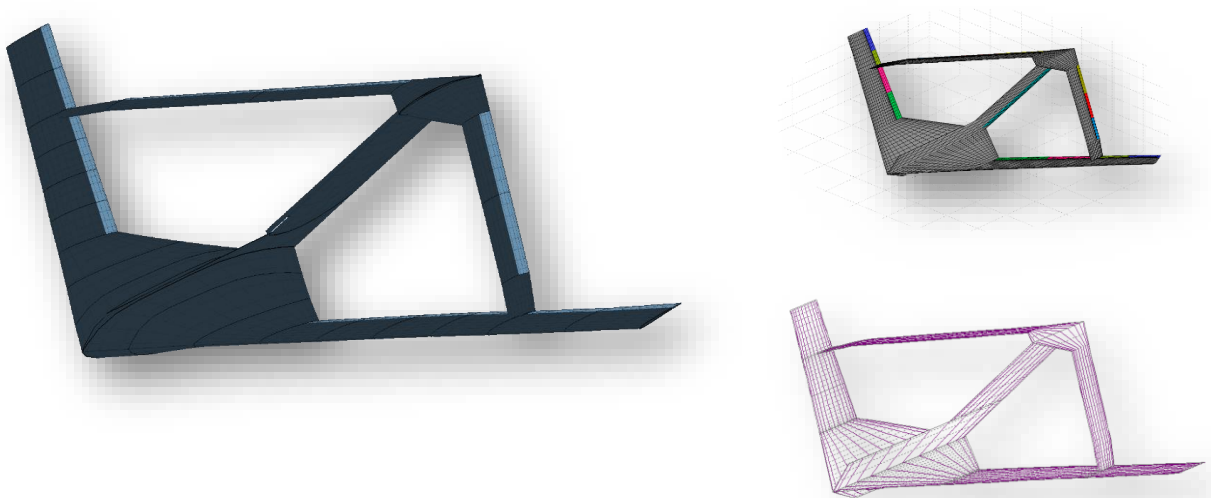


FIGURE 14 - VORTEX LATTICE MODELS OF BASELINE

Some additional corrections were performed to refine the VLM results. This included a detailed drag buildup of components such as antenna, landing gear etc to improve the overall confidence in aircraft polars. Additionally, since the VL methods only account for the lift induced drag, additional calculations were performed to determine profile drag contributions of the lifting surfaces. This involved the calculation of drag polars at 14 spanwise cross sections and integrating the predicted drag over the lifting surfaces based on local induced angles of attack.

3.1.2 Aerodynamic Corrections Using Higher Order CFD

Additional analysis was performed to validate the VL results and to determine critical aerodynamic properties with greater accuracy. These results were then used to augment the VLM results and this database served as the aerodynamic characterization used for all subsequent work.

3.1.2.1 Geometry Cleanup

The first step in modelling the configuration using higher order methods involved clean up and repair of the outer mold line geometry. The geometry supplied by Boeing was in the IGES format (due to export constraints the original parametric model could not be supplied) and consisted of three individual parts (the Fuselage and tail boom assembly, the main wing and the aft wing). In translating the geometry from its native format (CATIA) to IGES, many problems were generated. In order to attempt to describe the geometry using the IGES standard, complex surfaces such as shape fillets were discretized into very small segments (see

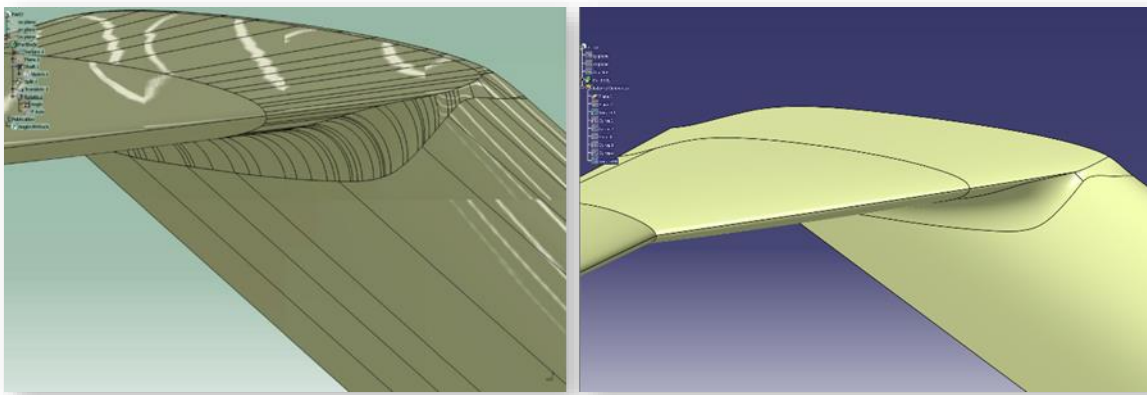


Figure 15 below). Many of these surfaces lacked both point and tangency continuity and required rebuilding. In addition, hundreds of other anomalies were introduced (sliver surfaces, overlapping and folded surfaces etc.). These problems had to be repaired in order to be used in downstream applications.

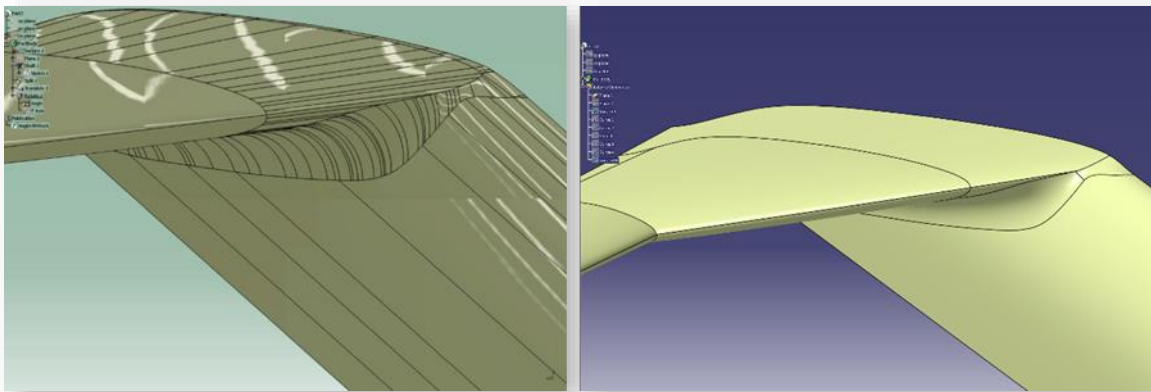


FIGURE 15 – BOOM GEOMETRY BEFORE (LEFT) AND AFTER (RIGHT) GEOMETRY CLEANUP

Repair work was performed using CATIA's surfacing capabilities and resulted in a water tight surface that was used to form a solid. This has allowed the import into ANSYS, ICEM and all other required software. This repaired OML was the basis of all subsequent analysis and design work.

3.1.2.2 Meshing

The fluid domain was modeled in CATIA in two parts. The first was a spherical domain that encloses the aircraft half model and the second is the entire remainder of the rectangular domain. This can be seen in the following figure showing the inner domain in red and the outer domain in white.

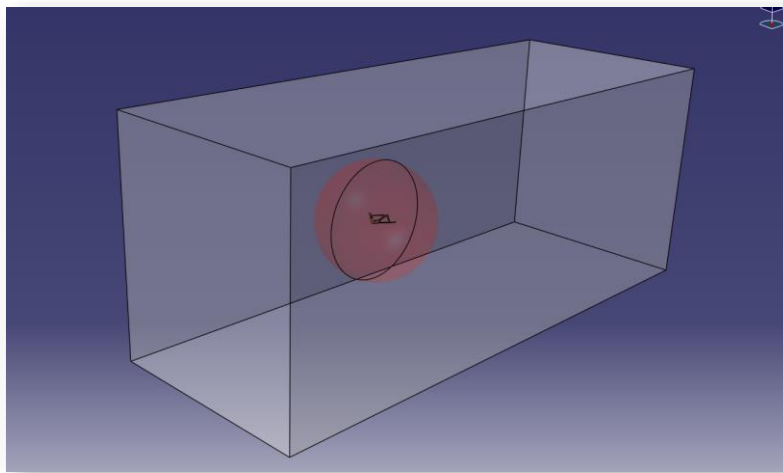


FIGURE 16 - COMPUTATIONAL DOMAIN

The reason for meshing the aircraft in two domains is that it allows the finer, more computationally expensive mesh at the aircraft surface, and immediate vicinity, to be meshed in fine detail once only. This domain can then be rotated (to do alpha and beta sweeps for instance) and only the outer rectangular domain would

require re-meshing. Also, this inner boundary could be assigned a moving reference frame which can allow the calculation of rate derivatives (it to calculate $\frac{dC_L}{dq}$).

ICEM[®] was used to generate the surface mesh using a patch independent algorithm. Next, the surface mesh was inflated to capture the boundary layer. Finally, the inner domain was filled using an advancing front algorithm. This inner mesh domain is then saved for use in all subsequent analyses (except for several that required re-meshing of the deflected control surfaces). This inner domain is then rotated to the desired trim point and a volume mesh generated to fill the outer domain. This resulting volume mesh was the basis of subsequent analyses using Fluent[®]. A half span mesh was also created to reduce computational expense where possible and is shown in the following figure.

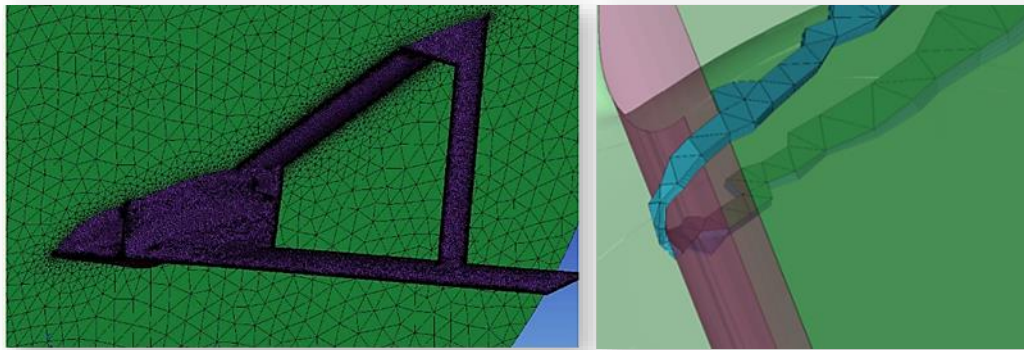


FIGURE 17 - SURFACE MESH OF BASELINE CONFIGURATION AND DETAIL SHOWING INFLATED BOUNDARY LAYER

3.1.2.3 Test Matrix

Due to the computational expense of the CFD runs a limited number of test points were evaluated. These test points are a subset of the most important parameters and serve to augment the VLM results which represent the majority of the aerodynamic modelling. Table 4 below outlines the test points chosen for the CFD analysis.

TABLE 4 - TEST MATRIX FOR CFD ANALYSIS

Test Point	Alpha	Beta	p	q	δAil_{OB}	$\delta Elev_{IB}$	$\delta Elev_{MID}$
0	-0.95	0	0	0	0	0	0
1	-10	0	0	0	0	0	0
2	-6	0	0	0	0	0	0
3	0	0	0	0	0	0	0
4	3	0	0	0	0	0	0
5	6	0	0	0	0	0	0
6	8	0	0	0	0	0	0
7	10	0	0	0	0	0	0
8	11	0	0	0	0	0	0
9	12	0	0	0	0	0	0
10	13	0	0	0	0	0	0
11	14	0	0	0	0	0	0
12	15	0	0	0	0	0	0
13	16	0	0	0	0	0	0
14	-0.95	3	0	0	0	0	0
15	-0.95	0	1	0	0	0	0
16	-0.95	0	0	1	0	0	0
17	-0.95	0	0	0	5	0	0
18	-0.95	0	0	0	0	5	0
19	-0.95	0	0	0	0	0	5

Here test point 0 corresponds to the predicted trim state and serves as the basis for following test points. Each subsequent point changes one condition as denoted by the numbers in red bold type face.

3.1.2.4 Analysis

In order to save computational time, wall functions were used to model the boundary layer, rather than resolving the near wall region with high density boundary layer elements and using a near wall modeling approach. The wall function approach is very popular because it is economical, robust and reasonably accurate. Since the viscosity affected region doesn't need to be resolved, it is widely used in the simulation of high Reynolds number flows. It is understood that this may not adequately capture the physics at high angles of attack and may not capture aircraft drag with such a high degree of certainty but it was decided that this is a valid tradeoff for the decreased solve times. This is especially true since this data is required mainly for developing linear controllers (tuned for reasonable angles of attack around the trim state) and subsequent flight testing would be performed to determine drag values etc. Boundary layer height and first cell thickness

values were determined for similar flow conditions over a flat plate and were used in the meshing process to determine prism inflation parameters.

The Reynolds-averaged Navier-Stokes equations (RANS) were used to model the flow. The problem is simplified by assuming the flow is incompressible since the Mach number at the desired test point is well below the transonic regime (approximately 0.12 at cruise). The turbulence model used is FLUENT's Realizable $\kappa - \epsilon$ model, which typically shows substantial improvements over the standard $\kappa - \epsilon$ model where the flow features strong streamline curvature, vortices and rotations. However, FLUENT cautions against the use of the model in cases where the domain includes both rotational and static subdomains as is the case in the pitch roll and yaw rate test points discussed earlier. In these cases the standard RNG $\kappa - \epsilon$ models have been used.

A segregated solver was used to analyze the problem for initial runs. Segregated solvers tend to be slower than the coupled solvers but have lower memory requirements. At the outset of this work 64 bit computers were not widely adopted and the RAM limit was quite low. Some additional analyses have been done throughout this work and in some cases run on 64 bit computers with up to 64GB of RAM, in which case the coupled solvers were used.

Mesh adaptation was performed on each run based on the value of the boundary layer thickness, or y^+ values. This adapts the mesh and refines it based on initial results calculated after a set number of iterations and can aid in convergence and overall accuracy of results.

Each test point was run and non-dimensional quantities calculated based on integrated forces and moments calculated in FLUENT's post processor using "User Defined Functions". The results from these runs were used to fill in the more extensive vortex lattice results described in a previous section. This database of results served as the basis for all subsequent analyses such as control surface scheduling and design, stability and control investigation and build-up of 6dof simulators. Figure 18 below shows some results for the alpha sweep and compares this to the results predicted by the augmented VLM (with corrections allowing for form drag of lifting surfaces and fuselage) describe previously.

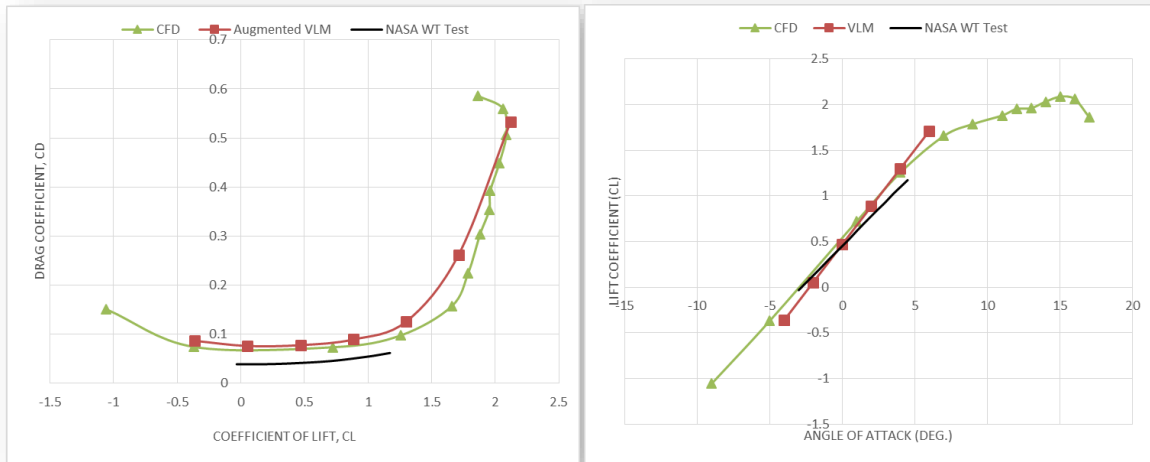


FIGURE 18 - COMPARISON OF AERODYNAMIC PREDICTIONS (VLM & CFD) WITH WIND TUNNEL RESULTS

Also of note in the above figures is the data corresponding to the Wind Tunnel Results obtained from work done at the NASA Ames Wind Tunnel by Boeing (see Figure 19 below). These results were not made available until two years after the initial study was performed but are included here as a comparison. From this comparison we can see that the wind tunnel drag values were much lower than those predicted analytically. This may be partially due to the addition of the drag components that were added to the analytical results due to antennae, landing gear etc.



FIGURE 19 - BOEING SENSORCRAFT IN THE TRANSONIC DYNAMICS TUNNEL AT NASA LANGLEY [55]

3.1.3 Stability Analysis

The stability derivatives resulting from the aerodynamic analyses, along with the scaled mass properties of the full scale aircraft, were used to compile the state space model of the aircraft. A subsequent Eigen mode analysis of the decoupled lateral/longitudinal sets of equations yielded and insight into the dynamic stability of the configuration. The following results represent the most adverse mass distribution in terms of the dynamic stability.

TABLE 5 - DYNAMIC STABILITY FOR BASELINE CONFIGURATION

Mode	Eigenvalues		$T_{1/2}$	$n_{1/2}$	Period	freq.	ζ	ω_n	τ
	real	Im	sec.	-	s	$1/s$			
Phugoid	-4.34E-03	0.4621	159.756	11.719	13.596	0.074	0.009	0.462	
Short Period	-2.92181	2.8577	0.237	0.108	2.199	0.455	0.715	4.087	
Dutch Roll	6.19E-02	1.6562	11.200	2.944	3.794	0.264	-0.037	1.657	
Roll	-4.65472	0	0.149						0.214836
Spiral	-3.76E-02	0	18.446						26.61826

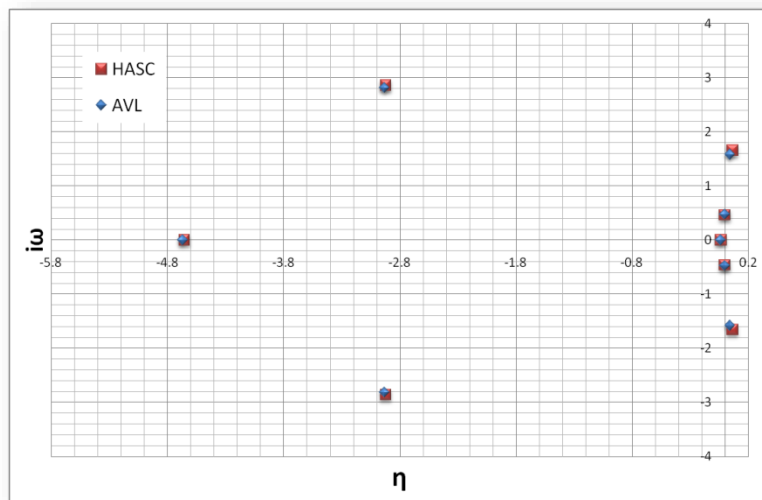


FIGURE 20 - EIGENVALUES OF BASELINE GEOMETRY

The results show that all modes are stable with the exception of the Dutch roll mode. Flying qualities are rated based on the guidelines outlined in [56]. All of the modes achieved highest rating for flying quality, level 1, in all

categories of flight with the exception of two. The Dutch roll mode is unstable and the Phugoid mode only achieved level 2 rating in all categories (A, B and C).

The level 2 rating is defined as having “Flying qualities adequate to accomplish the mission Flight Phase, but some increase in pilot workload or degradation in mission effectiveness, or both, exists”. The level 2 flying quality in the case of the Phugoid mode is not of large concern to the RPV pilot since the perceived flying qualities for small unmanned aircraft are quite different from that of full scale aircraft and small Phugoid instabilities are of little concern. Of greater concern however is the potentially unstable Dutch roll mode. The following design modifications were proposed as possible solutions to this problem.

3.1.4 Proposed Modifications

Three solutions are investigated here to deal with the lack of yaw stability and control authority.

3.1.4.1 Addition of Vertical Surface with Control Surface

The first solution involves the addition of a vertical tail surface aft of the tail boom which would be fitted with a control surface. Figure 21 below shows the model modified with this additional surface.

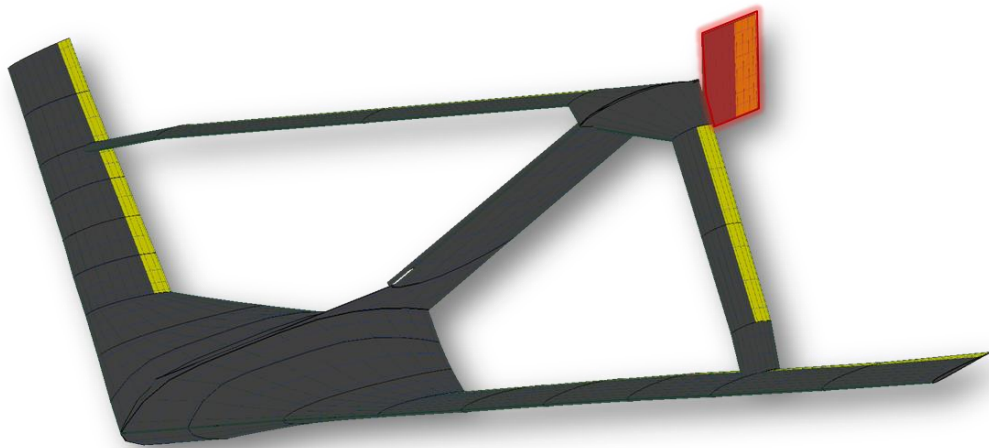


FIGURE 21 - CONFIGURATION WITH VERTICAL TAIL SURFACE

An analysis performed on this configuration shows its effectiveness at damping out the Dutch roll. The addition of the surface improved the Dutch roll mode to a level 2 flight quality while adding sufficient yaw authority. The other modes see little change as a result of this modification with the exception of the spiral stability mode which sees a drop in its time to double amplitude. The spiral stability mode does however maintain a level 1 quality rating.

TABLE 6 - DYNAMIC STABILITY FOR CONFIGURATION WITH ADDITION OF VERTICAL SURFACE

Mode	Eigenvalues		$T_{1/2}$	$n_{1/2}$	Period	freq.	ζ	ω_n	τ
	real	Im	sec.	-	s	$1/s$			
Phugoid	-4.34E-03	0.4621	159.756	11.719	13.596	0.074	0.009	0.462	
Short Period	-2.92181	2.8577	0.237	0.108	2.199	0.455	0.715	4.087	
Dutch Roll	-6.81E-02	2.0564	10.171	3.320	3.055	0.327	0.033	2.058	
Roll	-4.65472	0	0.149						0.214836
Spiral	-3.07E-02	0	22.598						32.60913

One potential drawback of this modification is its effect on the aeroelastic response of the aircraft. The addition of this surface has an effect on the lateral aerodynamic modes which may play a role in the aeroelastic modes.

3.1.4.2 Addition of Conventional Tail Boom

The pilot who was to be operating the RPV has voiced some concern about the amount of pitch authority that would be available to the aircraft. The VLM analysis showed adequate authority is available but it may have been desirable to include modifications to the early flight vehicle just in case. At a project design meeting between the USAF, Virginia Tech and the University of Victoria, LTCol Shearer and Maxwell Blair from USAF ARFL/AFIT suggested the addition of a conventional tail boom to the initial flight test article. This would add additional pitch authority from an elevator surface mounted to the new horizontal surface, while also adding the benefits described in the previous section. Figure 22 below shows the proposed modification to the baseline configuration.

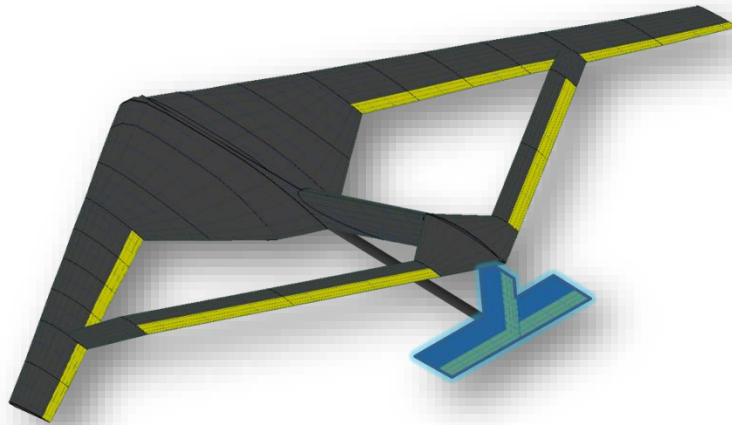


FIGURE 22 – CONFIGURATION WITH ADDITION OF CONVENTIONAL TAIL SURFACES

An analysis performed on this configuration shows the Dutch roll mode is made stable although only to a quality level of three. This is due to the fact that the tail, although the same size as in the previous case, is at a shorter distance from the cg. A further improvement is possible through increasing the size of the vertical stab and/or increasing the boom length. The other modes are affected by a small degree but not enough to change their flying quality ratings. The Phugoid mode was improved however but is still rated level 2. The results of these analyses are shown in Table 7 below.

TABLE 7- STABILITY FOR CONFIGURATION WITH ADDITION OF CONVENTIONAL TAIL SURFACES

Mode	Eigenvalues		T1/2	n1/2	P	f	ζ	ω_n	τ
	real	Im	sec.	-	s	1/s			
Phugoid	-5.35E-03 ±	0.4582	129.431	9.413	13.714	0.073	0.012	0.458	
Short Period	-3.25378 ±	2.8376	0.213	0.096	2.214	0.452	0.754	4.317	
Dutch Roll	-6.63E-03 ±	1.7277	104.551	28.672	3.637	0.275	0.004	1.728	
Roll	-4.67633 ±	0	0.148						0.213843
Spiral	-3.70E-02 ±	0	18.746						27.05026

The same potential drawback arises for this configuration that did with the previous. Making large changes in the aerodynamics will have an effect on the aeroelastic response of the aircraft. This is even more drastic with the addition of the horizontal surface as it affect the pitch/plunge of the aircraft in flight. Another potential drawback that existed with this solution was that the added mass at such a large distance aft of the cg would

make the trimming of the aircraft cg even more difficult (as it turns out a big challenge throughout testing was trimming the cg sufficiently forward to achieve desired longitudinal response).

3.1.4.3 Active Control Using Existing Surfaces

The final solution investigated involved scheduling the existing surfaces to gain some level of yaw authority which can then be used with an active yaw damping system. Yaw damper systems are quite common with RC aircraft and can be purchased inexpensively off the shelf. Their operation varies but most consist of a unit which is placed in-line between the remote receiver and the rudder servos. Some units also allow mixing of multiple surfaces for yaw control such as with y-tails.

Another more robust option investigated at the time was to use stability augmentation via an autopilot unit. When in autopilot mode the yaw is damped using the built in feedback loops, but the concern was in the flight regimes where the pilot is flying the aircraft in manual mode and the yaw damper was deactivated (as is the case with many autopilots). However, the Piccolo II autopilot (the autopilot ultimately chosen for the 5m aircraft) has a built in yaw damping feature which allows the pilot to control the aircraft remotely in manual mode while automatically mixing in rudder commands to damp out unwanted yaw. The primary mode of operation however would be the fly by wire mode in which all of the inner loop gains are handled by the autopilot and only high level commands are sent to the aircraft from the pilot (such as roll, yaw, bank and airspeed).

In order for these solutions to be effective and robust, an adequate degree of yaw authority is required. If no modifications are made to the geometry then the yaw control must come as a result of deflecting a combination of the existing controls.

This solution of only using existing surfaces, and not modifying the OML, was the most desirable in terms of maintaining a faithful aeroelastic response. Upon analyzing the alternatives and proposing them to the AFRL, the decision was made to follow this option as it was most faithful to the original configuration. There does exist the large drawback of added complexity due to advanced scheduling schemes and the danger of flying an

aircraft that is potentially unstable if fully manual control is required at any point during operations. As a result a greater emphasis was placed on simulation and reduced scale flight testing using models of increasing risk and complexity as will be presented in later sections.

3.2 Avionics and Control

Many control schemes are possible with so many control surfaces. Many options were envisioned and evaluated both analytically and experimentally. The following are a subset of options that were looked at and subsequently flown on reduced scale aircraft.

3.2.1 Crow Mixing of Surfaces for Drag Rudder Effect

The first scheme involved deflecting the outer flap down and outer elevator up on one side of the aircraft. The amounts for each deflection have to be chosen so as to minimize the effect on motion about the other axes, while achieving the required yawing moment. The effect on the roll is twofold; first, the increase in drag caused by the deflected surfaces acting at a distance outboard of cg causes a yawing moment. The second effect is caused by the resolved components of lift in the spanwise direction due to the dihedral/anhedral of the wings. This effect is shown in the following figure.

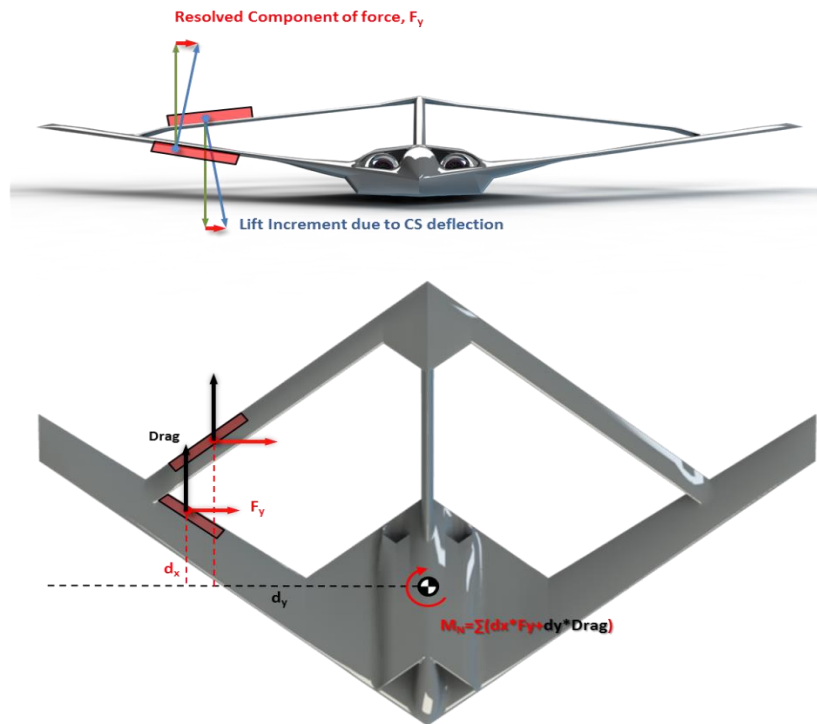


FIGURE 23 - EFFECT OF RESOLVED LIFT INCREMENT ON AIRCRAFT YAW

In order to ensure that the yawing moment resulting from these control surface movements is uncoupled from the other aircraft degrees of freedom as much as possible, a combination of deflections from other surfaces was required to trim the aircraft. The trim solution for this case is quite complicated as there exist an infinite number of solutions. In order to solve the trim equations additional constraints had to be added to achieve a unique solution. These included minimizing the controller effort (ie minimizing the sum of the square of deflections for all surfaces involved in trimming the aircraft) and using some surfaces only for one function (ie tying both inner elevators together to reduce the number of trim variables). This scheme showed good yaw authority and subsequent flights using reduced complexity models allowed a flat turn to be achieved through yaw input only.

3.2.2 Split Surfaces for Drag Rudder Effect

Several split surface options were investigated. This included split flaps at the outer elevator station and the outer flap station as shown in Figure 24 below. The vortex lattice method cannot account for the pressure drag effect of the split flap so a 2D CFD analysis was run on the local station for a sweep of split flap settings. These results were then integrated along the local span where the split flaps are employed in order to determine the effect of the drag rudder on the yaw, pitch and roll moments.

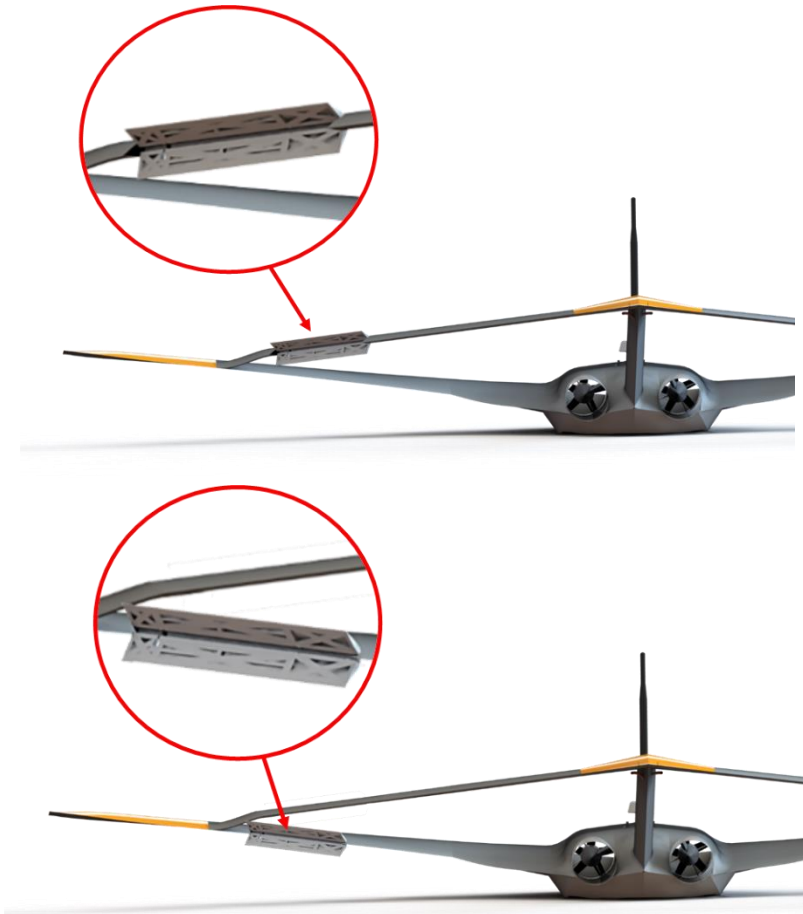


FIGURE 24 - LOCATIONS OF SPLIT DRAG RUDDERS AT OUTBOARD ELEVATOR (TOP) AND OUTBOARD FLAP (BOTTOM) STATIONS

The aft wing, outboard elevator split flap showed small amounts of yaw authority and was deemed ineffectual by pilots in subsequent flight-testing using the reduced complexity aircraft. The forward wing, outer flap location provided very good authority however and was the most effective of all proposed solutions at achieving yaw authority when flown on the smaller, reduced complexity models. However, fabrication proved very difficult due to the extremely thin cross section of the flap at that location and there was great concern that the surface would not be able to handle the high aero loads expected by the 5m aircraft. Another large advantage of the split flap control surfaces is that they could also be deployed as airbrakes in the landing and approach phase of flight.

3.2.3 Vertical Rudder in Boom

Analytical Calculations showed very low yaw authority for the rudder surface. However, tests were performed with the reduced complexity models in flight. While there was a minor effect on yaw there was also a degree of pitch coupling at high rudder deflections.

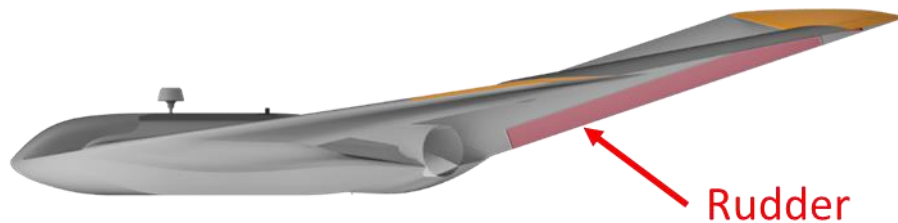


FIGURE 25 - SIDE VIEW SHOWING RUDDER LOCATION

3.2.4 Aileron Differential and Trim Tabs

Flight testing with the reduced complexity models showed that a great deal of the Dutch Roll oscillations are initiated at the outset of the banking maneuvers. This initial roll causes an adverse yawing moment which yaws out of the turn initially. The autopilot continues the roll and after a delay the aircraft reaches its maximum adverse yaw and begins to yaw back into the turn which accentuates the roll. This causes a large overshoot and initiates an oscillatory roll yaw coupling.

When the autopilot is set to limit the roll rate when initiating the bank the resulting Dutch roll oscillations are greatly reduced. However, if the adverse yaw can be further reduced this results in a more coordinated turn and prevents the large perturbations in yaw that then lead to the Dutch roll. The aircraft is still marginally stable in the Dutch roll but since it is not excited to the same degree takes much less time to damp out. This damping can be magnified even without direct yaw authority since the ailerons help to damp out the roll axis. Therefore it is very desirable to reduce the initial perturbation caused by the adverse yaw.

Two methods have been used to reduce the adverse yaw. The first involved aileron differential, where the aileron travelling up (ie the right aileron when rolling right) is deflected a larger amount than the aileron

travelling down. This effectively reduces the induced drag on the outer aileron and therefore reduces the adverse yaw. This is shown graphically in Figure 26 below.



FIGURE 26 - RIGHT ROLLING MANEUVER USING AILERON DIFFERENTIAL

The other method applied with great success was the addition of special drag tabs under the aileron. These effectively add unsymmetrical drag, when an aileron goes up the drag tab comes into the airflow and causes drag yawing the aircraft into the turn. On the downward deflected aileron the drag tab stays in contact with the underside of the wing and does not produce any additional drag. Figure 27 below shows this graphically.

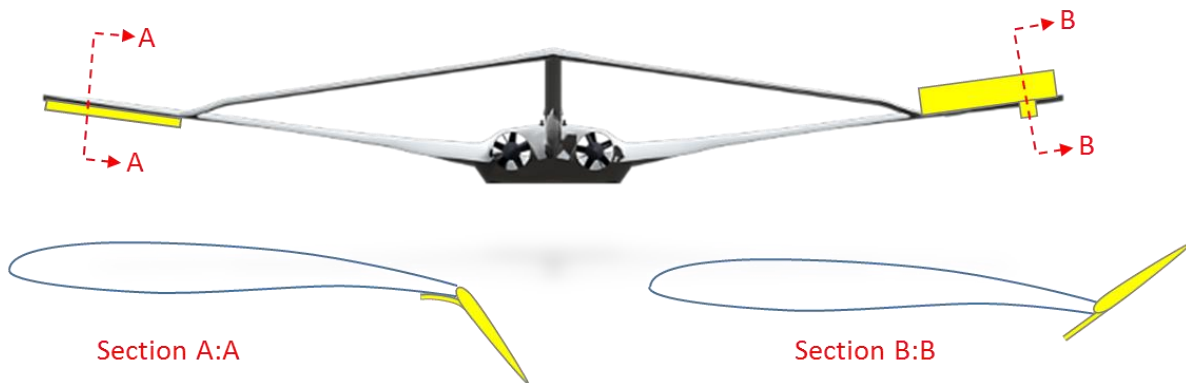


FIGURE 27 - FLEXIBLE DRAG TAB USED TO COUNTERACT ADVERSE YAW

Both of these methods were very effective in preventing the large yaw perturbations when entering a banked command and therefore very little Dutch roll was seen when flying in these configurations. There still exists some low level oscillations after entering/exiting banks and when yaw was perturbed by outside forces such as wind gusts. However, when the roll axis of the controller is properly tuned this scheme results in very acceptable handling qualities. The other advantage here is the simplicity since no complex mixing schedules

are required and very little trimming is required to balance the other axes of the aircraft. For these reasons these techniques were employed on all reduced and full scale aircraft.

3.3 Reduced Scale Testing and Simulation

The analytical characterization of the Joined Wing SensorCraft's aerodynamics, and subsequent stability and control analysis, predicted some undesirable behavior in Dutch Roll and an overall lack of authority in yaw. While several options were proposed in the previous section it was determined that simulations would need to be run to validate these proposed control schemes. In addition, the simulators would provide a means to train pilots and ground crew in preparation for actual flight tests. This section also includes a series of reduced scale flight tests that were performed in the lead up to the flight testing of the 5m RPV using a variety of the models of increasing size and complexity.

3.3.1 Simulation

Simulation for the JWSC FTP is broken into three categories: 6 Degree of Freedom (DoF) flight simulation, hardware in the loop simulation and pilot training. Each category is described in the following section.

3.3.1.1 6 Degree of Freedom Flight Simulation

A 6 DoF simulator was built using a variety of default and custom Simulink blocks. Matlab Aerospace Blockset and the Unmanned Dynamics Aerosim v1.2 Blockset provided some preconfigured physics modelling while custom blocks were developed to model non-linear aerodynamics, allow interfacing with RC controllers and output data for further analysis. The simulator is based on a set of first order aerodynamic terms but has been altered to allow non-linear aerodynamics to be modeled through the use of multi-dimensional lookup tables. This allows coefficients to be input for various angles of attack and sideslip angles where nonlinear aerodynamic terms have been captured (from CFD results for instance).

The simulator calculates the aircraft states and then outputs this to an open source flight simulator, FlightGear for visualization. A custom block has also been created and incorporated that allows the pilot to control the aircraft using a standard radio controlled (R/C) transmitter attached to the computer through the "training" port. Figure 28 shows a typical flight simulation with the Simulink model, custom gauges and FlightGear all running

simultaneously. This simulator is very robust and flexible. It has been used to model, tune and simulate a variety of autopilots used throughout this work (Micropilot, Procerus and Ardupilot).

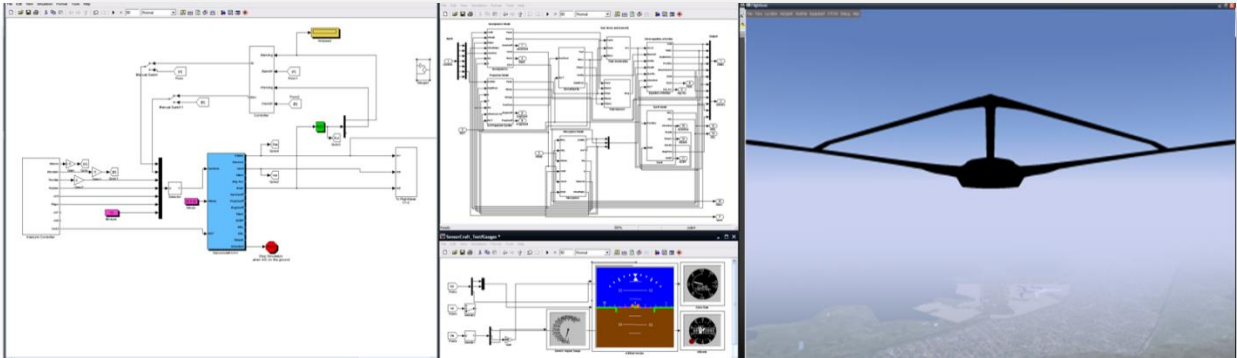


FIGURE 28 - SIX DEGREE OF FREEDOM FLIGHT SIMULATOR

More recently, the simulator supplied by CloudCap with the Piccolo autopilots has been used for software in the loop simulation. The CloudCap simulator interfaces with the ground control software developed for the Piccolo family of autopilots and can also be visualized using Open Source flight simulators. This solution has been valuable for training using the Piccolo ground control station software but is limited to their avionics only and has a limited set of physics that can be modelled. For instance, at the present time there exists no method to simulate turbine engines using the CloudCap simulator so a custom DLL had to be written to more accurately capture the physics of the 5m Joined Wing RPV.

3.3.1.2 Hardware in the Loop Simulation

The simulators have been taken one step further as hardware in the loop testing is performed that allows the aircraft autopilot to be incorporated into the simulation. The Micropilot 2128 THWIL (True Hardware In the Loop) system was used to evaluate their autopilot. The system uses National Instruments data acquisition hardware to interface the 2128 autopilot within the simulator built in Simulink. The hardware in the loop setup electrically stimulates all sensor outputs using analog to digital conversion, signal conditioning and pulse-width-modulation boards. This allows a higher level of fidelity by more closely replicating in-flight conditions while on the ground.

For Hardware in the Loop simulations involving the CloudCap autopilots, their supplied simulator tool is used. This simulator is also capable of HWIL testing by connecting the avionics to the computer through an integrated CAN bus. This setup was used extensively once the Piccolo was chosen as the primary autopilot.

3.3.1.3 Pilot Training in RealFlight® COTS Simulator

The unique configuration and flight characteristics of the JWSC makes flying the RPV a challenge for even the most experienced pilots. The 6 DoF simulators previously discussed address this problem by allowing the pilot to fly the simulator using a conventional R/C transmitter. Unfortunately, a gap between the simulation and reality still exists because the FlightGear visualization program was designed for manned aircraft simulation, and accordingly the flying sites and pilot locations (where the user can view the aircraft from) are not ideal for RPV flight simulation. In order to address these problems and further reduce the gap between simulation and RPV flight, a model was created for use in RealFlight G5, the most advanced R/C flight simulator in Knife Edge Software’s widely used R/C flight simulator line. A screenshot of the JWSC RPV in flight in RealFlight G5 is shown in Figure 29.

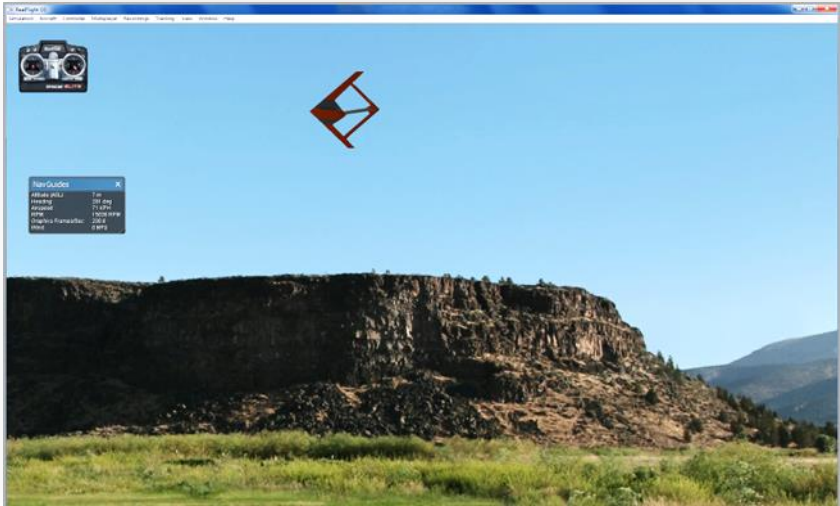


FIGURE 29 - SCREENSHOT FROM REALFLIGHT G5 SIMULATOR USED FOR PILOT FAMILIARIZATION

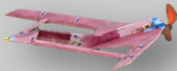
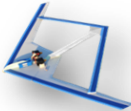
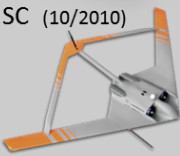

Since RealFlight is commercially available and easy to deploy it was a valuable tool to train pilots off site. The previously discussed 6 DoF simulators are complicated and difficult to deploy, beyond the capability of the pilots

using consumer grade computers in a home based environment. The RealFlight software made it easy to supply pilots with simple software that could be used for training and familiarization over the course of this work. The small tradeoff in terms of fidelity of the physics was worth it for this added degree of simplicity and pilots regarded it as a useful tool in the build up to flight test campaigns.

3.3.2 Reduced Scale Flight Testing

A key to the success of this work was the methodology adopted to minimize project risk through a series of reduced complexity flight tests using a series of models with increasing fidelity. This included development of quick and dirty models made of inexpensive materials, built using simple techniques, to investigate fundamental behaviors of the SensorCraft configuration. Over time these models were improved to the point that they shared the exact same scaled thrust, mass properties and outer mold lines of the full scale aircraft. In addition, many flights were performed with more conventional aircraft platforms in order to test avionics, instrumentation and train ground crew while removing the unknowns and challenges posed by the highly unconventional joined wing configuration. The following table summarizes some of the reduced complexity aircraft used in this work with additional information provided in the subsequent sub sections.

TABLE 8 – REDUCED COMPLEXITY MODELS USED IN THIS WORK

Name (First Flight)	Qty	MTOW Wingspan	Objective	Designed/Built By
FP Foamie (03/2010) 	1	1 kg 1.68m (3.67%)	<ul style="list-style-type: none"> • First flying model • Investigate predicted yaw instability 	<ul style="list-style-type: none"> • Tyler Aarons (VT)
TC Foamie (06/2010) 	3	2.1 kg 1.85 m	<ul style="list-style-type: none"> • Correct shortcomings of Foamie • TO and LDG strategies • Control Surface Scheduling 	<ul style="list-style-type: none"> • Jenner Richards (Uvic)
Mini SC (10/2010) 	8+	4.6 kg 1.85 m	<ul style="list-style-type: none"> • Control development • Test manufacturing techniques • Test Plan optimization 	<ul style="list-style-type: none"> • Jenner Richards (Uvic)
QT1.1 UAV (09/2009) 	4	23 kg 3.06 m	<ul style="list-style-type: none"> • Instrumentation testing • Flight test procedure development • Crew Training 	<ul style="list-style-type: none"> • Jenner Richards (Uvic)

3.3.2.1 Flat Plate “Foamie”

This first iteration of reduced complexity aircraft was conceived and built by Tyler Aarons of Virginia Tech, who at the time was responsible for developing the flight test plan and various instrumentation systems for the proposed 5m flights. The aircraft was built and flown at Virginia Tech in Blacksburg Virginia in the spring of 2010.

The model was of flat plate foam construction with a flying weight of 2.2 lbs. This aircraft was designed to serve as an experimental platform to test and validate proposed control schemes as well as address the yaw stability and control authority questions. The model, shown in flight in Figure 30, is constructed of 0.25 inch flat extruded polystyrene fanfold insulation underlayment board with carbon fiber arrow shaft spars. The streamer shown in Figure 30 is added to aid the pilot in referencing the aircraft during flight. The unique, diamond shape of the JWSC proved to be difficult to track, especially during turns, due to the similarities between the profile of the aircraft from the front and side when viewed from a distance.



FIGURE 30 - FLAT PLATE FOAMIE IN FLIGHT DURING A FLIGHT TEST.

When designing the model, a balance was struck between the simplicity and operability of the model and the desired accuracy of the representation of the flight dynamics of the full scale RPV. The reduced scale features dihedral, anhedral and sweep angles representative of the full scale geometry; however, the camber and complex spanwise twist distribution present in fore and aft wings was omitted due to the selected material. Additionally, the turbine propulsion system was replaced with a simplified, high thrust-to-weight ratio propeller setup for ease of operation and maintenance. Finally, the laminar flow airfoils selected for the full scale RPV are replaced by flat plates due to the small scale of the model and the chosen materials.

A series of flight tests were completed to first establish an acceptable CG location for the model and trim the aircraft. These initial tests showed that the configuration could be flown under manual control but several shortcomings were apparent. The first was the Dutch roll and lack of yaw authority using a conventional rudder and the second was poor flying qualities, likely due to the limitations of the building method. The aircraft tended to tip stall in turns and at high angles of attack and there was a large amount of pitch due to throttle input. The former was due to the lack of accurate twist distribution and airfoil shape along the wing while the latter was likely due to thrust line placement and or cg location.

3.3.2.2 Twist Corrected “Foamie”

The second sub-scale model created, the *EDF Twist Corrected Foamie*, was designed and built to correct the shortcomings of the *Flat Plate Foamie*. The model, shown in Figure 31, is constructed of extruded polystyrene foam wrapped in fiberglass with unidirectional carbon strips to provide stiffness to the lifting surfaces. When designing the model, the two primary goals were to include the proper twist distribution in both the fore and aft wings and to include an EDF propulsion system capable of providing accurately scaled thrust characteristics.

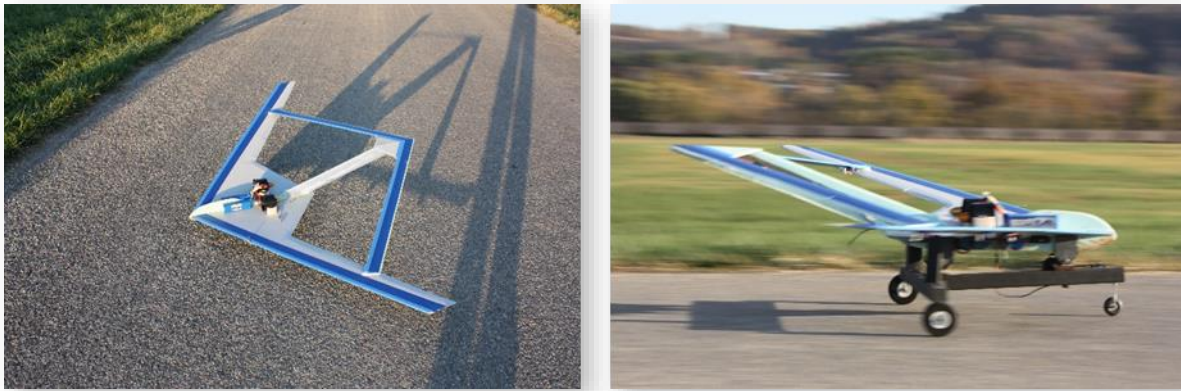


FIGURE 31 - TWIST CORRECTED FOAMIE

Preliminary flight testing showed a marked improvement over the *Flat Plate Foamie*. The twist distribution allowed stable flight and no tip stalling was noticed during normal operation maneuvers. Three of these aircraft were built and tested in flight operations spanning over 60 flights. During these flights many specific goals were achieved including.

- *Control Surface Schedule Testing – these aircraft had a full complement of control surfaces and were often modified to test additional ones such as split flaps. All of the control scheduling schemes introduced in the previous section were evaluated using these aircraft.*
- *Autopilot Testing – Due to the low cost of these airframes they were ideal test beds for experimental hardware and control algorithms. This aircraft was the first to fly with stability augmentation and in fully autonomous mode*
- *Launch and recovery – this aircraft was used to evaluate launch and recovery methods for the subsequent Mini SensorCraft configuration and the 5m RPV. Launch methods included hand,*

bungee and catapult launch as well as conventional landing gear and finally takeoff using a detachable cart (as pictured in Figure 31 above)

- *Pilot and Ground Crew Training – the Twist Corrected Foamie configuration served as an ideal platform for training pilots and ground crew. The low flight speed, light weight and foam construction minimized damage resulting from crashes and was easy to repair. The challenges posed by this marginally stable configuration required many flights to become accustomed to and proved to be invaluable to pilots as they learned to fly this aircraft. Autonomous flights required ground crew for setup and operation and these early flights served to train personnel and guide future operating standards and best practices.*

3.3.2.3 Mini SensorCraft R1

The final iteration of the reduced complexity flight test articles is the *Mini SensorCraft* configuration. This aircraft is a 37% scaled version of the 5m aircraft with an equivalent outer mold line. The aircraft is fabricated using wet layups consisting of carbon and epoxy and also served as an investigation into fabrication and building techniques that would be used on the larger 5m configuration. The tooling was made using a CNC machine built by the author out of Medium Density Fiber Board. The machined molds were plasticized using an epoxy based sealing compound and finished using wet sanding and polishing compound. Figure 32 below shows a completed mold, laying up of wing skins and finally, a fuselage section after being removed from its mold.

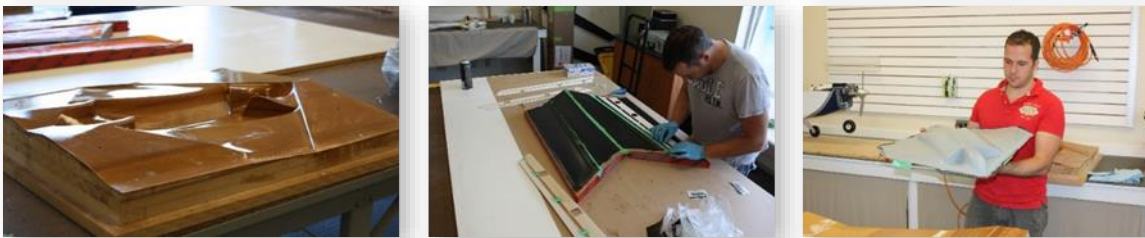


FIGURE 32 - MINI SENSORCRAFT CONSTRUCTION

The *Mini SensorCraft* has seen three iterations, the Generation 1 (G1), Generation 2 (G2) and Flexible (F1) configurations. During the reduced complexity phase being discussed presently the configuration was in the Rigid 1 stage. (The G2 configuration involved an internal redesign to provide additional payload capacity and instrumentation and is described further in Chapter 6 along with the flexible F1 configuration).

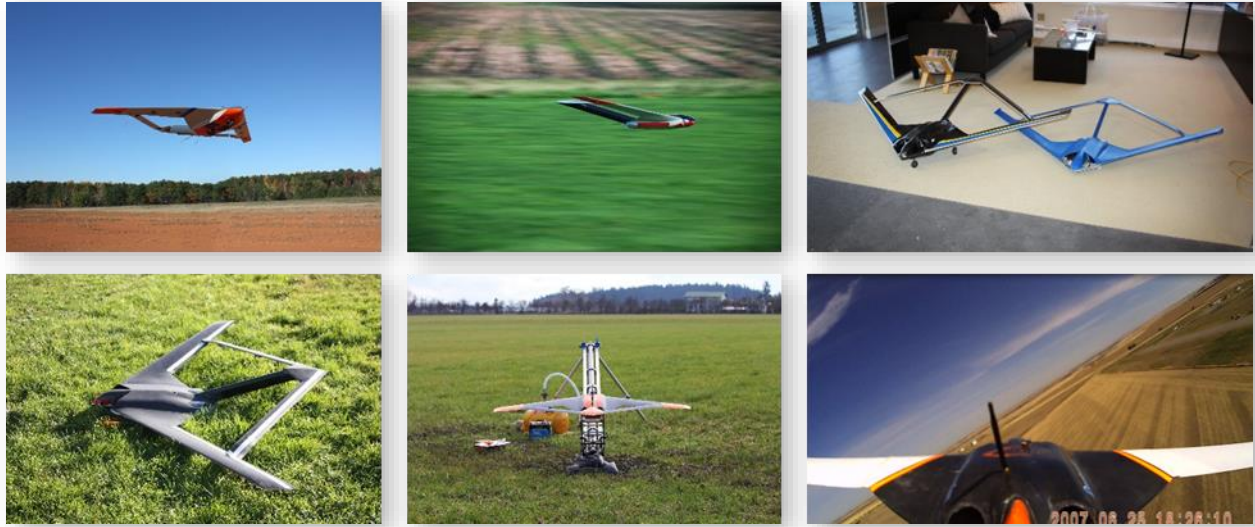


FIGURE 33 - VARIOUS GENERATION 1 MINI SENSORCRAFT RPVS

Figure 33 above shows seven of the G1 aircraft that were constructed. Two were always required to be on hand in the event that repairs needed to be carried out to an aircraft. Throughout this stage over 60 flights were conducted with these aircraft. The primary focus of these flights were as follows.

- *Parameter Identification and Aerodynamic Model Improvement – During all flights using the Mini SensorCraft, 6dof inertial data, airspeed, altitude, position and control surface deflections were logged. This information was post processed to determine aerodynamic parameters and further refined the aero model discussed previously*
- *Pilot and Ground Operator Training – this configuration showed larger Dutch Roll tendencies than the foam aircraft (closer to the theoretical predictions) and as such turned out to be a good training tool for pilots. They were used extensively in warm up flights by all pilots before flying the 5m aircraft.*
- *Autopilot Development and Tuning – Later flights with the Mini SensorCraft RPVs included the Piccolo Avionics (the same avionics flown in the 5m aircraft) which allowed autopilot evaluation and tuning.*
- *Instrumentation Evaluation – various sensors were evaluated and logged on board these aircraft.*
- *Ground/Flight Test Methodology Evaluation – procedures and testing methodology that was proposed for the 5m aircraft was evaluated on the Mini aircraft. This included the evaluation of full scale test points as well as ground test procedures such as static thrust and inertia testing.*

3.3.2.4 QT1.1

The QT1.1 platform is a UAV employing a more conventional configuration as seen in Figure 34 below. The UAV was developed and built by the author since at the time no adequate commercial solutions existed to meet the cost, reliability and flying qualities required.

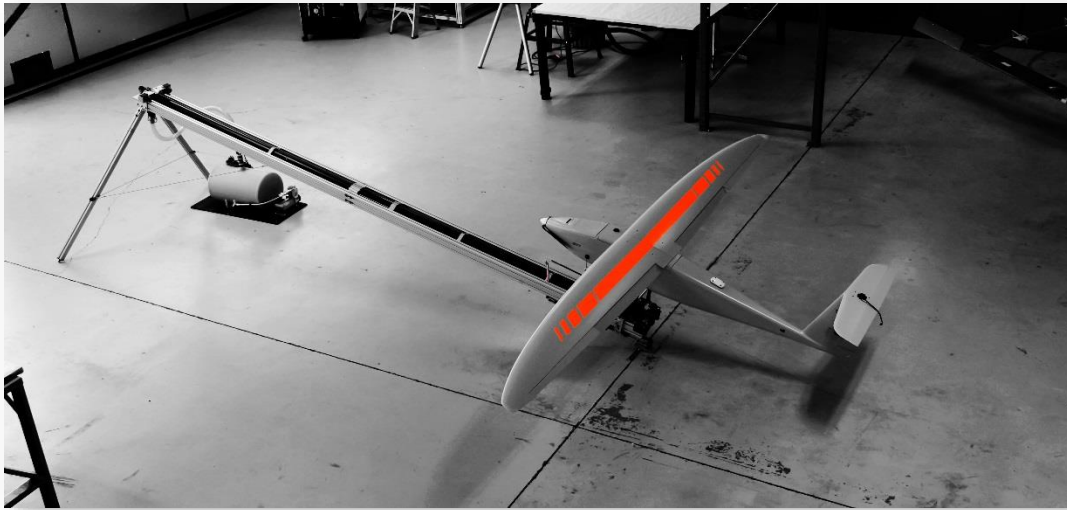


FIGURE 34 - QT1.1 UAV

The aircraft was extremely reliable and served as a platform to test avionics, instrumentation and piloting methods including First Person View, FPV, in which the pilot flies the aircraft from the ground station using a forward facing camera. The platform was used to evaluate all autopilots used in this work. When additional functionality or features were proposed for any of the SensorCraft RPVs they were usually evaluated using the QT1.1 platform. Figure 34 above shows one of the QT1's on the Pneumatic Launcher while Figure 35 shows a QT1 being launched in fully autonomous mode using the Piccolo avionics.



FIGURE 35 - AUTONOMOUS CATAPULT TAKEOFF TEST

3.5 Conclusions

Before the 5m configuration could be built and flown, a greater understanding of the Joined Wing SensorCraft configuration was required. Foremost was the aerodynamic properties and the resulting stability and control characteristics.

Initial studies using vortex lattice methods, supplemented with higher order CFD results, show that the aircraft overall exhibits reasonable flying qualities with the exception of a marginally stable Dutch Roll mode. Compounding the problem, the aircraft has little yaw authority due the lack of a conventional vertical tail and resulting poor effectiveness of a rudder surface. In order to effectively operate the configuration, it was decided that some combination of avionics, modifications to the aerodynamic shape and advanced control surface scheduling were required.

While some modifications to the outer mold line were investigated and shown to be effective, it was decided that this was too undesirable in terms of obtaining the scaled aeroelastic response. Therefore, it was decided to obtain reasonable dynamic stability characteristics through the use of stability augmentation using and autopilot. Several control surface schedules were investigate to determine an effective way to obtain yaw authority while still uncoupling other control axes. Two control schemes were chosen and subsequently used on the remainder of the aircraft used in this work.

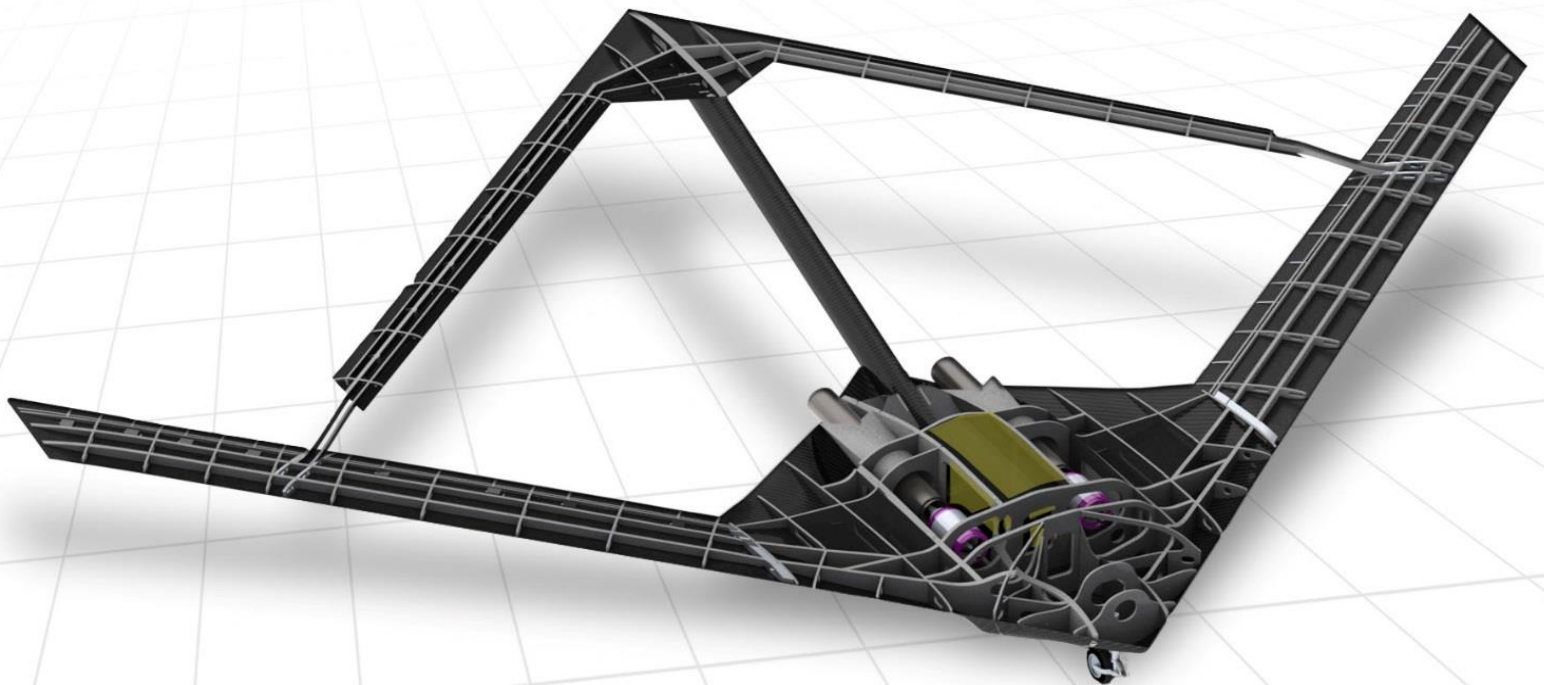
- *Damping Dutch roll using Drag Rudders located at the outer flap location on the forward wing.*
- *Damping of Dutch Roll using only the roll axis stabilization while also using a combination of aileron differential and drag tabs to prevent the large yaw perturbations due to roll commands.*

Several autopilots were evaluated and the Piccolo was determined to be the best choice due to its maturity, robustness of control architecture and leading technical support. This and other autopilots were evaluated using a variety of airframes as well as hardware in the loop and software based simulation.

A key to the success of a project of this magnitude is the incremental approach to both flight risk and complexity. A series of reduced scale aircraft were evaluated (ranging from flat plate foam models to 1.85m “Mini”

SensorCraft employing equivalent outer mold lines) in over 100 flight tests. They were instrumental in evaluating hardware, experimentally determining control schemes and training pilots/ground crew. These reduced scale aircraft continued to be flown throughout the duration of this project and lessons learned from this stage were directly transferable to the subsequent design and testing of the 5m configuration.

Chapter 4 - 5m Configuration Evaluation and Testing



4.1 Design of 5m RPV

The desired test point chosen to evaluate the Boeing SensorCraft corresponds a 5m span, tested at an elevation that corresponds to the predicted flight range in Foremost Alberta. Initially, a rigid aircraft was designed with the intention of gaining better understanding of system weights, space reservations and constraints on the structure imposed by flightworthiness requirements. The aircraft is not truly rigid but rather very stiff to ensure adequate safety margins and reduce the challenge of flexible lifting surfaces that would be imposed by aeroelastically equivalent wings. The ultimate intent was to first fly this rigid RPV to gain better understanding, train crew etc, and then re-wing the fuselage with the aeroelastically equivalent lifting surfaces.

This section outlines the process that went into sizing, building, ground testing and ultimately flight testing the 5m configuration. The section then concludes with some post processed results from initial flight tests and recommendations carried forward to subsequent aeroelastically scaled aircraft design.

4.1.1 Structural Sizing

A Finite Element Model was developed as the basis for the initial sizing of the structure. A conventional rib/spar design was developed with the bulk of the loading to be taken by the wing skins themselves. Each of the four wings (two forward, two aft) employed a forward and aft spar as well as a closeout spar along the aft of the wing just before the chord wise location of control surface cutouts. These spars were intended to act only as shear webs with most of the axial and bending loads taken by the spar cap that is integral with the upper and lower skins (like a monocoque structure). A cross section of the forward wing is shown below for clarity with shear webs shown in red, skins in yellow and conformal spar caps in blue.

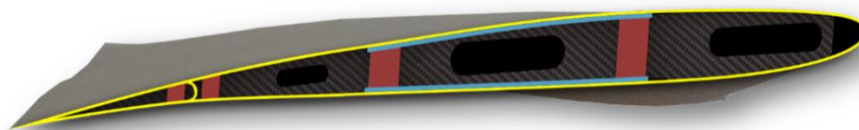


FIGURE 36 - WING CROSS SECTION SHOWING STRUCTURE MAKEUP OF WINGS

The fuselage structure was chosen to consist of a main load bearing skins with a series of bulkheads to prevent skin buckling, provide hard points for systems (ie engines, fuel tanks etc) and act as load paths to distribute external forces (for landing gear loads for instance). Figure 37 below shows the internal topology chosen as the basis for subsequent sizing. Pictured is a series of 2d surfaces that was subsequently meshed for downstream Analysis.

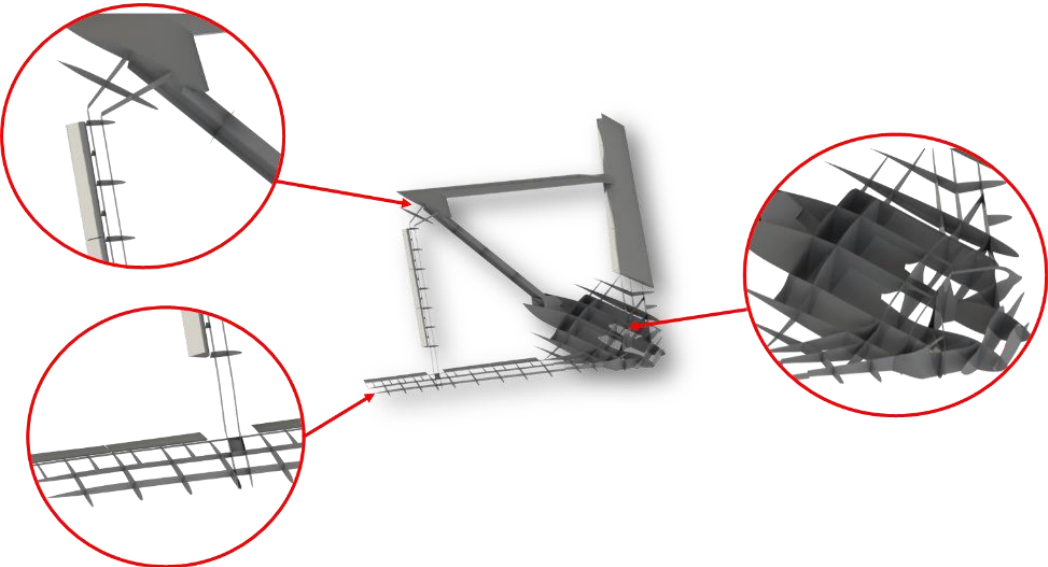


FIGURE 37 - INTERNAL AIRCRAFT STRUCTURE

Figure 37 shows control surfaces as well. Even though these are not loadbearing and typically could be excluded for structural sizing, their inclusion was critical for downstream investigations such as aeroelastic analyses where the overall structures mode shapes, including the control surfaces, are required.

Several meshes were generated of various fidelity for use in different analyses. The highest fidelity model, shown below, contains over 150,000 structural elements.

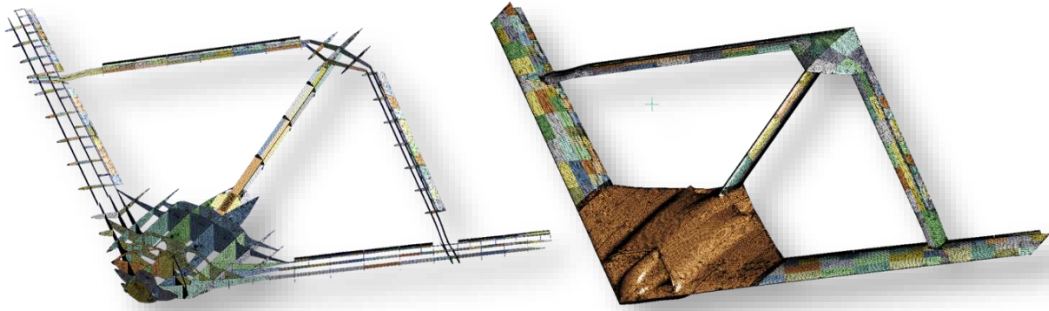


FIGURE 38 – INTERNAL AND EXTERNAL VIEW OF HIGH FIDELITY FE MESH

Materials used were primary composites, using 2d laminate shell elements. ANSYS Composites Pre-Post (ACP) was used to assign material properties to these elements using intuitive inputs such as laminate zones, number of plies and thickness as well as ply orientations. ACP then writes these laminate properties in a text based file format that can be read by the ANSYS structural model. Access to these text files allows layup properties to be changed parametrically by another application before the call to the ANSYS solver is made, allowing for integration into the optimization framework. Individual laminate properties were developed based on the constituent fabrics and resins using classical laminate theory. A combination of material was used in the laminates including plain weave and unidirectional carbon, plain weave fiberglass, Urethane Foam Core and plywood. Test coupons were also laid up to evaluate various laminates using a Tensile Testing Machine as shown in Figure 39.

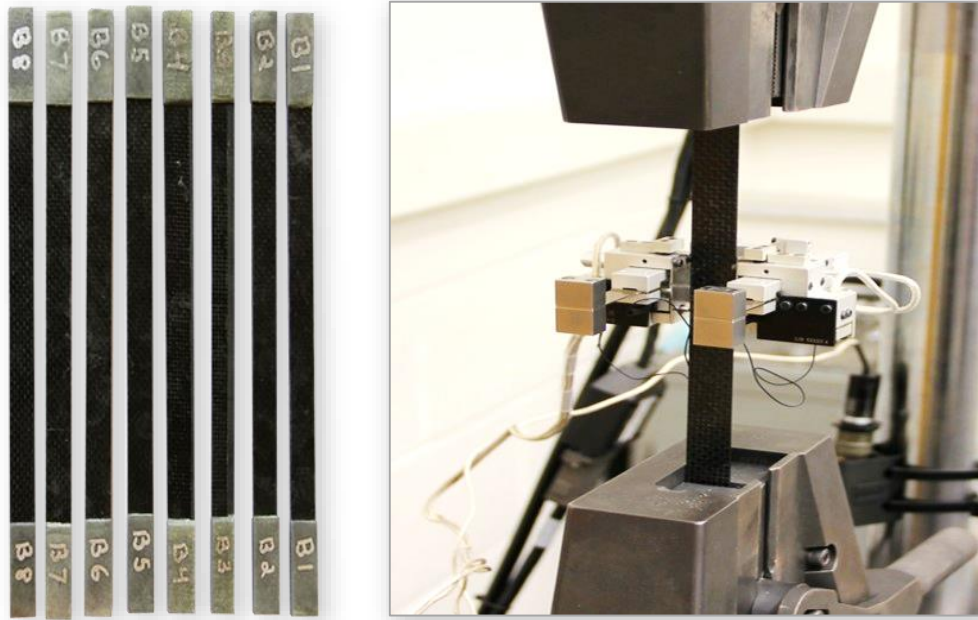


FIGURE 39 - SAMPLE TEST COUPONS (LEFT) UNDERGOING TENSILE TESTING (RIGHT)

Additional material properties were assigned to various parts in the FE model including 6061 aluminum for various structural members. Some additional reinforcements were included and were modelled using material properties for $\frac{1}{4}$ and $\frac{1}{2}$ hard plywood.

In order to accurately measure the mass of the structure additional modeling of components was achieved through the addition of point masses. Parts modelled in this manner included landing gear, avionics, fuel, engines and batteries. If a component was specified beforehand, it was modelled to capture the accurate mass and moments of inertia and applied to the point mass element. Otherwise, estimated values were assumed. In order to achieve the desired rigid body flight dynamics, the overall mass and moment of inertia of the entire aircraft had to match the scaled values of the full scale configuration. As such, trimming bays were designed into the structure and here tailored masses were added to the FE model in order to match the desired overall mass properties. Figure 40 below outlines the locations of these trimming bays.

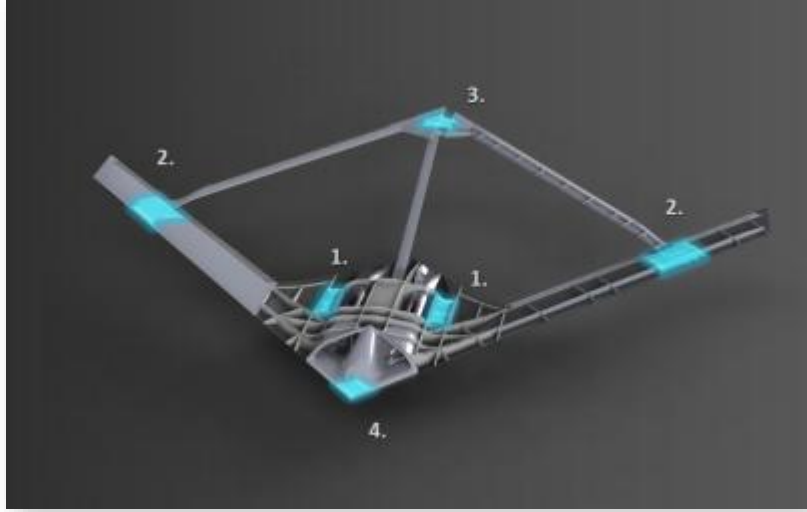


FIGURE 40 - LOCATION OF TRIMMING WEIGHT BAYS (1 IN FUSELAGE, 2 IN WINGS, 3 IN TAIL AND 4 IN NOSE)

Additional weight was modelled using line elements to represent the mass added by structural adhesives and fillets at all of the structural interfaces. In addition, paint and primer were modeled as distinct plies to capture the overall weight contribution. Due to the overall fidelity of this modelling, an early prediction of the overall empty weight of the structure could be calculated by removing mass of the fuel and trimming weights (leaving only those required to match cg location). This mass prediction was used as for subsequent modelling in the simulators and for planning initial flights that were performed at reduced weights.

Various loading conditions were applied to the structure by discretizing pressure loads calculated using the CFD Models described previously. These were calculated based on various expected worst case scenarios including a trimmed 3.5g pull-up maneuver (with fore and aft cg) and a negative 1.5g push-over. Additional loads were calculated based on calculated landing and taxiing loads as specified by Military Specifications. These loads were analyzed and combined into an envelope solution that was used to size the laminate build up in the skins and bulkheads.

An optimization was run after wrapping the ANSYS model in Phoenix Modelcenter®. The optimizer used discrete variables to determine the number of plies (defined using chosen bi and uni-directional fabrics) required in each ply zone. The optimizer was also allowed to change the ply direction of various zones making up the aircraft skin. Some post processing was required to reduce the complexity of the resulting layup schedule to ease manufacturing, with the final sequence shown in the following figures. The figures show the chosen material, where the bulkhead material specified consists of plain weave 5.7oz carbon with either a 6.4 or 12.7mm Divinice cell core (for thin and thick bulkheads respectively).



FIGURE 41 - FUSELAGE LAYUP

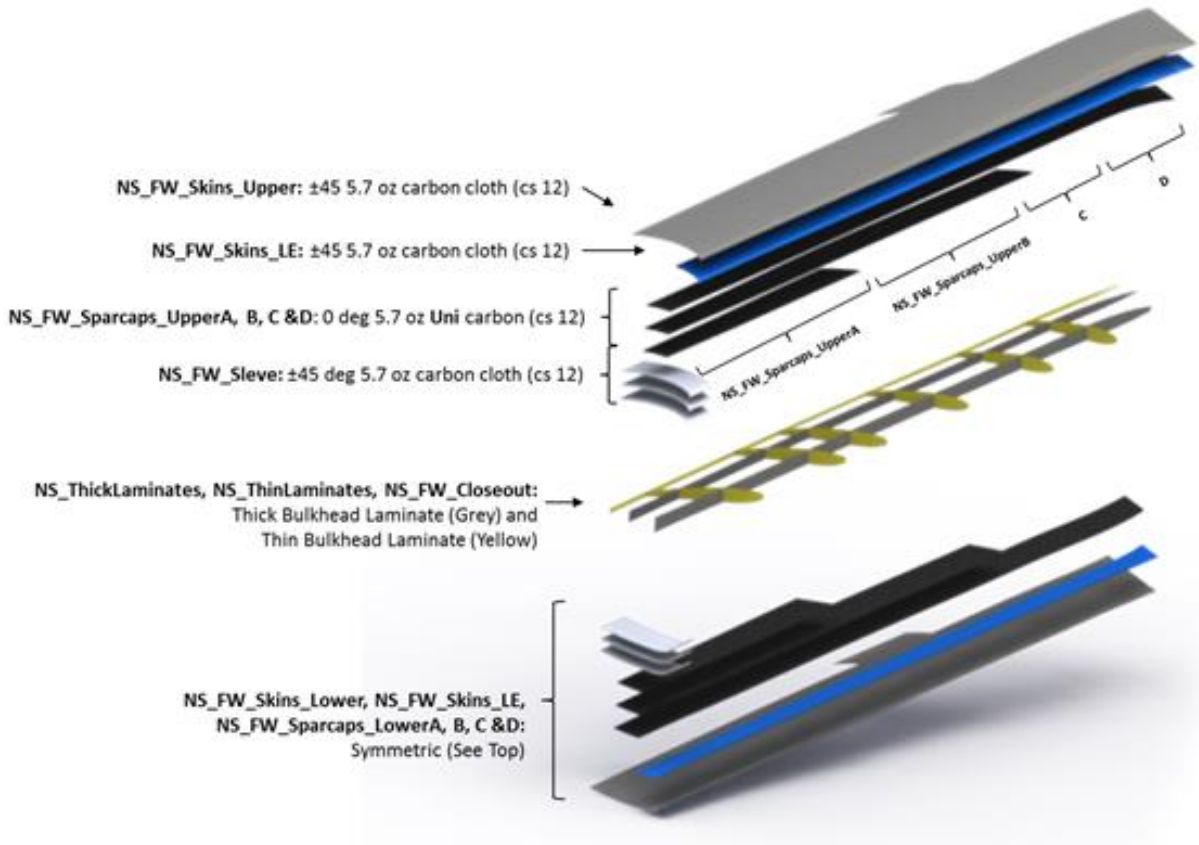


FIGURE 42 - FOREWORD WING LAYUP

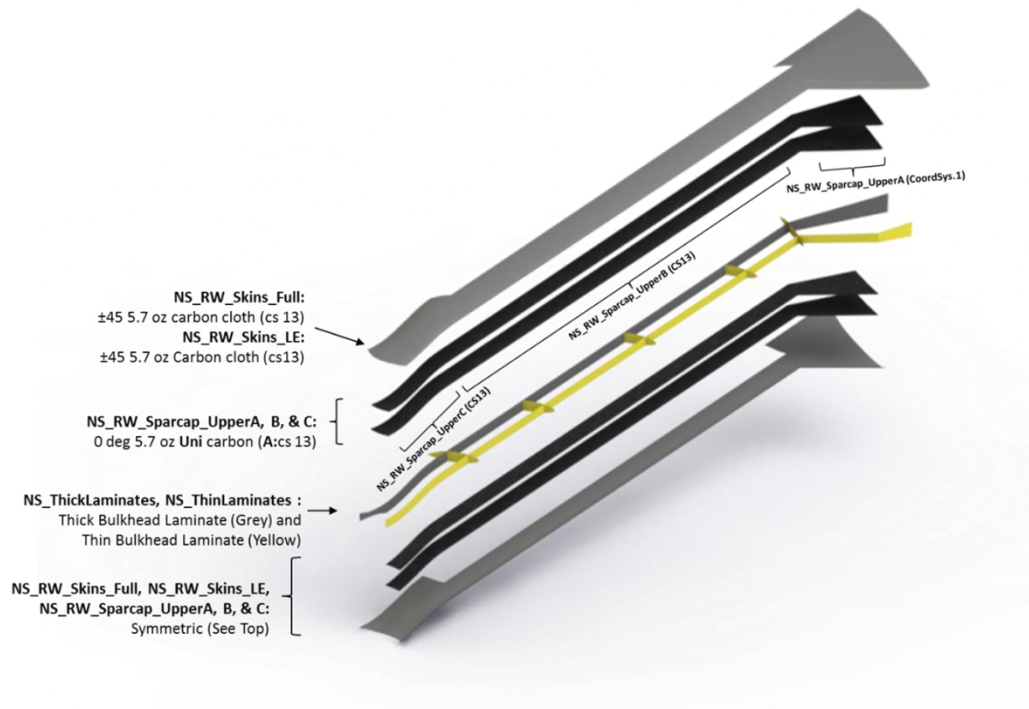


FIGURE 43 - AFT WING LAYUP

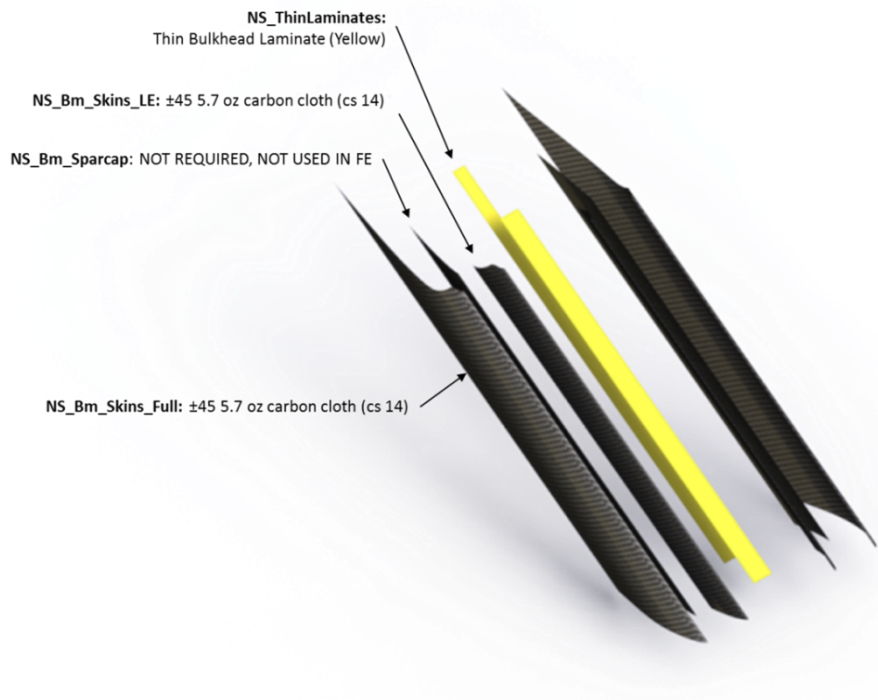


FIGURE 44 - BOOM LAYUP

4.1.2 Design of Propulsion System

The requirements of achieving faithful scaling necessitated the inclusion of jet turbines into the aircraft. Here, two Jet p-200 engines were chosen based on both the required scaled thrust and performance requirements chosen based on Military specifications for stall speed, climb rate and gradient and takeoff distance using the drag data calculated from previous aerodynamic analysis. As it turns out smaller engines (JetCat's next smaller model, the P-180s) would have met these requirements but through consultation with the pilots it was determined that the additional thrust afforded would outweigh the small weight and fuel consumption penalty. (Small scale aircraft often require additional excess thrust to get out of difficult situations due to the proximity to the ground and small time scales).

The engines were placed as far forward in the fuselage as possible to help shift the cg forward, as initial studies showed the structure was quite aft heavy. The required inlet opening size was calculated and no modifications were required to the supplied OML to feed the engines. Each engine was mounted in an internal compartment that was isolated from other bays and coated in heat reflecting tape. A custom titanium exhaust tube was passed through the existing exhaust outlet in the OML to transfer the jet exhaust out of the rear of the vehicle (as seen in Figure 45 below). This custom nozzle had a bell mouth opening and a double wall construction. The double wall insulates the thrust tube but also allows the jet of high speed gas exiting the tube to draw additional air around the outer plenum, thereby increasing mass flow and thrust. Special ceramic paint was applied at the outlet on the composite structure and then covered with stainless steel flashing to ensure no damage would be inflicted to the structure due to overheating (see Figure 46).

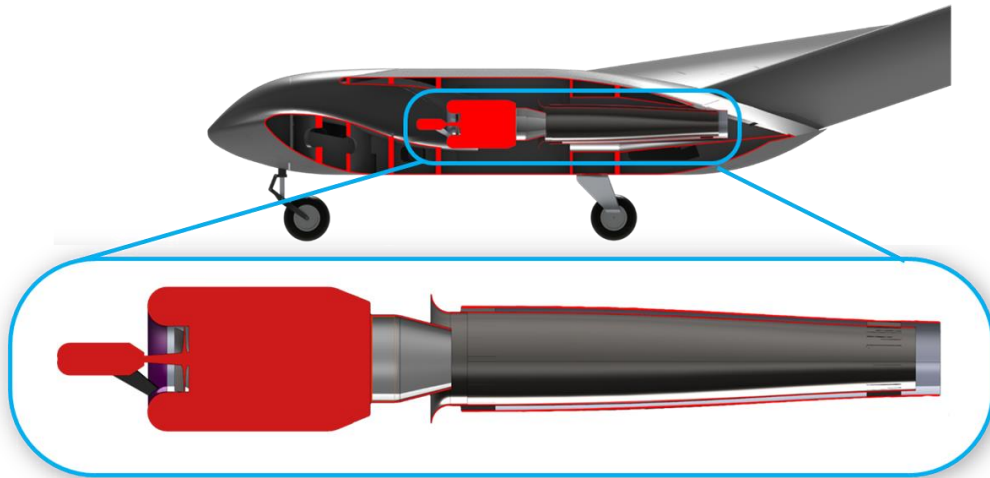


FIGURE 45 - CUTAWAY OF PROPULSION SYSTEM VIEWED FROM SIDE



FIGURE 46 - EXHAUST OUTLET SHOWING CUSTOM DOUBLE WALLED THRUST TUBE (LEFT) AND STAINLESS STEEL FLASHING ON STRUCTURE TO PREVENT HEAT DAMAGE TO STRUCTURE (RIGHT)

The JetCat P200-SX has many features which make it a safe and reliable choice for powering the JWSC RPV including a heavy duty starter, onboard RPM and exhaust gas temperature sensors and JetCat’s industry leading customer service. Two of the most important features are the Electronic Control Unit (ECU) and the Ground Support Unit (GSU). Below is a description of these features:

1. **JetCat Electronic Control Unit (ECU)** - The JetCat Jet-tronic ECU provides real-time closed loop control of the turbine, resulting in better starts, smoother idle and more reliable performance. The ECU, which features a Hitachi H8 16 bit microcontroller, has a fully automatic starting sequence which promotes safe, reliable starts. The ECU also monitors turbine RPM and exhaust gas temperature during flight via sensors in the turbine. Additionally, the ECU monitors fuel pump voltage, battery voltage and calculates statistical data including total fuel consumption, total turbine time, maximum RPM, run time. The ECU also monitors total turbine runtime. This is especially useful as JetCat requires each turbine to be sent in for maintenance every 25 hours of runtime. Typically this ECU is connected via a com port of a computer to view real-time data on a shop bench during testing. However, in this case a level shifter board was used so that the serial data could be passed through the autopilot and sent over the telemetry stream so as to be read in real time on the ground control station.
2. **Ground Support Unit (GSU):** Used for monitoring or prescribing (within operational limits) key parameters such as maximum RPM and minimum RPM, in real time, during startup and ground testing. The GSU may be connected or disconnected from the ECU at any time.

A series of thrust tests were performed to characterize engine parameters such as static thrust, fuel consumption and RPM vs throttle setting. The resulting data allowed the development of a refined fuel consumption model that was implemented in the simulators and used to update predicted fuel requirements. These fuel requirements were used for subsequent sizing of the fuel cell.

The fuel cell was sized based on required fuel, predicted unusable fuel allowance (calculated based on most adverse predicted aircraft attitude) plus a 10% reserve factor which would allow two go-arounds in the case of a balked landing. The overall capacity is 27 kg of Jet A1 with 23kg usable amount. The cell was custom fabricated out of Kevlar composites and contained a series of baffles to reduce fuel slosh. The inside was coated in a paint on, fuel safe sealant made for this purpose. The fuel cell contained a sloped bottom with a sump well that feeds

two fuel pickups (one for each engine) and venting ports. The fuel tank has a large screw off window that also served as the refueling door as pictured below.



FIGURE 47 - FUEL CELL USED IN 5M RIGID AIRCRAFT

This main cell feeds a pair of header tanks, one for each engine, that also serve as air traps. This insures that the engines won't flame out, even if the aircraft moves into an attitude that results in air being ingested into the fuel lines. Fuel flow data is calculated based on voltage supplied to the two fuel pumps rather than an inline fuel flow measurement. This resulted in a slightly inaccurate fuel prediction from telemetry which was accounted for in the flight test panning.

4.1.3 Landing Gear Design

Takeoff of the Geometrically Scaled RPV is accomplished via a tricycle style landing gear with steerable nose gear. The use of a tricycle arrangement of wheels gives stability during taxi testing and during the takeoff roll. Figure 25 shows the landing gear for the Geometrically Scaled RPV, including the custom designed oleo strut for the steerable nose gear.



FIGURE 48 - TRICYCLE LANDING GEAR LAYOUT AND CUSTOM OLEO STRUT

Sizing of the landing gear was accomplished using the method described in *Airplane Design* by Jan Roskam ^[57]. The gear is designed to allow the rear gear to move forward and aft to accommodate CG shift for various takeoff weights. The rear gear can be located at 5 places, equally spaced between the forward and aft CG limits of 910mm and 1107 mm aft of the nose, respectively.

Figure 49 presents the results of the gear sizing calculations for the Geometrically Scaled RPV for the aft most CG location (left) and the forward most CG location (right). All required criteria are satisfied for both configurations and Table 10 presents a summary of key design specifications for the landing gear.

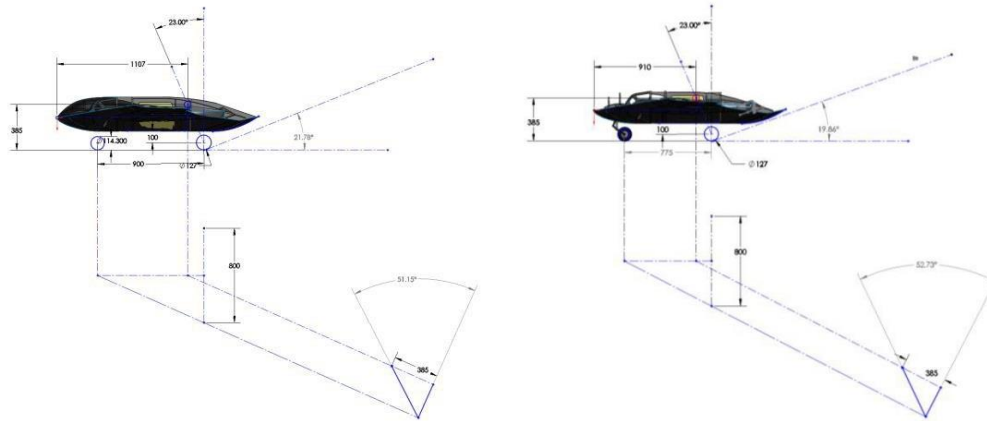


FIGURE 49 -GEAR SIZING OF THE GEOMETRICALLY SCALED RPV FOR AFT AND FOREMOST CG LOCATION

As with most designs implemented on the 5m RPV, initial testing was first performed on the reduced scale aircraft. Figure 50 below shows a Mini SensorCraft with equivalent scaled landing gear geometry that was used to assess the proposed design.



FIGURE 50 - MINI SENSORCRAFT USED TO EVALUATE PROPOSED LANDING GEAR GEOMETRY

The landing gear for a 90kg aircraft are not readily available off the shelf from the RC aircraft community. As such, they had to be designed and constructed from scratch. The landing gear were designed based on loads cases outlined by MIL specifications. The aft gear was designed using aluminum heat treated to the T6 state (initially annealed to O-state to allow bending). Additional strength was added through spring steel inserts that

run along channels machined into the cantilever gear arms. The rear gear were designed with 2 degrees of toe-in to help with tracking and 5 degrees of positive camber in the un-deflected state which resulting in a neutral camber when the weight is on the wheels.

The nose gear was designed as a steerable unit and included an air spring/damper system. This air spring system can be charged up using a hand pump before flight in order to achieve the desired stiffness depending on the takeoff weight, landing conditions etc. The forward gear was designed using a combination of 2024 aluminum and chromoly steep. Static and Dynamic FE analyses were run to size the components with some of the resulting models shown below.

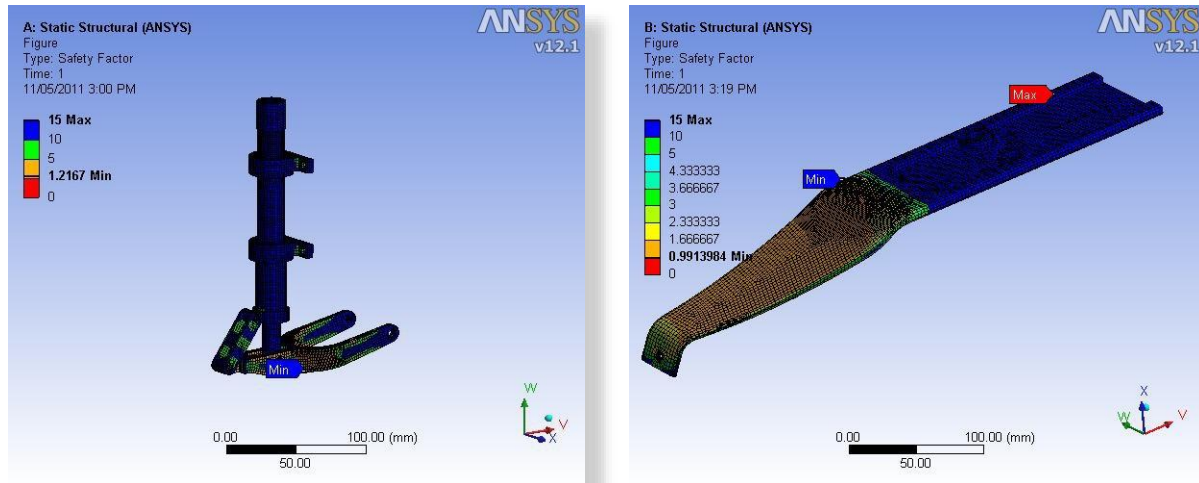


FIGURE 51 - FINITE ELEMENT ANALYSIS OF LANDING GEAR

In addition to these analyses, the reaction forces found here were applied to the fuselage FE model introduced earlier and used to design hard points and gusset plates in the fuselage to transfer landing loads safely through the structure. A servo was used to actuate the steering of the forward strut with a custom steering damper used to absorb excess shock due to an off angle landing (thereby preventing the stripping of gears in the steering servo).

A set of pneumatically operated brakes were chosen to arrest the aircraft. These brakes are actuated using a proportional valve actuated by a pulse width modulated signal supplied by the autopilot. Off the shelf wheels

were chosen from a scale f-16 RC model. These were pneumatic tires which added additional shock absorption but turned out to be the failure point for the aircraft flown in a subsequent flight test regime. The heavy weight of the aircraft caused the tread to be scrubbed off the tire and subsequently blew on a landing run out.

4.1.4 Power Management

Onboard power was supplied through Lithium Polymer (LiPo) Battery Packs. Each turbine ECU was powered using a separate 2S pack capable of 2+ hours of operation. Servo power was supplied through 4 separate, redundant 2S batteries regulated by a pair of Powerbox Royal power management systems. These units provided redundant, regulated, optically isolated power buses to feed servos and other avionics. It also provides servo matching and mixing capabilities. These features are critical; the servo matching is required since multiple servos are used on each control surface (for additional torque and redundancy) and matching allows individual tuning to ensure they do not fight each other through the range of servo travel. The custom mixing allows the complex control scheduling that the autopilot alone will not offer due to the limited amount of servo channel outputs (there are 16 outputs on the autopilot used here whereas the configuration employed 28 servos).

The forward section of the fuselage was used as the avionics compartment and housed both the batteries and power management units. A custom dashboard was created out of carbon plate to cover the avionics bay. The tray also hosts displays showing system health, power switches and pressure readouts for landing gear spring and brake accumulator pressure.

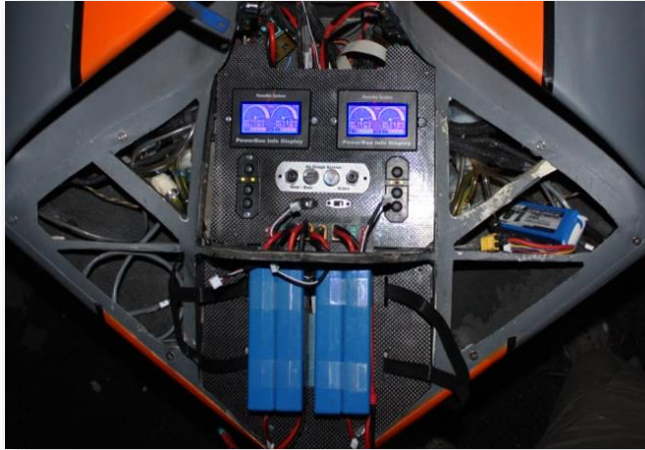


FIGURE 52 - AVIONICS BAY SHOWING BATTERY COMPARTMENT, SWITCH BANKS, PNEUMATIC FILL VALVES AND PRESSURE READOUTS

4.1.5 Avionics and Control

Primary control of the Geometrically Scaled RPV is accomplished via the onboard Cloud Cap Technology Piccolo II Autopilot. The autopilot provides fly by wire stability augmentation with the pilot providing high level commands such as pitch roll and throttle input. The autopilot's inner loops then control the surfaces to achieve these desire commands.

There are two communication links capable of controlling the aircraft through the Piccolo autopilot. The **Primary transmitter** is controlled by the **Primary Pilot** who is located outside the command station and is responsible for flying the aircraft under direct visual conditions. The **Primary Transmitter** communicates through a frequency hopping, 2.4GHz link with 6 satellite receivers placed throughout the aircraft. The autopilot polls all of the redundant receiver streams and picks the one with the highest receive strength quality to supply inputs to the fly by wire control system.

The second control link is passed through the autopilots telemetry link (which can offer up to 25km range). This link is controlled via the **Piccolo Tethered Transmitter** which is located at the ground control station. In this case the commands from the controller are passed through a physical wire to the Piccolo ground station and muxed into the Piccolo's primary 2.4GHz comms link. When activated, the **Tethered FPV Pilot** is then

capable of flying the aircraft through a dual redundant camera feed located at the tail of the aircraft. The intention here is that in the case of a **Primary Pilot** failure event (such as link failure, loss of visual orientation etc) the **Tethered FPV Pilot** could bring the aircraft back to a safe distance from the ground station (in order to re-acquire the primary control link or ensure the **Primary Pilot** regains visual regard) before potentially passing control back.

The third layer of control is a fully manual scheme that bypasses the autopilot completely (in the case of autopilot failure, autopilot gain errors etc). In this case the **RC Backup Pilot** can obtain control at any time during the flight by simply flipping a switch on the **Radio Control Transmitter**. Flipping this switch toggles the input selection channel on the RxMUX, changing the source of the servo commands to the aircraft. The RxMUX functions by having two input rails (one from the manual transmitter and one from the autopilot) and a single output rail feeding signals to the servo mixer, with the output controlled by a switch on the backup transmitter. The system is designed such that the backup controller can take control of the aircraft at any time, and in the event of signal loss with the primary controller, the switchover is automatic. One potential challenge is that since this control scheme completely bypasses the autopilot, there is no stability augmentation available. Figure 53 below shows the command and control hierarchy graphically.

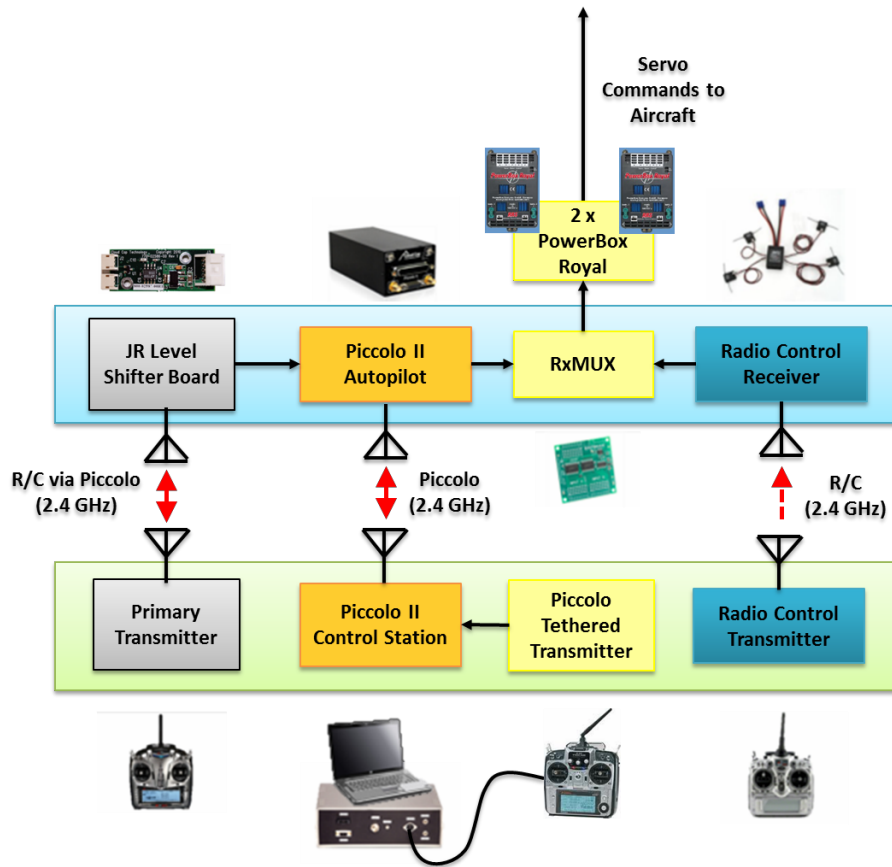


FIGURE 53 - PICCOLO II/ RxMUX SYSTEM CONCEPT

4.1.6 Camera Systems

The Geometrically Scaled RPV was fitted with a forward facing camera mounted on the top of the boom to provide emergency first person view (FPV) navigation in the event that the RPV inadvertently travels out of visual range. This camera provides a real-time video feed to the ground station at all times during the flight. The forward facing camera is a GoPro HD Hero digital camera which offers a 127° field of view and will record to flash memory (1080p at 30fps). This camera also output a standard definition video stream to dual onboard video transmitters which then relay the signal to the ground station. Due to shape of the aircraft and carbon fabrication, two transmitters are used in order to ensure signal and antenna diversity. A view from the FPV camera in flight is shown in Figure 54 below.



FIGURE 54 - IN FLIGHT VIEW FROM FPV CAMERA ON VERTICAL BOOM

The first video transmission link employs a 1 watt, FM analog unit broadcasting at a user selectable frequency with an omni-directional cloverleaf antenna. The receiver unit uses a 24dbi high gain directional dish antenna on the ground and the combination has a specified operating range of 25 miles. The second video link uses a 1.5 watt FM analog transmitter broadcasting in the 900 MHz spectrum. The airside antenna is an end feed dipole, omni-directional antenna linked to a receiver unit with a unity gain omni-directional antenna. The rated range for this system is 5 miles.

At the ground station, each receiver is fed into an Oracle Video Diversity Controller (shown below in Figure 55) to provide redundant video reception. The Oracle measures the video signal strength from each receiver, selects the video and audio stream with the strongest signal and forwards that signal to the output. This provides the best possible video quality and lessens the risk of a lost signal, which is key for emergency navigation purposes.



FIGURE 55 - VIDEO DIVERSITY SWITCH USED AT GROUND STATION

4.1.7 Ground Control Station

Two ground control stations were designed by the author as part of this work. The first consisted of a computer station with dual redundant power supplies with backup batteries, dual monitors and communications hardware for interfacing with all of the autopilots used in this work. This computer station was housed in a custom fabricated case which could fold up and be transported using a custom built trailer. The trailer was designed and fabricated by the author and included custom aircraft holding fixtures, work desks and a cabinet for housing the computer station while in transit. The trailer also has a fold out awning for protecting the operators from direct sunlight and inclement weather. The following figure shows the computer station both in the laboratory (where it was used in hardware in the loop testing) as well as in-situ during flight operations.



FIGURE 56 - INITIAL MOBILE COMMAND CENTER: COMPUTER STATION (TOP AND LOWER RIGHT), INTERIOR OF CUSTOM TRAILER (LOWER LEFT) AND DEPLOYED SETUP (LOWER RIGHT)

Part way through the project an improved command center was conceived and designed by the author. This **UVic CfAR Mobile Command Center (MCU)** is a full featured laboratory housed within a 2013 Mercedes Sprinter van. The MCU was designed to house three operators at three separate workstations: a backup pilot, the ground control station operator and the payload specialist.

A stock, extended length sprinter was chosen with the tandem axle configuration with the optional tow package as the basis for the command unit (see Figure 57 below). The aft portion of the vehicle was separated using a bulkhead in which the server rack was integrated. The server rack has slots for 4 3u servers and a variety of additional rack mount audio/video mixers. The bulkhead also houses the base station for a set of 5 wireless

Dave Clarke headsets, controls for the retractable legs and the pneumatic mast. An additional lockable cabinet houses all of the avionics required to interface to the aircraft.

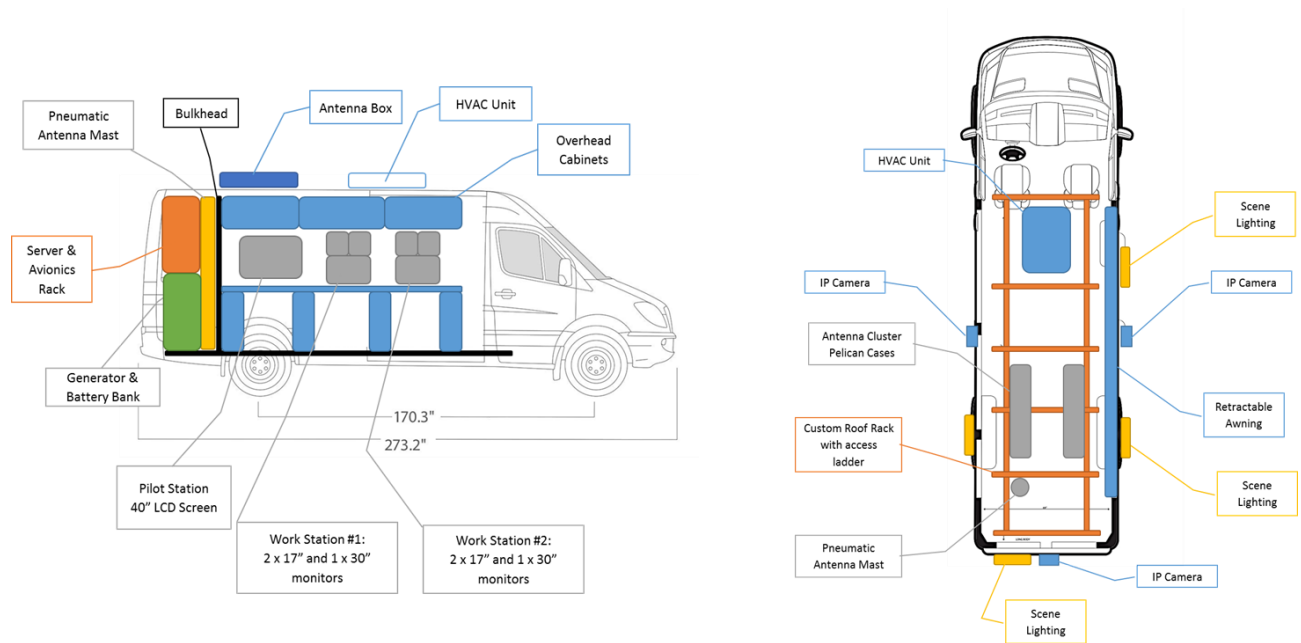


FIGURE 57 – INTERIOR SIDE VIEW (LEFT) AND EXTERIOR TOP VIEW (RIGHT) OF MOBILE COMMAND UNIT

Aft of the bulkhead is a bank of 8, deep discharge, lead acid batteries for backup power as well as a diesel generator that feeds off the vehicles main diesel tank. Charge controllers allow the van to be powered from a variety of sources including the generator, the battery bank or shore power. The generator, as well as the rear of the server racks, are accessed through the rear ambulance style doors.

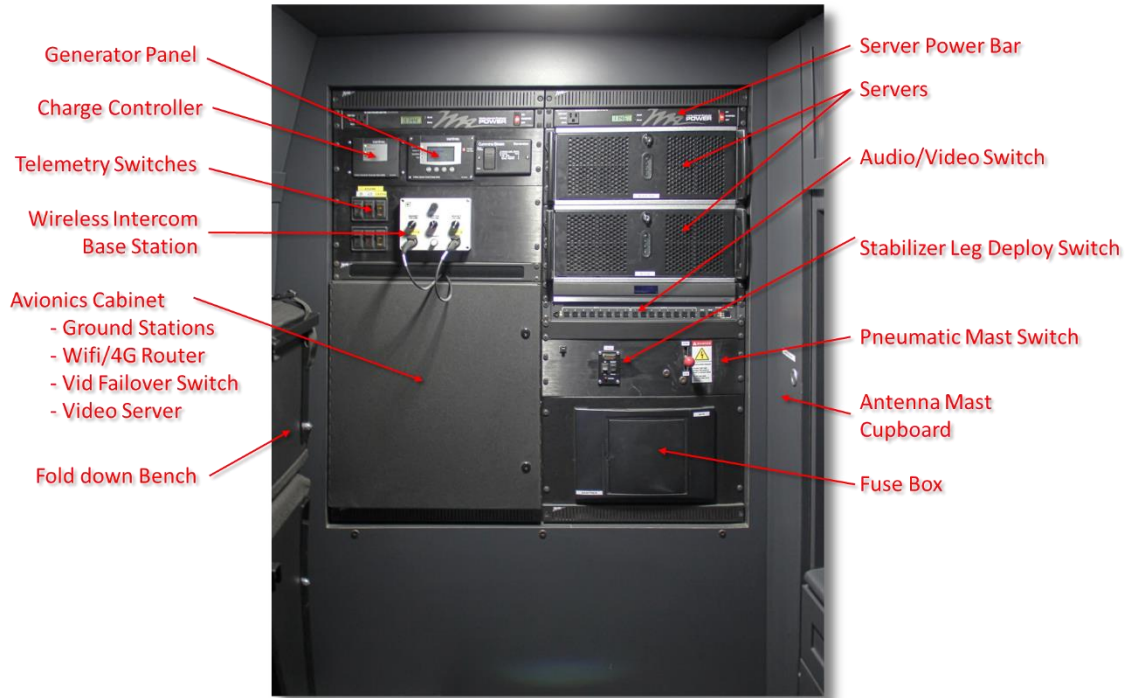


FIGURE 58 - AFT COMPARTMENT FROM INSIDE MAIN COMPARTMENT

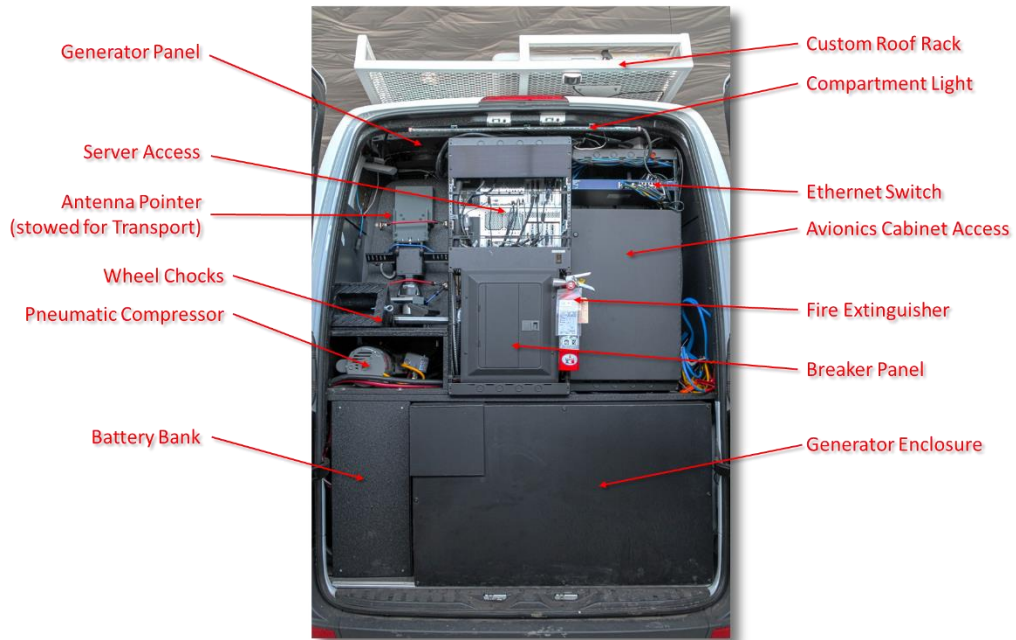


FIGURE 59 - AFT COMPARTMENT FROM REAR DOORS

The main compartments contains the three workstations and a fold up bed/couch. The left side of the vehicle includes cabinets for storage, the workstations themselves as well as the cabinet for the 45', retractable pneumatic antenna mast. This antenna mast is deployed using compressed air (the compressor is housed in the aft compartment) and has a three axis FLIR antenna pointer with continuous pan capability. A series of directional antenna can be quickly mounted to the antenna pointer for the variety of telemetry links employed in the vehicle. All roof and mast mounted data links can be turned off or on using a switch bank inside the vehicle. Retractable stabilizer legs are included under the van and are extended before deploying the mast in order to ensure stability of the vehicle.



FIGURE 60 – MAIN COMPARTMENT SHOWING THREE PRIMARY WORKSTATIONS

The outside of the vehicle has been heavily modified to include a series of cameras and ultra-high brightness scene lights for operating in the dark (including one spot light on the pointing antenna mount). A custom fabricated roof rack and access ladder allow the user to get onto the roof to service components or store equipment. The roof also houses two waterproof cases, one to store equipment and one to house a series of

modems and antenna. An HVAC system is also located on the roof that provides additional heat or air conditioning to the operators without requiring the running of the vehicles engine.



FIGURE 61 – EXTERIOR VIEW WITH ANTENNA MAST DEPLOYED (LEFT) AND AT NIGHT (RIGHT)

The MCU was designed to be flexible and allow future growth. As such, a wide variety of data and camera links is integrated into the unit and available to the user. These include the following

- *5 Watt, 2.4 GHz RC signal booster (RC controller plugs into this feed via wall connection) with Omni-directional and directional pointing capability*
- *433 MHz (1 Watt), 2 x 900MHz (1 Watt), 1.3 GHz (1 Watt), 2.4GHz (1 Watt) telemetry links with both Omni and directional antennae options*
- *900MHz (1 Watt), 2 x 5.8GHz (2 Watt) video down links with Omni and directional antennae*
- *5GHz (6.5 Watt) PtP Wi-Fi link with patch antenna*
- *4G LTE and Wi-Fi modem for local area networking*
- *ICOM Nav/Comm VHF Air Band transceiver for ground-air or ground-tower communications*
- *Novatel RTK Differential GPS antenna and base station*

4.2 Fabrication

The following section gives a very brief outline of the fabrication and assembly of the Rigid 5m RPV. This process took the author approximately 1 year between Aug 2010 and Sept 2011. Over this period, three UVic coop student were also employed to assist in the process.

4.2.1 Internals Fabrication

The internals of the aircraft are made primarily out of carbon/foam/carbon or carbon/plywood/carbon laminate materials. All of these laminate sheets were produced using wet layup vacuum bagging and/or Vacuum Assisted Resin Transfer techniques. The sheets were laid up on a single sided tool which consisted of a large, melamine sheet that was waxed and polished. In total 8 4'x8'x1/2" and 5 4'x8'x1/8" sheets of laminates were produced.

From these sheets the internal structure was machined. The internal ribs, sheer webs and bulkheads were all designed such that they interlock and self-locate (see Figure 62 below). The parts were machined using a 5 axis mill in order to capture the complex edging where the vertical bulkheads intersect the compound curvature of the OML.

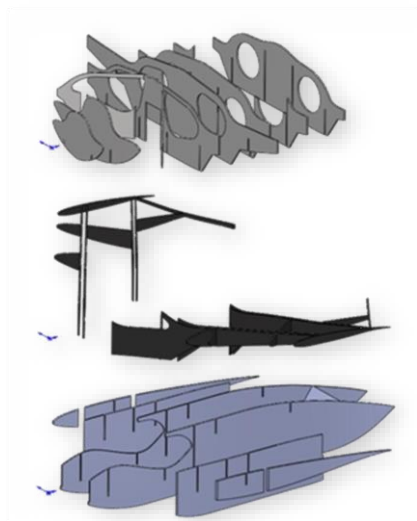


FIGURE 62 - EXPLODED VIEW SHOWING INTERLOCKING BULKHEADS

The machined bulkheads were then assembled and bonded together using glass filled epoxy and glass/epoxy tape along all joints. The figure below shows the final assembled fuselage internal structure.



FIGURE 63 - INTERNAL STRUCTURE OF RIGID RPV FUSELAGE

4.2.2 Tooling Fabrication

Tooling was designed and built as a set of 12 female molds. An example of the process is outlined in the figure below where we can see the process of developing the upper fuselage mold. The first step is to laminate the blank for the tool. Here a series of 26 1" sheets of Medium Density Fiberboard (MDF) was laminated using polyester resin. The picture shows the stack in a vacuum bag that was used to press the sheets together while drying. The next step involved loading the blanks into the 5 axis CNC mill at Camosun College (each blank weight in excess of 700lbs). The third step that is shown is the machining of the mold itself, a process that involved 5-axis tool paths and took over 16 hours of machine time. The final step involved plasticizing the mold using thinned epoxy, sanding and polishing to a high shine state and finally buffing and waxing to make a suitable mold surface.



FIGURE 64 - MOLD FABRICATION PROCESS

Additional tooling was required for several other components such as the composite ducts and fairings. One example was the inlet and outlet for the engines compartments. These tools were a very complex geometry and such were not easily fabricated in one piece using available CNC tools. As such, a series of 2d profiles were cut out of foam and stacked. Before milling the contours from the foam, a sheet of 18" ply was laminated onto it. These ply sections serve as hard templates embedded in the stacked foam plug and acted as guides for sanding the foam plug into a fair and smooth shape, while still preserving the required lofted accuracy. This layered building technique can be seen in the following figure on the left which shows the inlet tooling before the plug is covered in fiberglass and finished (as shown with the final outlet plug on the right).



FIGURE 65 - MALE PLUGS USED FOR PRODUCING AIR INTAKE SKINS (LEFT) AND OUTLET SKINS (RIGHT)

4.2.3 Composite Layups

The majority of the aircraft structure is defined by the outer mold line. The external structure of the aircraft was fabricated using the female tools described earlier using a wet layup, vacuum bagging technique. Two coats of Duratec® primer is sprayed into the waxed tooling before the composites are laid up. This ensures there are no pinholes in the final part and acts as an easily sand-able primer coat on the final parts.

The ply buildup, described in an earlier section, was laid up for each individual component (upper/lower forward and aft wings, Right/left half of boom, upper/lower fuselage) with a final layer of peel-ply. The peel-ply is left on right up the final bonding stage (where wing halves for instance are bonded together) and once removed allow a high energy surface for better bonding of the adhesive. Figure 66 below shows the process of laying up the bi-directional and uni-directional carbon in the fuselage's lower surface.



FIGURE 66 - LAYING UP BOTTOM FUSELAGE SKIN

Some additional parts were fabricated using the existing tooling. These included parts such as access panels and fairings. A good example is the upper access panel on top of the fuselage. In this case, a patch of composites are laid up in the upper fuselage tool and allowed to cure. The laminate is then taken out of the mold and trimmed to the correct access panel shape before being placed back into the tool. The upper fuselage skin is then laid up in the tool (on top of the trimmed access door) and allowed to cure. When removed from the mold

the access panel is detached from the skin and the access hole in the top of the fuselage is trimmed. The result is a conformal panel with a corresponding recess in the skin. Figure 67 below shows the top of the fuselage with the conformal cover installed and with the top access bay open.



FIGURE 67 - CONFORMAL FUSELAGE ACCESS DOOR

4.2.4 Final Assembly

Once the internal and the skins have been fabricated and allowed to cure, then next step involves bonding the structure together. The process is as follows.

1. First, a layer of Teflon release film is laid over the bottom skin (shown in green in Figure 68) which ensures no epoxy will adhere to skin at this stage. Then, fillets are added to the intersection between the lower skins and the internal structure, as well as a strip of fiberglass tape (the cross sections are shown as red L-sections in the figure).
2. Once cured, the internals are removed from the bottom mold (recalling that they will not adhere to the bottom skin because of the release film). They are then placed into the upper wing mold and adhered permanently to the upper skin using an attachment method similar to that described in the previous step (now shown in pink).
3. Then, structural adhesive is applied to the upper surface joints (shown in red) and the upper and lower molds are brought together. The molds are clamped together and are allowed to cure

- The part is then removed from the mold and trimmed. This results in a part with taped seams throughout and ensures adequate surface area for bonding of the internal structure to the skins.

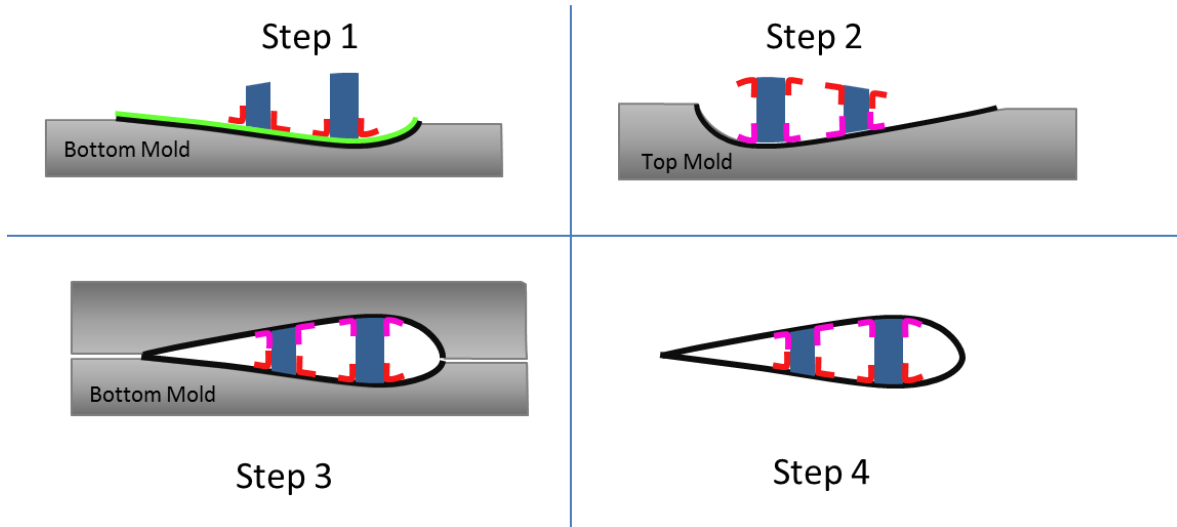


FIGURE 68 - PROCEDURE USED TO BOND INTERNAL STRUCTURE AND SKINS

These steps are also shown in the following figure. On the left we can see the internal wing structure in the top mold ready for bonding (step 2 above). On the right the adhesive is being applied to the taped flanges (part of step three) before subsequently assembling the molds/skins and clamping the assembly (bottom).



FIGURE 69 - ASSEMBLY OF WING STRUCTURE

The Final step after assembling and trimming all of the individual structural components was to assemble the entire aircraft. This required the design and fabrication of a precise assembly jig to ensure that all of the parts were aligned prior to drilling hard points used for subsequent joining. Figure 70 below shows the CAD design of the fixture as well as the aircraft in the physical jig.

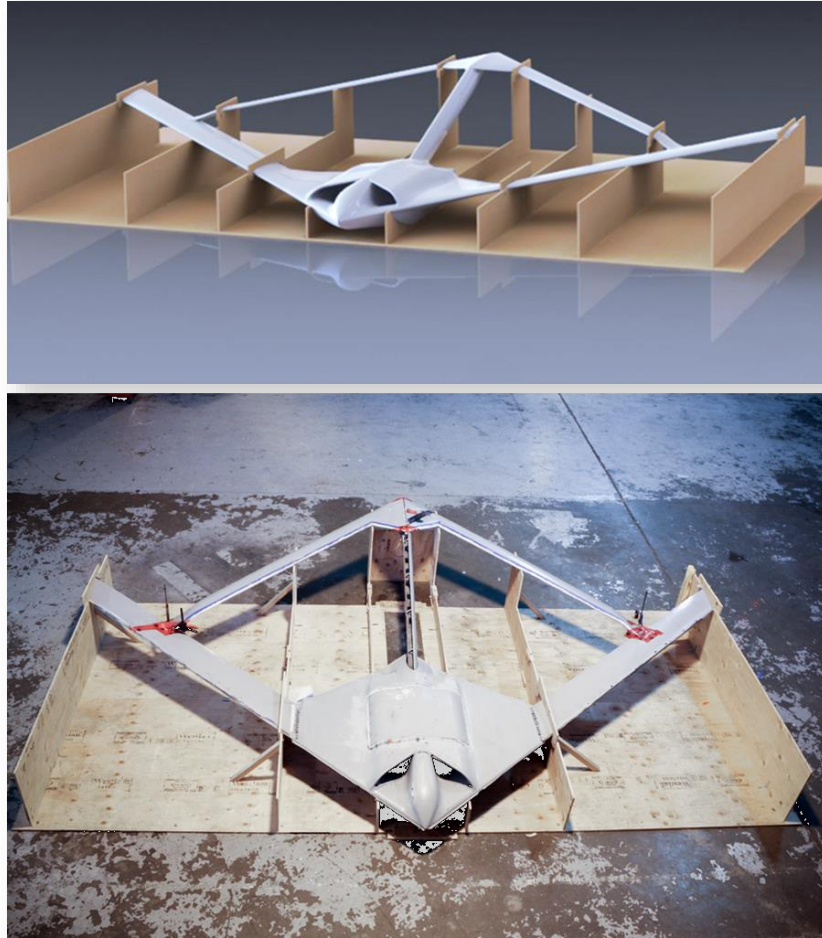


FIGURE 70 - ASSEMBLY OF THE AIRCRAFT USING CUSTOM JIG

4.2.5 Part fabrication and Integration

Many individual parts were required to be fabricated and integrated into the aircraft. These included CNC'd aluminum hard points for hinges, servo mounts, threaded inserts etc., as well as all of the avionics wiring bundles. The list is too extensive to outline here but Figure 71 below shows some of the additional parts that were developed and integrated into the wings. Similar parts were required for other surfaces while the fuselage require many hard points, custom wiring and various components to complete installation of flight critical systems.

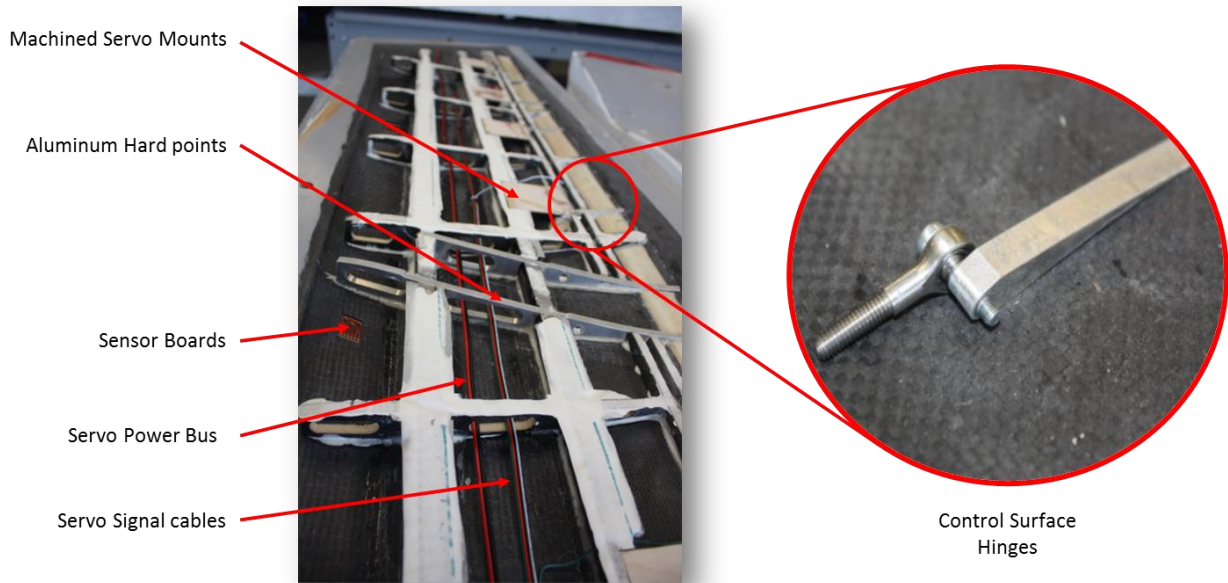


FIGURE 71 - SOME OF THE CUSTOM COMPONENTS FABRICATED (FORWARD WING SHOWN)

After all systems were installed the aircraft went through extensive checkout tests (subject of another section) and was painted. A high visibility orange was used in contrast to a matte grey color for the top of the aircraft. The bottom used florescent yellow stripes (90° offset from stripes on top of aircraft) to aid the pilot in referencing the aircraft. Figure 72 below shows the final paint scheme chosen

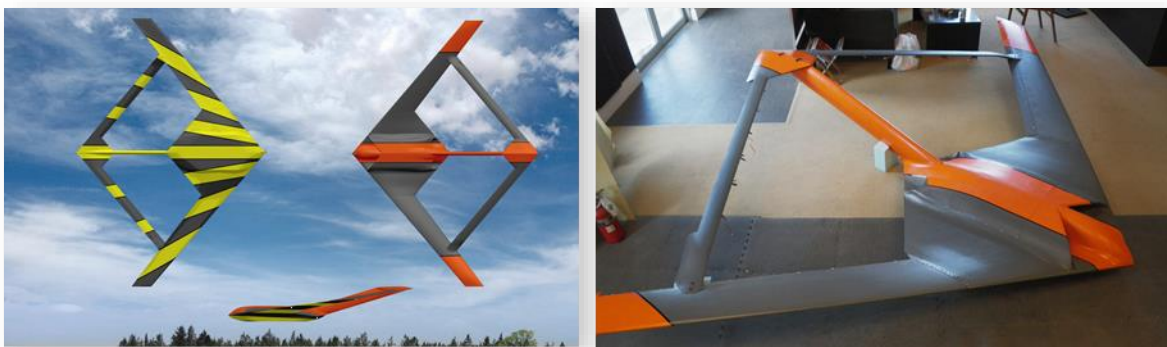


FIGURE 72 - PAINT SCHEME CHOSEN FOR AIRCRAFT RIGID RPV (LEFT) AND ACTUAL AIRCRAFT AFTER PAINT (RIGHT)

4.3 Flight Test Planning

Flight Test Planning was primarily the Responsibility of Tyler Aarons and Jeff Garnand-Royo from Virginia Tech and was the subject of their respective Theses ^[58] ^[59]. However, since UVic was primarily responsible for operations some assistance was given in the form of developing test procedures, checklists and training material. While a great deal of work was invested by the author at this stage, the details are not included here. However, the work completed at this stage have since served as the basis for the operating procedures and best practices applied at the University of Victoria Center for Aerospace Research (UVic CfAR).

4.4 Ground Testing

This section outlines the ground tests that were conceived and carried out to meet airworthiness requirements imposed by the UASF flight directorate. It should be noted that a large portion of the ground testing was performed in conjunction with Mr. Tyler Aarons and Jeffery Garnand Royo of Virginia Tech who were responsible for instrumentation of the aircraft and flight test planning.

4.4.1 Static Thrust Test

An installed static thrust test was completed to verify the performance of the engines as integrated in the aircraft. These results were compared to bench tests performed on the engines as well as manufacturers published data. Vibrations were logged at several points in the airframe to check for any resonance that could potentially interfere with sensors, the inertial measurement units etc.

Throughout the testing, throttle percentage, throttle command, exhaust gas temperature, fuel flow rate and RPM were also recorded. A total reduction in static thrust over published data of 4.8% was noted on the bench while installed thrust was reduced by 10.4%. The manufacturer claims that these numbers are well within expected values. Figure 73 below shows the static thrust test rig developed for the tests.

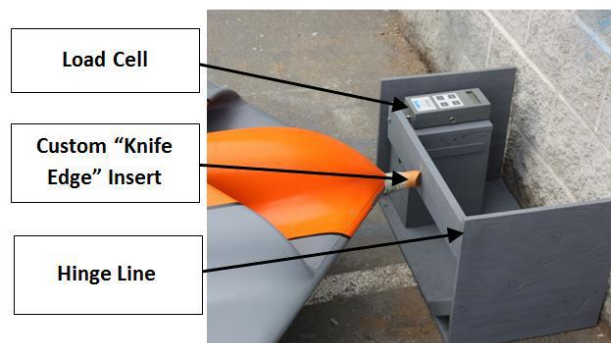


FIGURE 73 - INSTALLED STATIC THRUST TEST RIG

4.4.2 Bifilar Pendulum Test (BFPT)

A Bifilar Pendulum test was completed in order to experimentally determine the mass moments of inertia of the GSRPV and compare them to the as-modeled values generated by the FE model and subsequent detailed

mass breakdown. The Bifilar Pendulum test presented here was used only to determine the mass moments of inertia about the principle axes (Roll, Pitch, Yaw).

A custom cage assembly was constructed to hold the aircraft in the three principle orientations and trimmed to ensure the center of gravity corresponds to that of the aircraft. The assembly was hung from a pair of filaments separated by a known distance, rotated about a vertical axis passing through the center of gravity and allowed to oscillate. The moments of inertia were calculated from the period of the oscillations with the contribution of the cage assembly subtracted out. Figure 74 shows a test of the aircraft in the roll orientation.

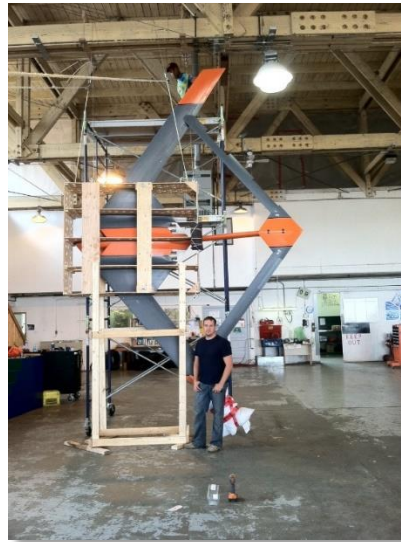


FIGURE 74 - AUTHOR IN FRONT OF BFPT ABOUT PITCH AXIS

The Bifilar Pendulum Test provided accurate experimental mass moments of inertia for the GSRPV. An object of known inertia was tested, and a small 1.85% error validated the method used. Testing of the GSRPV provided excellent correlation with the as-modeled, predicted data for the roll and yaw orientations. The pitch orientation had the largest error between the modeled and measured values; however, several potential sources of this error were identified and can be corrected for future iterations of this test.

TABLE 9 – SUMMARY OF BIFILAR PENDULUM TEST RESULTS FOR THE GSRPV

Principle Axis		Value	Units
Roll	Experimental	29.25	$kg\ m^2$
	Predicted	28.64	$kg\ m^2$
	Difference	2.13	%
Pitch	Experimental	25.59	$kg\ m^2$
	Predicted	33.53	$kg\ m^2$
	Difference	23.68	%
Yaw	Experimental	56.08	$kg\ m^2$
	Predicted	59.99	$kg\ m^2$
	Difference	6.52	%

4.4.3 Static Load Testing

A static structural loading test was completed to experimentally validate the structural design and fabrication of the GSRPV and ensure that the as-built structure was capable of withstanding the predicted aerodynamic loading required to complete all planned flight maneuvers.

The CFD model was used to determine the most adverse loading case and the resulting spanwise load required. The pressure distribution was approximated using three lumped masses along the span of the forward wing. The loading was accomplished using sand bags applied to the underside of the aircraft as it was placed upside down to allow the upward aero loads to be approximated by gravity. The loads were placed at 0.5 g increments up to a total of 3gs. The GSRPV successfully withstood loading up to a 3g load, at the flying weight, without permanent structural damage. The right forward wing loaded to 3g is shown in the following figure.



FIGURE 75 - STATIC LOADING OF AIRCRAFT

The setup used for the initial static test has several limitations in terms of reproducing desired loading. As a result, an updated loading rig was built that allows load applications at 22 locations on the forward and aft wings in any direction using a system of turnbuckles and force gauges.



FIGURE 76 - IMPROVED STATIC LOADING RIG SHOWING LOADING OF FRONT WINGS

4.4.4 Landing Gear Drop Test

The landing gear drop test was done to evaluate the as-built design of the landing gear to see whether or not it can withstand the required loads upon landing. Utilizing FAR 23 section 725 requirements, a drop height of the landing gear was calculated such that the gear would be at the required descent rate at the point of impact with the ground. The landing gear for the GSRPV was mounted to a frame designed to replicate the geometry of the aircraft. Weights (sand bags) were added to the rig and distributed such that the CG of the system corresponded to the CG of the overall RPV. The loaded rig was raised above the ground and was released utilizing a custom constructed single point release mechanism to assure the proper orientation of the rig at impact as per the required Federal Aviation Regulations. Accelerometers were applied to the rig to measure the actual loading history of the assembly and used in a loads analysis of the structural model.



FIGURE 77 - LANDING GEAR AT IMPACT (LEFT); LANDING GEAR AFTER TEST (RIGHT)

4.4.5 Range and Electro Magnetic Interference (EMI) Tests

A variety systems on board the aircraft communicate with the ground station over a range of frequencies. These links include primary and backup command and control as well as a telemetry downlinks on 2.4GHz (frequency hopping) bands and cameras downlinks on 5.8GHz and 900 MHz. The Aircraft is constructed primarily of carbon fiber which blocks the signal path in different orientations. Several techniques were employed to evaluate the range and interference. These included the use of signal attenuators to simulate communications at a distance and placing transmitters/receivers on other aircraft flown at remote locations at set distances away from the corresponding receiver being tested. The tests confirmed issues in terms of range and signal quality which were overcome through the use of solutions such as tuned ground planes, directional antennae, antenna masts on groundside and radio transparent compartments for antenna.

4.4.6 Additional Testing

A wide range of additional testing was required performed and included usable fuel tests, low and high speed taxi tests (to evaluate handling and braking performance), control surface actuator load testing/ phase margin test etc. All tests were deemed successful and served to show flightworthiness to the AFRL flight directorate who granted permission to operate the aircraft in accordance with a Transport Canada Special Operating Certificate.

4.5 Reduced Complexity Flight Tests

Due to overall complexity of building and testing the 1/9th scale aircraft, a series of flight tests of incremental complexity were also performed to familiarize the team with the joined wing configuration and its characteristics (these were introduced previously in Chapter 3). The reduced complexity flight tests were completed utilizing a 38% model of the Geometrically Scaled JWSC RPV. These models, deemed “Mini SensorCrafts”, had a 1.85m wingspan utilizing twin 72 mm diameter electric ducted fans.

The aircraft had the exact scaled outer mold line as the full scale and also have scaled overall thrust and mass. The reduced complexity flight tests ranged from initial proof of concept flights for the JWSC configuration to more advanced performance characterization, including stall speed tests and investigation into Dutch roll tendencies for the JWSC configuration. The most important contribution of the reduced complexity flight tests were invaluable insight into the flight performance and handling qualities of the JWSC configuration and as a test bed for autopilot control law development. Additional testing was performed in the buildup to the 5m testing to further investigation flight maneuvers and test procedures that were proposed on the 5m configuration. Figure 78 below presents the Mini SensorCraft in flight.



FIGURE 78 - MINI SENSORCRAFT FLEET (LEFT); MINI SENSORCRAFT IN FLIGHT

4.6 Flight Testing

The following sections outline the initial flight testing of the geometrically scaled aircraft in Foremost Alberta. In addition, a summary of the post flight analysis is included as well as recommendations leading into flights of the aeroelastically scaled test article.

4.6.1 Flight Test Location

The Foremost, Alberta airstrip is a low traffic civilian airstrip off which the Canadian Centre for Unmanned Vehicle Services (CCUVS) operates small UAV programs. Figure 79 below shows an aerial photo of the Foremost Airstrip as well as the total approved airspace for the flight test of the GSRPV.



FIGURE 79 - AERIAL PHOTO OF FOREMOST AIRSTRIP (LEFT), APPROVED AIRSPACE (RIGHT)

The total approved airspace was defined as a 2.5km radius circle centered at Foremost's runway. This is the airspace which Transport Canada approved for flight operations. The "Safety Template," or the airspace in which all flight operations were allowed to continue uninterrupted, is shown above in green and was a 2.0 km radius circle centered at the runway truncated 0.5 km west of the approved airspace boundary and 0.5 km north of Provincial Highway 61. All planned flight tests would remain well within the Safety Template (as shown by the racetrack flight path presented in blue). Immediately outside of this safe zone, the rest of the approved airspace, shown in yellow, is known as the Caution Zone. Normal Operations would avoid flight in this region due to its inclusion of Provincial Highway 61. Immediately outside of the Caution Zone is the Kill Zone, shown

in red. If the aircraft had entered the kill zone, the failsafe would be automatically executed terminating the flight. The maximum permitted flight altitude was 700 ft.

4.6.2 Flight Test

The first flight of the GSRPV took place in Foremost Alberta on Saturday October 15, 2011 and consisted of a 7 minute 58 second flight completed entirely in fly-by-wire mode. Figure 80 presents a picture of the aircraft in flight from a ground perspective (left) and an installed tail boom camera perspective (right).



FIGURE 80 - GSRPV FLIGHT FROM GROUND PERSPECTIVE (LEFT); TAIL BOOM CAMERA PERSPECTIVE (RIGHT)

The pilot was able to successfully complete both figure 8 and racetrack patterns, well within the airspace allotted for the flight. The nominal cruise speed range of 35-45 m/s provided an ample speed range to complete all flight maneuvers in a slow, controlled manner while still avoiding stall. During the flight, Dutch roll oscillations were noticeable, but the fly-by-wire mode was able to damp them to the point where they did not negatively affect the flight.

After completing several racetrack patterns and figure 8s, a mock approach was successfully completed. Satisfied with the performance during the mock approach, a landing attempt was made. After completing the downwind leg, the aircraft was brought parallel to the runway. A gentle glide slope was maintained during the entire approach and a soft touchdown was made completing a successful flight. Figure 81 presents a picture of the GSRPV on final approach.



FIGURE 81 - GSRPV ON FINAL APPROACH

After touchdown, the aircraft veered towards the near side of the runway. The pilot attempted to control the aircraft; however, he was unable to kill the engines below idle. He called for the backup pilot to take control. The backup pilot immediately took control, corrected the rollout and shut down the engines. During final roll out, the left rear tire blew due to the large side forces experienced, but no damage was caused to the aircraft. The aircraft rolled to a stop, bringing the GSRPV flight test program to a successful completion.

4.7 Post Flight Analysis

This section serves as a summary of the initial flight of the Geometrically Scaled, 5 meter SensorCraft. The data logged on-board the aircraft was analyzed in order to better understand the flight envelope and to use it for subsequent mission planning and tuning of the autopilot.

4.7.1 Mission Summary

The mission profile of the GSRPV flight is shown below in Figure 82.

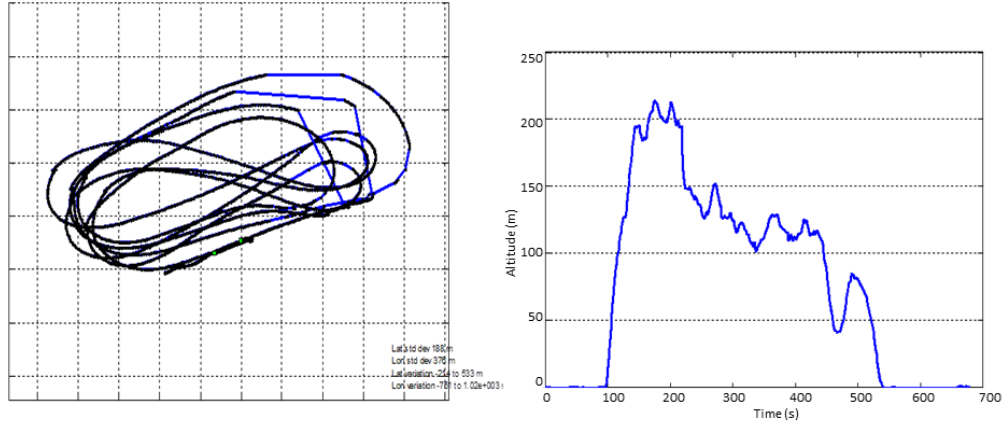


FIGURE 82 - AIRCRAFT GPS POSITION (LEFT); ALTITUDE PROFILE FOR FLIGHT (RIGHT)

The following table summarizes some of the limits imposed before the flight and the actual values achieved.

TABLE 10 – SUMMARY OF MISSION LIMITS

	Target	Actual Values
Vmin, Vmin	21.4 m/s	30.49 m/s
Takeoff Speed, VTO	25.6 m/s	34.2 m/s
Nominal Cruise Speed, VCruise	35-45 m/s	40.47 m/s
Do Not Exceed Speed, VNE	65 m/s	47.14 m/s max speed
Approach Speed, VApproach	25.6 m/s	31.07 m/s
Operating Altitudes, AGL	100-213 m	101-214 m
Max Distance from Operator	1500 m	796 m

4.7.2 Takeoff

The aircraft took off into a partial cross wind with a headwind component of 3.5m/s . During the takeoff run the aircraft achieved a forward acceleration of 0.529 g . The aircraft experienced 0.2595 g of lateral load due to steering input which was well below the limit placed on the aircraft by the autopilot of 0.4 g . This meant the pilot had full steering authority.

The aircraft accelerated to a rotation speed of 27.7 m/s before the pilot commanded gradual elevator input up to a maximum deflection of -19.4 degrees . The rotation time to pitch, before lifting off, was approximately 2.5 seconds and liftoff was achieved at a speed of 34.16 m/s and a distance of 163 m . The maximum Z acceleration

experienced during the lift off was **1.6 g**. Figure 26 below shows the throttle position and airspeed during the takeoff run.

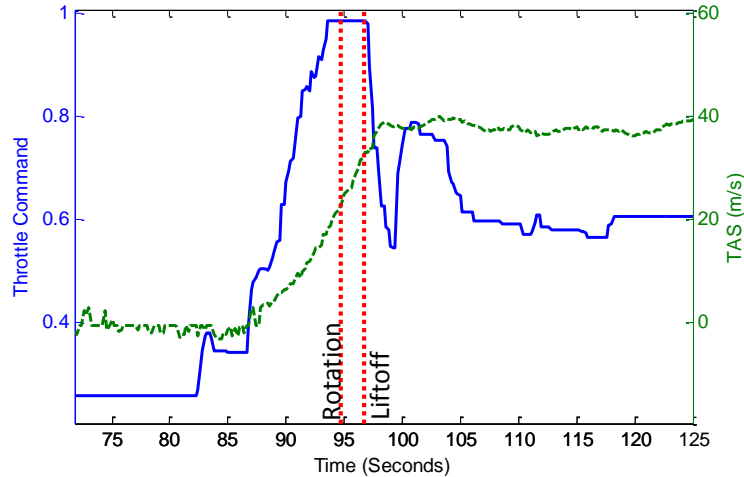


FIGURE 83 - AIRSPEED AND THROTTLE DURING TAKEOFF RUN

Upon lifting off, the aircraft climbed at an average vertical speed of **4.0 m/s (7.11 m/s maximum)**, while maintaining an average climb speed of **38.2 m/s ($C_L=0.585$)**. This corresponds to a climb fraction of **1.79**. The climb took **44 seconds** at which point the pilot began to level out at approximately **202 m AGL**.

Immediately after takeoff the aircraft displayed some rolling oscillations with maximum amplitude of **22.5 degrees** at a frequency of **1.18 Hz**, before decaying throughout a climbing bank as shown in Figure 84

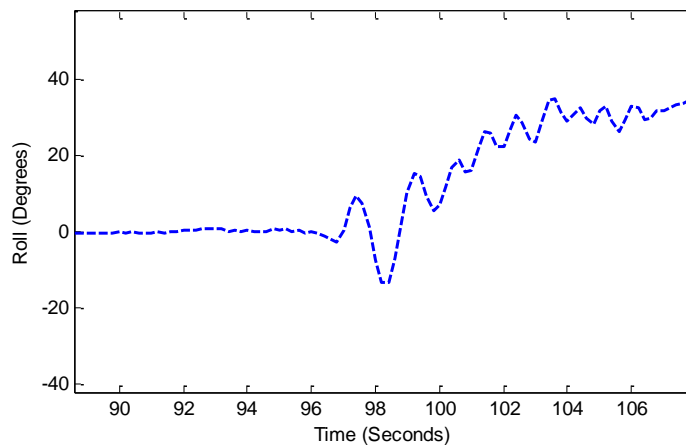


FIGURE 84 - AIRCRAFT ROLL IMMEDIATELY AFTER TAKEOFF

4.7.3 Cruise Segment

The cruise portion of the flight was performed at an average altitude of **143 m** AGL with a minimum altitude of **101 m**. The maximum altitude reached was **214 m**. The average throttle setting over the cruise segment was **48.52%** which corresponds to an average thrust of **117.8N** at a fuel consumption of **564 ml/min**. The average cruise speed was **40.47 m/s** ($C_L = 0.5047$) with the min/max speeds of **32.65** and **47.1 m/s** respectively. This fell closely within the cruise target speeds set out for the pilot before the flight (based on Mini SensorCraft operating speeds) of **35-45 m/s**.

Several points were chosen throughout the cruise segment to investigate C_L vs C_D . Figure 85 shows the normalized values of vertical rate, the X acceleration, throttle position and roll with the points chosen for investigation shown as red dots.

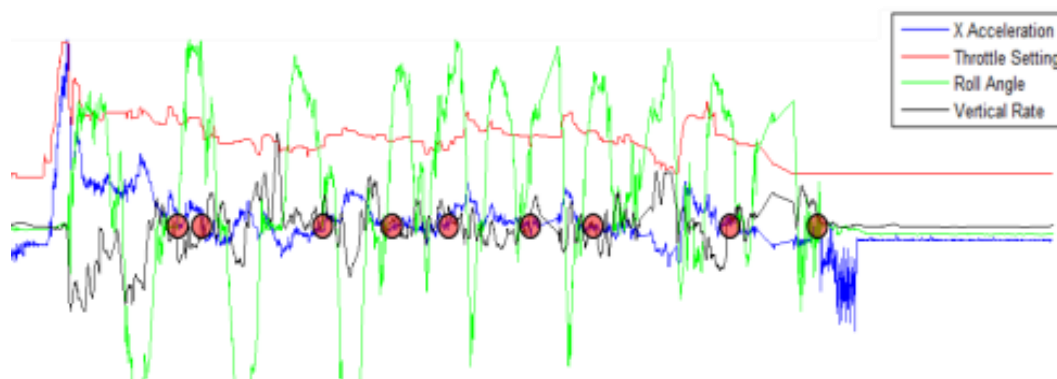


FIGURE 85 - POINTS CHOSEN TO INVESTIGATE C_L AND C_D

The points chosen correspond as closely as possible to simultaneous conditions of steady throttle input, zero X acceleration and zero vertical rate. C_L is calculated based on the aircraft's mass at that point in the flight (allowing for fuel burn), the aircraft's airspeed and the instantaneous bank angle. The C_D was calculated based on predicted thrust from throttle percentage and assumes that X acceleration and climb rate are zero. Figure 86 shows the results overlaid on a polar plot of a CFD analysis used for mission planning as well as the vortex lattice results that are the basis for the simulators.

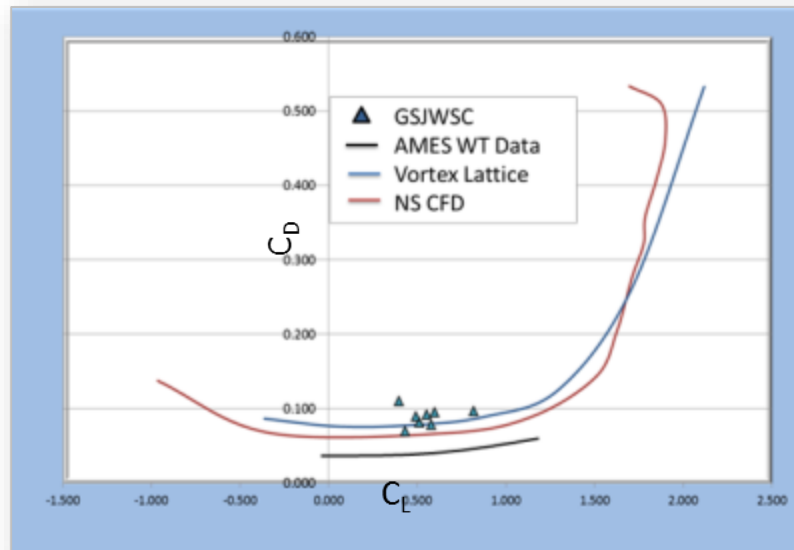


FIGURE 86 - COMPARISON OF CALCULATED POLARS VS FLIGHT TEST DATA

The data presented above shows some spread but appears to validate the models around this operating range. The CFD and Vortex Lattice Model (VLM) results show good agreement while the wind tunnel results from tests performed by Boeing in the NASA Ames WT slightly under predict the drag. This is likely due to the fact that the WT model did not have antenna, landing gear, servos in the airstream etc. The VLM polar is closer to the flight test data as expected since a base drag (C_{D0}) was added based on Mini Sensorcraft flight test results. (The VLM also accounts for form drag, in addition to induced drag, by interpolating station-wise airfoil polars based on local flow conditions).

During the flight, the elevator travel was between **-25.57 degrees** and **1.74 degrees**. The trimmed elevator deflection was approximately **-8 degrees** which was expected considering the forward cg location chosen for the flight. These elevator values were well within the minimum and maximum limits set in the autopilot which are **-35** and **30 degrees** respectively. Aileron travel was between **-35 and 12.5 degrees** which corresponds to the limits set in the autopilot (aileron differential is used which accounts for the non-symmetric endpoints). However, the saturation of the aileron inputs only occurred on the landing approach (likely as a result of the

low speed roll oscillations and over tuning of roll gains as will be discussed later). Aileron travel throughout flight can be seen in Figure 87.

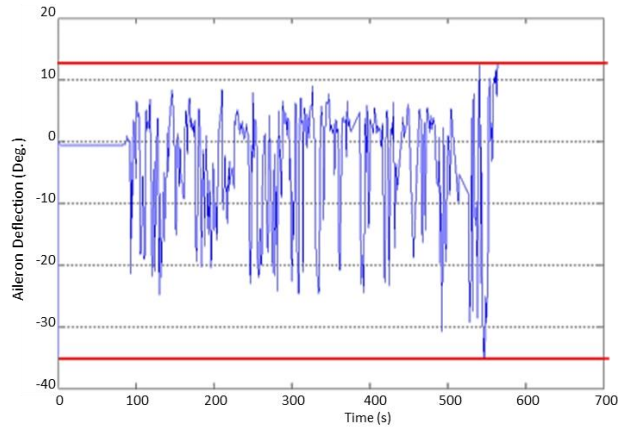


FIGURE 87 - AILERON TRAVEL THROUGHOUT FLIGHT

The minimum Z acceleration experienced during flight was 0.594 g during a pitch down maneuver while the maximum experienced was 1.82 g during a 50 degree banked turn. Figure 88 below shows the Z acceleration during flight, as well as the predicted loading required to maintain the aircraft's bank angle at that instant.

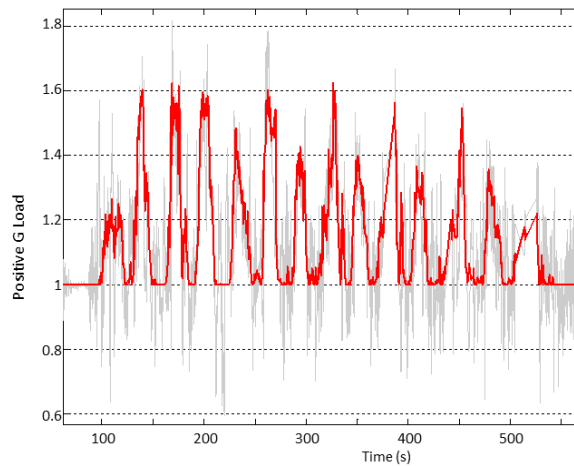


FIGURE 88 - Z-ACCELERATION THROUGHOUT FLIGHT

The large amount of noise is expected due to atmospheric conditions and structural elasticity. However, the autopilot is forward of the cg by approximately 0.3 m and therefore rotational accelerations may have an effect on the Z accelerations. Further investigation will be performed to determine the effect of this coupling.

Some mild roll oscillations was observed over the cruise segment and its frequency was averaged over three points in the flight. The frequency is **1.296 1/s** at an average speed of **41 m/s**. The amplitude at these points is very low at approximately **3 degrees**.

4.7.4 Range and EMI

The Range and EMI were the biggest issues in the lead up to the flight and are still the biggest area of concern. The figures below shows that the Acknowledgement Ratio (ACK) ratio fell below recommended values (should be >90) for large portions of the flight and in some cases the signal was dropped all together.

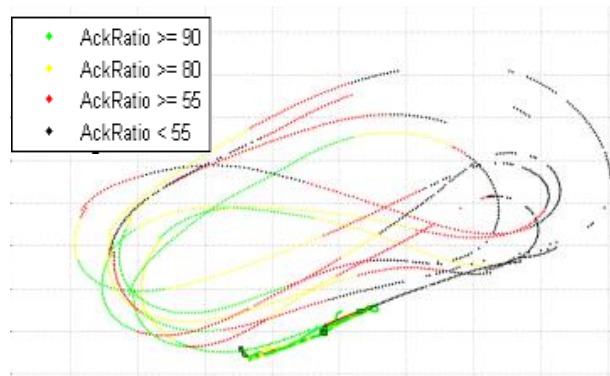


FIGURE 89 - ACKNOWLEDGEMENT RATIO ALONG FLIGHT PATH

It was partially due to this poor communications link that this initial flight test was cut short at only one flight. Since discovering these communications issues in flight, work has been done to reduce the problem and solutions include making the vertical tail boom RF transparent for better line of sight to antenna during flight as well as replacing modems with 900MHz band frequencies that will not interfere with any existing systems on the aircraft.

4.7.5 Landing Segment

Two landing approaches were made. The first resulted in a go-around before landing on the second. The base leg of the first landing approach was **487 m** and the second was **580 m**. The approach leg for the landing was **650 m** long with average approach speed of **31.1 m/s**, which corresponds to an approach fraction of **1.45** ($V_{\text{Approach}}/V_{\text{min}}$). The average vertical rate on approach was **-3.8 m/s** resulting in an approach slope of **-7.0**

degrees. The final speed was **25.3 m/s**, resulting in a final descent fraction of **1.18** ($V_{\text{Final}}/V_{\text{min}}$). The final vertical rate was **3.7m/s** resulting in a final slope of **-4.5 degrees**.

During touchdown the minimum g-loading was **0.667 g**. The rollout distance was **292 m** with a maximum negative X acceleration due to braking of **-0.298 g**. The maximum lateral acceleration due to steering loads was **0.4 g** which saturated the limits imposed by the autopilot. This means that the autopilot limited the nose steering in order to not exceed **0.4 g**. Wing rock was observed during the final approach. The frequency was measured at **0.769 Hz** with amplitude of approximately **12.2 degrees**.

4.7.6 Fuel Usage

This section summarizes the fuel usage within flight and the comparison of predicted values with those measured in flight. From this a refined estimate of flight duration is determined for subsequent flights and recommendations are made in order to increase the overall mission duration

4.7.6.1 Unusable Fuel

An analysis of the aircraft's orientation shows that the initial estimate of **6.1 kg** unusable fuel was overly conservative. An unusable fuel test was performed in the lead up to the flight (Section F) in which a most adverse aircraft orientation was chosen with **19.3 degrees** pitch down attitude and **15 degrees** roll. A review of the flight test data was performed to determine the direction of the instantaneous acceleration vector throughout flight. This then corresponds to the free surface orientation of the fuel.

Results show that the most adverse orientation in flight was **-12 degrees** pitch and **3.5 degrees** roll. Only six combinations of roll/pitch were investigated during the unusable fuel tests but the nearest test was for **-13.4 degrees** pitch and **10 degrees** roll, which corresponds to **4.3 kg**.

Choosing a new unusable fuel amount of **4.3 kg** is still conservative and could be reduced further if additional unused fuel tests were run nearer the conditions achieved in flight. Also, at the most adverse flight condition there still exists a **3.4 second** buffer fuel can still be fed to the engines from the header tanks, even though no

fuel would be picked up from the main tank. However, due to the catastrophic results of an engine flame-out, an unusable fuel amount *of 4.3kg* is a good choice considering data on hand.

4.7.7 Mission Duration

The remaining fuel drained from after the flight was **11.0 kg** and a total of **4.5 kg** of fuel was used. The calculated fuel usage over the flight based on throttle settings is shown in Figure 90.

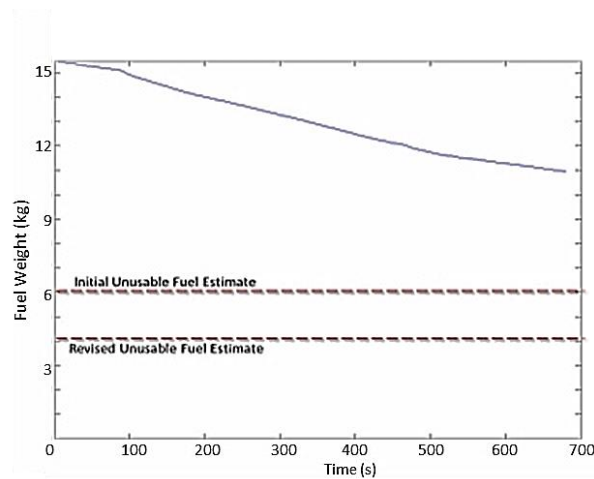


FIGURE 90 - FUEL BURN OVER MISSION

Based on the calculated average fuel burn for the cruise segment, an additional **10.5 minutes** of cruise duration is possible based on the initial **6.1 kg** unusable fuel estimate. Using the revised unusable fuel value of **4.3 kg**, an additional **14.4 minutes** of cruise is obtainable. (The cruise time for this flight was **4.87 minutes**).

If additional cruise time is required beyond these numbers, the unusable fuel amount would have to be reduced through the use of a fuel sump, flapper doors, larger header tanks etc. If usable fuel were brought down to a value of **1 kg**, the cruise time could be increased by **21.5 minutes**, bringing the total cruise time to **26.4 minutes**.

4.7.8 Roll Oscillations/Dutch Roll

Our analytical models predicted a marginal Dutch roll stability for the SensorCraft. During initial manual flights, with the Mini SensorCrafts, this instability was manifested as an almost uncontrollable roll oscillation. This led to the necessity for the autopilot to damp out oscillations and results in a much more controllable aircraft.

Even with the use of fly by wire, some degree of roll oscillations was still observed. Table 9 below shows the measured roll oscillations frequency observed during takeoff, cruise and landing, as well as the calculated Dutch roll frequencies calculated from our models.

TABLE 11 – MEASURED ROLL OSCILLATIONS VS CALCULATED DUTCH ROLL FREQUENCY

Flight Phase	AC mass /Velocity	Measured Wing-Rock Frequency/Amplitude	Calculated Dutch Roll Frequency
	Kg/m/s	Hz/Degrees	Hz
Takeoff	67.1/38	1.18/22.5	0.351
Cruise	65.1/41	1.296/3.0	0.366
Landing	63.0/25	0.769/12.2	0.328

Immediately after the initial flight it was felt that this roll oscillations was a result of the autopilot not sufficiently damping the Dutch roll mode and that an increase in lateral control gains was required. However, it can be seen in the above data that the measured Dutch roll frequency throughout flight was at a much higher frequency than predicted by the computational models, although the general changes in frequency at each flight phase are consistent. This brought into question a) the validity of the computational models and b) the assumption that the roll oscillations was due to the marginal Dutch roll. An investigation was performed to determine the root cause of the discrepancy.

An analysis of Mini SensorCraft data was performed to compare to theoretical predictions. The roll oscillations were measured and a Power Spectral Density analysis was performed from flight test data to determine the frequencies as shown in Figure 31 and Figure 32.

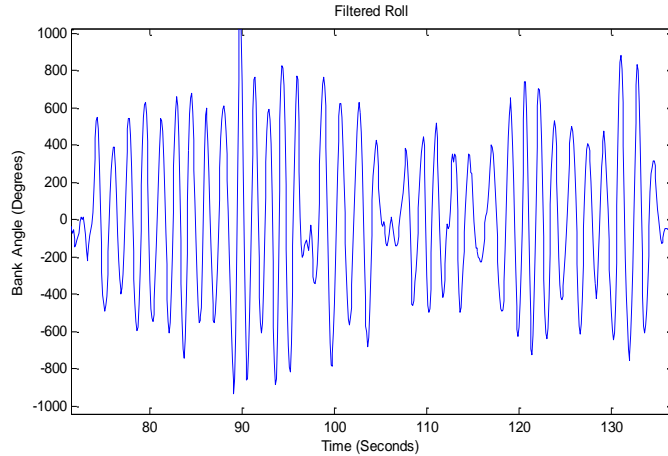


FIGURE 91 - SAMPLE OF MINI SENSORCRAFT FLIGHT DATA SHOWING ROLL OSCILLATIONS

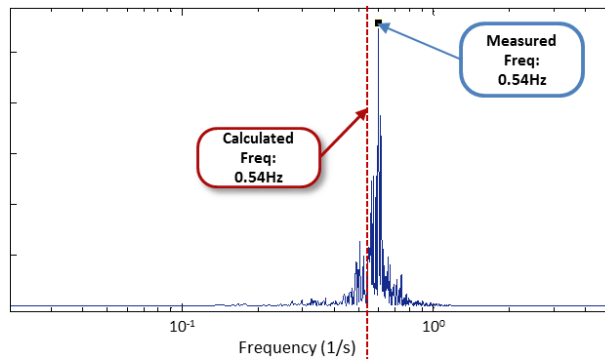


FIGURE 92 - PSD ANALYSIS OF MINI SENSORCRAFT ROLL ANGLE SHOWING ROLL OSCILLATION FREQ.

The measured frequency of 0.606Hz was very close to the predicted value of 0.54Hz and serves to validate the computational model. This same level of agreement is observed for many sets of flights and across many flight conditions. This resulting confidence in the dynamic model pointed towards the possibility of the closed loop roll control loop in the autopilot being over tuned and driving the faster oscillations observed in flight.

Simulations were performed for both open and closed loop responses to a chirped bank command using the 6dof simulator. As expected, the open loop control predicts a frequency of oscillation similar to the analytical model (the basis of the 6dof) which is similar to that predicted by scaling the Mini SensorCraft's response to the GSJWSC test point. However, when the autopilot is modeled in the loop, the resulting oscillations are

quickly damped out (with some overshoot) with a higher frequency, as observed in flight. Figure 93 and Figure 94 show the open and closed loop response to the chirped bank command.

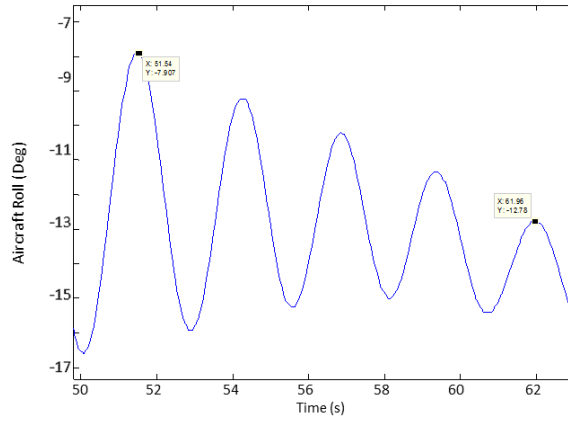


FIGURE 93 - SIMULATED OPEN LOOP RESPONSE OF GSJWSC TO CHIRPED BANK COMMAND (0.384 Hz)

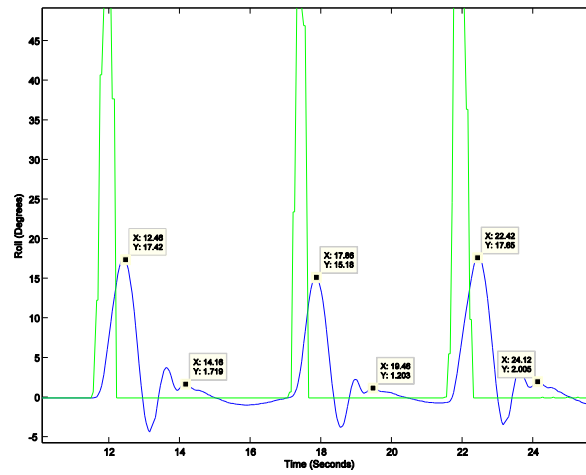


FIGURE 94 - SIMULATION OF ROLL RESPONSE TO CHIRPED BANK COMMAND (GAINS FROM FLIGHT TESTS)

4.8 Conclusions

There are many complexities involved in developing a flight worthy aircraft for measuring in-flight behaviors. Many of the components required for a UAV larger than the 35kg RC aircraft upper limit have to be custom designed and fabricated. In this case most components, from landing gear to servo mounts, needed to be designed and specified. Some items such as the engines and servos can be purchased off the shelf but special attention is required to ensure their reliability and modifications are required to incorporate them into such a complex aircraft.

Some challenges faced here were the requirements for redundancy, both in terms of systems and operation. Custom solutions were required to ensure that several levels of redundant control were achievable based on all of the conceived failure scenarios. This included the use of three separate pilots with separate command links to overcome autopilot failures, loss of communications, flight outside of visual limits etc.

One of the largest challenges was in terms of communications and electromagnetic interference. Due the large number of data links and command/control links, the aircraft had a lot of problems regarding interference. This was compounded by the large blanketing caused by the structure that was made primarily of carbon fiber. Special attention was focused on placement of antennae with redundant antennae used as often as possible. However, in retrospect it would be wise to have made nonstructural portions of the aircraft out of radio transparent materials and place safety critical antennae at these locations (for instance, making the boom out of glass and embedding antennae inside).

Ground testing made a big difference in terms of the success of the 5m evaluation phase. A thorough and systematic approach to the ground testing ensured a flight worthy aircraft was taken to Foremost and many bugs had been caught and fixed in this initial testing stage. Flight test planning was also of great importance with a very large emphasis on check lists and contingency plans.

The flight of the 5m aircraft went very well, with the chosen control scheme being very effective at controlling the aircraft. The pilot reported good flying qualities throughout the flight envelope but there was still some minor wing rock oscillations. Post processing and simulation showed this to be due to over tuning of the lateral control loops. Subsequent model tuning and loop gain optimization resulted in a simulated response with much less wing rock. These updated parameters served as the basis for future flights of the smaller “Mini” SensorCraft configurations.

The blowout of the left main tire on roll out cut the flight test campaign short and further emphasized the importance of developing custom components rather than relying on hobbyist grade parts. Despite this shortened flight test campaign the 5m platform proved to be very stable and reliable. It was proven that the 5m platform is feasible for future investigation of flexible configurations. In addition, the lessons learned and the procedures developed will serve as a foundation for all future efforts, both in terms of the SensorCraft and all other UAV

Chapter 5 - Aeroelastically Scaled to Aeroelastically Tuned Demonstrator



5.1 Linearly Scaled 5m Aircraft Modifications

After the successful flight of the geometrically scaled RPV, the 5m platform was proven to be a feasible and effective configuration for subsequent testing of a Linear Aeroelastically scaled wing set. The plan was to further refine the aeroelastically scaled design, using the scaling framework introduced previously. Finalized component weights, space reservations and minor modifications to the outer mold line (such as access panels) could now be captured and implemented in the framework as planned.

Around the same time, the client (USAF Research Laboratory) began shifting their priority to the nonlinear static response of the aircraft. The idea is that the linearly scaled aircraft could be pushed to high g loading cases that would allow the investigation of several phenomenon predicted by their in house studies.

Two linear elastic scaling studies were performed in parallel, one by the author and one by Charles Eger^[60] of Virginia Tech. Eger's work was performed using the Finite Element model developed and analyzed by the author with the main difference being that the framework used here employed ANSYS FE software, whereas the VT model was converted to NASTRAN. In addition, the full scale FE model supplied by Boeing was export controlled and while not available to the author was available to the VT students. Boeing's model was used on occasion to generate the required baseline data that was used as inputs to the authors scaling framework.

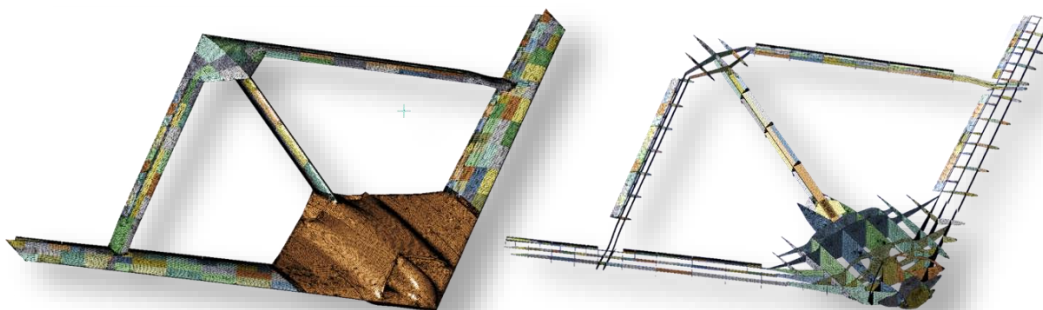


FIGURE 95 – INTERNAL AND EXTERNAL VIEW OF HIGH FIDELITY FE MESH

Upon further analysis, using a high fidelity FE Model developed for the refined scaling work, it started to become apparent that the baseline aircraft supplied by Boeing was very stiff and when scaled down to the 5m

size would be too stiff to display sufficient and measurable nonlinear responses. The USAF and Boeing were asked about this problem and after some deliberation it was stated that the configuration that was released to us (**Boeing-410-E8**) was a “pre weight optimized model”, and therefore had a very stiff structure. Subsequent design studies by those entities had yielded several subsequent configurations which showed these large nonlinearities that they had mentioned were of concern. Unfortunately, at the time these update models had remained classified. Gaining clearance for the new configuration would not happen in the remaining timeframe of the current work and therefore, an alternative plan was devised.

The US Air Force removed the “**Aeroelastically Scaled**” requirement and replaced it with “**Aeroelastically Tuned**”. This would allow the design of a much more flexible aircraft, capable of investigating any of a number of structural nonlinearities. The intent was that several candidate designs would be generated and the Air Force would choose the one which most closely matched their weight optimized model for further investigation. An initial study was performed here to investigate the primary structural nonlinearities and the main effects of several key parameters such as joint stiffness and material properties.

5.2 Investigation of Nonlinearities and Design Space Exploration

Two forms of nonlinearity had been identified by the Air Force and Boeing. The first form was the so called boom reversal. This involved the aft most tip of the boom deflecting upwards under a trimmed load case in the linear region and then reversing and deflecting down as the load increases. (As it turns out the reverse was also possible, where the boom deflects down in the linear region and then reverses to deflect up as the load steps increase). The second form of nonlinearity was the buckling of the aft wing. Both of these effects were to be studied using a parametric model.

Two frameworks were developed. The first one was based on a low fidelity (LF) beam model (~50 beam elements) while the second was based on the high fidelity (HF) model introduced previously (~150k shell elements). The intent was to use the LF model to quickly sweep across many design variables to explore the

design space and then run some optimizations to maximize the nonlinear response. These results were then applied to the HF model to see if they held in a more accurate model.

5.2.1 Low Fidelity Analysis

The low fidelity model was created using ANSYS and consisted of Beam 188 elements running along the 25% chord or the main lifting surfaces. A simple truss structure was used to model the fuselage and MPC 184 general joint elements were used to model interfaces between physical parts such as fuselage (Fuse), forward wing (FW), boom and rear wings (RW). The structural members were modelled as rectangular tubes consisting of the default aluminum alloy material. Figure 96 below shows the beam locations relative to the aircraft's planform as well as a visualization of the beam cross sections of the baseline design.

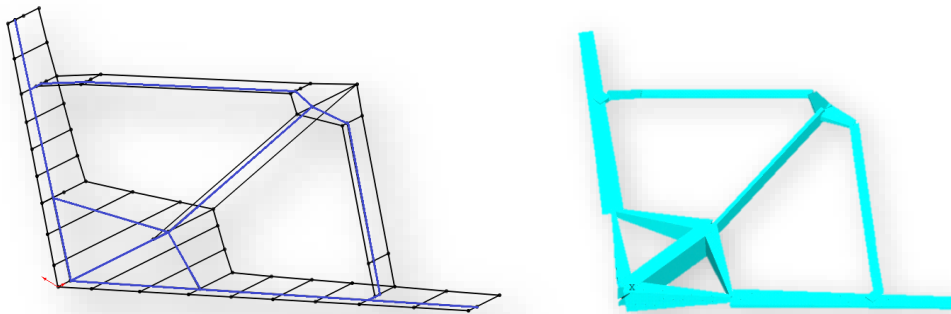


FIGURE 96 - BEAM LOCATIONS SHOWN IN BLUE (LEFT) AND VISUALIZATION OF THEIR CROSS SECTIONS (RIGHT)

The model was paramatized based on the properties of the FE model. Joint rotational stiffness' were exposed as variables to adjust the flexibility of the structural interfaces. Figure 97 below shows the joints modelled, with the X,Y and Z annotations signifying which degrees of freedom were used as variables for each joint.

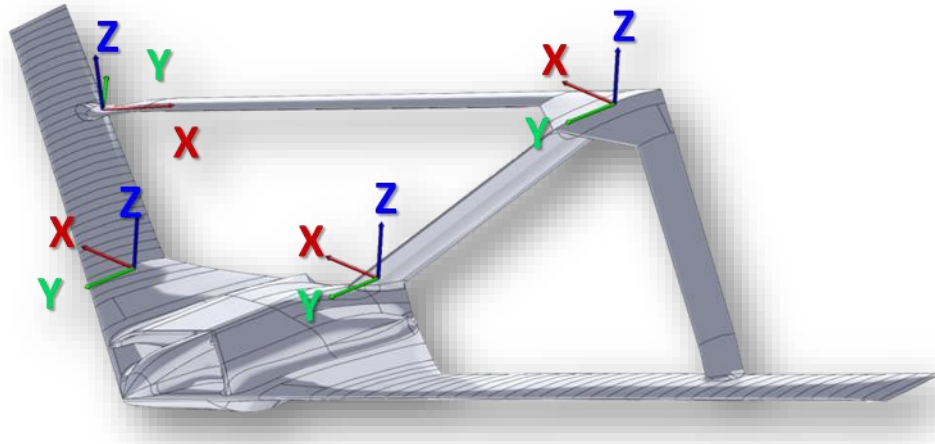


FIGURE 97 - DOFS USED AS DESIGN VARIABLES IN PARAMETRIC STUDIES

The running stiffness of the structural components were paramatized using the beams' cross sectional geometry. Since the beam was modelled as a tube, the cross sectional moments of inertias and the polar moment of inertia could all be uncoupled and varied using three geometric parameters (beam width, height and wall thickness). An additional parameter allows beam stiffness to be tapered along the length.

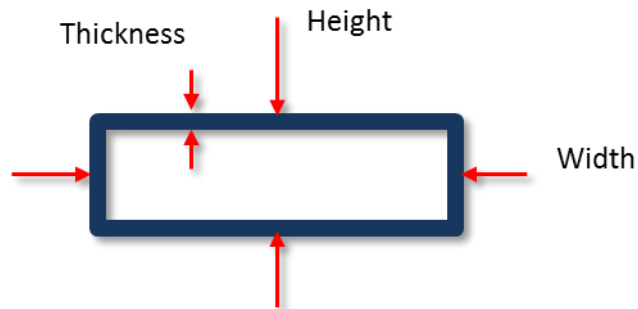


FIGURE 98 - GENERIC BEAM CROSS SECTION SHOWING THREE VARIABLES USED TO TUNE STIFFNESS

The model was integrated into a ModelCenter® based framework that was used to automate the analysis process of exploring the design space. A linear analysis branch was also included that was used to tune beam model to match the experimental load test results of the geometrically scaled 5m RPV (to create a baseline structural model to center the design space and to tune the fuselage structure which subsequently remained

unchanged). The main features of the framework are listed below with a graphical representation shown in Figure 99.

1. **Preprocessing Script** – this created ModelCenter Variables and linked them to the ANSYS inputs. This framework included several user activated switches to change the run case parameters in the ANSYS model (such as follower force effects, meshing parameter etc) as well as mathematical relations to uncouple the cross sectional moments of inertia using the geometric parameters.
2. **Parallel Linear Run Cases** – this allowed 1-4 linear static cases to be run in parallel. Separate branches allowed models with slightly different topologies and load cases to be run simultaneously. This was helpful in matching experimental data that was produced from static load tests. These tests were performed with and without the aft wings attached and allowed the linear model to be tuned to match both the forward wing and boom stiffness parallel to the full configuration tests. Each solution branch also includes scripts used to calculate objective functions and constraint checks as well as perform some post processing of results.
3. **Modal Analysis Branch** – a modal analysis could also be run by itself or in parallel with the static load cases. The branch was used to parse and sort the modal solutions and also to calculate mass properties.
4. **Nonlinear Branch** – this was the branch used to investigate the nonlinear response of the aircraft. It output the time histories for the analysis and a Matlab script was used to process this data. The post processing involved calculating objectives such as nonlinearity parameters (to quantify how “nonlinear” the configuration is) and saving results to the hard-drive.
5. **Post Processing branch** – this module rendered the baseline mesh as well as the linear and nonlinear nodal deformations. This branch could also calculate multi-objective functions based on individual objectives determined by the previous branches.

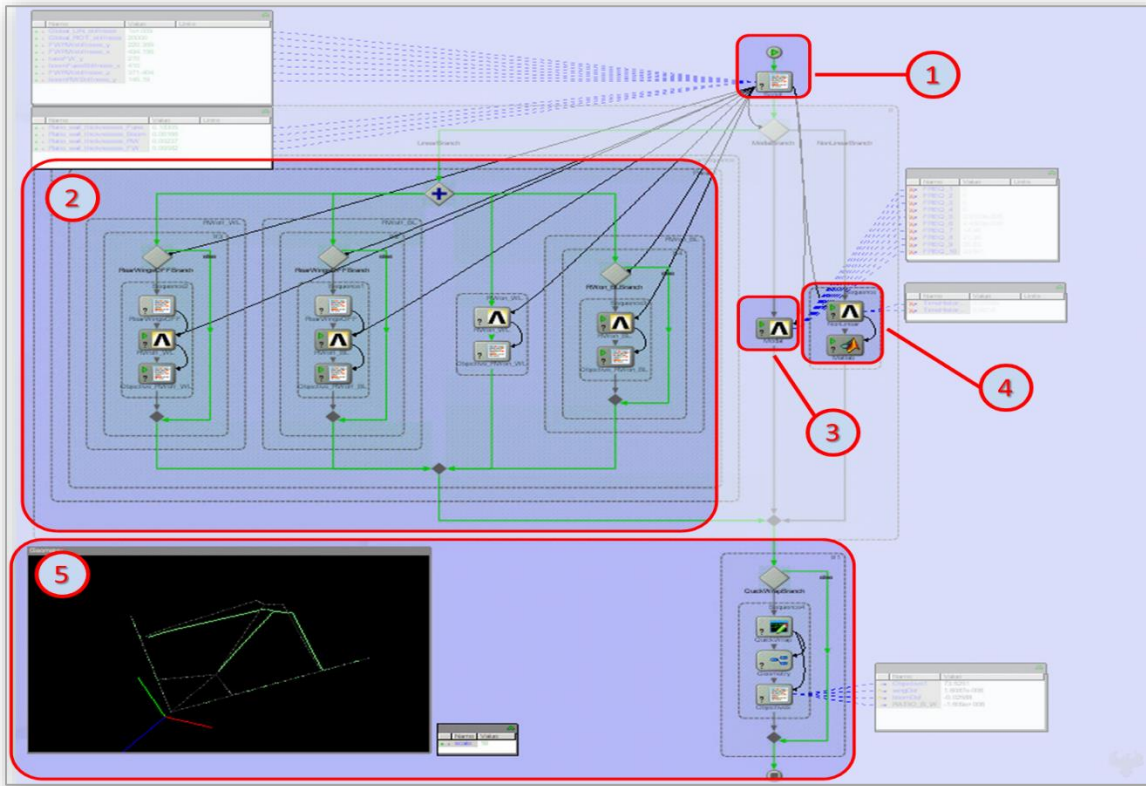


FIGURE 99 - FRAMEWORK USED TO MATCH EXPERIMENTAL RESULTS AND INVESTIGATE NONLINEARITIES OF JOINED WING

The first study run with the framework involved the matching of experimental load case results determined from static loading tests of the geometrically scaled 5m RPV. This ensured that when sensitivities were taken they would be done so around a feasible design point that was based on some realistic structural response. It also served to tune the fuselage properties which were subsequently held constant for the remaining studies. The four linear branches ran 4 parallel load cases that corresponded to those applied experimentally. These load cases are shown below.

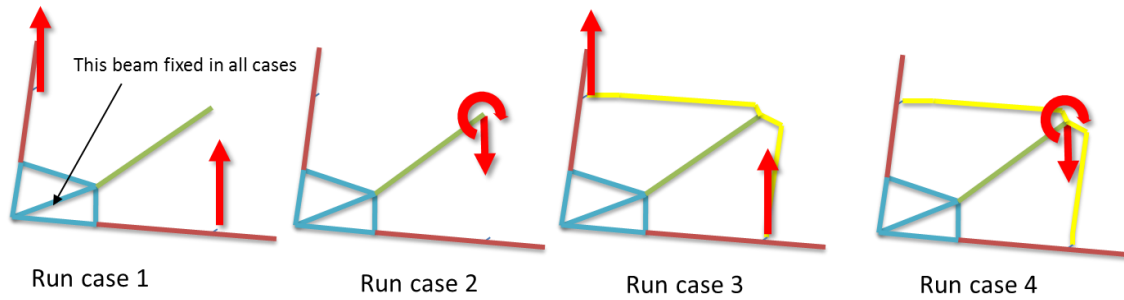


FIGURE 100 - LOAD CASES USED IN TUNING BASELINE BEAM MODEL

Next, a series of sensitivity studies were performed on the joints and the stiffness' of the structural members in order to understand which parameters affect the structural response the most. This was done to primarily reduce the dimensionality of the design space by determining which parameters could be ignored in subsequent higher fidelity and nonlinear investigations. Figure 101 below shows the sensitivities of flexibility due to the joint stiffness's for one of the load cases analyzed (point loads applied on joints with magnitude chosen to yield equivalent forward wing root bending moments to a 3.5g pull-up maneuver).

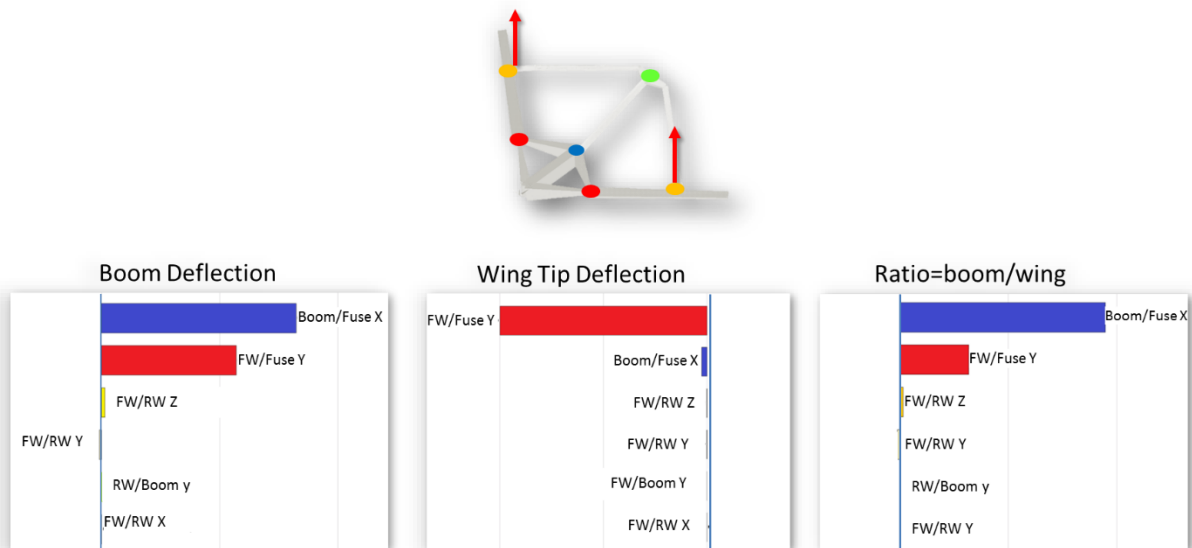


FIGURE 101 – NONLINEARITY SENSITIVITIES DUE TO JOINT STIFFNESS'S (PARAMETERS WITH LITTLE TO NO EFFECT ARE NOT SHOWN)

Similarly, an investigation into the effects of the running stiffness of the main structural components was performed for several load cases. Figure 102 below shows the results for the same load case described previously.

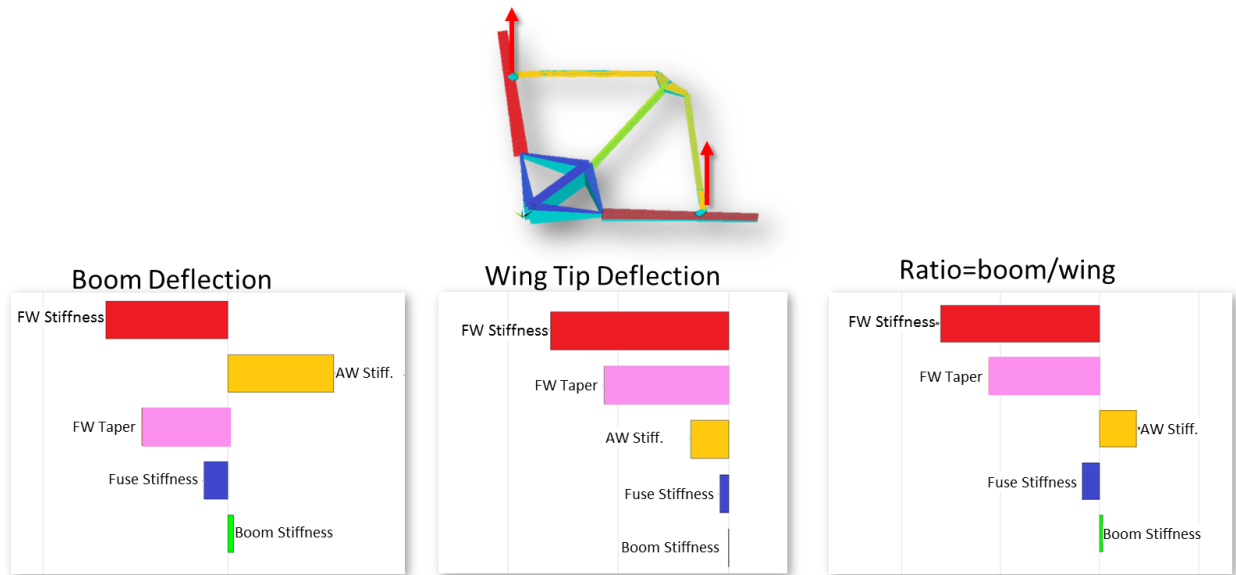


FIGURE 102 - SENSITIVITY TO STRUCTURAL MEMBER STIFFNESS (PARAMETERS WITH LITTLE TO NO EFFECT ARE NOT SHOWN)

Sensitivities of the nonlinear response were also investigated using this low fidelity model. The two nonlinear responses of interest mentioned earlier were looked at. Measures of nonlinearity were calculated for boom reversal (**Reverse Factor**) and aft wing buckling (**Buckling Factor**). An additional form of nonlinearity was also noted and tracked in this process which involved either a stress stiffening or softening of the boom and a large nonlinear deformation due load stepping (**NL Factor Boom**).

The effects of both joint and structural stiffness were investigated. The results of these tests are shown in Figure 103 and Figure 104 below.

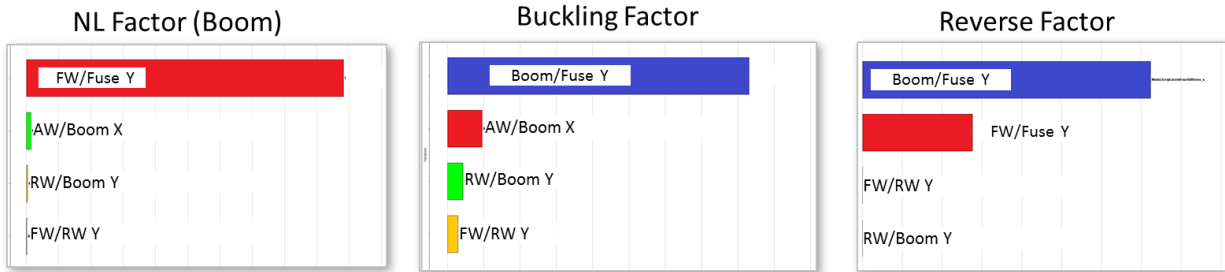
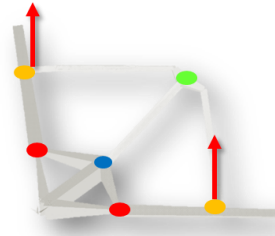


FIGURE 103 - EFFECT OF JOINTS ON NONLINEAR RESPONSE (PARAMETERS WITH LITTLE TO NO EFFECT ARE NOT SHOWN)

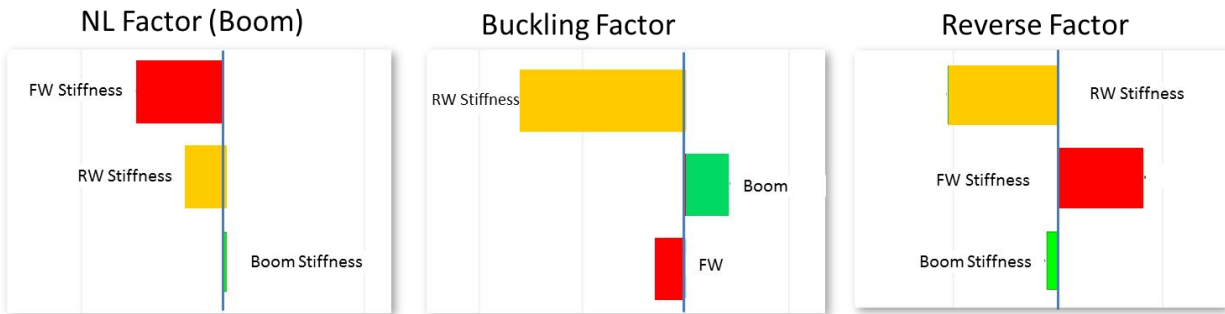
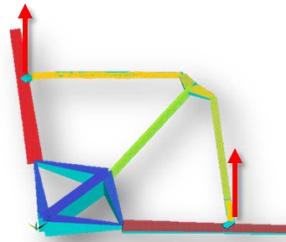


FIGURE 104 - EFFECT OF RUNNING STIFFNESS ON NONLINEAR RESPONSE (PARAMETERS WITH LITTLE TO NO EFFECT ARE NOT SHOWN)

A subset of the parameters with the largest effect on the nonlinear response was chosen to further investigate the design space. They included the FW, RW and Boom stiffness as well as the FW/Fuse Y axis joint stiffness as well as the Boom/Fuse Y axis joint stiffness. A regular grid was used to build the Design of Experiments in order to explore the design space. Each variable was analyzed at 7 values resulting in a total of 7^5 or 16807 separate

nonlinear runs being analyzed. After completing the runs, all three nonlinearities were captured in the design space, with some designs showing boom reversal (up and then down as well as down then up), nonlinear boom tip deflection and aft wing buckling. Figure 105 below shows the projection of the design space into two dimensions (RW and Aft Wing Stiffness with the vertical axis showing a measure of nonlinearity). In this one slice of the design space we can see different forms of nonlinearity including geometric stiffening of boom tip (1), boom up/down reversal (2) and boom softening (3).

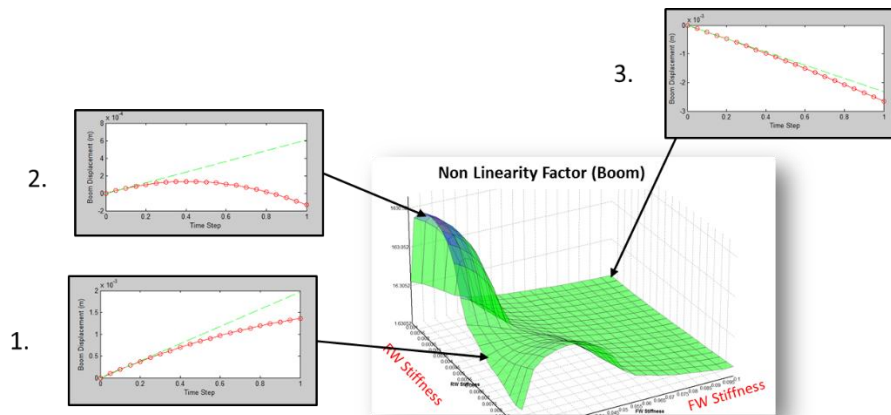


FIGURE 105 - PART OF DESIGN SPACE SHOWING DIFFERENT NONLINEAR RESPONSES

Through interrogation of the design space, three candidate designs were chosen; One showing the largest amount of boom reversal, one showing a large amount of boom tip softening and one demonstrating large aft wing buckling response. These three designs were used as the starting point for three separate gradient based optimizations meant to further maximize the nonlinear response using the High Fidelity Model. The resulting designs were then proposed as candidates to the US Air Force and Boeing as possible starting points for the Aeroelastically Tuned RPV design.

5.3 Aeroelastically Tuned SensorCraft RPV for Investigating Aft Wing Buckling

Of the three candidate designs presented to the USAF, the one which they felt was of greatest interest was the design exhibiting aft wing buckling response. This was in a large part due to the fact that this phenomenon was

present in their weight optimized model (which could still not be released due to clearance limitation) and also because while interesting, the boom reversal phenomenon observed in this model, as well as their own, was on a very small scale. There was some concern that this small deflections may be difficult to measure in flight due to noise, control surface loads, turbulence etc.

The design displaying the large aft wing buckling, proposed previously, served as the basis for a more in-depth investigation using a nonlinear aeroelasticity framework developed by Anthony Ricciardi of Virginia Tech ^[52]. This framework was used to couple the aerodynamic loading and structural response at various trim states. This allowed further refinement the nonlinear response of the baseline design while also calculating design constraints based on safe operating limits.

This new design that was modelled inside Mr. Ricciardi's framework consisted of similar geometry as the preceding model with the exception that the aft wing was modelled now as a series of beams making up a ladder structure (see Figure 106 below). The forward wing was again modelled as a rectangular cross section with variable height acting as the main tuning parameter. Further optimizations were performed by Mr. Ricciardi to further increase the aft wing buckling response while still obeying several new constraints (such as material limits, control surface reversal etc). The end result of his study was specifications for a beam model of the forward inboard wing and aft ladder spar. These specifications served as the final design driver for the detailed design presented in the next chapter.

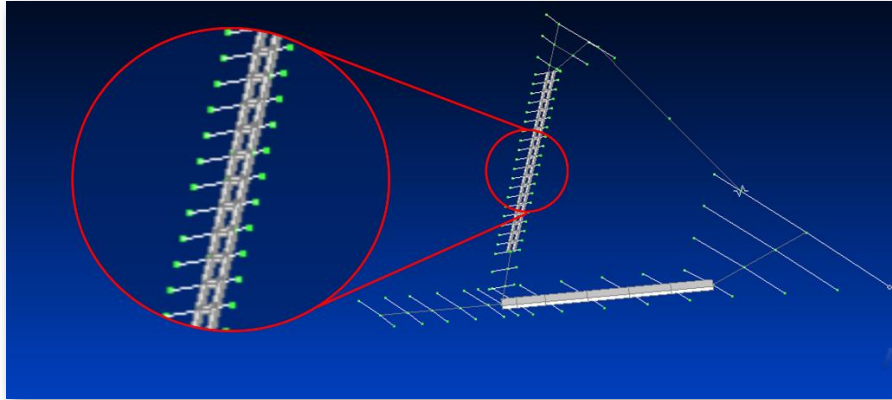


FIGURE 106 - STRUCTURAL LAYOUT OF STRUCTURAL MODEL USED IN AEROELASTIC FRAMEWORK

5.4 Aeroelastically Tuned “Mini” SensorCraft Configuration

Upon reaching a final structural layout there was a great deal of concern with all parties over the amount of flexibility that was introduced in the airframe. The additional flexibility posed a great challenge in terms of stability and control since the aerodynamics would now change as a function of loading. Some concerns were brought up that the control algorithms would not be able to adapt to the flexible configuration since there was no structural state feedback and control surface reversal may play a roll if operating limits were exceeded. Another big concern was that the added complexity and risk was making it much more difficult to obtain flight permissions from Transport Canada.

As a result of these concerns, it was decided to develop the aeroelastically tuned aircraft in the “Mini” SensorCraft Configuration (1.85m span). This reduced overall risk since the aircraft at this size has much less kinetic energy and does not carry jet fuel on board. Also, since the “Mini” aircraft can be flown locally in Victoria, several flight test campaigns would ultimately be feasible vs the single 10 day flight envelope that would be possible if the large aircraft were flown in Foremost Alberta. Details for the design and testing of this Aeroelastically Tuned “Mini” SensorCraft are outlined in the next chapter

5.5 Conclusions

A more detailed scaling study was performed using a high fidelity FE model, updated to reflect the as built mass, stiffness and volume constraints determined through the building of the 5m Rigid RPV. These investigations showed that the Joined Wing SensorCraft configuration supplied by Boeing at the outset of this project (**Boeing 410 E8**) was too stiff to show the desired amount of nonlinear behavior. Upon consultation with Boeing, it became known that this supplied configuration was an early, pre weight optimized design, and that the latest, more flexible configuration was classified and could not be cleared within the timeframe of this project.

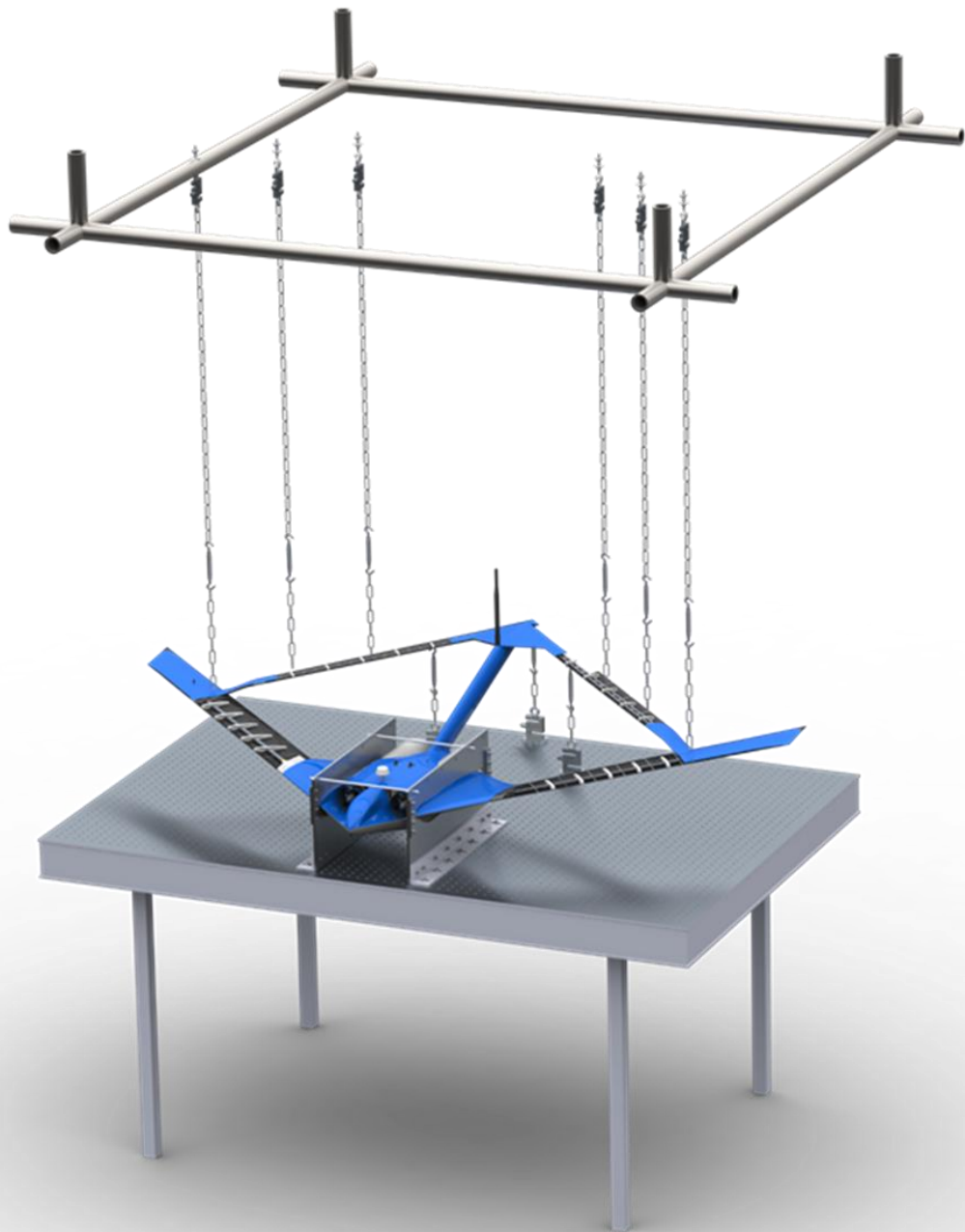
Therefore the decision was made to release the Aeroelastically Scaled constraint, and change to an Aeroelastically Tuned design. This would then allow further softening of the structure and would result in an aircraft that shows similar nonlinear phenomena to those seen in Boeing's latest configuration. Sensitivity studies showed that several nonlinearities are achievable through variation of key structural parameters such as joint and wing stiffness'. Three distinct nonlinearities were shown which included either stress stiffening/softening of the boom tip deflection, a specific form of the boom nonlinearity where the boom deflects in one direction in the linear region and then reverses at higher load steps and finally aft wing buckling. The latter case was chosen by the Air Force as the response of greatest interest.

The aft wing buckling case was further refined by Anthony Ricciardi^[52] from Virginia Tech. Anthony proposed a ladder type construction for the aft wing and further optimized the forward/aft wing stiffness' using a fully nonlinear aeroelastic framework. The final sizing that resulted from his sizing would serve as the basis for my subsequent design of an aeroelastically tuned flight test article.

After submitting the final design concept, a great deal of concern was raised regarding the potential safety risks of flying a marginally unstable aircraft with greatly increased flexibility. In order to reduce risk, both in terms of safety and in terms of schedule, the decision was made to fabricate the aeroelastically tuned design at the reduced, 1.85m "Mini" SensorCraft scale. This would greatly reduce the difficulty of gaining flight clearance

from Transport Canada and allow for multiple flight test windows since the smaller aircraft could be flown locally rather than having to travel to Alberta, as is required with the 5m aircraft.

Chapter 6 - Nonlinear Test Article Design, Testing and Tuning



6.1 Aeroelastically Tuned Mini SensorCraft Design

This section outlines the design of a flightworthy mini SensorCraft that will exhibit the desired structural nonlinearities within the limits of safe operating conditions. The first stage in the design process involves an evolution of the previous Generation 1, Rigid Mini aircraft in order to improve mass and balance, payload volume and manufacturability. A basic internal structure is then chosen that will allow for sufficient compliancy, strength, ease of manufacturability and assembly. The new structure models are parametric and thereby allow the optimization of their geometry to tune the mass and stiffness properties until a desirable response can be achieved. Once the final computational design is achieved a detailed design phase is started in order to generate manufacturing instructions, detailed part drawings, instrumentation specifications and communications system designs.

6.1.1 Redesign of Generation 1 Mini SensorCraft Configuration

At the outset of this phase only one Generation 1 Mini SensorCraft was available (G1-007) and it had been subjected to several hard landings. For this phase it was determined that two new aircraft would be built. One flexible aircraft (JGR10-F1) to investigate the nonlinear response in flight, and during ground tests, as well as two new rigid aircraft (JGR08-G2 and JGR09-G2). These rigid aircraft would serve as test beds for new pilots, flight test maneuvers, instrumentation systems and autopilot.

Before manufacturing the three new aircraft a redesign was required for the Generation 1 Minis. The two Generation 2 Rigid aircraft, as well as the Flexible aircraft, require additional payload capacities (both weight and volume) in order to house the additional instrumentation. An additional challenge was the anticipated aft weight distribution of the new instrumentation. This aircraft has been difficult to trim (cg too far aft) in all of its configurations so all internal were reconfigured to shift weight as far forward as possible.

Figure 107 below show the updated internal layout of the new configuration. Here the batteries have been moved as far forward as possible and a new battery hatch designed so that they can be swapped without flipping the aircraft upside down (in comparison with the G1 design). The motors have been moved as far

forward as possible and are no longer buried in the fuselage. The G1 aircraft had the engines buried in the fuselage and were fed through an inlet duct which was expected to limit the flow and result in reduced thrust and endurance.

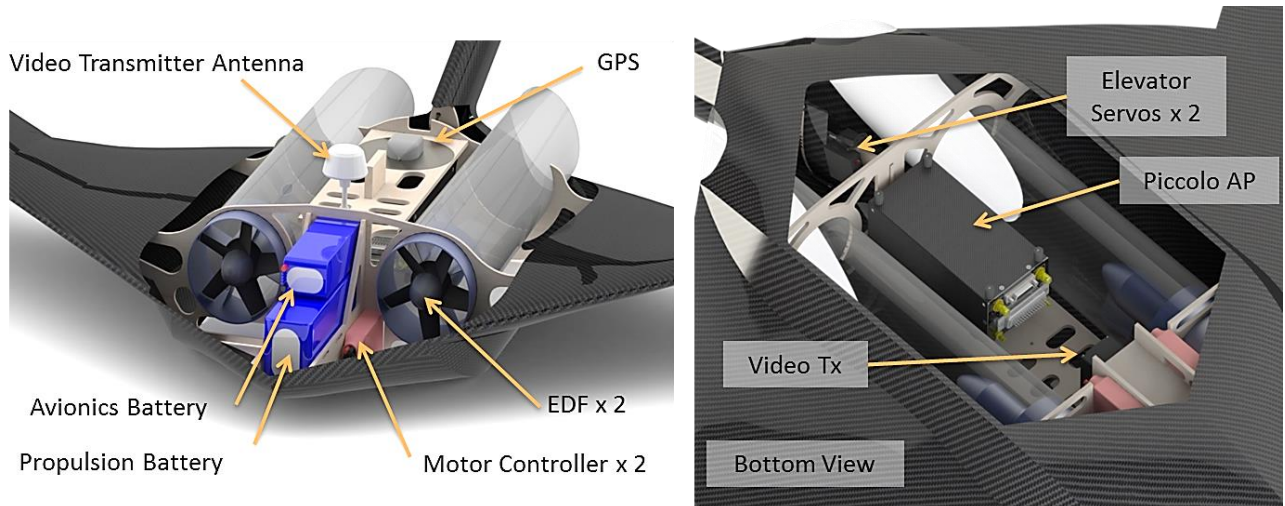


FIGURE 107 – UPDATED INTERNAL LAYOUT OF GENERATION 2 MINIS

The speed controllers were sized up and moved into the forward battery bay to both increase the airflow and shift the cg forward. The servos which actuate the elevators were moved from the aft wing to the fuselage compartment and actuation transferred to the control surfaces using push rods as seen in Figure 108 below.

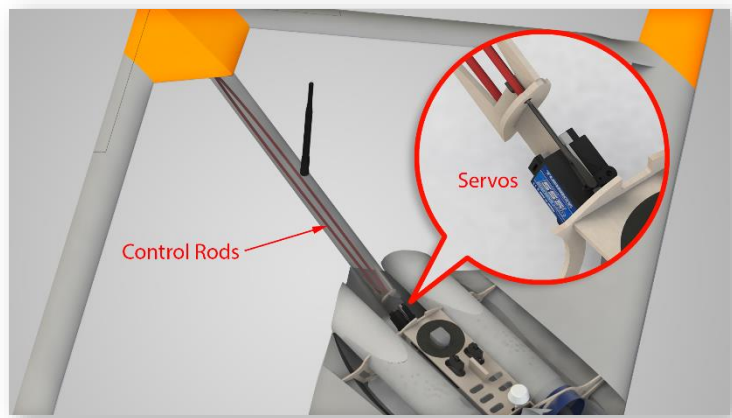


FIGURE 108 - UPDATED ELEVATOR SERVO LOCATIONS AND CONTROL RODS

A video transmitter was also added on the front bulkhead for transmission of the pilot view camera feed. A relay was added in line with the transmitter in order to turn on or off in flight via an autopilot feed through. This was deemed important in case of interference between the camera transmission and the GPS or autopilot telemetry link. The camera used is a GoPro Hero3 which has been used successfully in the past as a live pilot view on the 5m test article. The camera placement of the 5m aircraft was at the top of the boom at the intersection of the aft wings. The placement of the camera in this aft position is not feasible on the Mini configurations due to cg considerations so a custom bracket was designed to move the camera to the base of the boom. The ability to slide this mount forward and aft also serves as a means to trim the aircraft in the field. Figure 109 below shows the camera mounted on the movable boom bracket.



FIGURE 109 - CUSTOM BRACKET USED TO MOUNT GOPRO AND ADJUST CG

A large challenge with these small scaled RPVs is electromagnetic interference and blanketing of the comms link signal. In this configuration this has been addressed by ensuring better antenna separation than was employed on the Generation 1 aircraft. Additionally, the previous aircraft were constructed entirely from carbon fiber which shadowed the antenna at certain aircraft orientations and resulted in dropped comms and degraded range. In the latest generation large portions of the fuselage were designed using s-glass/epoxy laminates which are transparent to the RF bands used on board the aircraft. Figure 110 below shows the RF transparent portions of the new design as see through whereas the carbon laminates are shown opaque.

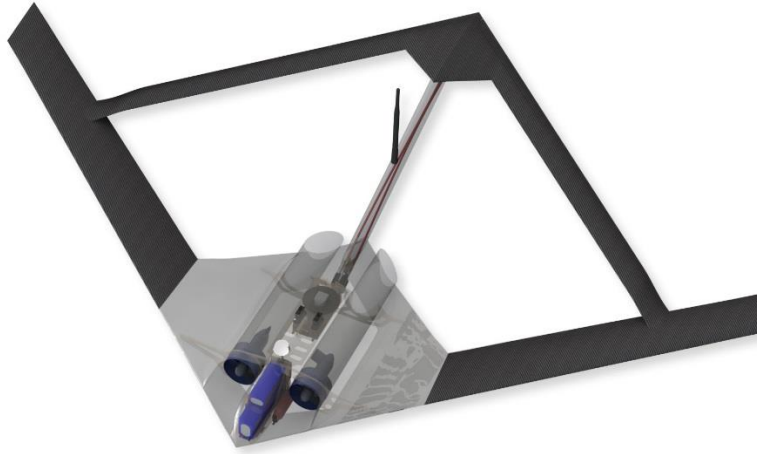


FIGURE 110 - RF TRANSPARENT PORTIONS OF MINI STRUCTURE (SHOWN TRANSPARENT)

The control surface locations are slightly altered from the supplied full size aircraft geometry and the previous flown GSRPV and G1 Minis. Several control surface scheduling schemes have been both simulated and tested using reduced scale aircraft, previous Mini SensorCraft, and the GSRPV. The scheduling that will be used in the initial flight test of the Mini SensorCraft is summarized in Table 3. For the primary control surface schedule, roll command uses the outboard ailerons, and pitch command uses the elevators. The primary ailerons will utilize aileron differential (40% down, 60% up mixing).

TABLE 12 - CONTROL SURFACE SCHEDULING

Surface	Function
Inboard Aileron	Flap or Secondary Aileron
Outboard Aileron	Primary Aileron
Elevator	Primary Elevator

The primary change for this configuration is the movement of the elevators inboard onto the boom strake. The addition of a compliant aft wing has a large effect on the elevator control surface design. If elevator control surfaces are the same size and locations as those adopted on the Generation 1 aircraft then two problems arise. The first is the potential for control surface binding in the highly deformed state and the second is the potential for the control surface to add stiffness to the aft wing which would change depending on the actuation state of the surface. As a result the elevators were both shifted inboard as well as decreased in overall span as can be seen in Figure 111 below.

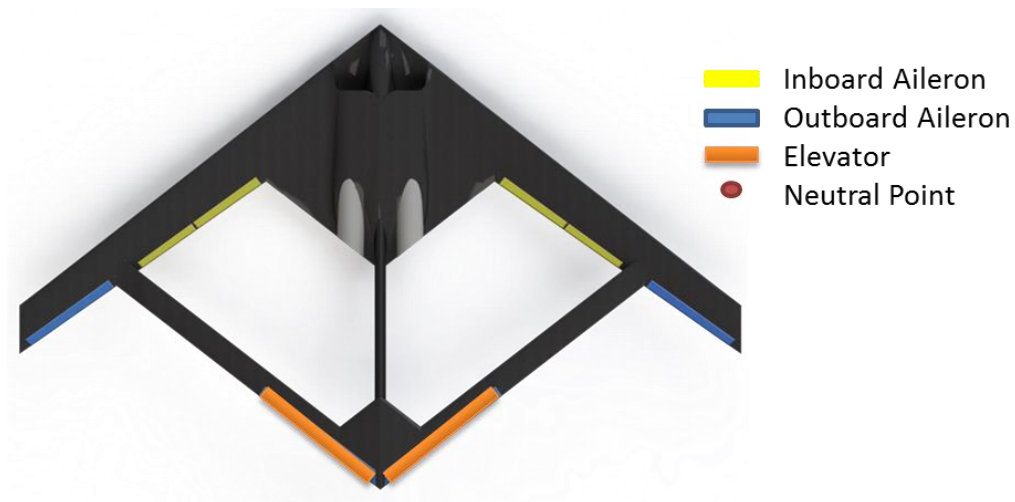


FIGURE 111 – CONTROL SURFACE LAYOUT

This shift inboard minimizes the spanwise portion of the control surface that is joined to the compliant portion of the aft wing (shown in blue) and also moves the aerodynamic center of the elevator more aft (thereby helping regain some of the control authority lost in shortening their span). In addition, only two hinge points are used on each elevator and each of these is a spherical type joint with one translational dof along the hinge line freed on the inboard spherical joint to allow for relative spanwise motion between the two hinges under large bending deformations. The result is a configuration which allows no bending moments to be passed to the control surface which will increase modelling certainty and reduce the likelihood of the control surface from binding. The hinge design is pictured in Figure 112 below.

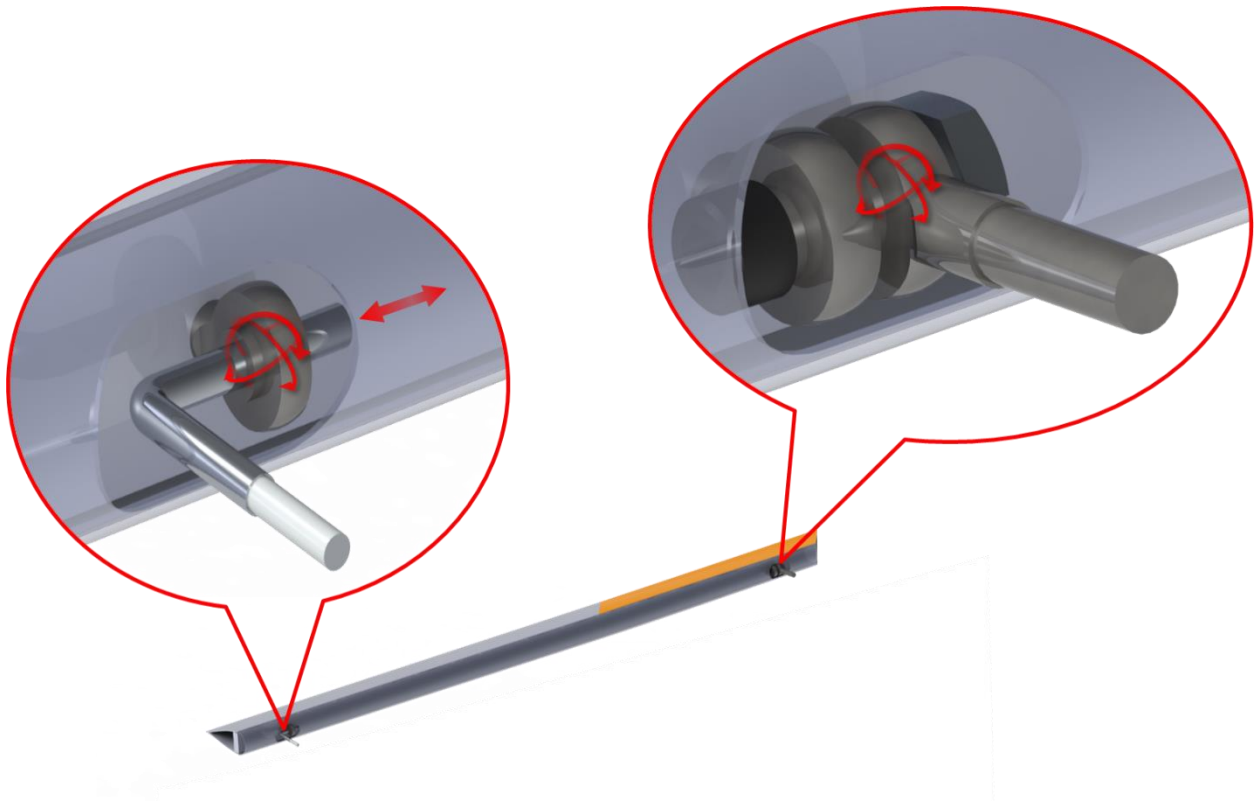


FIGURE 112 - CLOSE-UP OF RIGHT ELEVATOR SHOWING CONSTRAINED DEGREES OF FREEDOM

The exhaust ducting for the G2 aircraft is now required to be longer due to the forward placement of the motors. Previously, 1/16" Mylar sheeting was wrapped into a tapered, tubular shape and tacked into place within the aircraft. For the new aircraft an aluminum mandrel was machined using a CNC lathe with the correct taper ratio calculated based on the average flying speed of the aircraft. Two plies of 1.7oz fiberglass was vacuum bagged on the mandrel before being removed with compressed air and trimmed. Both the exhaust tubes and electric ducted fans are mounted using silicone rubber in an attempt to attenuate the high frequency vibrations caused by the fans.

The two Generation 2 minis outlined here, and portions of the subsequent flexible variant, use conventional composite construction. Parts are fabricated similarly to Generation 1 Minis and the 5m RPV, with composite load bearing skins and plywood or laminate bulkheads, shear webs and ribs. The load bearing skins are typically carbon/foam/carbon construction with a choice of bidirectional and uni-directional weaves depending on

location. As mentioned previously some areas of the aircraft are now constructed of fiberglass due to its RF transparency.

6.1.2 Detailed Design of Aeroelastically Tailored Model

In order to investigate the nonlinear aft wing buckling behavior predicted by theoretical studies, a redesign of the internal structure was required. The following section summarizes the layout of this structure in the flight test article as well as some of the non-structural components required to achieve a flight worthy aircraft.

6.1.2.1 Design Methodology

There are many potential complexities of scaling an aeroelastic response to a much reduced scale such as the Mini SensorCraft Configuration (~4% full scale). One of the challenges is to design a structure with the desired flexibility using common materials and conventional building techniques. Often, the use of conventional fabrications techniques, such as those used previously on the mini SensorCraft, would require skin thickness that are unrealistically thin or material properties that are not feasible. Even they were achievable, undesirable effects such as skin buckling and damage due to everyday handling would be inevitable. As a result, a less conventional configuration is chosen here which uses tailored aluminum spars and a series of non-load bearing aerodynamic panels as shown in the following figure.

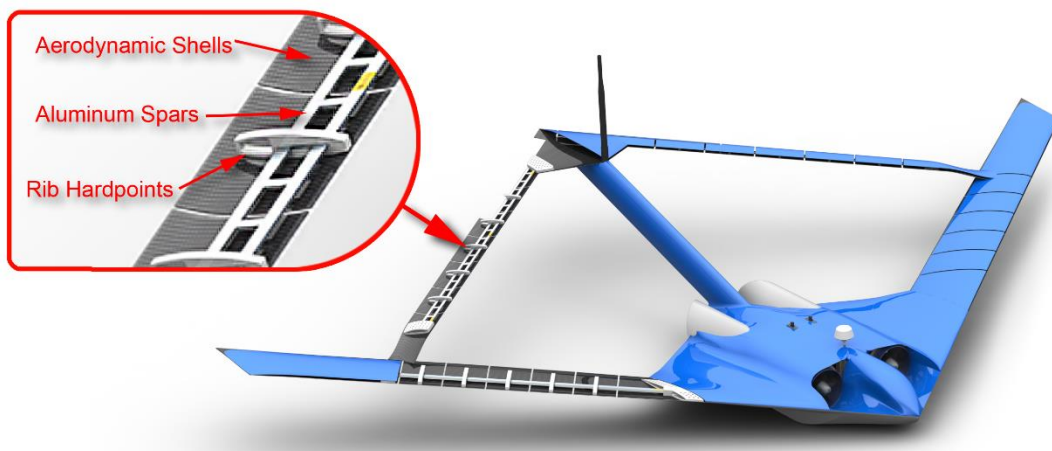


FIGURE 113 - MAIN COMPONENTS OF COMPLIANT STRUCTURE

The load bearing structure of the forward and aft wings are made of aluminum and have a very shallow cross section. This allows them to deform a great deal without causing failure in the outermost fibers of the beam. (This in in contrast to the monocoque structure of the 5m Rigid aircraft wing which resulted in a very stiff structure that experienced wing skin buckling at large deflections).

6.1.2.2 Structural Design (Non-Compliant Portions of Airframe)

Some structural components are common between the Generation 2 Rigid aircraft and the Aeroelastically Tuned model. The Aeroelastically Tuned model uses similar fuselage and boom construction methods but are re-winged with a set of compliant lifting surfaces as will be discussed in a subsequent section. Additionally, the structural response of the outer portion of the forward wing (outboard of the fore/aft wing joint) has very little effect on the aft wing's structural response. As a result, this portion of the wing does not been to be overly compliant, nor does the exact structural response need to be characterized analytically. Therefore, similar techniques are adopted in their fabrication to that of the Generation 1 and 2 Mini SensorCraft (carbon and glass monocoque construction).

6.1.2.3 Structural Design (Compliant Structure)

As Mentioned Previously, the forward and aft wings require additional flexibility beyond that which can be achieved using conventional monocoque fabrication techniques. Instead, shallow cross section spars are used in the main forward and aft lifting surfaces as shown in the following figure.

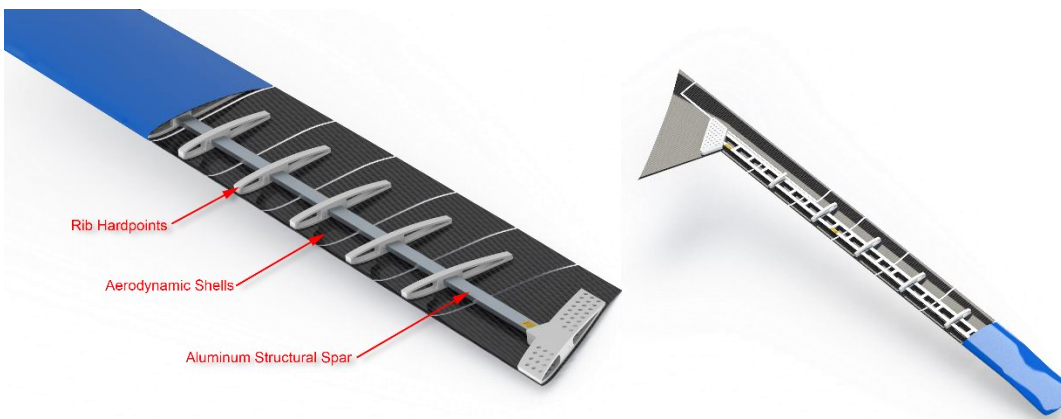


FIGURE 114 - FORWARD AND AFT WING INTERNALS (LEFT AND RIGHT RESPECTIVELY)

This compliancy of this shallow cross section spar requires that no load be passed to the skin of the aircraft as this would add unwanted stiffness. However, an aerodynamic shape is required for the wing cross section so a series of aerodynamic shells are designed to attach to the spars at certain spanwise locations. Each of these aerodynamic shells is attached at only one point to the underlying spar which ensures no load is transferred to it. See Figure 115 below for clarification.

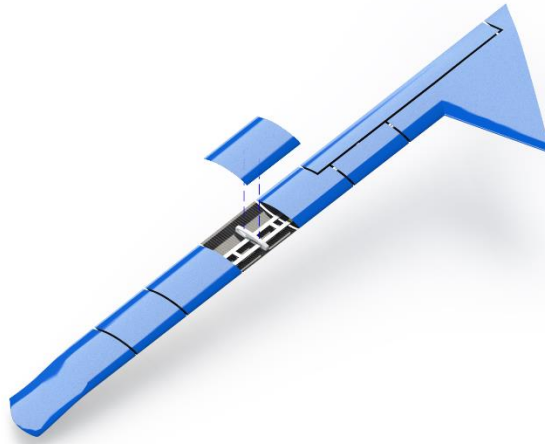


FIGURE 115 - AERODYNAMIC SHELLS EMPLOYING SINGLE LINE OF ATTACHMENT ENSURING NO LOAD TRANSFER TO SKINS

Each shell has a small spanwise gap between itself and the neighboring shell preventing contact or binding when the aircraft wing is bending. In order to prevent high pressure air underneath the wing from leaking to the top surface (and thus spoiling the lift), special sealing tapes have been chosen. The first tape is a flexible polymer which bridges the gap and sticks to both panels on either side of the gap. While this will take no load in compression it will offer stiffness when the gap is opened up. While this load bearing is undesirable in tension, this tape will only be used in the upper skin of the forward wing which is anticipated only to in compression under normal positive g loads. For the underside of the forward wing and both top and bottom of the aft wing, a special “hinge sealing” tape will be used and is pictured below.



FIGURE 116 - HINGE SEALING TAPE SHOWING ADHESIVE ALONG ONE EDGE ONLY

This tape is made of a clear stiff Mylar material and is adhesive only on one edge. This tape is adhered to the inboard portion of a gap and allowed to overlap the adjoining panel. This creates a type of lap joint that, while adhered on one side, is free to slide on the outboard portion of the gap. Figure 117 below shows the two different gap treatments, the left showing the upper forward wing using the flexible tape with the right picture showing the underside employing the lap type joints.



FIGURE 117 - GAP SEALING TECHNIQUES (LEFT SHOWS FLEXIBLE TAPE AND RIGHT SHOWING LAP JOINT USING HINGE TAPE)

6.1.2.4 Instrumentation Design

In order to observe and quantify the nonlinearity of the structural response, a variety of sensors are required. The primary sensor for investigating the response will be strain gauges along the aft wing spar in order to measure bending strain. Due to the Wolkovitch Effect it is anticipated that the forward spar of the aft wing ladder structure will exhibit the greatest compression leading to more deflection due to buckling. An additional pair of gauges is placed at the root of each wing in order to measure the bending strain experienced in the forward wing. Figure 118 outlines the locations chosen for strain measurements.

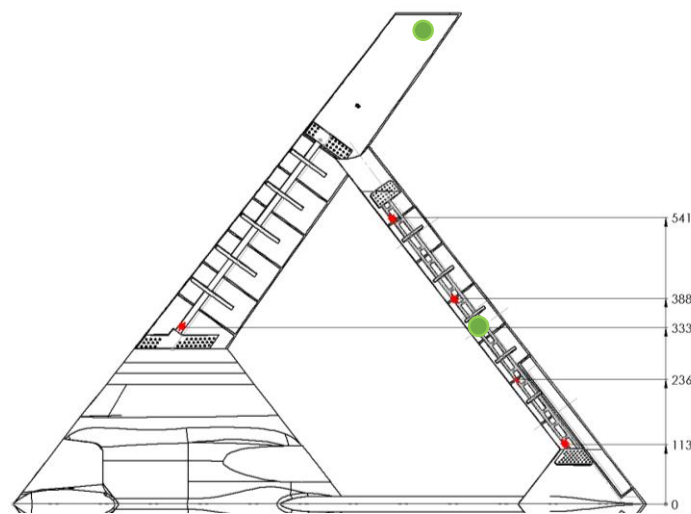


FIGURE 118 - STRAIN GAUGE (RED) AND ACCELEROMETER (GREEN) SPANWISE LOCATIONS (MIRRORED ON LEFT SIDE OF AC)

Also shown in Figure 118 are locations of 3-axis accelerometers. The accelerometers are chosen primarily for the ground test phase where the static measurements can reveal twist at local aft wing stations. They are also used to get modal response during dynamic vibration tests.

The final means of quantifying the structural response is through optical measurements. Digital SLR cameras will be used during ground testing at each load step. Photomodeler® Software is used to extract 3D measurements and models from photographs taken with the camera at various locations. The measurements are then confirmed at various points on the model using measurements acquired with dial indicators. During flight testing a more basic camera will be used to view the aft wings from rear facing camera. Rough

measurements can then be made after flight using a custom script written in Matlab® that maps the approximate deflections based on target location and deflection in pixels. Figure 119 shows the view from the aft facing camera that will be logging during flight.



FIGURE 119 - CAMERA FIELD OF VIEW FOR CAPTURING AFT WING STRUCTURAL RESPONSE IN FLIGHT

Data acquisition is divided into two scenarios. Ground based testing will allow the use of larger, lab based equipment with higher sampling rates and resolutions. A miniaturized system is designed for flight testing that has lower sampling rates but is smaller, has onboard logging and is capable of passing a real-time feed to the ground at a reduced frequency. Details of the ground and air based test measurement are presented in a Section 3.

6.2 Fabrication

This section acts as a very brief overview of fabrication of the various aircraft, test rigs and instrumentation.

The final section summarizes the as built properties that were measured using the final test articles.

6.2.1 Structural components

The structure of the G2 Rigid Mini's were fabricated by Jon Harwood of Harwood Custom Composites. The fabrication of miscellaneous parts (such as thrust tubes, Pitot Static Tubes etc) was performed by the author.

All wiring and integration was completed by the Author and Jeff Garnand at the UVic CfAR hangar in Sidney BC.

The structural elements of the flexible aircraft were fabricated by the author and assembled at UVic CfAR.

Many of the internal components for the flexible aircraft were fabricated using rapid prototyping technologies.

This work was completed using both Stereo Lithography and fused deposition methods at Camosun College.

Various machined parts were also fabricated at the machine shop at the University of Victoria using a combination of manual and CNC machines.

6.2.2 Test Rigs and Instrumentation

The structural elements of the testing rigs were fabricated by the author and coop student Simon Moffat. Most of the components were machined using the UVic machine shop and assembled at University laboratories.

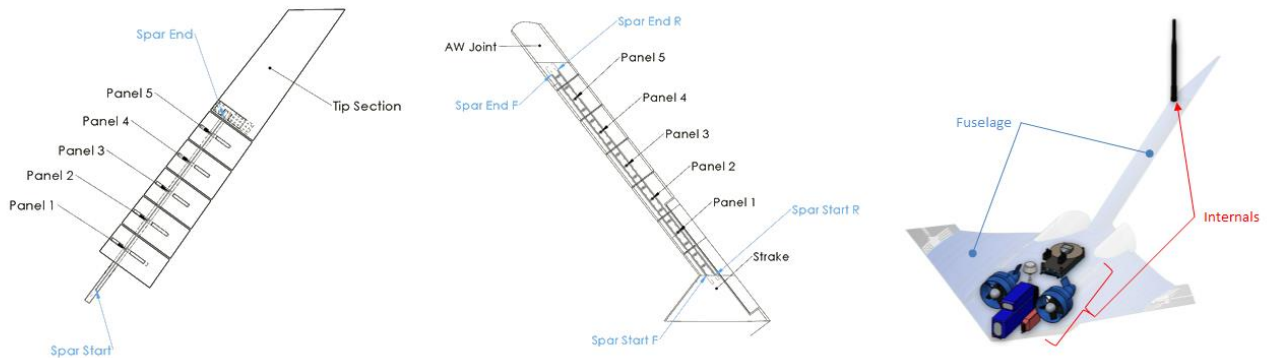
Instrumentation systems were assembled and tested at UVic CfAR facilities. Prototyping of custom PCBs was contracted out with the final assembly performed using a manual pick and place machine and reflow oven at Camosun College.

6.2.3 As Built Data

Upon completion of the structural fabrication a series of measurements were required to gain updated mass properties of the structure as an input for the nonlinear aeroelastic model. These details are critical in subsequent nonlinear aeroelastic analysis.

Some structural members such as the wing spars and strake were weighed and their approximated running mass used to apply beam properties to the FE structural models. In these cases the center of mass of each item was measured and transformed to the aircrafts coordinate system. Other items, such as aerodynamic panels, had no equivalent feature in the FE models and were subsequently modelled as point masses connected to structural members using rigid elements (inertias about these components cg assumed to be negligible).

Heavier items, such as the internals and the boom/fuselage, were also modelled as point masses in the FE model but here their inertial properties were considered significant. The boom/fuselage's properties were measured using a bifilar pendulum setup to determine overall moments of inertias. The remaining internal parts (such as motors, batteries etc) were modeled in a CAD environment and their mass properties altered until their overall mass and cg were matched. The following figures and tables show the modelled items and their associated properties.



Forward Wing

Component	Mass [g]	CG Loc			Modelled As
		x [mm]	y [mm]	z [mm]	
Panel 1	25	374.7	410.6	48.7	<i>point mass</i>
Panel 2	22	420.3	472	56.3	<i>point mass</i>
Panel 3	22	466	533.4	64	<i>point mass</i>
Panel 4	22	511.6	594.8	71.6	<i>point mass</i>
Panel 5	20	557.2	656.2	79.3	<i>point mass</i>
Tip Section	120	643	752	91	<i>Running mass</i>
Spar	66	-	-	-	<i>Running mass</i>

Aft Wings

Component	Mass [g]	CG Loc			Modelled As
		x [mm]	y [mm]	z [mm]	
Strake	70	1070	50	182	<i>Running mass</i>
Panel 1	15	983.5	201.8	159.3	<i>point mass</i>
Panel 2	15	924.9	278.1	148.6	<i>point mass</i>
Panel 3	15	866.3	354.4	137.9	<i>point mass</i>
Panel 4	15	807.7	430.6	127.2	<i>point mass</i>
Panel 5	15	749.2	506.9	116.5	<i>point mass</i>
AW Joint	41	696	590	103.85	<i>Running mass</i>
Ladder Spar	36	-	-	-	<i>Running mass</i>

Fuselage

Component	Mass [g]	CG Loc			Inertia			Modelled As
		x [mm]	y [mm]	z [mm]	Ixx [g mm ²]	Iyy [g mm ²]	Izz [g mm ²]	
Fuselage/Boom	950	401	0	40	33016747.04	58859451	87507480	<i>pt mass w/inertia</i>
Internals	1892	210	0	16.9	3508576	1702365	4837476	<i>pt mass w/inertia</i>

FIGURE 120 - AS BUILT MASS PROPERTIES OF AEROELASTICALLY TUNED AIRCRAFT

6.3 Ground Test Planning

This section outlines the proposed testing required for the flexible aircraft investigation. A series of ground tests were planned in order to quantify the static and dynamic structural response of the Aeroelastically Tuned Mini Configuration. Additional tests are proposed in order to confirm flightworthiness of the configurations in order to determine characteristics such as inertial properties, installed thrust and autopilot tuning.

6.3.1 Static and Dynamic Load Testing

A series of static loading cases is chosen in order to systematically evaluate the individual structural components of the aircraft. This begins with tests to isolate the forward wing and boom stiffness's followed by load cases to quantify the response of the fully assembled aircraft. A final load case was chosen to represent maximum expected flight loading in order to clear the aircraft for flight.

The potential locations for load application is shown in Figure 121 below. These points correspond to hard points within the structure and the numbers and locations are chosen in order to accurately simulate distributed loads seen in flight. No loads are applied on the forward wing outboard of the aft/forward wing joint as the structural response of this portion of the wing is not deemed to be of large importance to the aft wing response nor is its structural integrity under question (due to high safety margin chosen in sizing this portion of the structure).

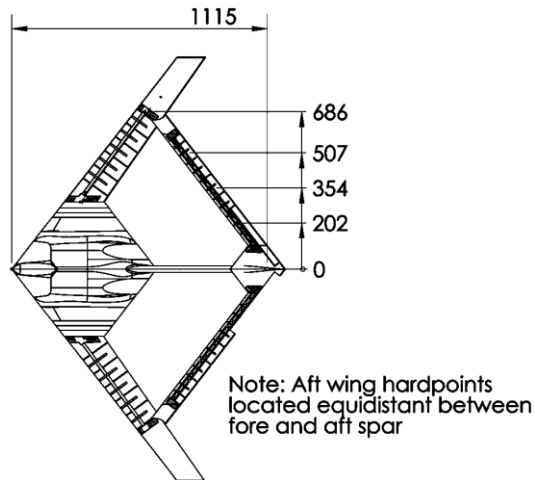


FIGURE 121 - HARD POINT LOCATIONS USED FOR LOAD APPLICATION (MIRRORED ON LHS)

The assumed boundary is a fixed condition at fuselage and forward wing interface inboard of the forward wing crank. This condition is reproduced in the ground testing through the use of a holding jig that will clamp the aircraft along a line of contact shown in Figure 122.

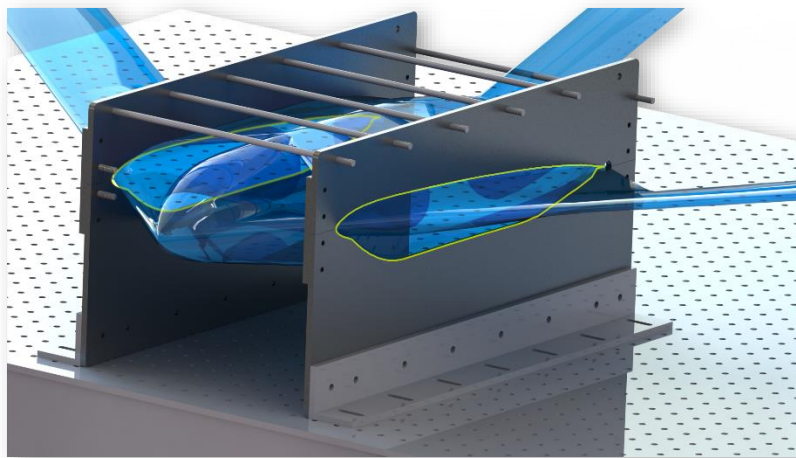


FIGURE 122 - LINE OF CONTACT BETWEEN AIRCRAFT AND TEST FIXTURE

6.3.2 Load case 1a: Forward Wing Loading

The first load case involves the application point loads to the cantilevered front wing at a station corresponding to the intersection of the forward and aft wings (stations 686 in Figure 121 above). A point load is chosen that produces a root bending moment on the wing equivalent to maximum predicted moment seen by the forward

wing during a 3g pull up maneuver (with aft wings attached). This value corresponds to a 660N point load for each wing as seen in Figure 123 below. During testing, this load is applied in 5 equal load increments and measurements taken with both a steel ruler and using Photodeler® software. Additionally, strain readings are taken to determine the bending strain at the root of the forward wing and compared to theoretical values determined using classical beam theory.

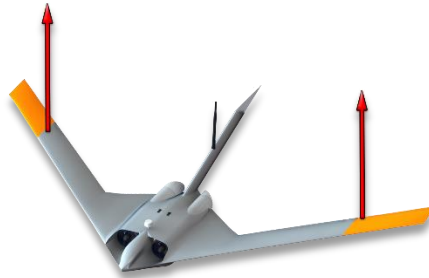


FIGURE 123 - LOAD CASE 1A LOADING

6.3.3 Load Case 1b: Boom Loading

In order to capture the stiffness of the boom and the boom/fuselage interface an incremental load is applied to the tip as seen in Figure 124 below. This load has no physical significance other than it will deflect the boom more than any expected flight load will. A load of 3.8N was applied in five equal increments and measurements taken using steel ruler.

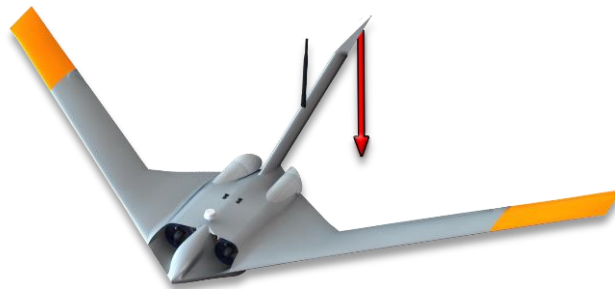


FIGURE 124 - LOAD CASE 1B LOAD APPLIED TO BOOM

6.3.4 Load Case 1c: Dynamic Structural Response of Forward Wings

The third test case involves capturing the dynamic response of the forward, cantilevered wings. This involves the excitation of the forward wings using a series of impact excitations at various spanwise locations and subsequent frequency measurements using the strain gauges at the wing roots. The spectral response is then calculated in real-time using a Fast Fourier Transform.

6.3.5 Load Case 2a: Forward Wing and Boom Loading of Assembled Configuration

For this loading case, forward wing and boom loads are chosen in which result in boom and wing root bending moments equivalent to those seen in a 3g pull up flight maneuver (11.9N per forward wing and -1.16N on boom). This coarse approximation of loads is deemed sufficient in this case as the actual flight response is not desired but rather an easily reproducible load case to compare to the analytical model and to serve as the basis for downstream model tuning. The loading is applied as shown in Figure 125 below and measurements are taken using strain gauges, rulers and Photomodeler®. In order to fully investigate the linear to nonlinear transition, load increments are chosen at 8.3%, 16.7%, 33%, 50%, 67%, 83% and 100% of full load.

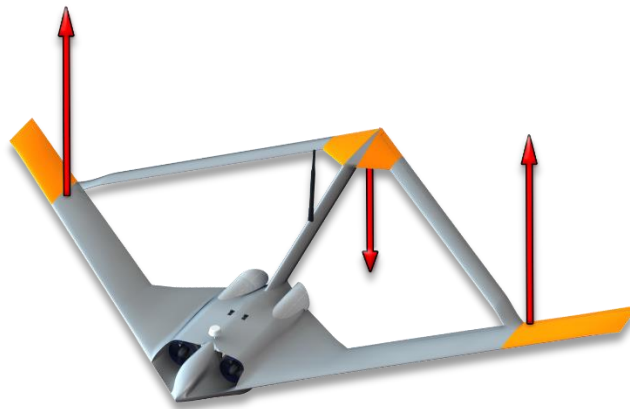


FIGURE 125 - LOAD CASE 2A LOADING

6.3.6 Load Case 2b: Equivalent 3g Pull-up Flight Maneuver Clearance

The final loading case is one which corresponds to a 3g pull-up maneuver at the predicted trim state for flight testing. Forward wing loads are condensed to point loads at the wing joints while the aft wing load distribution is approximated as a series of loads applied at 3 stations at each aft wing and one at the boom station. The quantities of these loads will be generated by a nonlinear aeroelastic analysis using a structural model that was

tuned based on the structural response measured from previous load case results. Figure 126 below shows the load application points for this load case.

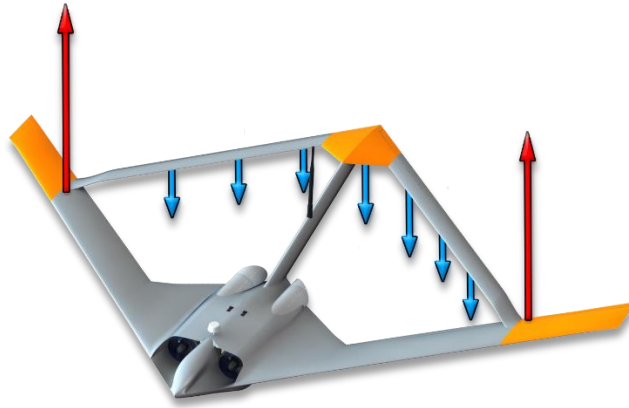


FIGURE 126 - LOAD CASE 2B LOADING

6.3.7 Load Case 2c: Dynamic Structural Response of Aircraft

The last test case involves capturing the dynamic response of the forward and aft wings. This involves the excitation of the forward and aft wings using a series of impact excitations at various spanwise locations and subsequent frequency measurements using the strain gauges and accelerometers along the wings. The spectral response is then calculated in real-time using a Fast Fourier Transform.

6.4 Ground Testing

The previous section outlined the planning and justification of the chosen test matrix. This section outline the implementation of those tests including a description of the physical test setup and procedures, as well as results. In addition, the section briefly describes so of the tuning methods and results of the analytic model tuning based on the measured results.

6.4.1 Static Load Testing

A rigid and precise static loading test rig is crucial in gaining confidence in the measured response of the aircraft. A lot of work was performed to ensure that the designed test fixture was both accurate and very rigid to ensure minimal deflections and modal frequencies largely separated from the predicted aircraft response.

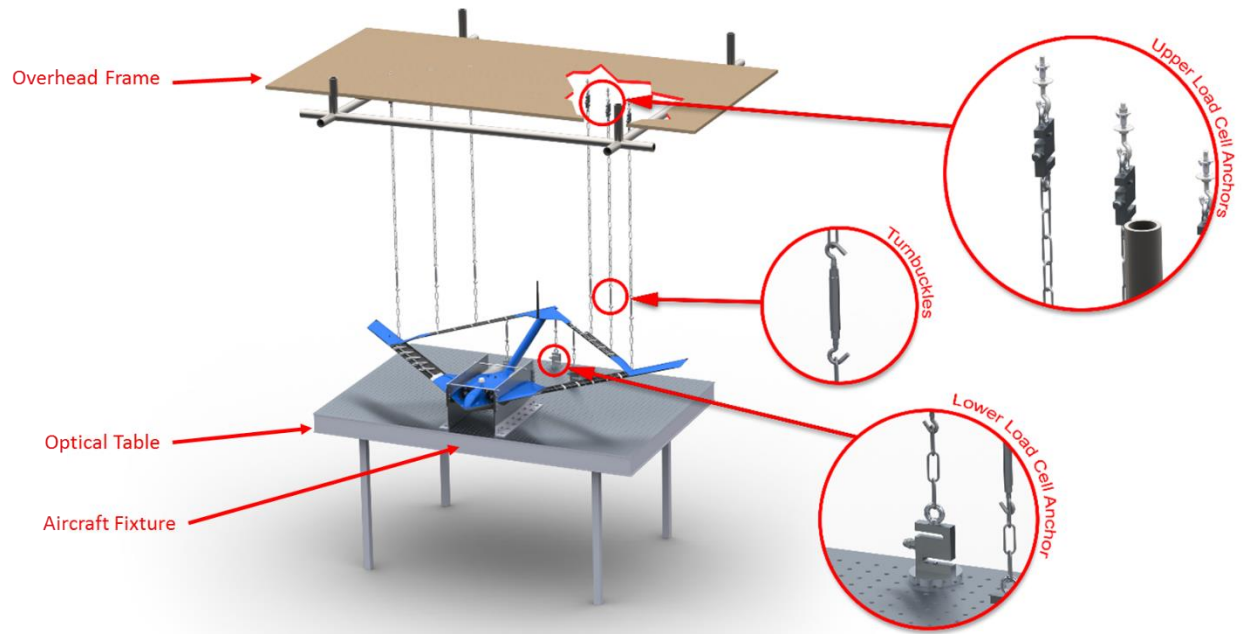


FIGURE 127 - STATIC LOADING TEST SETUP

The final setup is shown in Figure 127 above. Here we can see the main components of the rig. Starting from the bottom is the optical table which is both very rigid and mounted on damped supports. The optical table's top is made of a ferrous material which allows the use of magnetic hard points used in load applications. The table also has an array of ¼-20 threaded holes which are used to hold down the aircraft specific fixture.

The aircraft holding fixture is machined from ¼ aluminum plate. The fixture is based on the outer mold line of the aircraft and as a result, a very good line of contact is made along the entire station and the aircraft. This results in no free-play and very little movement of the aircraft in the translational axes. The spanwise location of the jig corresponds to the rapid increase in span and chord thickness due to the fuselage wing connection as seen in Figure 128 below. This location is chosen as it is thought to further reduce translation and rotation as the forward wing is subjected to bending loads.

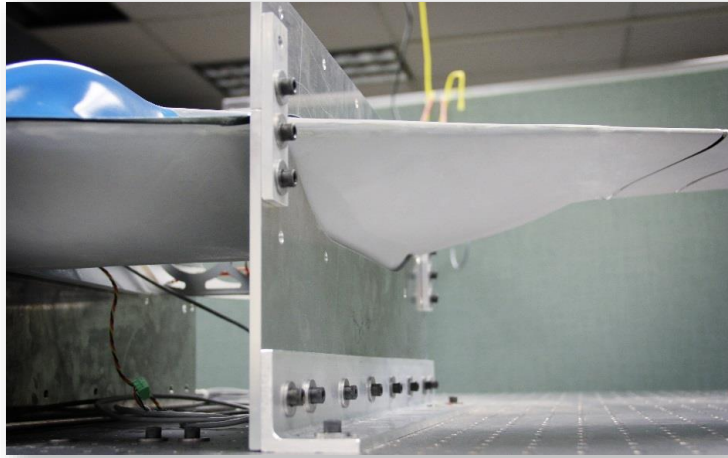


FIGURE 128 - AIRCRAFT/JIG CONTACT

The aircraft is loaded using a series of anchored chains that are whose lengths are changed using turnbuckles. These loads can be applied in either a positive or negative z direction depending on their anchoring location. For positive loads, the chains are anchored to the ceiling of the lab whereas negative loads involve anchoring the chains to the table top below the load application using permanent magnets. The holding force of the magnets is very high and they offer very fine adjustment in terms of location. It is suggested that future version of the rig adopt this same technique for the overhead anchor points through the use of a steel clad sheet placed above the aircraft.

6.4.1.1 Load application

This section outlines the details of applying, measuring and acquiring the data using a custom developed user interface.

6.4.1.1.1 Load Sensing

Loads are applied using turnbuckles as described in the preceding sections. The load steps are applied by iteratively adjusting the various turnbuckles until the desired loads are achieved at each station. Since the load anchor points are fixed throughout the load steps, follower forces are not accounted for. However, since the analytical model can output non-follower forces this was determined not to be of concern.

The magnitude of the applied loads are measured using a series of S-type load cells from Phidgets Inc[®] as pictured in Figure 129 below. Bridge completion is performed by the Phidget Bridge board that will be discussed in the following section.

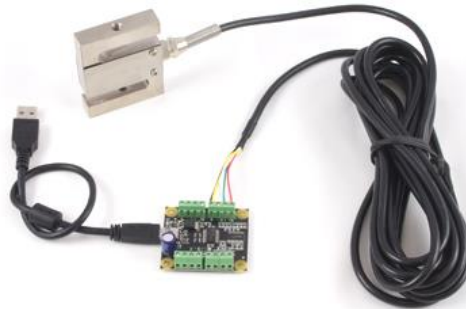


FIGURE 129 – PHIDGET[®] LOAD CELL AND 1046 DATA ACQUISITION BOARD

6.4.1.1.2 DAQ for Load Readings

Figure 129 above also shows the PhidgetBridge 1046 interface. Each board will accept four load sensors and will poll each channel at up to 125Hz. This data is multiplexed and passed through a USB connection to the host computer. This board comes with an example LabView code that was modified to allow ingestion of the load cell readings into the LabView interface

6.4.1.1.3 GUI for Reading Applied Loads

A graphical user interface was developed in order to assist in load cell calibration, process the raw data from the load cells as well as display/record the readings in an easy to use interface. The final interface of the PhidgetBridge is shown below, each control and indicator will be explained in the subsequent figures and table.

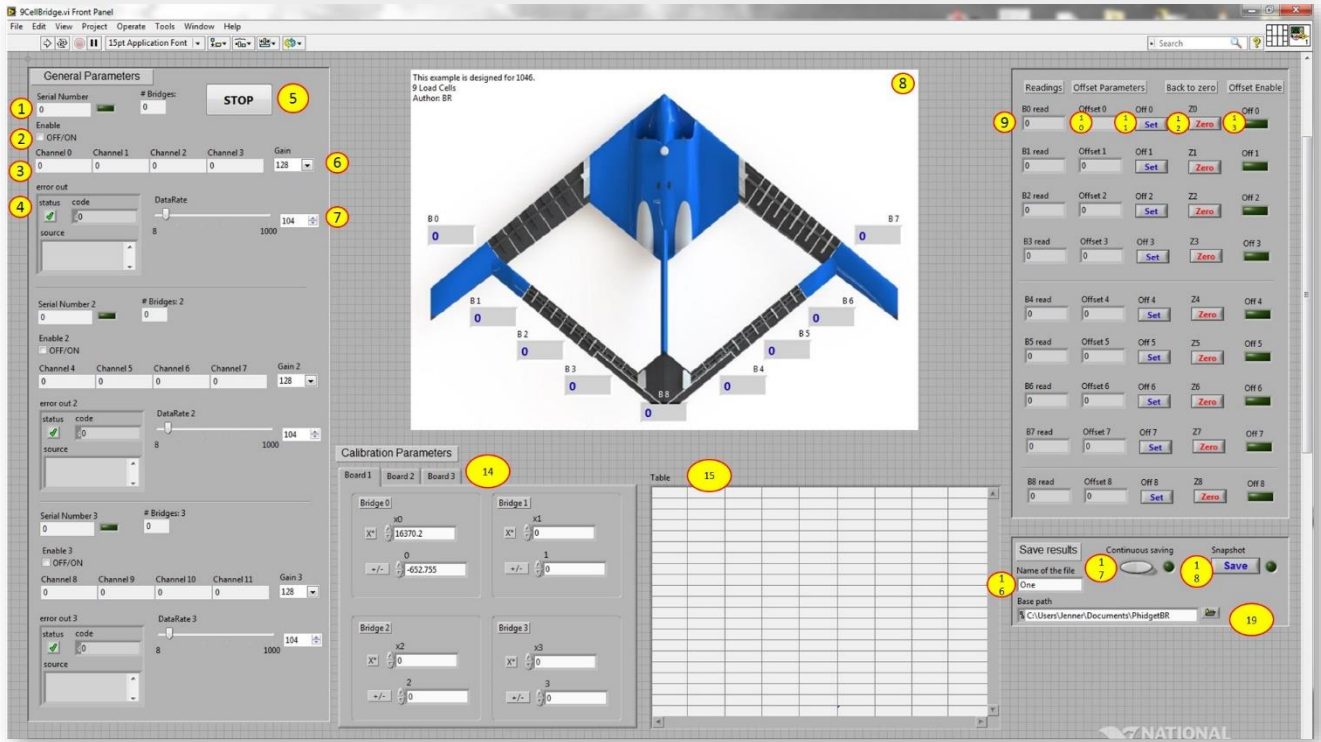


FIGURE 130 - LOAD APPLICATION INTERFACE

TABLE 13 - LOAD APPLICATION INTERFACE DETAILS

Number	Description
1	Indicates the serial number of each Phidget Bridge board (each board has its own serial number), the led turns on when correctly attached to the USB port.
2	For start the measurement the Enable Chart must be selected (One for each board).
3	The result of the measurement of each load cell is displayed in the charts called <i>Channel#</i> in mV/V.
4	In the Error case, if the program is running properly a tick will be displayed, if not a red X and the code of the error (see data errors in Phidget bridge datasheet).
5	Used to stop VI
6	Set the gain (a big value of gain will show a more precise result), the default value is 128 which is the maximum.
7	Set the data rate according to the application, once calibrated each bridge, using a fast measurement (low value) is recommended.
8	The figure shows the places where the load cells are, corroborate the numbers of each board according to the Serial Number and the Number displayed in the Channel# cases.
9	Raw value in grams once calibrated, without offset.
10	Indicates the offset value of each load cell in grams.
11	Set the offset in the required moment.
12	Reset the offset, back to zero.
13	The LED indicates when the offset is enabled.
14	Set the calibration formulas, using the Ph calibrations software for establishing the values is recommended before start the measurement (select between tabs for each board).
15	When the Saving data buttons are enable, the value of each load cell will be displayed in the table, it resets just when the program is stopped and run then.
16	Write the name of the file where the data is going to be stored.
17	Press the button if a continuous saving is needed (Latched).
18	Press the button if a snapshot of the values is required (Push button).
19	Write the path of the destination for the file generated.

6.4.1.2 Collection of Strain Readings

The following section describes the methods employed to measure, filter and process the strain data resulting from airframe loading.

6.4.1.2.1 Strain Sensing

Strain is measured through the use of foil type strain gauges. In order to measure the strain this type of sensor, it must be connected to an electric circuit that is capable of measuring the minute changes in resistance corresponding to strain. Strain gage transducers usually employ four resistive elements that are electrically

connected to form a Wheatstone bridge circuit (Figure 131). A Wheatstone bridge is a divided bridge circuit used for the measurement of static or dynamic electrical resistance. The output voltage of the Wheatstone bridge is expressed in millivolts output per volt input. The Wheatstone circuit is also well suited for temperature compensation. The number of active strain gages that should be connected to the bridge depends on the application. For example, in this case we are interested in measuring bending strain (while rejecting axial strain) two gauges are connected on opposite sides of a beam. In this arrangement, one can effectively double the bridge output for the same strain as well as compensate for temperature variations.

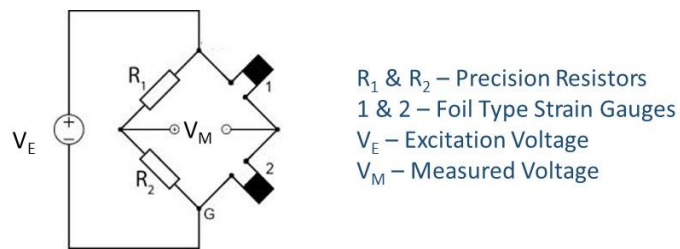


FIGURE 131 - HALF BRIDGE CCT USED TO MEASURE BENDING STRAIN

As can be seen in Figure 131, several key components are required to complete the bridge circuit. In this case the precision resistors are 350 OHM $\pm 0.1\%$ precision type from Vishay Precision Group. Excitation Voltage, V_E , is supplied using a bench top power supply. A total of 8 bridge completion circuits were required and custom board was developed using through-hole proto board. The finished bridge completion board is shown in Figure 132.

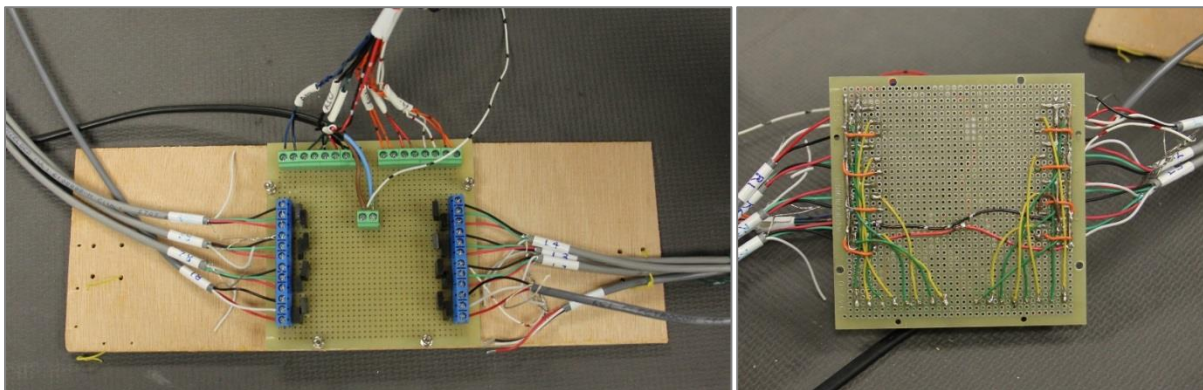


FIGURE 132 - CUSTOM BRIDGE COMPLETION CIRCUIT USED FOR STRAIN BASED GROUND TESTING MEASUREMENTS

6.4.1.2.2 DAQ for Strain Data

The differential measurements across the bridge circuits is achieved using a National Instruments XXXXXX Digital Acquisition Unit. The unit has 16bit resolution and is capable of measuring 8 differential measurements at up to 31 kS/sec. The large sampling rate proved useful as it allow a large sampling window to be used in a moving average type filter, thereby markedly improving the signal quality for dynamic measurements.

Due to the limited number of differential inputs, simultaneous strain readings of the 8 aft wing locations and readings from the forward wing (or accelerometers) was not possible. Therefore when additional inputs were required, a National Instruments USB-6001 unit was used. This unit can take up to 4 differential inputs but at a significantly lower 10 kS/sec with 12 bit resolution. Despite the lower specifications the unit was still adequate for dynamic measurements using strain gauges within the required range (0-100Hz).

6.4.1.2.3 GUI for Reading Strain Results

A second GUI was developed for displaying strain and writing results to disk. The interface displays both numeric and dial gauge indicators readouts of strain as well as and strip charts to show time based history. A spectral analysis is also performed and displayed in a chart. Details of the GUI are given in the following Figure and Table.



FIGURE 133 - CUSTOM INTERFACE FOR CALCULATING, FILTERING AND DISPLAYING MEASURED STRAIN

TABLE 14 - MEASURED STRAIN GUI DETAILS

Number	Description
1	Numerical and Dial indicators outputting strain readings at four stations on right aft wing in microstrain
2	Numerical and Dial indicators outputting strain readings at four stations on left aft wing in microstrain
3	Strip chart showing time history of right aft wing strains at four stations
4	Strip chart showing time history of left aft wing strains at four stations
5	VI stop button to halt calculations and displaying of data
6	Warning LED (and buzzer) which activates when strain reaches 80% of calculated maximum
7	Tare button to zero strain readings
8	Spectral response for real time dynamic analysis of the system
9	Button to activate real time FFT analysis
10	Bar graph showing strain at aft wing stations. Blue and red line represent 3g and 1gx3 predicted response

6.4.1.3 Other Measurements

A variety of other means were used to measure the structural response of the aircraft. These included optical and physical measurements of displacement as well as accelerometer based measurements to determine angular deflections and dynamic response.

6.4.1.3.1 Photomodeler

Photomodeler requires that the camera used to acquire images be calibrated using a printed target array. The procedure was followed here with reasonable results. Although several calibration attempts were made, only one resulted in acceptable results. It is assumed that the lack of consistent accuracy may be due to poor lighting conditions in the lab as well as small changes in focal length resulting from the camera autofocus. Typically a camera can be set to fixed focus for larger targets but due to the small size of the model (short focal length), varying camera distance from target (due to cramped conditions in lab) and large aperture required by the lighting conditions, the camera had a very short depth of field and refocusing was required at different stations. Despite these issues the Photomodeler results showed consistent results within $\pm 1\text{mm}$ when compared to physical measurements.

Once the camera/lens were calibrated a series of calibrated targets were applied to the aircraft as well as a fixed reference frame (in this case the optical bench) as shown in Figure 134 below.

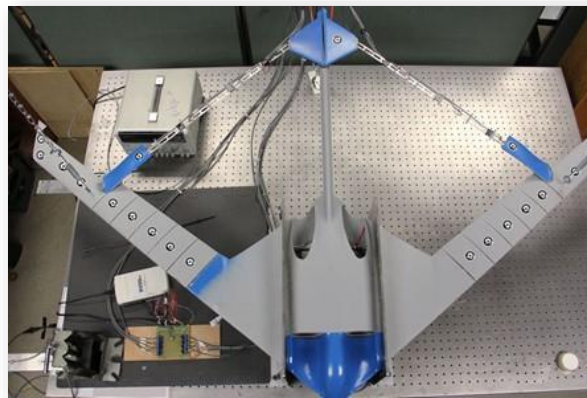


FIGURE 134 - TOP VIEW SHOWING OPTICAL TARGETS

Approximately 20 shots were taken at each load step and processed in Photomodeler. A text file was then generated for the specific targets mentioned previously. Several manual reference points were also chosen such as the wing tip since it was impractical to center a target at this location. Figure 135 below shows some results for this process at several locations along the aircraft, along with the unreformed geometry.

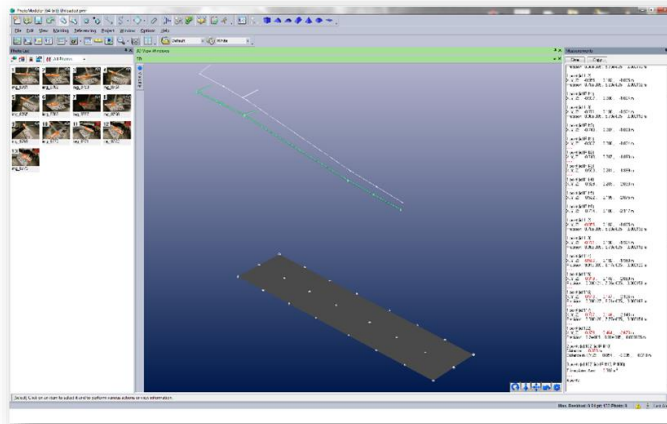


FIGURE 135 - PHOTOMODELER INTERFACE SHOWING DEFORMED AND UNREFORMED GEOMETRY

6.4.1.3.2 Physical Measurements

A series of physical measurements were also performed as a means to benchmark Photomodeler's results. These measurements were taken at several equivalent points throughout the structure (such as the wing tip). Additional measurements were taken at various locations along the remainder of the aircraft in order to obtain backup data in case Photomodeler data failed at a particular time step.

All measurements were of vertical displacements and were taken with a steel ruler with respect to the planar top of the optical bench. The assumed error was chosen as $\pm 0.5\text{mm}$ as this was one half of the smallest increment on the ruler.

6.4.1.3.3 Accelerometer for Angular Rotations and Dynamic Response

A 3-axis, ADXL335 accelerometer from Analog Devices was also used on some test cases (Shown in Figure 136). This accelerometer outputs three single ended signals for each axis and as a result only two could be used

simultaneously on the 8-channel NI USB-6009 DAQ. Two strain gauges was sufficient for dynamic response measurement of the forward wing to determine primary bending modes. However, angular deflections were measured at 8 spanwise locations on the forward and aft wings. Therefore, one accelerometer was used and moved throughout the structure to measure rotations at each load step.

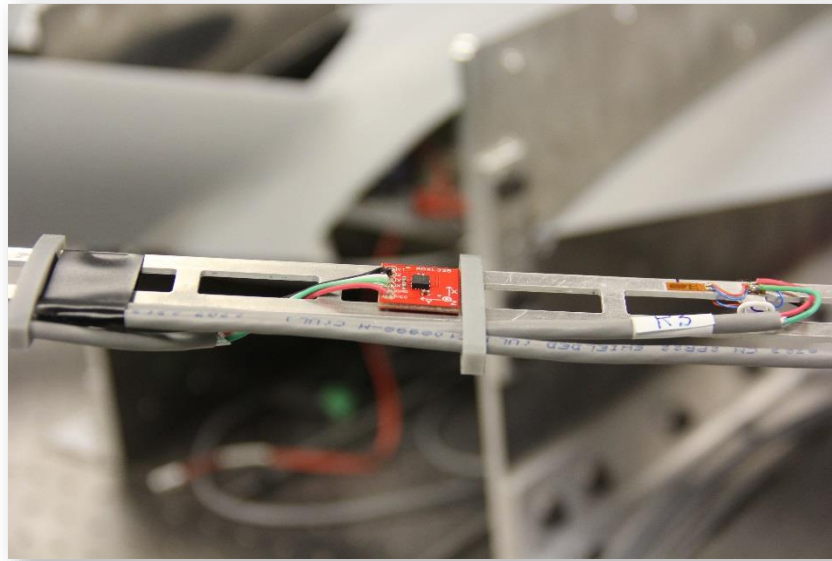


FIGURE 136 - 3-AXIS ACCELEROMETER ON AFT WING

6.4.1.4 Test Results

The following section compares the test results against analytical predictions made using Anthony Ricciardi's initial NASTRAN model. Results of a model tuning process are then summarized and this new analytical model compared to the experimental results. The resulting, tuned structural model was then passed to Anthony Ricciardi for nonlinear aeroelastic analysis using his custom framework. Finally, the results of this analysis, including trim states, at the predicted points in the operating envelope.

6.4.1.4.1 Results comparison

The as built mass and inertia properties (see Section 6.2.3) were applied to the NASTRAN model and an equivalent discretized 1g and 3g load cases analyzed using SOL 106 with follower forces turned off. These results were used as the basis of comparison with experimental measurements.

FE analyses were run for load cases 1a, 1b and 2a. These load cases were defined in Section 3 previously but are also summarized in the following figure.

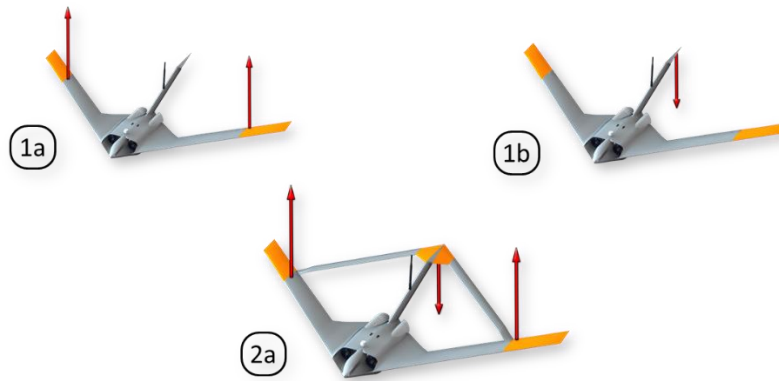


FIGURE 137 - LOAD CASE SUMMARY

First a comparison of deflections during loading cases 1a and 2a. Comparing the analytical and experimental displacements resulted reasonable agreement as can be seen in Figure 138 below. Here we can see that the initial structural model over predicts the forward wing stiffness, while under predicting the stiffness of the boom.

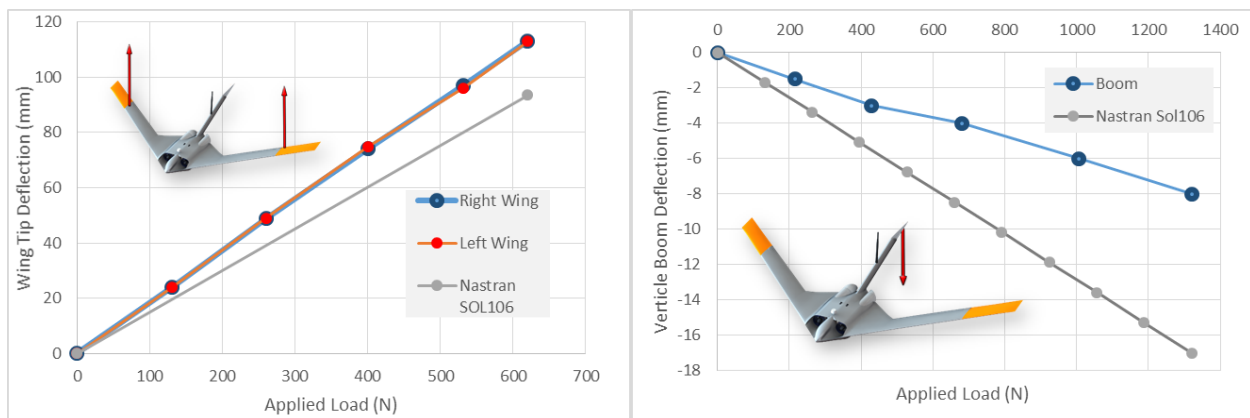


FIGURE 138 - CANTILEVER WING AND BOOM TEST RESULTS VS BASELINE FE MODEL

Figure XX shows a comparison of the measured and predicted strain at the forward wing root subjected to load case 1a (no strain gauges installed on boom, therefore no results for load case 1b). These results also show the baseline model under predicted strain.

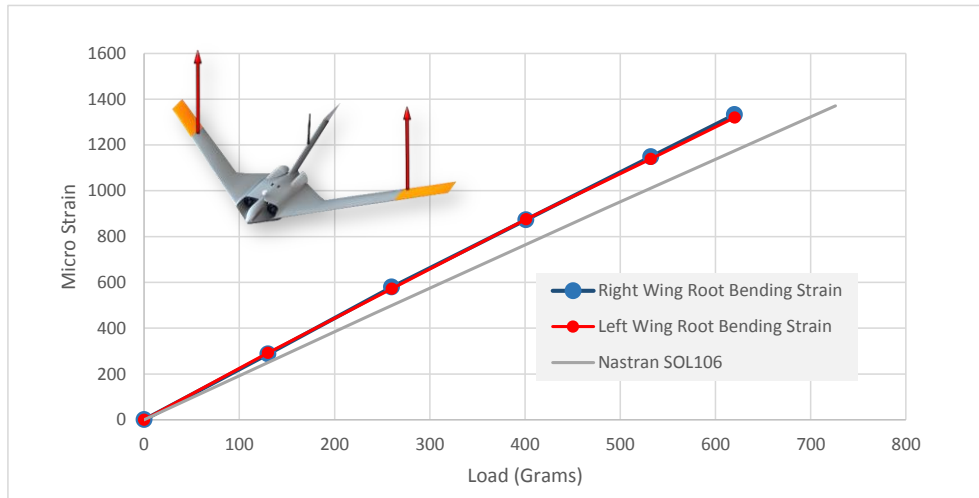


FIGURE 139 - COMPARISON OF MEASURED STRAINS WITH THOSE PREDICTED BY BASELINE FE MODEL

A modal analysis was also run using the NASTRAN model to determine the first flexible body modes. These were compared to experimental results found by performing a spectral analysis on accelerometer readings recorded after subjecting the wing structure to several impacts. Figure 140 below shows the NASTRAN results overlaid onto the spectral response from the experiment. Here we can again see good agreement with the first 3 modes with a distinct frequency shift to the right for the NASTRAN predictions. This again is likely due to this initial Nastran model over predicting the front wing stiffness.

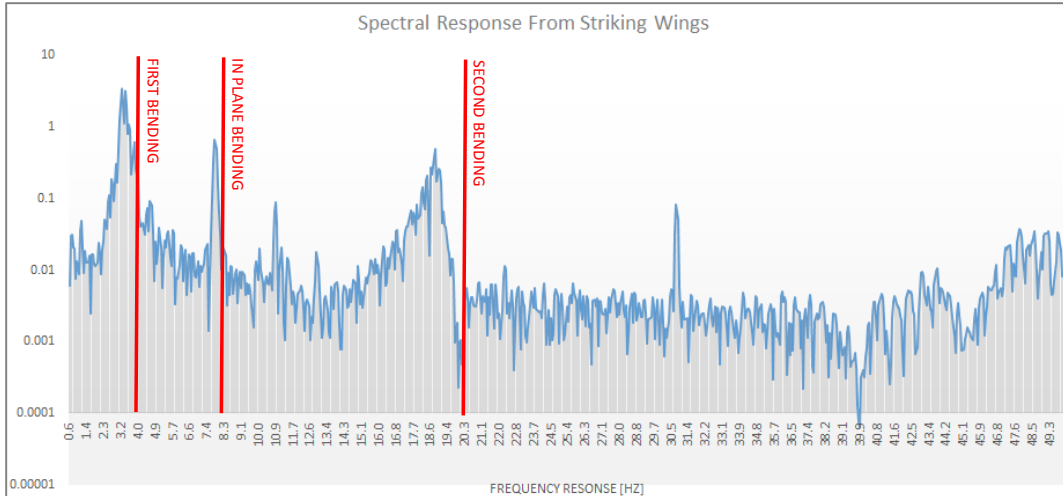


FIGURE 140 – SPECTRAL RESPONSE OF CANTILEVER WING (BLUE) VS PREDICTED (RED)

Discrepancies were most likely due to errors in modelling the non-compliant composite structures. Many of the material and cross sectional properties were modelled based on approximate cross sections and assumed material properties for the composite bodies. Many of these structures would benefit from a multi-objective optimization that sought to match both the displacements and strain results. This is the subject of the following section.

6.4.1.4.2 Model Tuning

As mentioned previously, initial material properties chosen for the composite portions of structure were rough estimates. It was desired to update several of these initial estimates in order to better match the experimental data. The first step however was to update the original NASTRAN model to better capture the as built geometry. One update was to the aluminum spar dimensions. The initial design specified a forward wing spar height of 4mm whereas the as built part ended up at 3.63mm. Similarly, the aft wing spar thickness was reduced from 1.6mm to 1.55mm.

Figure 141 below shows the inner forward wing portion that was originally modelled using a constant cross section beam. However, to better capture the running stiffness of this portion of the beam, the three elements making up this section were gradually tapered with the same approximate ratio of the actual test article.



FIGURE 141 – FE MODEL OF SENSORCRAFT CONFIGURATION SHOWING UPDATED TAPED BEAM INBOARD WING SECTIONS

The baseline FEM modeled the portions of the aft wing ladder spars as a singular element (the spanwise portions connecting each rung). However, since the gauge locations were located at the middle of these portions (see Figure 142) an additional node was placed at the midpoint of each element. Some small geometry updates were also included to better capture the as built geometry and more accurately simulate the applied load location, these are also noted in the figure.

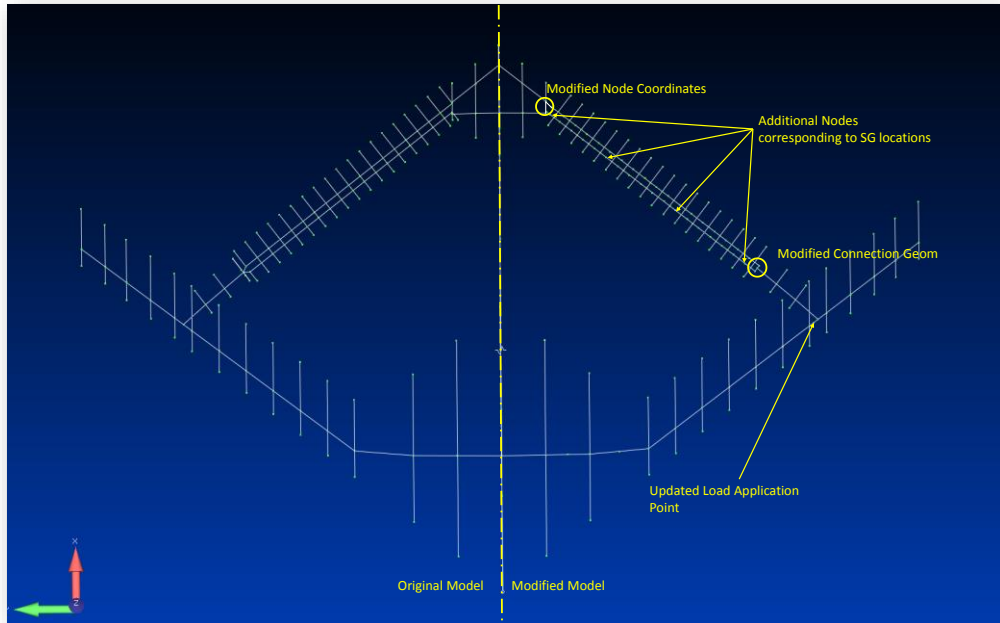


FIGURE 142 - MODIFICATIONS TO BASELINE NASTRAN MODEL TO CAPTURE AS TESTED CONFIGURATION (BASELINE ON LEFT, UPDATED RIGHT)

This is critical in accurately capturing the correct strain values as the bending moment at each rung/spar interface sees a discontinuity due to the effect of the rungs passing on a discrete bending moment at these locations (as shown in Figure 143).

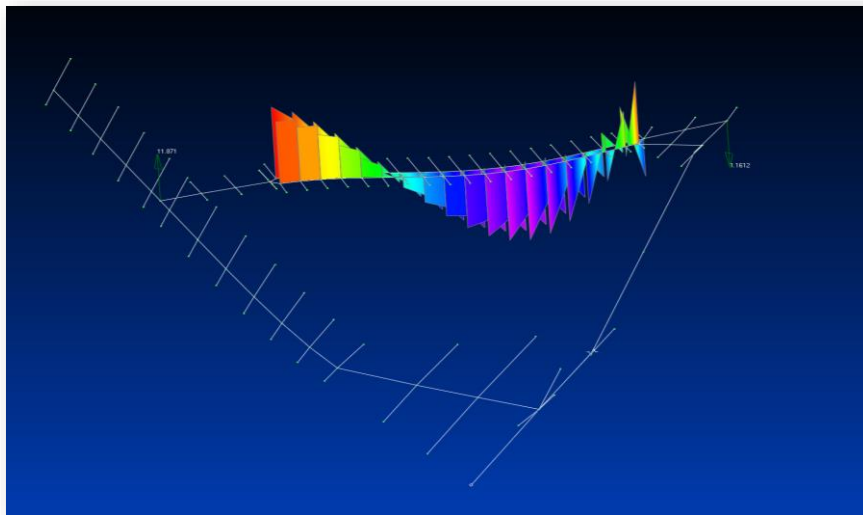


FIGURE 143 - DISCREET BENDING MOMENT DISTRIBUTION DUE TO LADDER SHAPED AFT SPAR

The final modification to the baseline model was the reassigning of material properties to the structural elements in order to achieve discrete properties across each portion of the structure. This would allow for more control over individual stiffness's of various entities in the subsequent tuning process. FigureXX shows the initial distribution of 3 material properties vs the updated model with 7.

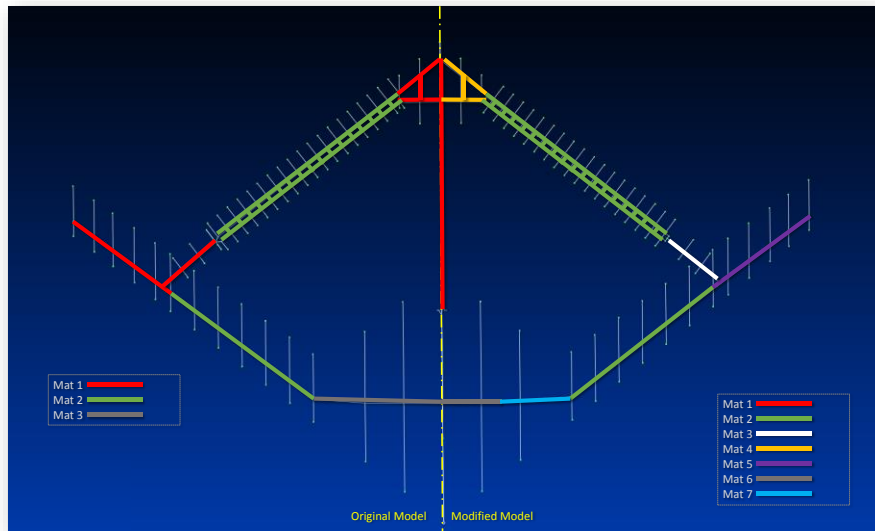


FIGURE 144 - MODIFIED MATERIAL PROPERTIES USED IN SUBSEQUENT OPTIMIZATION (BASELINE ON LEFT, UPDATED RIGHT)

ModelCenter process control software was used to integrate Nastran and Matlab in order to tune the analytical model. A screenshot of the process can be seen in Figure 145.

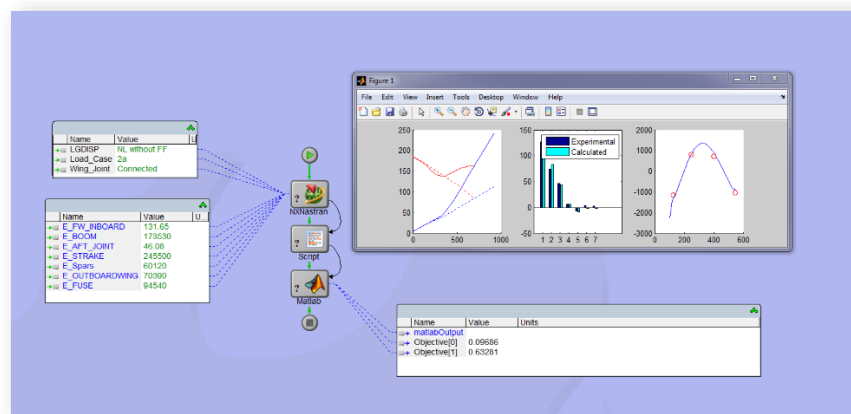


FIGURE 145 - MODELCENTER PROCESS USED TO TUNE BASELINE MODEL

A series of optimizations were performed in order to minimize the error in displacements as well as the aft wing strain values. The displacement error was calculated as the RMS error of the experimental readings (FE model is only a semi-span model so experimental measurements are averaged across the left and right side of the aircraft). The resulting in 7 discrete locations used for displacement comparison are shown in Figure 146 below (note, similar measurements taken left half of aircraft and averaged with right side to compare to analytical half model).

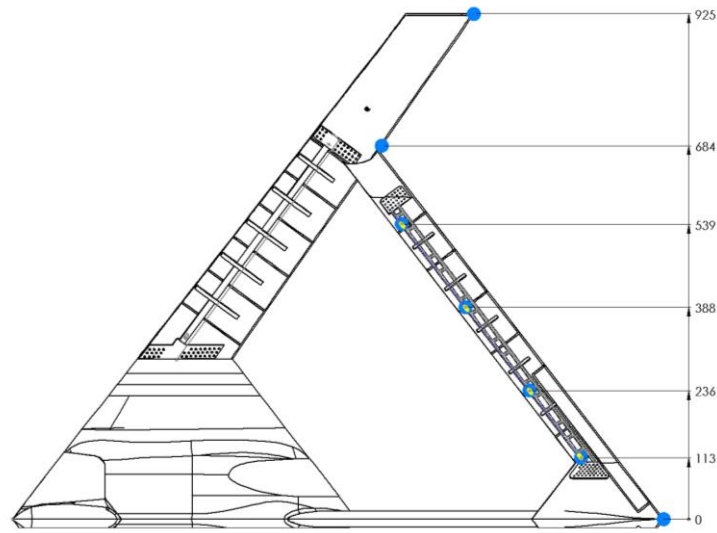


FIGURE 146 – LOCATIONS USED TO MEASURE STRUCTURAL DISPLACEMENTS

Strain errors were again RMS values calculated based on the difference between the measured and calculated values at the locations shown above (also with the experimental results being averaged over each semi-span, left & right). Both the strain and displacement RMS errors were normalized based on the baseline NASTRAN model response, resulting in an error of one for each. Figure 147 below shows the Strain and Displacement results for the baseline FEM model. The leftmost figure shows a front view of the deformed and un-deformed model (z-displacements only) with the middle figure showing a bar graph of measured vs predicted deflections at the 7 measured locations on the aircraft. Finally, the rightmost figure shows the calculated strain in blue along the aft wing compared to the measured values represented by red circles.

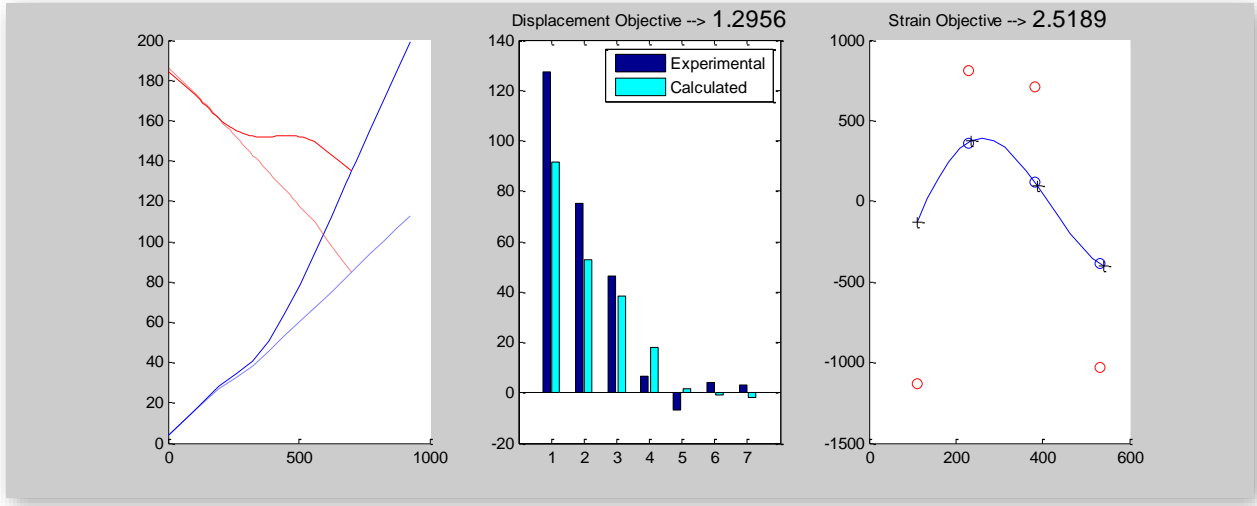


FIGURE 147 - STRAIN AND DISPLACEMENT RESULTS OF BASELINE FEM CONFIGURATION

A series of genetic optimizations were performed with the goal of optimizing both displacement and strain objectives. This resulted in a Pareto front which allows a design to be chosen based on a tradeoff between the two objectives. After exploring the optimal solutions a design point was chosen based on a weighing of 1:2 for displacement and strain respectively. Figure 148 below shows several designs on the Pareto front with the chosen design shown in greater detail in the subsequent figure.

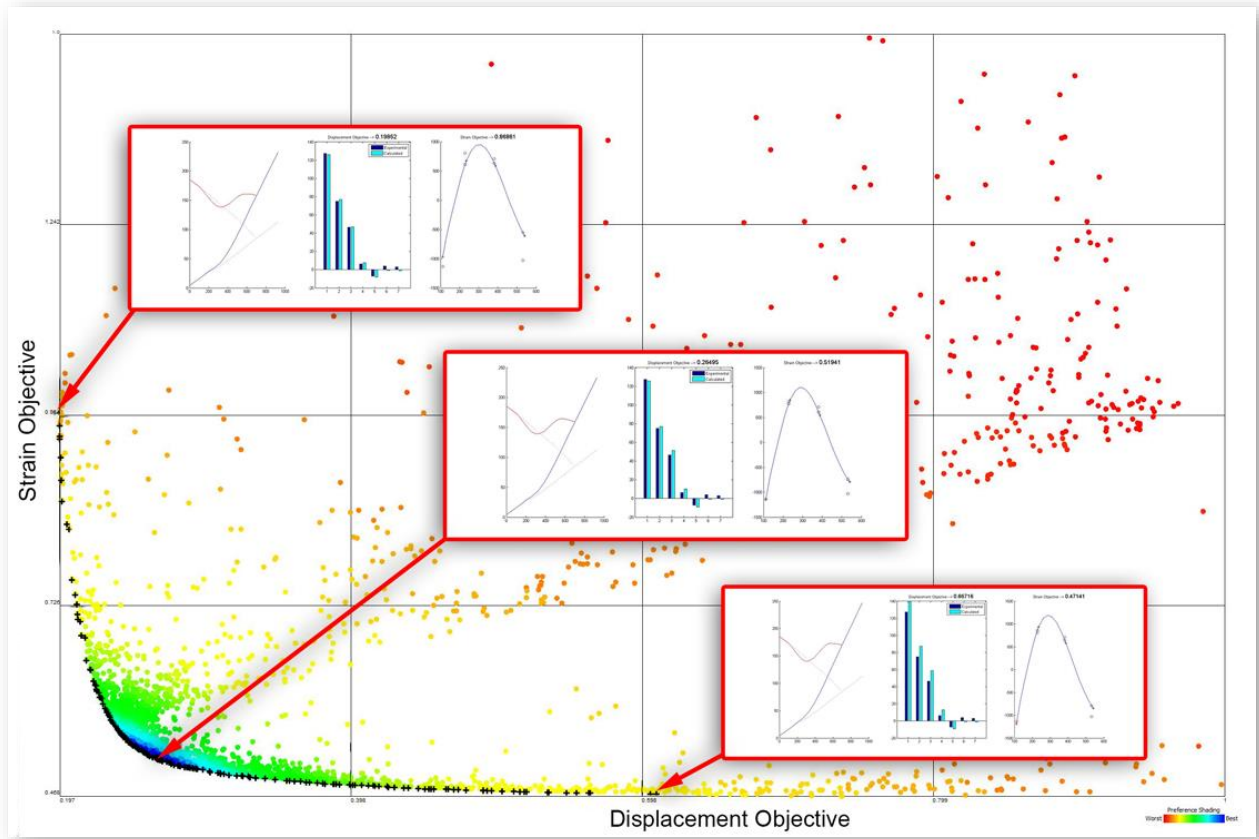


FIGURE 148 - PARETO FRONT SHOWING OPTIMAL DESIGNS IN TERMS OF MINIMIZED DISPLACEMENT AND STRAIN RMS ERRORS

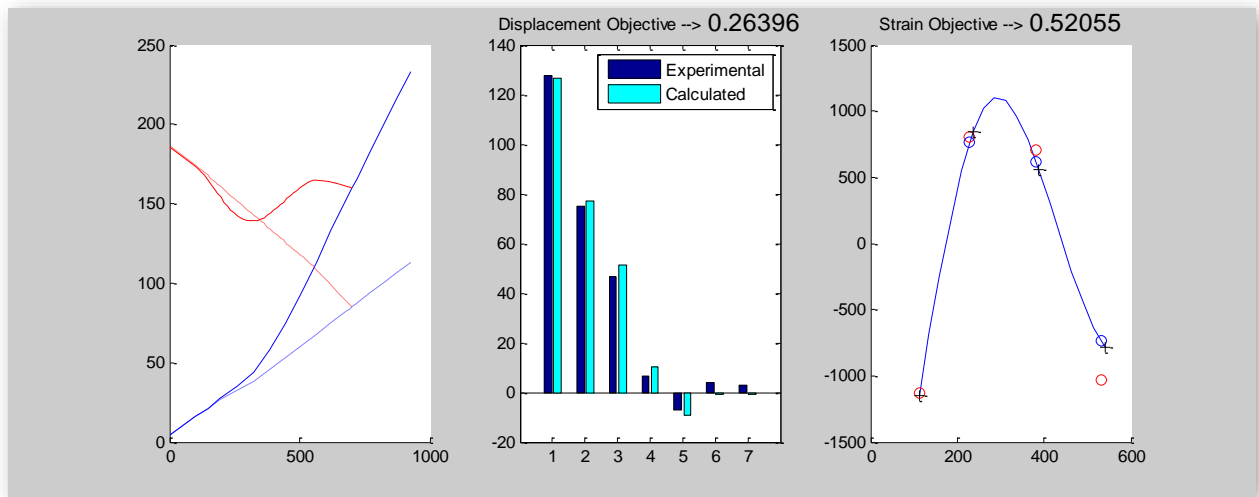


FIGURE 149 - STRAIN AND DISPLACEMENT RESULTS OF OPTIMIZED FEM CONFIGURATION

Comparing Figure 147 and Figure 149, we can see a vast improvement in both the strain and displacement objectives. Two discrepancies are still present however. The first is the predicted boom down reaction of the FE model vs the upward deflection seen in the experiments. It is suspected that this is due to the modelling of the boundary conditions which allow no force to be passed inboard of the fuselage constraint whereas in reality some loading may pass through the holding fixture through the composite skins and as a result affect the booms response. Further work may be performed to improve this results although the small error is likely irrelevant for the purposes of this tuning exercise. The second discrepancy is in the strain reading on the aft wing at the most outboard station. This strain error is quite a bit larger than at the other stations and is unexplained at present. This is likely due to unknown boundary conditions where the end of the ladder is bonded into the rapid prototyped hard point in the outboard section of the aft wing. Future work could focus on improving these results but overall the results are very encouraging.

This resulting modified NASTRAN model was then passed back to Anthony Ricciardi for processing through the nonlinear framework to determine trim states, aeroelastic response and resulting loading for use in flight clearance load tests Described in Section 6.

6.4.2 Flightworthiness Checks

The following section briefly describes some of the ground testing that was performed to determine the flight worthiness of the aircraft used in flight testing. Much of this work was performed under the guidance of Jeffery Garnand Royo during his recent visit to the Center for Aerospace Research in Victoria BC.

The following figure summarizes the ground testing (including the static load tests described earlier) process flow that is used in order to clear each aircraft for flight with each subsequent section explaining the individual tests in greater detail.

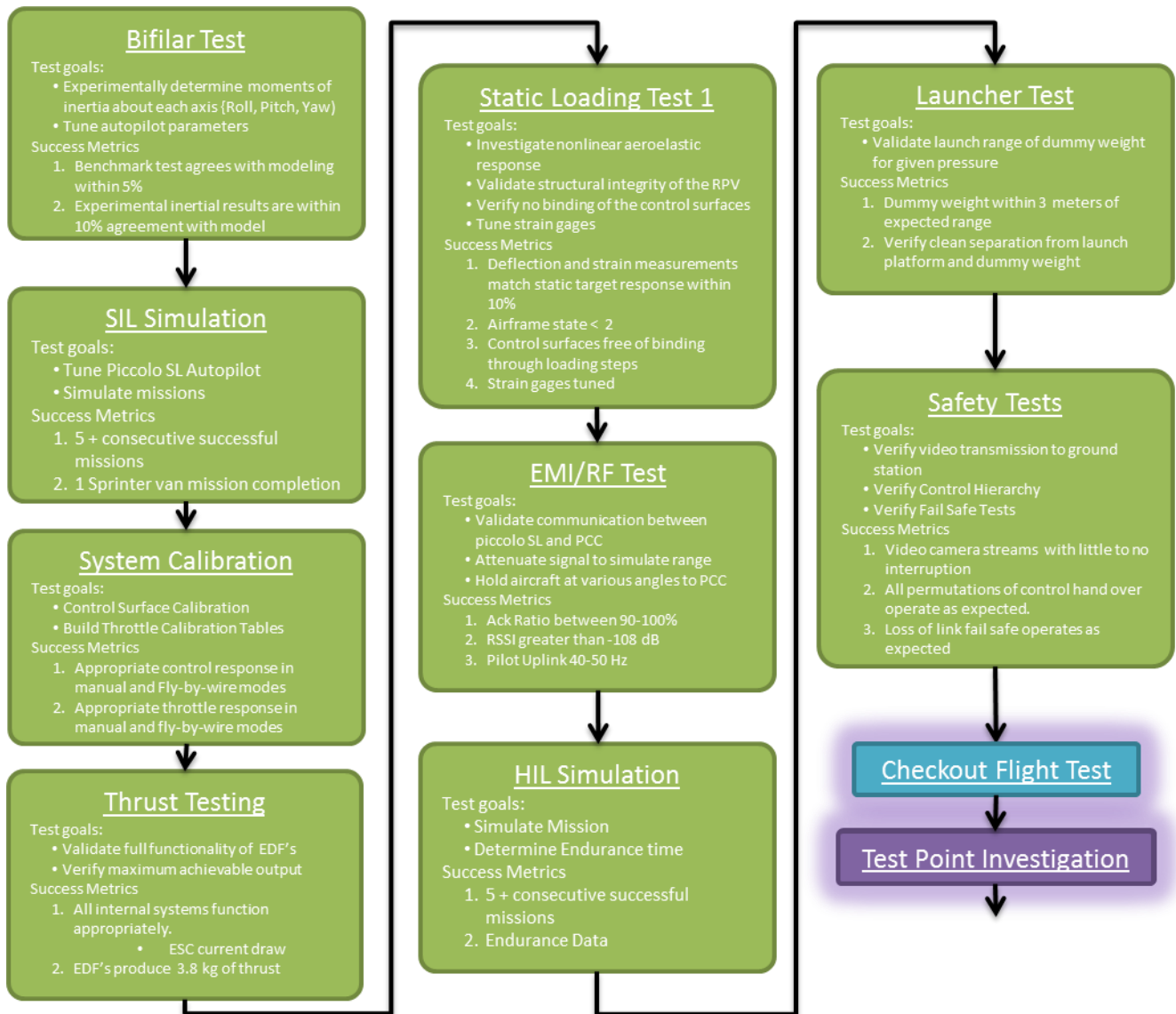


FIGURE 150 - TESTING PROCESS FLOW

6.4.2.1 Bifilar Pendulum Tests

A series of Bifilar Pendulum Tests (BPT) were performed in order to measure the inertial properties of the flight test articles (both the G2 Rigid and the flexible configuration). The details of these tests were described in previous works, however, a brief description will be given here for reference.

A custom rig was developed to hold the aircraft while it is suspended with two wires. These wires are connected along the rig so as to ensure the rig comes to rest in the chosen principle axis (ie with the aircraft primary x, y,

or z axis vertical). The empty cage is then oscillated in all three axes and the resulting data used to calculate the inertia of the cage. The aircraft were then inserted in the rig and again oscillated in each orientation to determine the overall inertias of the rig and aircraft. The inertia of the rig was then subtracted to determine the principle moments of the aircraft. Since the aircraft were flown at different weights and cg locations, these baseline results were modified on a per flight basis using a spreadsheet to account for added trimming weight and cg travel. Figure 151 below shows a BPT being performed in the pitch axis.



FIGURE 151 - BIFILAR PENDULUM TEST IN PITCH AXIS

6.4.2.2 Software in the Loop Testing (SWIL)

A variety of other testing was performed. These included a series of Software in the Loop tests. These tests served four primary purposes...

- 1) Tune and validate autopilot gains and settings
- 2) Train ground crew and pilots prior to each flight test
- 3) Validate flight test plan and evaluate chosen test maneuvers
- 4) Provide simulated data to validate post processing workflow and test algorithms developed to distil flight test data

6.4.2.3 Static Thrust Tests

A series of static thrust tests were performed on the electric ducted fans (EDFs) chosen to power the aircraft. This also included installed tests using the custom thrust measurement rig shown below. The objective of the test was to validate the predicted thrust and endurance as well as to build thrust vs throttle command tables for subsequent tuning of the autopilot.

6.4.2.4 EMF

As series of range and interference tests were performed to ensure adequate communications between the aircraft and command/control links. Range tests were performed by driving the aircraft to the extents of the flight test range and monitoring the telemetry, video, and RC control links. Each link was turned on or off in sequence to see their effect on the other links in order to reduce the risk of interference and cross talk. No discernable interference was observed through any combination of active links so next the vehicle was orientated in a variety of roll, pitch and yaw attitudes beyond what would typically be seen if flight. At this maximum expected range (1.8 km) the comms. were slightly degraded with the primary data link and RC control link still being above acceptable limits. The video link dropped out in various orientations but this was likely due to the close proximity of the aircraft to the ground which greatly reduces the link quality due to the ground blocking the antenna emission pattern. This reduced video range was determined acceptable since the initial set of flights do not rely on flying through the video link and incremental testing will be performed to slowly prove the range capability of both video and telemetry links.

6.4.2.5 Other Testing

The standard set of tests including systems checks, control surface stress tests and electrical system load tests were also performed. In addition, a series of tests was performed using a variable dummy mass to determine the relationship between aircraft weight and takeoff speed vs Pneumatic Catapult charge pressure by systematically firing and measuring the exit velocity of the launcher. Figure 152 below shows some post processed video used to determine the launch speeds, accelerations etc.

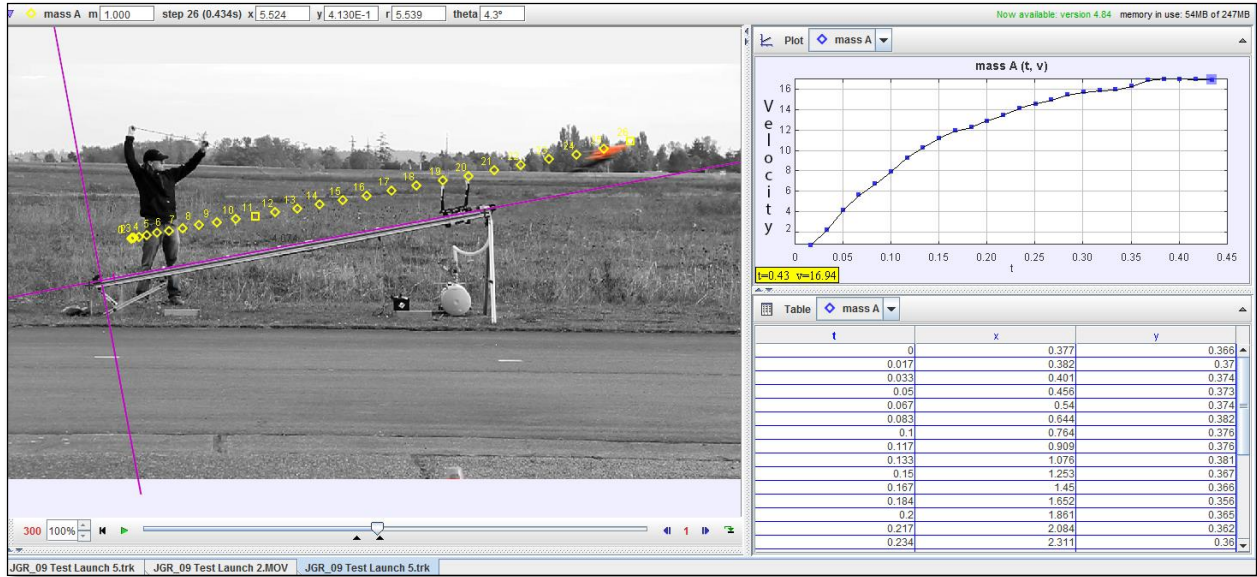


FIGURE 152 - CALCULATION OF LAUNCH SPEEDS AND TRAJECTORIES IN PREPARATION FOR FLIGHT TESTING

Upon completion of these tests a series of Hardware in the Loop tests were performed to simulate the missions and confirm the correct operation of the hardware aboard the aircraft. These tests were performed before each individual day of testing on an ongoing basis.

6.4.3 Modifications to Instrumentation System for Flight Based Measurements

In order to carry out measurements in flight several modifications were required to the instrumentation and DAQ described for the ground testing. This included updating electronics to reduce overall size, weight and power consumption as well as the development of an onboard system capable of both logging and transmitting real time data. The following section outlines the modified instrumentation.

6.4.3.1 System Design

The basic system consists of eight in-wing sensor units (each corresponding to a strain reading locations on aft wing) and a central data logger. The data logger also outputs a data stream to the aircraft's autopilot, which will pass the information to a ground station at a reduced sampling rate in order to prevent competition with flight-critical telemetry. Figure 153 below shows the instrumentation system architecture from the strain gauges to the GUI at the pilots HUD station in the ground control station.

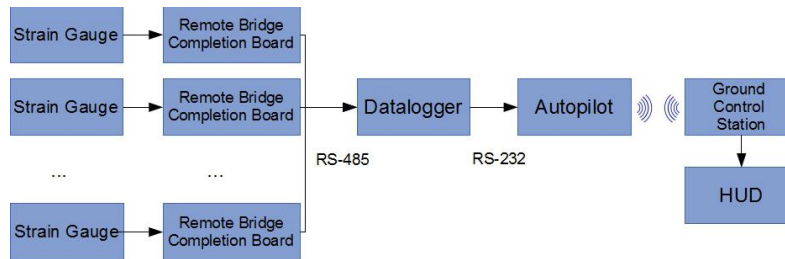


FIGURE 153 - HARDWARE ARCHITECTURE FOR CAPTURING STRAIN DATA IN-FLIGHT

As the aircraft uses electric motors as well as various servo and radio systems, the potential for noise over the communication lines is high. For this reason, RS-485 was chosen to link the remote bridge completion boards (RBCB) to the data logger. RS-485 uses a differential signal which excels at rejecting common-mode noise. RS-485 also allows the use of a daisy-chain network topology, reducing the number and therefore weight of conductors required.

The autopilot used for this project is the Piccolo SL+, by Cloud Cap Technology. The Piccolo provides a serial pass-through function for payload-to-ground-station communications. This pass-through can be accessed using either RS-232 or CANBUS protocols. RS-232 was selected for this project for ease of use, but it is not a differential protocol, raising the risk of signal noise. To prevent this, the data logger will be placed close to the autopilot, minimizing conductor length and noise induction.

The data logging system is based on the Logomatic v2, from SparkFun Electronics. The Logomatic uses an NXP LPC2148 ARM7 processor, and includes a Micro SD card for data storage. One major advantage of the LPC2148 is the inclusion of two UARTs for serial communications. This allows the allocation of one serial channel for the wing strain gauges, and a separate line entirely for the autopilot. The daisy-chain format of the RS-485 network requires the use of individual ID numbers for each separate node, which would be difficult to implement for the Piccolo autopilot.

Finally, the in-wing RBCB were designed by Wanjohi Mugo, a University of Victoria Electrical Engineering student and can be seen in Figure 154 below. Each individual strain gauge incorporates a 16-bit analog-to-digital converter (ADC) that feeds into an ATMEGA328 8-bit microcontroller. The inclusion of the

microcontroller simplifies communications a great deal. The ADC uses a synchronous communications protocol, which is extremely difficult to use in a daisy-chain polling environment.



FIGURE 154 - CUSTOM DESIGNED PRINTED CIRCUIT BOARD FOR REMOTE STRAIN READINGS

6.4.3.2 Firmware Development

The Logomatic v2 is open-source hardware, and SparkFun provides a basic firmware package that allows direct serial data logging. Heavy modification was required to meet the needs of the project, as the original SparkFun firmware only included support for input on one serial line, and essentially just dumped whatever was received into the Micro SD card. The new firmware developed for the project operates the following main loop:

- Poll strain gauge values.
- Add to working data buffer.
- If data buffer is full, write to SD card and switch to secondary buffer.
- Once every n loops, write out current values to autopilot pass-through.

The data is written to the SD card in a comma-separated value (CSV) format, and includes basic timing information using the Logomatic's onboard real-time clock:

```
18,11,48,32176,32186,32196,32206,32216,32226,32236,32246,
```

The first three numbers represent hours, minutes, and seconds. Higher-accuracy timing is currently being implemented, which will add a decimal value to the seconds field. Each remaining number represents a sensor value in base ten. As the ADC is a 16-bit system the possible values range from 0 to 65535, although the actual

strain gauges are unable to reach those limits. The CSV format is easily analyzed using common spreadsheet software or MATLAB.

6.4.3.3 Stability and Data Rate Testing

A system of testing the developed firmware was created using an Arduino Mega microcontroller to replicate the behavior of the wing sensor nodes. The current system polls the complete set of sensors at a rate of 66 Hz, logging data at 329 kB/minute. A final overnight stability test showed consistent results over an 18-hour period, greatly exceeding the aircraft flight time of ten minutes or less. Figure 155 demonstrates the stability of the logged results, with the Arduino sending out a series of ramping values.

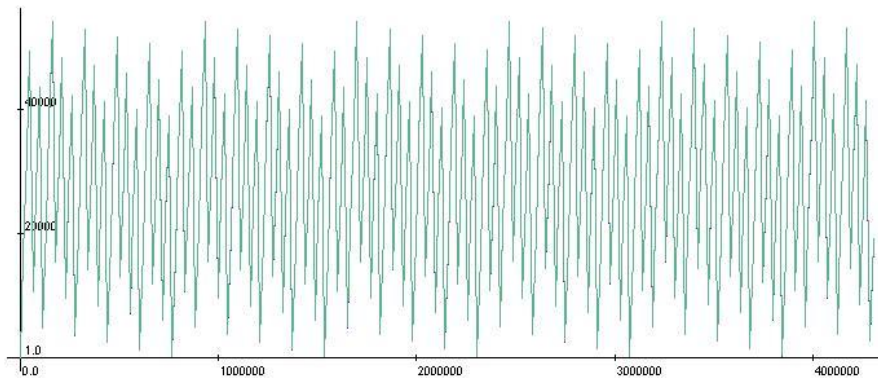


FIGURE 155 - DATA LOGGER OUTPUT, 18-HOUR TEST

Although the test did take place in an ideal environment, no outliers or dropped frames were encountered. In excess of four million lines were logged, over 32 million individual sensor values. Fig. 2 actually shows eight separate streams, but the volume of data recorded renders them indistinguishable. This shows great promise in terms of adapting the data-logging system to other applications, such as a tethered aerostat.

6.4.3.4 Pilot Station Based GUI

An updated user interface is also required for monitoring real time data at the ground station. Figure 156 below shows the pilot station Heads Up Display (HUD) which will be viewed in a Picture in Picture view at the Piloting Station (46" TV in Ground control station from which the pilot will navigate the aircraft for precision maneuvers using the forward facing camera).



FIGURE 156 - PILOT STATION HEADS UP DISPLAY

The HUD shows a real-time strip chart of the aircraft states as well as dial indicators for the strain at the aft wing locations. An audible buzzer also sounds when the prescribed strain limits are reached. In addition to the instrumentation readouts there is also the forward facing camera feed as well as an artificial horizon to aid in the navigation of the aircraft.

6.4.4 Flight Clearance Load Testing

The final phase of ground testing involves a final static load test to determine if the aircraft can take the predicted maximum load as calculated using the Nonlinear Aeroelastic Tool described previously and ASWING aeroelastic simulation code developed by Prof Mark Drela.

ASWING calculates the static, time domain dynamic, and frequency domain response of an aircraft [46] [47] [48] [61] and was used to determine the predicted static aeroelastic loading at several operating points throughout the flight test envelope. The test also served as a means to validate the updated, in-flight telemetry system described in the previous section.

6.5 Flight Test Planning¹

This provides a brief outline of the flight test planning phase. This work included determining flight test goals, procedures and logistics. A series of flights were planned using the G2 Rigid minis as a build up to subsequent flight tests using the Aeroelastically Tailored vehicle.

6.5.1 Rigid Flights

The Rigid Mini flights serve as a stepping stone to flights using the compliant aircraft. They are seen as a low risk means to develop and validate safe flying characteristics, determine achievable loading conditions during flight, train pilots and ground crews and supply data to dry run post processing tools and methodologies. As such, the following goals were defined.

6.5.1.1 Primary Objectives

1. Validate correct integration and tuning of Piccolo flight control systems.
2. Demonstrate accurate and successful data acquisition/ logging of Instrumentation system.
3. Safely validate flight test methodology and test points that will be used in subsequent compliant flight tests.

6.5.1.2 Secondary Objectives

1. Determine Feasibility of First Person View (FPV) piloting for precision maneuvers
2. Validate Real time sensor stream over telemetry link
3. Verify operating envelope including stall characteristics and operating speeds
4. Determine more precise estimate of endurance and time on station
5. Train additional ground crew

¹ This work was primarily performed by Jeffery Garnand Royo [58] with some help from the author, but is included here for completeness

6.5.1.3 Tertiary Objectives

1. Perform flight maneuvers with full autopilot
2. Generate sensor data and validate post processing methodologies

A series of flights were planned in order to achieve the goals mentioned above. Of primary interest is the tuning of the Piccolo autopilot (which has not been flown in the Mini configuration at outset of this phase) to ensure controllability throughout the envelope while still allowing sufficient authority to the pilot to perform require test maneuvers.

Test maneuver investigation involves performing push-over/pull-up doublets as well as windup turns. Flights were planned to investigate achievable loading in all three of the primary control modes of the aircraft (Fly-by-wire, manual, FPV/manual and FPV/fly-by-wire). Should time permit, the tertiary objective of using the fully autonomous mode of the piccolo SL autopilot to perform flight maneuvers were planned.

6.5.2 Flexible Flights

The overriding goal of these flight is to validate the safe flying characteristics of the compliant structure and to investigate the aeroelastic response of the aft wing in both linear and nonlinear regimes. To do so, the following set of objectives was defined.

6.5.2.1 Primary Objectives

1. Obtain steady state strain readings for various loading cases ranging from 1g level flight to a 3g maneuver
2. Demonstrate controllability of flexible configuration using COTS Piccolo autopilot.
3. Verify feasibility of 1.85m test point for collecting clean inertial and structural response

6.5.2.2 Secondary Objectives

1. Collect sufficient data through onboard sensors to quantify flying qualities
2. Obtain dynamic structural response data to validate structural predictions

6.5.2.3 Tertiary Objectives

1. Accurately measure aft wing deflections using on board cameras

Here a series of 3 flights were planned to achieve the objectives. The first would be a checkout flight consisting of gentle controlled maneuvers to determine the controllability of the aircraft and to collect sufficient low g structural response data.

The second and third flights would build up to higher loading conditions to obtain the desired aft wing loading. The details of the maneuvers required to achieve this are outcomes of the Rigid aircraft flight testing described in the previous section.

6.6 Flight Testing

This section outlines the flight test results to date using both the Rigid Generation 2 aircraft as well as the Aeroelastically Tuned model.

6.6.1 Generation 2 Rigid Flights

The following section outlines the flight tests performed to date including the completed Generation 2 rigid flight test articles. The flights are broke down into Airworthiness Checkout Flights, Test Point Evaluation and Autonomous Flight.

6.6.1.1 Checkout Flights

A series of five initial checkout flights were performed in order to train flight and ground crews, validate and tune the Piccolo autopilot and to perfect a new launch method using a pneumatic catapult (see Figure 157 below).



FIGURE 157 - FLIGHT TESTING OF GENERATION 2 MINI

A large problem during the initial tests was the takeoff segment immediately after exiting the launcher. This was determined to be a result of several issues. First the aircraft elevator trim was causing a slight pitch up motion after takeoff when the pilots sticks were centered and the pilots initial response was to pull up. this resulted in a violent pitch up motion that bled airspeed and caused a stall. Another concern was the lack of elevator effectiveness which was determined to be to the low launch speed and to overprediction of the effectiveness in the modelling. In subsequent flights the autopilot was modified to allow for the reduced effectiveness by changing the $C_{m_elevator}$ term in the first order inversion term (telling the autopilot that the surface is less effective is analogous to increasing the proportional gain). The neutral point of the elevator was also trimmed (trailing edge down) 4° to avoid the initial pitch up. These changes, combined with increasing pilot experience, resulted in very good takeoff behaviour in subsequent flights. During the initial flights gain tuning was performed resulting in good flying qualities while operating in fly by wire mode.

6.6.1.2 Test Point Evaluation Flights

The next set of three flights involved investigation of the test point maneuvers. A series of push-over/pull-up maneuvers were performed to determine the ability for a pilot in fly by wire mode to induce a desired verticle load. It was found that the pilot had difficulty in achieving a desired steady state load condition while readings were transmitted from the ground station operater via the headsets. Better steady state results were achieved if the autopilot g limiter was set at the desired value and the pilot “buried the sticks”. However, the maximum

load achieved using this technique was 2.2g (even when the limiter was set higher) due to a lack of pitch rate authority. Figure 158 below shows flight test results of the maneuvers resulting in the largest g loading.

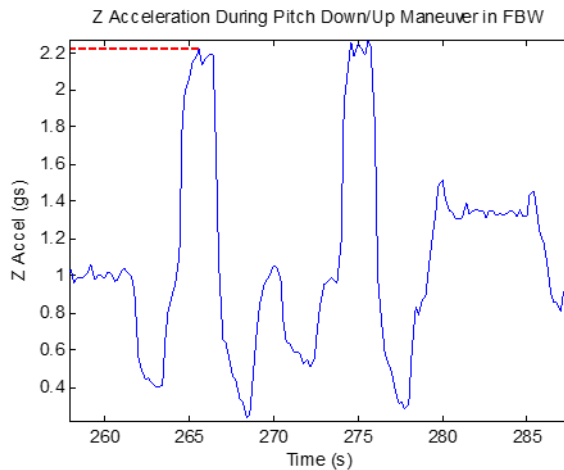


FIGURE 158 - Z-ACCELERATION DUE TO PILOT INDUCED DOUBLET MANEUVER

Future flights would allow more aggressive tuning of the pitch loop but great care is required not to overtune the aircraft to the point that it would exhibit marginal stability at any points in the envelope. To date these additional tuning flights have not been performed.

During these flights the windup turn maneuver was also investigated. Here a maximum load of 1.5gs was achieved. This was limited by the maximum bank angle limit imposed by the autopilot. While this parameter can be adjusted it was determined that unsafe conditions would arise if the bank angle was raised much further beyond the existing limit. For instance a 3g load would require a 70 deg bank which would be well beyond the safe limits specified by the manufacturer of the autopilot.

6.6.1.3 Autonomous Flight

One autonomous flight was performed during which several doublet commands were performed. The doublet command is a special feature of the Piccolo autopilot that can only be commanded when the aircraft is in full

auto mode. In this application the command temporarily turns off control of the pitch axis (and optionally the off axis loops as well) and commands a fixed deflection of the elevators for a prescribed time.

Results from these tests were very promising with good steady state loading results even at high loading conditions (see Figure 158 below). However, one large area of concern is the extremely violent pitching of the aircraft and the rapid loss of altitude at the higher g loadings. One distinct outcome of these tests, especially with the flexible aircraft, is that the autopilot will be unable to reliably recover the aircraft once the command is done and the autopilot comes back online.

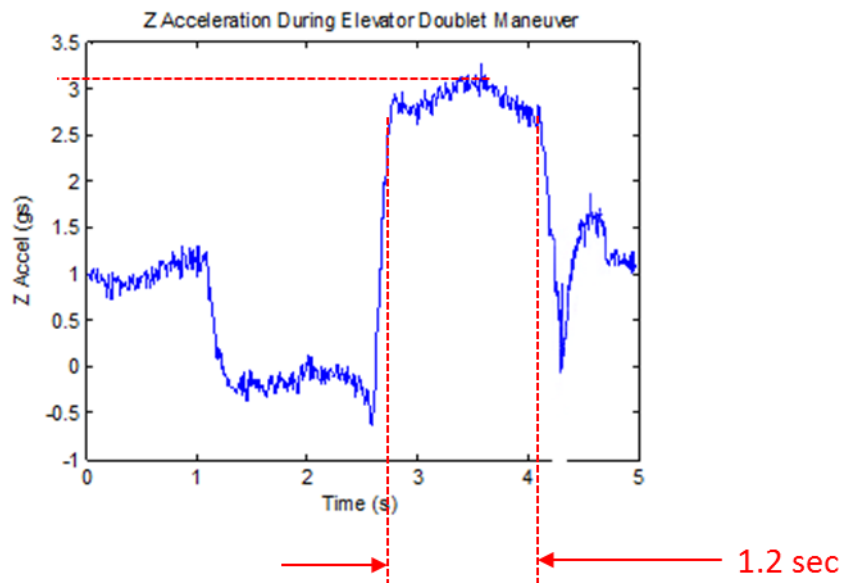


FIGURE 159- Z-ACCELERATION DUE TO AUTO-PILOT INDUCED DOUBLET MANEUVER

6.7 Aeroelastically Tuned Mini Flights

The flights of the aeroelastically tuned model are planned as future work with the main goal of providing an aeroelastically tuned, flight worthy vehicle having been met. As part of this future work, a series of three testing phases has been planned. The first set of flights will be checkout tests consisting of gentle maneuvers meant to increase pilot comfort and ensure the aircraft is controllable and no adverse aero-structural effects are present. The second phase of testing will involve transitioning to the first person flying mode with the secondary pilot taking over control in the GCS and performing maneuvers while monitoring the inertial and

structural loading in real-time. At present three incremental flights are planned that will gradually build up to the 3g push over pull up maneuver expected to create the greatest nonlinear response. The last set of tests is optional and would involve flying in full autonomous mode and initiating a series of scripted commands such as the elevator doublets.

6.8 Conclusions

An aeroelastically tuned SensorCraft was designed and constructed based on the improved, Generation 2 Mini SensorCraft configuration. Several techniques were employed to ensure adequate structural compliance while still preserving the aerodynamics and ensuring flight worthiness.

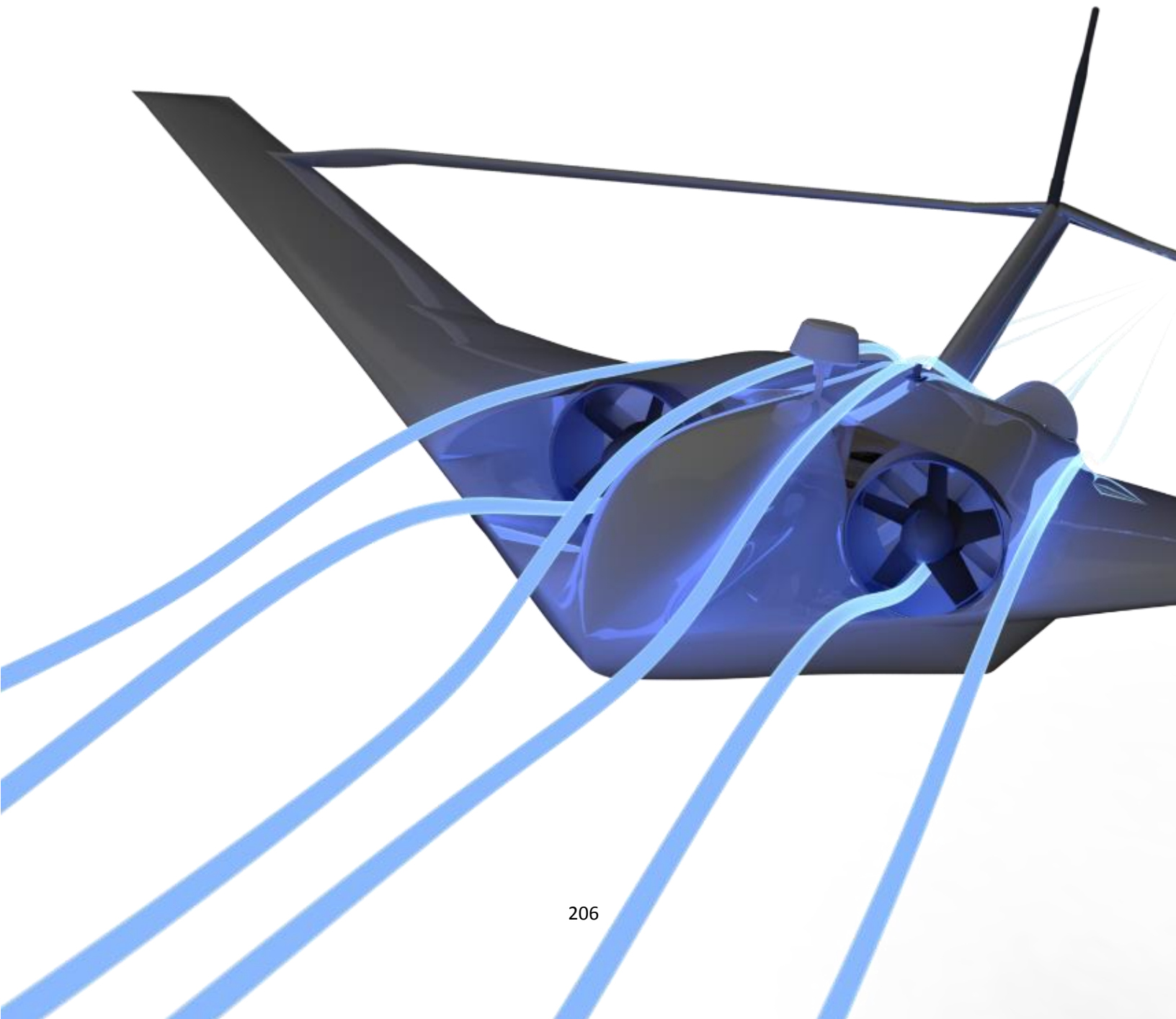
This highly flexible structure had to be tested in both static loading and ground vibration experiments. This required a custom laboratory setup including data acquisition hardware, instrumentation and post processing user interfaces to record and interpret the data. The results from these experiments agreed quite well with the analytical models. These experimental results were then used to further refine the analytical model through an optimization study where material properties and configuration geometry were varied in order to tune the FE model's response. The resulting tuned FE model agreed very well with the experimental results.

Due to the small size of the Mini Configuration, a full set of custom instrumentation had to be built for the flight vehicle. This required custom PCB bridge completion boards that would fit within the small internal volume of the aft wings and then feed the signals to a central DAQ board. This board then processed the data, sending some for onboard storage while simultaneously down sampling the data and sending to the ground station over the autopilot's telemetry link.

A custom pilot operating station interface was developed to allow the pilot to monitor aircraft structural response in flight. This allows the pilot to fly by instruments in order to achieve the required loading for the desired test point. This new method of piloting required a great deal of testing which was carried out using a conventional QT1 UAV and the rigid, Generation 2 Mini SensorCraft.

The flexible mini has undergone final testing and is awaiting its initial flight test campaign. These flights are scheduled for the fall of 2014 under a follow on project that will be run in collaboration with Boeing Directly (as compared to the majority of this work which was with Boeing indirectly, through the US Air Force).

Chapter 7 - Conclusions and Future Work



7.1 Conclusions

At the outset of this work, the USAF requested a series of reduced scale and complexity aircraft to test and validate the Boeing Joined Wing Concept. University of Victoria, in collaboration with Virginia Tech, committed to design, build, instrument, test and fly these aircraft. The desire was to ultimately fly a 1/9th scale aircraft to investigate the linear aeroelastic response of the configuration.

The intent in the Feasibility stage was to determine whether the full sized aircraft could be scaled down to a 5m span ($\sim 1/9^{\text{th}}$ scale) and flown at or near sea level. Some simplifying assumptions were made regarding the governing physics and a set of scaling laws developed which were used to map characteristics from full to model scale. Several constraints were imposed based on physical quantities that cannot be easily manipulated (such as air viscosity and the gravitational constant) but these were shown to likely be of little consequence to the overall usefulness of results.

Since the internal structure of the full scale aircraft is classified, the internal details were not made available. However, the modal response of the full scale aircraft was supplied and it was shown that if the aerodynamics can be preserved (by scaling the outer mold line), a linear aeroelastically equivalent model can be achieved if the mode shapes and scaled frequencies are reproduced.

A quick initial study was summarized with the aim of proving that the chosen reduced scale design point was feasible. Using geometric parameter optimization to tailor the mass and stiffness distribution, it was shown that a feasible model could likely be produced that would have sufficient stiffness using common building materials, yet remain light enough to allow incorporation of all supporting systems required for a flight worthy aircraft.

An advanced Scaling Framework was introduced that is capable of optimizing more complex and representative aircraft geometry in a repeatable and automated way. A test case was run using a simplified cantilever wing

design and showed very good results. This framework was then applied to a simplified beam model of the joined wing configuration in an attempt to match the first six mode shapes and frequencies.

While results using the simplified joined wing configuration were very promising, it was apparent that the optimization problem is very sensitive to the mass distribution and therefore the locations and weights of all the supporting systems. As a result it was determined that the first step must be to more accurately determine the space and component weight reservations throughout the aircraft. This would be achieved in the design of the Rigid 5m RPV (as detailed in the following chapter) and only after all components were defined would the final scaling be performed on a higher fidelity FE model.

Before the 5m configuration could be built and flown, a greater understanding of the Joined Wing SensorCraft configuration was required. Foremost was the aerodynamic properties and the resulting stability and control characteristics.

Initial studies using vortex lattice methods, supplemented with higher order CFD results, show that the aircraft overall exhibits reasonable flying qualities with the exception of a marginally stable Dutch Roll mode. Compounding the problem, the aircraft has little yaw authority due the lack of a conventional vertical tail and resulting poor effectiveness of a rudder surface. In order to effectively operate the configuration, it was decided that some combination of avionics, modifications to the aerodynamic shape and advanced control surface scheduling were required.

While some modifications to the outer mold line were investigated and shown to be effective, it was decided that this was to undesirable in terms of obtaining the scaled aeroelastic response. Therefore, it was decided to obtain reasonable dynamic stability characteristics through the use of stability augmentation using and autopilot. Several control surface schedules were investigate to determine an effective way to obtain yaw authority while still uncoupling other control axes. Two control schemes were chosen and subsequently used on the remainder of the aircraft used in this work.

1. *Damping Dutch roll using Drag Rudders located at the outer flap location on the forward wing.*
2. *Damping of Dutch Roll using only the roll axis stabilization while also using a combination of aileron differential and drag tabs to prevent the large yaw perturbations due to roll commands.*

Several autopilots were evaluated and the Piccolo was determined to be the best choice due to its maturity, robustness of control architecture and leading technical support. This and other autopilots were evaluated using a variety of airframes as well as hardware in the loop and software based simulation.

A key to the success of a project of this magnitude is the incremental approach to both flight risk and complexity. A series of reduced scale aircraft were evaluated (ranging from flat plate foam models to 1.85m "Mini" SensorCraft employing equivalent outer mold lines) in over 100 flight tests. They were instrumental in evaluating hardware, experimentally determining control schemes and training pilots/ground crew. These reduced scale aircraft continued to be flown throughout the duration of this project and lessons learned from this stage were directly transferable to the subsequent design and testing of the 5m configuration.

There are many complexities involved in developing a flight worthy aircraft for measuring in flight response. Many of the components required for a UAV larger than the 35kg RC aircraft upper limit have to be custom designed and fabricated. In this case most components, from landing gear to servo mounts needed to be designed and specified. Some items such as the engines and servos can be purchased off the shelf but special attention is required to ensure their reliability and modifications are required to incorporate them into such a complex aircraft.

Some challenges faced here were the requirements for redundancy, both in terms of systems and operation. Custom solutions were required to ensure that several levels of redundant control were achievable based on all of the conceived failure scenarios. This included the use of three separate pilots with separate command links to overcome autopilot failures, loss of communications, flight outside of visual limits etc.

One of the largest challenges was in terms of communications and electromagnetic interference. Due the large number of data links and command/control links, the aircraft had a lot of problems regarding interference. This

was compounded by the large blanketing caused by the structure that was made primarily of carbon fiber. Special attention was focused on placement of antennae with redundant links used as often as possible. However, in retrospect it would be wise to have made nonstructural portions of the aircraft out of radio transparent materials and place safety critical antennae at these locations (for instance, making the boom out of glass and embedding antennae inside).

Ground testing made a big difference in terms of the success of the 5m evaluation phase. A thorough and systematic approach to the ground testing ensured a flight worthy aircraft was taken to Foremost and many bugs had been caught and fixed in this stage. Flight test planning was also of great importance with a very large emphasis on check lists and contingency plans.

The flight of the 5m aircraft went very well with the chosen control scheme being very effective at controlling the aircraft. The pilot reported good flying qualities throughout the flight envelope but there was still some minor although undesirable wing rock oscillations. Post processing and simulation showed this to be due to over tuning of the lateral control loops. Subsequent model tuning and loop gain optimization resulted in a simulated response with much less wing rock. These updated parameters served as the basis for future flights of the smaller “Mini” SensorCraft configurations.

The blowout of the left main tire on roll out cut the flight test campaign short and further emphasized the importance of developing custom components rather than relying on hobbyist grade parts. Despite this shortened flight test campaign the 5m platform proved to be very stable and reliable. It was proven that the 5m platform is feasible for future investigation of flexible configurations. In addition, the lessons learned and the procedures developed will serve as a foundation for all future efforts, both in terms of the SensorCraft and all other UAV platforms used by the participants.

A more detailed scaling study was performed using a high fidelity FE model updated to reflect the as built mass, stiffness and volume constraints determined by building the 5m Rigid RPV. These investigations showed that the Joined Wing SensorCraft configuration supplied by Boeing at the outset of this project (**Boeing 410 E8**) was

too stiff to show the desired amount of nonlinear behaviors. Upon consultation with Boeing, it became known that this configuration was an early, pre weight optimized design, and that the latest, more flexible configuration was classified and could not be cleared within the timeframe of this work.

Therefore the decision was made to release the aeroelastically scaled constraint and change to an aeroelastically tuned design. This would allow further softening of the structure and result in an aircraft that shows similar nonlinear phenomena that were seen in Boeings latest configuration. Sensitivity studies showed that several nonlinearities are achievable through variation of key structural parameters such as joint and wing stiffness'. Four distinct nonlinearities were proposed which included either stress stiffening/softening of the boom tip deflection, a specific form of the boom nonlinearity where the boom deflects in one direction in the linear region and then reverses at higher load steps and finally aft wing buckling. The latter case was chosen by the Air Force as the response of greatest interest.

The aft wing buckling case was further refined by Anthony Ricciardi^[52] from Virginia Tech. Anthony proposed a ladder type construction for the aft wing and further optimized the forward/aft wing stiffness' using a fully nonlinear aeroelastic framework. The final sizing that resulted from this sizing would serve as the basis for the subsequent design, by the author, of an aeroelastically tuned flight test article.

After submitting the final design concept a great deal of concern was raised concerning the potential safety risks of flying a marginally unstable aircraft with a greatly increased flexibility. In order to reduce risk, both in terms of liability in case of a crash and in terms of schedule, the decision was made to fabricate the aeroelastically tuned design at the reduced, 1.85m "Mini" SensorCraft scale. This would greatly reduce the difficulty of gaining flight clearance from Transport Canada and allowed for multiple flight test windows since the smaller aircraft could be flown locally rather than having to travel to Alberta, as is required with the 5m aircraft.

An aeroelastically tuned SensorCraft was designed and constructed based on the improved, Generation 2 Mini SensorCraft configuration. Several techniques were employed to ensure adequate structural compliance while still preserving the aerodynamics and ensuring flight worthiness.

This highly flexible structure had to be tested in both static loading and ground vibration experiments. This required a custom laboratory setup including data acquisition hardware, instrumentation and post processing user interfaces to record and interpret the data. The results from these experiments agreed quite well with the analytical models. These experimental results were then used to further refine the analytical model through an optimization study where material properties and configuration geometry were varied in order to tune the FE model's response. The resulting tuned FE model agreed very well with the experimental results.

Due to the small size of the Mini Configuration, a full set of custom instrumentation had to be built for the flight vehicle. This required custom PCB bridge completion boards that would fit within the small internal volume of the aft wings and then feed the signals to a central DAQ board. This board then processed the data, sending some for onboard storage while simultaneously down sampling the data and sending to the ground station over the autopilot's telemetry link.

A custom pilot operating station interface was developed to allow the pilot to monitor aircraft structural response in flight. This allows the pilot to fly by instruments in order to achieve the required loading for the desired test point. This new method of piloting required a great deal of testing which was carried out using a conventional QT1 UAV and the rigid, Generation 2 Mini SensorCraft.

7.2 Recommendations and Future Work

The flexible mini has undergone final testing and is awaiting its initial flight test campaign. These flights are scheduled for the fall of 2014 under a follow on project that will be run in collaboration with Boeing Directly (as compared to the majority of this work which was with Boeing indirectly, through the US Air Force).

This follow on project will see the flight testing of the Flexible Mini SensorCraft as it preliminary stage before proceeding with the larger scale aircraft (possibly the 5m configuration or a slightly smaller 3m model). The larger scale aircraft will combine all of the lessons learned through the design, construction and testing of the aircraft used in this work and will be used to investigate nonlinear static and dynamic response as well as gust load alleviation schemes

Literature Cited

- [1] David Lucia, "The SensorCraft Configurations: A Nonlinear Aeroelastic Challenge for Aviation," , 46TH AIAA/ASME/ASCE/AHS/ASC STRUCTURES, STRUCTURAL DYNAMICS AND MATERIALS CONFERENCE, Austin, 2005.
- [2] Bradley Sexton, Brian Foist, Eric Reichenbach, and Terry Britt, "AIR VEHICLE TECHNOLOGY AND INTEGRATION RESEARCH (AVIATR)," Dayton, AFRL-RB-WP-TR-2010-3072, 2010.
- [3] Ben Smallwood, "Structurally integrated Antennas on a Joined Wing Aircraft," Air Force Institute of Technology, Dayton, MSc Thesis 2003.
- [4] J. Wolkovitch, "The Joined Wing: An Overview," *Journal of Aircraft*, vol. 23, no. 3, pp. 161-178, March 1986.
- [5] I.M. Kroo, J.W. Gallman, and S.C. and Smith, "Aerodynamic and Structural Studies of Joined Wing Aircraft," *Journal of Aircraft*, vol. 28, no. 1, pp. 74-81, January 1991.
- [6] Y. I. Kim, G. J. Park, R. M. Kolonay, M. Blair, and R. A. Canfield, "Nonlinear Dynamic Response Structural Optimization of a Joined-Wing Using Equivalent Static Loads," *Journal of Aircraft*, vol. 46, no. 3, pp. 821-831, May 2009.
- [7] D J Lucia, "The Sensorcraft Configurations: A Non-linear Aeroservoelastic Challenge for Aviation," in *46th AIAA/ASME/ASCE/AHS/ASC Structures, Structural Dynamics and Materials Conference*, 2005.
- [8] M., Canfield, R., Roberts, R. Blair, "Joined-wing aeroelastic design with geometric nonlinearity," , IFASD International Forum on Aeroelasticity and Structural Dynamics, Amsterdam, 2005.
- [9] S C Smith, I Kroo, and S E Cliff, "The Design of a Joied Wing Demonstrator Aircraft," in *AIAA Aircraft Design Meeting*, vol. AIAA-87-2930, 1987.
- [10] E. Livne, "Aeroelasticity of Joined-Wing Airplane Configurations: Past Work and Future Challenges - A Survey," April 2001.
- [11] H. H., Jhou, J., and Stearman Lin, "Inluence of Joint Fixity on the Aeroleastic Characteristics of a Joined WIng Structure," vol. Paper 1990-0980. 31st AIAA/ ASME/ASCE/AHS/ASC Structures, Structural Dynamics and Materials Conference, Long Beach CA, April 1990.
- [12] Jason Robinson, William A. McClelland and Jason Bowman Maxwell Blair, "A Joined Wing Flight Experiment," Dayton, Final Report AFRL-RB-WP-TR-2008-3101, 2008.
- [13] M., and Canfiled, R. A. Blair, "A JOINED-WING STRUCTURAL WEIGHT MODELING STUDY," , 43rd AIAA/ASME/ASCE/AHS/ASC Structures, Structural Dynamics, and Materials Confernece, Denver, 2002.
- [14] R.A. Canfield, M. Blair C.C. Rasmussen, "Optimization Process for Configuration of Flexibel Joined Wing," *Structural and Multidisciplinary Optimization*, vol. 37, no. 3, pp. 265-277, January 2009.

- [15] L Demasi, Bhasin, P C Chen, and Wang Z, "Dynamic Nonlinear Aeroelastic Analysis of The Joined Wing Configuration," , 53rd AIAA/ASME/ASCE/AHS/ASC Structures, Structural Dynamics & Materials Conference, Honolulu, 2012.
- [16] L Demasi, R Cavallaro, and Bertucelli, "Post-Critical Analysis of Joined Wings: the Concept of Snap-Divergence as a Characterization of the Instability," , 54th AIAA/ASME/ASCE/AHS/ASC Structures, Structural Dynamics & Materials Conference, Boston, 2013.
- [17] R Cavallaro, L Demasi, and A Rassariello, "International Forum on Aeroelasticity and Structural Dynamics," , International Forum on Aeroelasticity and Structural Dynamics, Honolulu, 2012.
- [18] L Demasi, R Cavallaro, and Bertucelli, "Risks of Linear Design of Joined Wings: a Nonlinear Dynamic Perspective in the Presence of Follower Forces," , 54th AIAA/ASME/ASCE/AHS/ASC Structures, Structural Dynamics & Materials Conference, Boston, 2013.
- [19] E. O. Macagno, "Historico-critical Review of Dimensional Analysis", " *Journal of the Franklin Institute*, vol. 292, no. 6, 1971.
- [20] A Vaschy, "Sur les lois de similitude en Physique," *Annales Telegraphiques*, pp. 22-28, 1892.
- [21] P W Bridgeman, *Dimensional Analysis*. London : Yale University Press, 1922.
- [22] R I Bisplinghoff, H Ashley, and R L Halfman, *Aeroelasticity*. Cambridge: Addison-Wesley, 1955.
- [23] NATO Science and Technology Organization, *Manual on Aeroelasticity*.: Advisory Group for Aerospace Research and Development, 1971.
- [24] Jenifer Heeg, Charles V Spain, and J A Riviera, "Wind Tunnel to Atmospheric Mapping for Static Aeroelastic Scaling," in *45th AIAA/ASME/ASCE/AHS/ASC Structures, Structural Dynamics & Materials Conference*, Palm Springs, 2004.
- [25] Mark French and F E Eastep, "Aeroelastic model design using parameter identification," *Journal of aircraft*, vol. 33, no. 1, pp. 198-202, 1996.
- [26] Mark French, "An application of structural optimization in wind tunnel model design," , AIAA/ASME/ASCE/AHS/ASC Structures, Structural Dynamics and Materials Conference, Long Beach, 1990.
- [27] E H Presente, "Innovative Scaling Laws for Aeroelastic and Aeroservoelastic Problems in Compressible Flows," University of California, Los Angeles, PhD Thesis 1999.
- [28] E H Presente and P P Friedman, "Aeroelasticity in Compressible Flow and Aeroelastic Scaling Considerations," in *International Symposium on Fluid-Structure Interactions, Aeroelasticity, Flow Induced Vibrations and Noise*, Dallas, 1997.
- [29] E H Presente and P P Friedman, "Aeroservoelasticity in Compressible Flow and Its Scaling Laws," in *39th AIAA/ASME/ASCE/AHS/ASC Structures, Structural Dynamics, and Materials Convergence*, Long Beach, 1998.

- [30] E. H. Presente and P P Friedmann, "Aeroservoelasticity in Subsonic Flows and Associated Scaling Laws," in *AIAA/ASME/ASCE/AHS/ASC Structures, Structural Dynamics, and Materials Conferences*, Kissimmee, 1997.
- [31] P P Friedman, D Guillot, and E Presente, "Adaptive control of aeroelastic instabilities in Transonic Flow Regimes," *Journal of Guidance, Control, and Dynamics*, vol. 20, no. 6, pp. 1190-1199, November 1997.
- [32] E H Friedman and P Peretze, "Rotary Wing Aeroelastic Scaling and its Implications for Adaptive Materials Based Actuation," in *6th SPIE Symposium on Smart Structures and Materials*, Newport Beach, 1999.
- [33] Pedro Pereira, Luis Reis de Almeda, and Antonio Costa, "Research and Development of a Scaled Joined-Wing Flight Vehicle," IST, Lisbon, EOARD Final Report 2006.
- [34] P Pereira, L. Almeida, and A. Suleman, "Aeroelastic Scaling and Optimization," , 48TH AIAA/ASME/ASCE/AHS/ASC STRUCTURES, STRUCTURAL DYNAMICS, AND MATERIALS CONFERENCE, Honolulu, 2007.
- [35] C Cesnik and Z Wan, "Geometrically Nonlinear Aeroelastic Scaling for Very Flexible Aircraft," , 54th AIAA/ASME/ASCE/AHS/ASC Structures, Structural Dynamics and Materials Conference, Boston, 2013.
- [36] C E S Cesnik and Su W, "Geometrically Nonlinear Aeroelastic Scaling for Very Flexible Aircraft," , 54TH AIAA/ASME/ASCE/AHS/ASC STRUCTURES, STRUCTURAL DYNAMICS, AND MATERIALS CONFERENCE, Boston, 2013.
- [37] ZONA Technology, Inc, *ZAERO Theoretical Manual 8.5*. Scottsdale, 2011.
- [38] MSC.Nastran Inc, *MSC.Nastran Version 68 Aeroelastic Analysis User's Guide*. Santa Ana, 2004.
- [39] M J Patil and D H Hodges, "Flight Dynamics of Highly Flexible Wings," *Journal of Aircraft*, vol. 43, no. 6, pp. 1790-1799, 2006.
- [40] D A Peters and M J Johnson, "Finite State Airloads and Deformable Airfoils on Fixed and Rotating Wings," Washington University, Seattle, MSc Thesis 1994.
- [41] D A Peters, W M Cao, and S karunamoorthy, "Finite State Induced Flow Models Part I," *Journal of Aircraft*, vol. 32, no. 2, pp. 313-322, March 1995.
- [42] D H Hodges, "A Mixed Variational Formulation Based on Exact Intrinsic Equations for the Dynamics of Moving Beams," *International Journal of Solids and Structures*, vol. 26, no. 11, pp. 1253–1273, 1990.
- [43] D H Hodges, "Geometrically Exact, Intrinsic Theory of Dynamics of Curved and Twisted Anisotropic Beams," *AIAA Journal of Aircraft*, vol. 41, no. 6, pp. 1131-1137, June 2003.
- [44] S Ricci and L Cavagna, "A Fast Tool for Structural Sizing, Aeroelastic Analysis and Optimization in Aircraft Conceptual Design," in *50TH AIAA/ASME/ASCE/AHS/ASC STRUCTURES, STRUCTURAL DYNAMICS, AND MATERIALS CONFERENCE*, Palm Springs, 2009.
- [45] S Ricci, L Cavagna, and L Travaglini, "Gust Loads Assessment: a Multi-Fidelity Approach," in *International Forum on Aeroelasticity and Structural Dynamics (IFASD 2011)*, Paris, 2011.

- [46] Mark Dreal, "Integrated Simulation Model for Preliminary Aerodynamic, Structural and Control Law Design of Aircraft," , 40th AIAA SDM Conference, St Louis, 1999.
- [47] Mark Drela, *ASWING 5.81 Technical Description - Stead Formulation*. Boston: MIT, 2008.
- [48] Mark Drela, *ASWING 5.81 Technical Description - Unsteady Extension*. Boston: MIT, 2008.
- [49] C E S Cesnik and E L Brown, "Modelling of High Aspect Ratio Active Flexible Wings for Roll Control," , 43rd AIAA/ASME/ASCE/AHS Structures, Structural Dynamics, and Materials Conference, Denver, 2002.
- [50] C E S Cesnik, J Zhang, and W Su, "Correlations between UM/NAST Nonlinear Aeroelastic Simulations and Experiments of a Cantilever Slender Wing," , IFASD International Forum on Aeroelasticity and Structural Dynamics 2009, Seattle, 2009.
- [51] C E S Cesnik and W Wu, "Nonlinear Aeroelastic Simulation of X-HALE: a Very Flexible UAV," , 49th AIAA Aerospace Sciences Meeting Including the New Horizons Aerospace Exposition, Orlando, 2011.
- [52] Anthony P. Ricciardi, "Geometrically Nonlinear Aeroelastic Scaling," Virginia Polytechnic Institute and State University, Blacksburg, PhD Thesis 2013.
- [53] NASA, High Angle of Attack Stability and Control (HASC) Code, refer to NASA Contractor Report 4712.
- [54] Harold Yongren Mark Drela, Athena Vortex Lattice (AVL) Code, <http://web.mit.edu/drela/Public/web/avl/>.
- [55] NASA Langley Research Center, High Angle of Attack Stability and Control 95.
- [56] Jan Roskam, *Airplane Flight Dynamics and Automatic Flight Controls*. Lawrence, Kansas 66044: DARcorporation, 1995.
- [57] Jan Roskam, *Airplane Design Volumes I-VII*. Lawrence: DAR Corporation, 2005.
- [58] Jeff Garnand-Royo, "Design and Evaluation of Geometric Nonlinearities using Joined-Wing SensorCraft Flight Test Article," Blacksburg, Thesis 2013.
- [59] Tyler Aarons, "Development and Implementation of a Flight Test Program for a Geometrically Scaled Joined Wing Sensorcraft Remotely Piloted Vehicle," Virginia Polytechnic Institute and State University, Blacksburg, MSc Thesis 2011.
- [60] Charles Eger, "Design of a Scaled Flight Test Vehicle Including Linear Aeroelastic Effects," Virginia Polytechnic Institute and State University, Blacksburg, MSc Thesis 2013.
- [61] Mark Drela, *ASWING 5.81 User Guide*. Boston, 2008.
- [62] Mark French, "Design of Aeroelastically Scaled Wind Tunnel Models Using Sensitivity Based," 1993.
- [63] The Boeing Company, "Selected Results from Test of Model on Sting," NASA Langley, Hampton VA, 2008.
- [64] ZONA Technology, Inc, *ZAERO Users Manual 8.5*. Scottsdale, 2011.

- [65] MSC.Software Corporation, *MSC.Nastran 2005 Quick Reference Guide, Volumes I & II*. Santa Ana: MSC.Software Corporation, 2004.
- [66] C E S Cesnil and E L Brown, "Active Wing Warping Control of a Joined Wing Airplane Configuration," , 44th AIAA/ASME/ASCE/AHS Structures, Structural Dynamics, and Materials Conference, Norfolk, 2003.
- [67] D A Peters and He Cheng, "Finite state induced flow models. II - Three-dimensional rotor disk," *Journal of Aircraft*, vol. 32, no. 2, pp. 323-333, March 1995.